Final Report

Application of Tools to Measure PCB Microbial Dechlorination and Flux into Water During In-situ Treatment of Sediments

SERDP Project ER-1502

August 2011

Joel Baker
Chih-wei Chang
University of Washington

Kevin Sowers
University of Maryland

Upal Ghosh
Piuly Paul
University of Maryland Baltimore County

Birthe Kjellerup
Goucher College

SERDP
DOD • EPA • DOE

Report Documentation Page

Form Approved
OMB No. 0704-0188

1. REPORT DATE	2. REPORT TYPE	3. DATES COVERED
AUG 2011	**N/A**	**-**

4. TITLE AND SUBTITLE	5a. CONTRACT NUMBER
Application of Tools to Measure PCB Microbial Dechlorination and Flux into Water During In-situ Treatment of Sediments	5b. GRANT NUMBER
	5c. PROGRAM ELEMENT NUMBER
6. AUTHOR(S)	5d. PROJECT NUMBER
	5e. TASK NUMBER
	5f. WORK UNIT NUMBER
7. PERFORMING ORGANIZATION NAME(S) AND ADDRESS(ES) **University of Washington**	8. PERFORMING ORGANIZATION REPORT NUMBER
9. SPONSORING/MONITORING AGENCY NAME(S) AND ADDRESS(ES)	10. SPONSOR/MONITOR'S ACRONYM(S)
	11. SPONSOR/MONITOR'S REPORT NUMBER(S)

12. DISTRIBUTION/AVAILABILITY STATEMENT
Approved for public release, distribution unlimited

13. SUPPLEMENTARY NOTES
The original document contains color images.

14. ABSTRACT

15. SUBJECT TERMS

16. SECURITY CLASSIFICATION OF:			17. LIMITATION OF ABSTRACT	18. NUMBER OF PAGES	19a. NAME OF RESPONSIBLE PERSON
a. REPORT	b. ABSTRACT	c. THIS PAGE			
unclassified	**unclassified**	**unclassified**	**SAR**	**147**	

TABLE OF CONTENTS **Page Number**

LIST OF TABLES

LIST OF FIGURES

LIST OF ACRONYMS

AC	active carbon
cPCR	competitive polymerase chain reaction
DELPCB	polychlorinated biphenyls water quality model for Delaware Estuary
dHPLC	denaturing high performance liquid chromatography
DMSO	dimethyl sulfoxide
DNA	Deoxyribonucleic Acid
dNTP	dinucleotide triphosphate
DOC	dissolved organic carbon
ETM	estuarine turbidity maxima
HOCs	hydrophobic organic chemicals
HPLC	high performance liquid chromatography
INS	inorganic solids
KC1	potassium chloride
OC	organic carbon
PAH	polycyclic aromatic hydrocarbon
PBDEs	polybrominated diphenyl ethers
PCB	polychlorinated biphenyls
PCR	polymerase chain reaction
PES	particle entrainment simulator
POM	polyoxymethylene
POM-SPE	polyoxymethylene solid phase extraction
qPCR	real time polymerase chain reaction
rRNA	ribosomal ribonucleic acid
SERDP	Strategic Environmental Research and Development Program
SOD	sediment oxygen demand
SPME	solid phase microextraction
STORM	shear turbulence resuspension mesocosms
TCC	total suspended solids
TOC	total organic carbon
TVC	trapped vortex combuster
USEPA	U.S. Environmental Protection Agency

Executive Summary

This study addresses the Strategic Environmental Research and Development Program (SERDP) Statement of Need CUSON-06-03: *Assessment and Measurement of Processes Impacting the Fate and Transport of Contaminants in Sediments*. The specific high priority needs addressed in this study are: 1) To develop and evaluate site characterization tools to measure the rates of important sediment chemical/physical/biological processes affecting the fate and transport of contaminants, and 2) To understand and quantify sediment exchange processes with overlying water. The project began in early Summer, 2006, and this report includes progress through December 2007 in this multi-year study. Our initial goals were to examine sediments from representative riverine and estuarine systems with well-characterized polychlorinated biphenyls (PCB) contamination histories. Since these sediments will be used for more detailed laboratory studies of dehalogenation, activated carbon (AC) amendments, and sediment-water exchange, an important goal of the first project year was to characterize the PCB levels *and* the presence of dehalogenating organisms. Only those sediments with sufficiently high PCB levels and active populations of dehalogenating microbes are suitable for subsequent experiments, and the results from these first year evaluations drive our initial 'go-no go' decision.

Sediment was collected from the Anacostia River (a tributary to the Potomac River in Washington, D.C.), the Buffalo River and the Grasse River (both in upstate New York), from several locations within Baltimore Harbor (Maryland) and from Hunters Point (San Francisco Bay, California). The Anacostia River is contaminated with PCBs from a number of sources, including activities at the Washington Navy Yard. Pilot-scale *in situ* capping studies are on-going in the Anacostia River. The Grasse River is a U.S. Environmental Protection Agency (USEPA) Superfund site that contains high levels of PCBs in the vicinity of an industrial facility. Based on our characterization of these sediments, we chose to focus the remaining detailed studies on the Grasse River sediments. Initial screening of the Anacostia, Buffalo, and Grasse River sediments show active PCB dechlorinating microbes at each site. PCB concentrations and dechlorinating activity were highest at the Grasse River. Levels of PCBs in the Buffalo River sediments may be too low for these sediments to be used in subsequent studies, so the Grasse River sediments are likely the best freshwater candidate sediments.

Results to date compare the PCB levels and availability across the sediment types. Incubations of Grasse River sediments with and without AC additions are underway in order to assess the dehalogenation activity of the native microbial populations. We have optimized and applied molecular techniques to characterize the dehalogenating community, proving a link between the observed activity and the putative organisms. Due to the likely variable redox conditions in contaminated sites such as the Grasse River, we added a series of aerobic incubations to assess the potential for aerobic degradation of PCB congeners. These studies, while still in progress, suggest modest degradation of many congeners that is reduced in the presence of AC. Finally, we have developed and calibrated a dynamic sediment-water exchange model of PCB transport that included particle coagulation and kinetically-limited partitioning.

This page is intentionally left blank

OBJECTIVES

This study addresses the SERDP Statement of Need CUSON-06-03: *Assessment and Measurement of Processes Impacting the Fate and Transport of Contaminants in Sediments*. The specific high priority needs addressed in this study are: 1) To develop and evaluate site characterization tools to measure the rates of important sediment chemical/physical/biological processes affecting the fate and transport of contaminants, and 2) To understand and quantify sediment exchange processes with overlying water. Contamination of sediments with persistent, bioaccumulative toxins such as PCB is a vexing problem, causing significant risk to humans and wildlife and commonly requiring expensive and disruptive remediation programs. The traditional approach is to assess risk by comparing the *total* contaminant concentration in the sediment to risk-based benchmarks, and to remediate sites by *removing* sediments for burial or treatment elsewhere. This approach explicitly assumes the contaminants measured in the solid phase are available to organisms and, therefore, present a risk. Recent studies have shown that strongly-sorbing solid phases such as soot and AC present in sediment significantly reduce bioavailability of hydrophobic pollutants, such that the *total* measured concentration may overestimate exposure and risk. These 'supersorbents' may result from natural processes (fires), inadvertent anthropogenic additions (coal gas manufacturing plants), or purposeful additions for *in situ* remediation. This study centers around how these particles influence microbially-mediated dehalogenation reactions and dissolved-sorbed partitioning of PCBs.

The overall hypothesis of this study is that the extent of biogeochemical reactivity and mobility of sedimentary contaminants is controlled by desorption to support dissolved concentrations. This study employs two new assessment tools to quantify the bioavailability of sediment-bound contaminants to evaluate the efficacy of *in situ* AC treatments. First, an MPN-PCR-based assay recently developed by K. Sowers detects and quantifies indigenous PCB dechlorinating species in soils and sediments. Microbial dehalogenation is not only an important sink for PCBs in sediments, but also may be used as a probe of PCB speciation and bioavailability. Second, we have recently developed and deployed an experimental system to accurately quantify PCB desorption rates from sediments under realistic levels of turbulence and bottom shear (Schneider *et al.*, 2007). A solid phase microextraction (SPME) technique rapidly measures truly dissolved PCB congeners in sediment suspensions, allowing desorption kinetics and bioavailability to be determined (Schneider *et al.*, 2006). These two assessment tools are used to compare PCB availability to total solid phase concentrations to directly examine PCB mobility in historically contaminated sediments. We are amending these sediments with AC to explore how addition of strongly sorbing solids alters microbial dehalogenation and PCB release from sediments. This approach has both fundamental and applied aspects–the AC additions are tools to study PCB speciation in sediments and pilot-scale evaluations of a promising *in situ* remediation technique. Our broad goal is to assist in the development of the next generation of contaminated sediment management tools.

Study 1. Development and Application of Molecular Techniques to Characterize *in situ* Dechlorination of PCB Congeners

The objective of this study was to optimize molecular techniques for characterizing the abundance and activity of dehalogenating microbial communities in natural and activated carbon-amended sediments. Specific objectives are:

1. Complete microbial characterization sediments from Grasse River, Hunters Point, CA, Anacostia River, D.C., and Hudson River, NY.
2. Opitmize molecular techniques for selected site (Grasse River) including denaturing HPLC (dHPLC) for community diversity analysis, cPCR for quantitative assessment of dehalogenators and dehalogenation activity microcosm assays.
3. Develop protocol for extraction of community deoxyribonucleic acid (DNA) from activated charcoal
4. Conduct microbial assessment of activated charcoal amended sediments.

Results

1. Complete microbial characterization sediments.

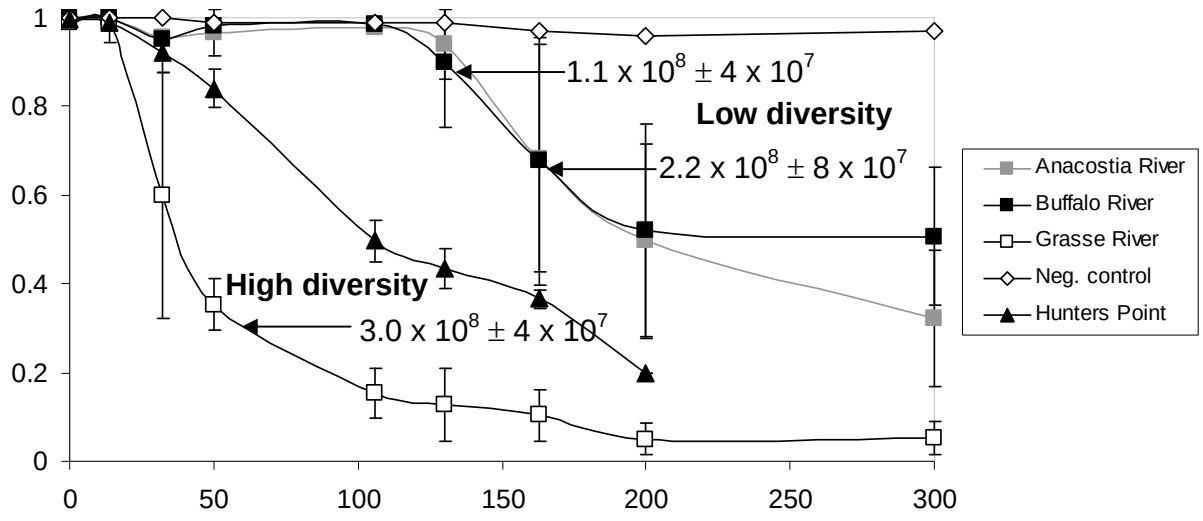

Figure 1.1 *Results from activity assays showing the dechlorination potential for PCB116 (2,3,4,5,6-PCB), which is fully chlorinated on one of the two biphenyl rings making all dechlorination processes potentially possible. (◊ Anacostia River; ◦ Buffalo River; ▫ Grasse River; ▪ Negative control.)*

Microbial characterization of Anacostia River, D.C., Buffalo River and Grasse River, NY was completed. These three locations were chosen based on their history and their current level of PCB contamination. Microbial characterization of these three sites was provided in last annual report. Grasse River was the most actively dechlorinating site of the three (Figure 1.1).

Although the qPCR showed that the numbers of dechlorinating bacteria was similar in all three sites, dHPLC indicated that the diversity was lower in the Grasse Rivers site. Although counterintuitive, the results suggest that at sites with a history of organohalide contamination, diversity analyses may be more informative than qPCR alone. Our working hypothesis is that low diversity suggests that an active population of dehalogenators has been enriched, whereas sites with high diversity may not be active and as a result there is no active enrichment for the dehalogenating population. Analyses at other sites in ongoing to determine whether there is a relationship between diversity and *in situ* activity.

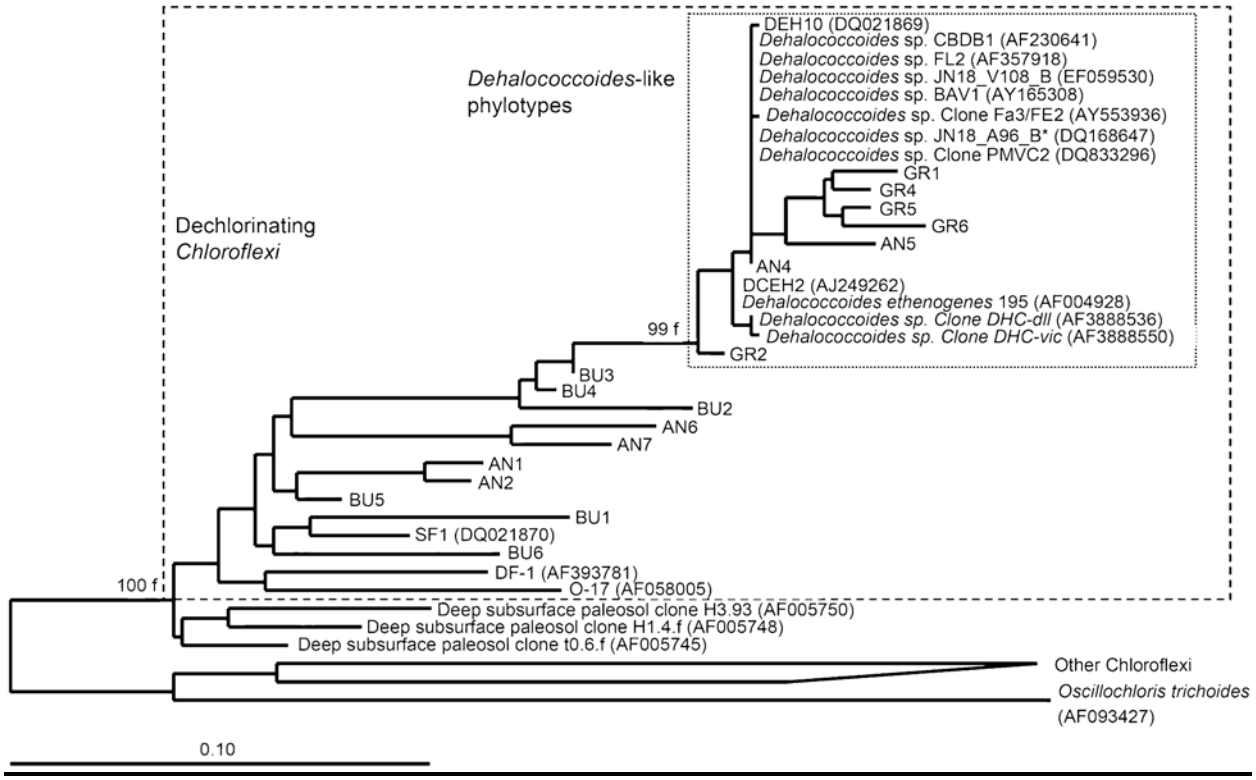

Figure 1.2. Phylogenetic tree showing the relationships between the phylotypes identified in Anacostia (AN), Buffalo (BU) and Grasse (GR) River sediments and the closest dechlorinating species within the dechlorinating Chloroflexi group. Dashed box indicates confirmed dechlorinating bacteria reported previously and putative dechlorinating phylotypes from this study. Accession numbers are indicated in parentheses. The tree was calculated by the neighbor joining method and supported by FITCH (Ludwig et al., 2004). The scale bar indicates 10 substitutions per 100 nucleotide positions.

To determine whether there was a relationship between differences in the dechlorination activity or congener distribution and the composition of indigenous dechlorinating bacterial communities, DNA was extracted from the sediments and analysed by DHPLC to characterize the community profiles of putative dechlorinating phylotypes (Figure 2). Comparative sequence analyses of

DNA obtained from the DHPLC showed that five phylotypes related to *Dehalococcoides* with sequence similarities _ 99% were identified in Grasse River sediment. This was a relatively homologous population as most active PCB impacted sites have phylotypes related to both the *Dehalococcoides* and DF-1/*o*-17 clade.

2. Optimize molecular techniques for selected site (Grasse River) including denaturing HPLC (dHPLC) for community diversity analysis and cPCR for quantitative assessment of dehalogenators.

A three step analysis is used to characterize the dehalogenating population in a sample. cPCR provides a qualitative assessment of the size of the dehalogenating population (Figure 1.2). This assay utilizes specific primers develop in our laboratory to selectively detect and enumerate only 16S rRNA genes from dehalogenating bacteria. dHPLC provides qualitative assessment of the dehalogenating population using specific primers to identify individual phylotypes and determine overall diversity of dehalogenators. Since 16S rRNA genes do not indicate that dehalogenating activity is occurring, the molecular assay are supported by activity assays that confirm the rates and specific pathways of PCB dehalogenation. The combined assays provide an overall assessment of the effect of treatments on the microbial population and it ability to reductively dechlorinate PCBs.

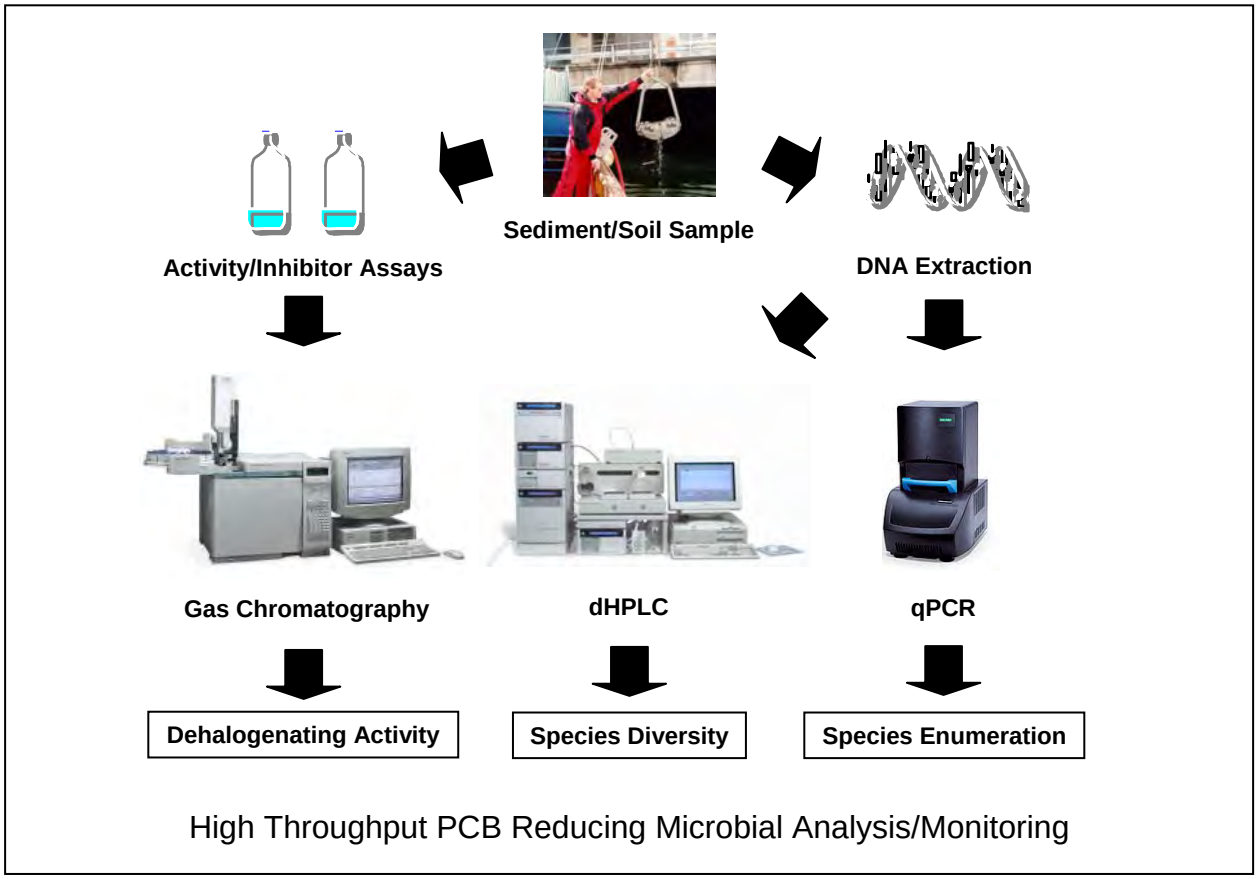

Figure 1.3. *Illustration of three-part assessment to determine the effect of treatments on microbial growth and PCB dehalogenating activities.*

2a. Enumeration of putative PCB dechlorinating bacteria by competitive PCR.

Primers 348F/884R that target the 16S rRNA genes of putative dechlorinating bacteria (5) are used to develop a competitive PCR assay using the Competitive DNA construction kit #RR017 according to the manufacturer's instructions (TaKaRa Bio Inc., Japan). The final size of the amplified target is 536 bp and the difference in size between the amplified target DNA and competitor DNA is 10% (54 bp). The number of copies constructed for this competitor is calculated as $OD_{260} \times 9{,}430^{12}$ equaling $6{,}4\times10^{12}$ copies μl^{-1} according to the manufacturer's instructions (TaKaRa Bio Inc, Japan). The specificity of the competitor is confirmed by using 16S rRNA genes from PCB dechlorinating bacteria DF-1, o-17 and DEH10 (5, 15) and non-dechlorinating bacteria *Desulfovibrio* sp., *Escherichia coli* and the aerobic PCB degrading bacterium *Burkholderia xenovorans* LB400 (3). Addition DNA samples extracted from two pristine inland sites on Baffin Island, Canada are used as negative controls. Enumeration of putative dechlorinating bacteria in the sediment samples using the cPCR assay is performed in triplicate with template DNA extracted from 0.75 g of sediment. The enumerated 16S rRNA genes copies from the cPCR assay is normalized to the dry weight content in the sediment samples. DNA extraction was linear in the range from 0-4 g of sediment (data not shown). A ten-fold dilution series of the competitor is used against unknown DNA from by using the PCR conditions described below with the substitution of 5 µl of competitor and 29.5 µl of nuclease free water. The intensity of the PCR products is measured by densitometry with image analysis software (Quantity One, Biorad, Hercules, CA). One 16S rRNA gene copy per cell was assumed based on the genome sequences of *Dehalococcoides ethenogenes* (13) and CBDB1 (9). The cPCR analysis was performed for putative dechlorinating bacteria as a group and not for the individual dechlorinating phylotypes. All samples were also tested with the universal primer set 341F/907R (10, 12) as a positive control to screen for PCR inhibiting components. Both the primer locations and PCR fragment size are similar for the universal and specific primer sets to minimize the effects of PCR bias.

2b. Community analysis by denaturing HPLC (DHPLC).

DHPLC analyses is performed using a WAVE 3500 HT system (Transgenomic, Omaha, NE) equipped with an ultraviolet detector. The primers 348F/884R are used for specific PCR amplification of 16S rRNA genes from putative dechlorinating bacteria within the *Chloroflexi* (5). PCR was conducted in 50 µl reaction volumes using the following GeneAmp reagents (Applied Biosystems, Foster City, CA): 10 mM Tris-HCl, 75 mM KCl, 0.2 mM of each dNTP in a mix, 1.5 mM $MgCl_2$, 1.6% DMSO, 2.5 units of AmpliTaq DNA Polymerase, 50 pM of each primer, 1 µl of DNA template and 34.5 µl of nuclease free water. For the PCR reaction (40 cycles), the initial denaturation step is 95°C for 2 min, followed by denaturation at 95°C for 45 s, primer annealing at 58°C for 45 s, elongation at 72°C for 60 s, a final extension step at 72°C for 30 min and a final holding step at 4°C. PCR products of the correct length are confirmed by electrophoresis using a 1.5% agarose gel prior to analysis by DHPLC. The 16S rRNA gene fragments are analyzed in an 8 µl injection volume by DHPLC with a DNASep® cartridge packed with alkylated nonporous polystyrene-divinylbenzene copolymer microspheres for high-performance nucleic acid separation (Transgenomic, Omaha, NE). The oven temperature is 63.0ºC and the flow rate is 0.5 ml min^{-1} with a gradient of 55%-35% Buffer A and 45%-65% Buffer B from 0-13 minutes. The analytical solutions used for the analyses are: Buffer A, Buffer B, Solution D and Syringe Wash Solution (Transgenomic, Omaha, NE). Analysis was performed using the Wavemaker version 4.1.44 software. An initial run is used to identify

individual PCR fragments and determine their retention times. Individual peaks are eluted for sequencing from a subsequent run and collected with a fraction collector based on their retention times. The fractions are collected in 96 well plates and dried using a Savant SpeedVac system followed by dissolution in 15 µl nuclease free water. Re-amplification is performed following the protocol described above and PCR products were confirmed by DHPLC to ensure that only one species was present in the individual fractions. The PCR amplicons are electrophoresed in a 1.5% low melt agarose gel and the excised fragment was purified for sequencing using Wizard® PCR Preps DNA Purification Resin/ A7170. The separations are all based on detection with UV at 260 nm resulting in a relatively high background on the chromatograms due to the presence of for instance remaining primers and unspecific DNA. However, this does not impact the subsequent sequencing.

Both of these assays are now used routinely by our laboratory to assess the suitability of sites for bioaugmentation and to monitor the effectiveness of different bioaugmentation strategies.

3. Develop protocol for extraction of community DNA from activated charcoal.

A critical factor in the proposed research is the development of a protocol for isolating DNA from the carbon treated sediment. DNA adsorbs irreversibly to AC, so it will be necessary to isolate cells from the carbon before attempting DNA extraction. We tested the efficiency of different protocols for extraction of PCB dechlorinating bacteria from sediment with granular AC used in our micrcosms studies and compared the results with controls that do not contain AC. An optimized protocol was developed using the MoBio Power Soil Kit that employs the standard recommended protocol with 0.75 g of wet sediment containing AC in stead of 0.25 g is used to obtain sufficient DNA for downstream applications. Briefly, the protocol is as follows: 1) the sediment slurry is mixed with lysing buffer/PowerBeads and subsequently vortexed for 10 minutes; 2) four different solutions were used sequentially used to remove non-DNA organic and inorganic material including cell debris, humic substances and proteins that would inhibit downstream DNA applications; 3) the DNA is finally captured in a spin filter that was washed with ethanol to remove residual salts, humic acids and other contaminants; 4) the clean DNA is eluted from the spin filter by adding 100 µl of PCR grade water.

4. Microbial assessment of activated charcoal amended sediments.

Sample grabs (20 liters) were taken form Grasse River and homogenized. Untreated samples and samples treated with AC were inoculated into medium for to determine the dechlorination potential of indigenous microbial communities in the sediment samples. Ten ml of anaerobically prepared F-medium was prepared in 25 ml anaerobe tubes sealed under N_2-CO_2 (80:20) with butyl rubber septa. Micrososms were set up in triplicate contained 4.0 g of sediment with and without AC. The treatments included 1) addition of congener 2,3,4,5,6-CB to a final concentration of 50 ppm; 2) no congener addition (weathered PCB only); 3) sterile controls autoclaved twice for 20 min at 121^{o}C on day one and day three prior to adding PCB. The cultures were incubated at 30ºC in the dark and sampled anaerobically over the course of 336 days for DNA extraction and PCB analysis. For PCB analysis samples (1 ml) were anaerobically transferred and extracted by Accelerated Solvent Extraction using USEPA Method 3545. The total amount of the individual congeners, respectively, were quantified in each replicate sample with a 7-point calibration curve using the surrogates PCB 14, 65, 166 at a standard range of 2, 5, 10, 20 ug/L and internal standards PCB 33 and 204 at 4ug/L. The Calibration table was made

using Mullins Mix - Aroclors 1232, 1248, & 1262 at these amounts for curve 30, 61, 183, 610, 1830ug/L.

Study 2. Intrinsic Bioavailability of PCB Congeners in Historically-Contaminated Sediments.

The availability of PCBs was examined in spiked sediment from the Anacostia, Buffalo, and Grasse Rivers according to the method described previously (Jonker and Koelmans, 2001). Briefly, 2,3,4,5,6-pentachlorobiphenyl (2,3,4,5,6-CB, Accustandard, CT) was dissolved in acetone prior to the start of the experiment. Polyoxymethylene, $(-CH_2-)_n$ (POM) sheets (obtained from the Norwegian Geotechnical Institute, Oslo, Norway) were cut into strips of 20 mg. Before use, the strips were cold-extracted with hexane and methanol for 30 minutes each followed by air-drying. The experiment was initiated by transferring 10 g dry sediment from each of the three rivers to 250 mL brown amber glass bottles (I-CHEM^{TM}, Rockwood, TN) and deionized water (240 mL) with sodium azide (1000 mg L^{-1}) was added. After manual mixing 4 µg of 2,3,4,5,6-CB dissolved in acetone were added and mixed by rotation at 3te, rpm for 24 hours. POM strips (100 mg) were then added to the mixture and the bottles were shaken horizontally for two weeks at 20 ± 0.9ºC. After two weeks, the POM strips were removed from the mixture, rinsed with deionized watet, cleaned with moist tissue paper and immediately stored in methanol until extraction. The POM strips were Soxhlet extracted for three hours with 125 mL methanol as described previously (Jonker and Koelmans, 2001). All of the extracts were concentrated to 1 mL using a nitrogen condenser (N-EVAP^{TM} 111 nitrogen evaporator, Organomation Associates, Inc., Berlin, MA) followed by exchange with acetone and finally hexane. A final clean-up was performed, where the dried and concentrated extract was passed through a deactivated silica gel column for the removal of organic interferences (Office of Solid Waste, 1996).

The sediment samples from Anacostia, Buffalo and Grasse Rivers were selected for examination due to the differences in their historical sources of contamination and the current levels of PCBs, which ranged two orders of magnitude (Table 1). Anacostia and Buffalo Rivers were both contaminated with a mixture of Aroclors in addition to numerous other contaminants originating from mixed industrial sites (Crane, 1993; USEPA, 2007a,b). In contrast, Grasse River was contaminated with A1248 that was used for aluminum production at this industrial site since the 1930's (EPA, 2005). Although Grasse River had the highest concentration of total PCBs, it also had the lowest average number of chlorines per molecule (Table 1). A comparison of PCB homologs from the three locations sowed that Anacostia and Buffalo River homolog profiles were most similar to the profile of Aroclor 1254 (A1254), whereas the Grasse River profile was most similar to the A1248 profile (Table 1). However, a statistical evaluation ($p<005$) of the homolog distribution compared with the distribution in several Aroclor mixtures described from Frame *et al.* (1996) showed that Anacostia River had a profile that was different from the profiles of all known Aroclors but closest to the profile of A1254. The profile of Buffalo River was not significantly different from the A1254 profile. The results of the analyses were consistent with historical information about the main sources of contamination for Anacostia, Buffalo, and Grasse Rivers.

The particle size distributions of the three sediments were similar with more than 60% of the samples below 63 µm, representing mainly silt and clay, and less than 10% above 250 µm (Table 1). Total organic carbon (TOC) levels in Anacostia and Buffalo River sediments were approximately half that in the Grasse River sediment. An evaluation of the PCB availability was performed for the three PCB-spiked sediments using the polyoxymethylene solid phase

extraction (POM-SPE) test and the results showed that the availability of the spiked PCBs was significantly higher ($p<0.05$) in the Buffalo River sample compared to Grasse and Anacostia Rivers (Table 1). In general a high level of PCB availability (as measured by the POM-SPE test) indicates high chemical activity (*i.e.*, weakly adsorbed PCBs). In the case of the Buffalo River, the reason for the high availability was likely a result of site geochemistry since this sample contained silt and had a low TOC content compared to Anacostia and Grass River sediments (Table 1).

Table 1. Characterization of PCBs in Anacostia, Buffalo, and Grasse River sediments

	Anacostia	Buffalo	Grasse
Total PCB concentration (ng/g-dry)	335	40	6820
Average no. of chlorine atoms/biphenyl	5.7	5.2	3.8
Percent of PCB with <6 Cl atoms/biphenyl	64	71	87
Percent of PCB with <5 Cl atoms/biphenyl	22	42	73
Sediment Size Fraction (%)			
>1000 µm	1.1	3.2	0.4
250-1000 µm	6.0	5.1	1.4
63-250 µm	6.7	18.4	31.4
<63 µm	86.2	73.3	66.9
Dry matter content (%)	50.4 (1.1)[a]	90.6 (0.2)	39.1 (0.3)
Black carbon (%) chemical oxidation/thermal CT0375 for 24 hours	0.462/0.612		0.155/0.392
Total organic carbon (%)	3.0 (0.5)	2.0 (0.2)	5.2 (0.3)
PCB availability (µg/g)[b]	0.102 (0.033)	0.533 (0.123)	0.207 (0.046)

[a]*Mean values are given and figures in brackets are standard deviations (n=3)*
[b]*PCB availability was determined by the POM-SPE test.*

Study 3. Impact of Activated Carbon on Volatilization and Microbial Bioavailability of PCBs in an Aerobic Sediment Slurry

3.1. INTRODUCTION

PCBs are a class of manmade hydrophobic organic compounds that exist as a legacy contaminant in the environment. A novel development in *in-situ* remediation of PCB contaminated sediment involves application of strong engineered sorbents such as AC to sequester PCBs and other hydrophobic organic chemicals (HOCs) (Ghosh et al., 2011). Due to repartitioning of HOCs into AC, the bioavailable fraction and the porewater concentration of these chemicals is reduced. Microbial processes play an important role in attenuation of HOCs in the environment. Besides several other factors, bioavailability is an important aspect that controls biodegradation of HOCs. Specifically the black carbon content of sediment or soil is the most significant factor influencing the bioavailability of HOCs. It is hypothesized that bacteria is able to degrade organics that are available in the freely dissolved state. For HOCs adhered to strongly sorbed surfaces it is believed that bacterial adhesion to these particles enables degradation. Several studies have reported negative correlation between PAH degradation and presence of black carbon in sediment or soil (Yang et al., 2009, Rhodes et al, 2008, Cornelissen et al., 2005).

The objective of the present study was to assess the effect of AC on microbial transformation of PCBs in aerobic sediment slurry by tracking changes in the mass of PCBs over time and comparing it to abiotic controls. The setups were kept aerobic to mimic the biologically active layer of sediment.

Sediment from Grasse River was chosen for this study because the surficial sediment PCB profile shows the dominance of lower chlorinated PCBs (Figure 3.1) which are more amenable to aerobic degradation and also because this sediment exhibited a higher dechlorination activity and had a greater abundance of *Dehalococcoides* phylotypes (Kjellerup et al., 2008). The lower Grasse River in Massena, NY has been a site of a pilot scale application of AC as a remediation method for PCB contaminated sediments. This ongoing pilot study has demonstrated the effectiveness of AC in reducing PCB bioavailability for tests done both *in-situ* and *ex-situ* using *Lumbriculus varigatus* as a test organism.

One major question that arises is whether AC amendment to reduce bioavailability can also result in significant reductions in the natural rates of attenuation of PCBs through biodegradation and volatilization processes. Since carbon application is mostly surficial, possibly impacting the aerobic zone of sediments, the biological process that can be potentially impacted is aerobic degradation. The present study evaluated loss of PCBs from field sediments through aerobic biodegradation and volatilization with and without AC amendment. PCB-impacted field sediment from Grasse River was used for this study. The sediment was characterized for PCB content, equilibrium partitioning between sediment and water, PCB distribution among different particle size and density classes, and desorption kinetics. The sediment was then used for aerobic degradation studies performed in laboratory mesocosms in a slurry form.

3.2. MATERIALS AND METHODS

3.2.1 Sediment and Activated Carbon

Grasse River sediment was collected in 2006 prior to AC application. The sediment was homogenized by mixing well by hand. The moisture content of the sediment was determined to be 70.02± 0.6% and the TOC content was 5.92± 0.9 % as measured for three replicates. The dose

of AC added to the sediment was 3% which was half the TOC content of the sediment. The type of AC used was TOG of mesh size 50X200 (Calgon Corp. Pittsburgh, PA).

3.2.2 Experimental Set-up

Five grams of wet sediment was spiked with 5 ml of nutrient solution (Furukawa et al., 1979) and transferred to a 50 ml conical flask. The following treatments were tested:

(i) Control: without addition of AC or sodium azide
(ii) Abiotic control: sediment mixed with sodium azide (1000 mg/L)
(iii) Treatment 1: sediment mixed with 3% AC
(iv) Treatment 2: sediment mixed with 3% AC and sodium azide (1000 mg/L)

The volume of each flask was brought up-to 20 ml by adding DI water. Each treatment had three replicates. The mouths of the flasks were capped with polyurethane foam plugs to allow air exchange while preventing PCB loss from the system through volatilization. Each flask was wrapped in aluminum foil to prevent algal growth. The flasks were placed on a horizontal shaker (Bellco Biotechnology, NJ) at 4 rpm and kept at room temperature. The mesocosms were monitored periodically for evaporation loss and DI water was added to maintain the volume at 20 ml. Treatment sets were harvested at 60 days and 1 year interval for total PCB analysis of the sediment and the foam plugs.

3.2.3 Chemical Analysis

3.2.3.1 Extraction of sediment

PCBs in sediment were extracted following EPA method 3550B. The overlying water layer was removed with a glass pipette and filtered through a glass fiber filter paper (GF/C; Whatman, Maidstone, England). About 3 ml of hexane was added to the vial containing the filtrate and shaken vigorously. The vial was allowed to stand for the aqueous layer and the solvent layer to separate. The hexane was pipetted into a 40 ml glass beaker. This process of liquid-liquid extraction of the water layer was done for a total of two times. To the pooled hexane in the 40 ml beaker, the sediment from the conical flask was added along with the filter paper that was used to filter the overlying water. The filter paper was shredded with the help of a stainless steel spatula. Sodium sulfate (granular, anhydrous) was added to the beaker and mixed till the contents were free flowing. This was followed by immediate addition of about 20 ml of extraction solvent mixture (hexane:acetone [1:1 v/v] [Pesticide grade]). PCB #14 and #65 were added to the sample before extraction as surrogate spikes to check the efficiency of the extraction process. The contents of the beaker were extracted using an ultrasonic disrupter (Model 500, Sonic Dismembrator, Fisher Scientific) for a total of six minutes (pulsing for half minute on and half minute off). After extraction, the solvent was decanted and filtered through a glass fiber filter paper in a glass funnel that was placed on a 250 ml conical flask. Extraction was performed for a total of three times. After the final extraction, the entire contents of the beaker was transferred to the filter paper and rinsed with the extraction solvent. All the extract was filtered and collected in the same flask for cleanup.

PCB cleanup was done following USEPA SW846 Methods 3630C (silica gel cleanup) and method 3660B (sulfur cleanup). The extract was concentrated under a gentle stream of nitrogen over a warm water bath. To about 1 ml of the concentrated extract, approximately 0.1 g of activated copper powder was added and mixed vigorously on a shaker for at least 30 minutes for removal of sulfur. The copper treated extract was passed through a 3% deactivated silica gel column using hexane (pesticide grade) as the eluting solvent. The silica gel cleanup step removes

organic interferents from the sample. Clean PCB samples were concentrated to a required volume under a gentle stream of nitrogen for injection into the gas chromatograph.

3.2.3.2 Cleaning of foam plugs

Foam plugs were Soxhlet cleaned with hexane for 12 h, followed by air-drying before use. Clean foam plugs were extracted in triplicate as described below to obtain a background concentration of PCBs. The total PCBs detected was less than 1% by mass of the PCBs detected in the experimental foam plugs and hence was not subtracted during compilation of the data.

3.2.3.3 Extraction of foam plugs

Each foam plug was placed in a 40 ml glass vial along with approximately 30 ml of hexane (pesticide grade) as the extraction solvent. A predetermined volume of PCB #14 and #65 were added to the sample as surrogate spike. The vials were placed on a horizontal shaker (Bellco Biotechnology, NJ) for extraction, overnight. Hexane was removed from the vial with a glass pipette and replaced with fresh hexane. The extraction process was repeated for a total of three times. The extracted hexane was pooled, concentrated, and cleaned using silica gel as described above before analysis.

3.2.3.4 PCB Analysis

PCB congener analysis was performed on a gas chromatograph with a micro electron-capture detector (6890N, Agilent Technologies, Santa Clara, CA). A 60 m X 0.25 mm X 0.25 µm fused silica capillary column (RTX-5MS, Restek US, Bellefonte, PA) was used with helium as the carrier gas at constant flow of 1 mL/min. The oven temperature program began at 100°C and was increased at the rate of 2°C/min to 280°C, followed by an increase of 10°C/min to 300°C and was held at this temperature for 6 mins. Quantification of the target PCB compounds was performed using a multi-level calibration. Identification of PCB congeners was carried out by comparison of retention times in the chromatogram with that of PCB standards purchased as hexane solutions from Ultra Scientific (North Kingstown, RI). PCB 30 and 204 were used as the two internal standards because they are not present in commercial Aroclor mixtures. Using this method 89 PCB congeners, including some coeluting peaks were identified and quantified. Coeluting peaks were quantified as the sum of the individual congeners.

3.2.3.5 Desorption kinetics study

PCB desorption kinetic studies were conducted using whole sediments and Tenax adsorbent resin used as an extractant following Ghosh et al. (2003). One gram wet untreated or AC treated sediment sample was transferred into 12 ml vials. Ten millilitres of ml DI water with 1000 mg/l of sodium azide and 0.2 g Tenax beads (40-60 mesh, Suppelco, PA) were added to each vial. The vials were placed on a roller and mixed continuously. At each sampling time (6 hours, 1, 2, 5, 10, 30, and 60 day), the Tenax beads were harvested and fresh Tenax beads were added to the vials. PCBs were extracted from the harvested Tenax beads with a mixture of hexane and acetone (50:50).

3.2.3.6 Aqueous Equilibrium study

Sediment-water equilibrium tests were performed in 1 L amber glass bottles with Teflon lined caps (Ghosh et al., 2000). The slurry of water-sediment with weight ratio of 20:1 was mixed on a roller at 3-4 rpm at 23 ^{o}C in darkness. Sodium azide (1000 mg/l) was added to inhibit microbiological growth. After two weeks, the mixture was removed from the roller and

the coarse particles were allowed to settle. Colloidal particulates were removed from solution following the alum flocculation procedure described in Ghosh et al. (2000).

3.2.3.7. Sediment fractionation in size and density classes

Wet sieving was performed to separate the sediment into four size fractions (<63 μm, 63-250 μm, 250-1000 μm, and >1000 μm) as described in Ghosh et al (2000). The larger size fractions (>63 μm) were composed primarily of sandy grains, coal-derived particles, and woody material. It was possible to wash off the lighter density particles from the heavier sand particles by swirling with water in a beaker and draining off the entrained lighter particles giving two separate fractions which we define as "light" and "heavy". This process was repeated several times until most of the lighter material was removed. Materials in the fine fraction (<63 μm) were density separated using a cesium chloride solution having a specific gravity of 1.8. Five grams of wet sediment and 40 mL of cesium chloride solution were centrifuged at 2000 rpm for 10 min in 50-mL glass centrifuge tubes. The fine lighter particles floated to the top and were decanted off and collected in filter paper and washed with water several times. The heavy clay and silt were similarly washed several times to remove cesium chloride. Each of these size and density separated fractions were then analyzed for PCBs.

3.3. RESULTS AND DISCUSSION

3.3.1. Sediment characterization

Total PCB concentration in sediment was 2.5 mg/kg. The distribution of PCB mass by homolog at the start of the experiment (day 0) is shown in Figure 3.1. The PCB profile of the sediment shows that the dominant homologs are the di, tri and tetracholorobiphenyls, which together constitute more than 70% of the total PCB mass. Aqueous equilibrium results are shown in Figure 3.2. As expected based on differences in aqueous solubilities of the PCB congeners and relative abundance in sediment of the lower chlorinated PCBs, the equilibriated aqueous phase is dominated by the mono, di, and trichlorobiphenyls. The most dominant congeners in the aqueous phase are PCBs 4 and 10 (di) which co-elute together, followed by PCB 1 (mono) and PCBs 5 and 8 (di). These five dominant congeners represent 61% of total PCBs in the aqueous phase. An important implication of this finding is that for this sediment, the mono and dichlorobiphenyls are in high abundance in sediment and sediment porewater and will likely be greatly available for aerobic degradation and volatization in the surficial aerobic zone of sediments.

Sediment fractionation into size and density classes are shown in Figure 3.3. While, 90% of the sediment mass is associated with the heavy density fraction, primarily in the <63 micron fraction, 70% of the total PCBs are associated with the lighter density organic fraction, mostly in the 63-250 micron size fraction. As expected based on PCB partitioning, organic matter in the sediment is the primary carrier of PCBs.

As illustrated in Figure 3.4, desorption kinetic studies showed that the PCBs in the study sediments are weakly sorbed and readily desorbed into tenax adsorbent resin. For the four dominant PCB homologs, over 90% desorption is achieved within a month. Thus PCBs in this sediment are readily available with a high fast desorption fraction. No major difference in desorption kinetics was observed among the different PCB homolog groups.

3.3.2 Change in PCBs in Sediment

3.3.2.1 Mesocosms without carbon amendment

After one year of incubation the sediment showed a decrease in the mass of lower chlorinated PCBs as compared to the abiotic control (Figure 3.5). For the abiotic control the decrease in di and trichlorobiphenyls after 60 days was 56 and 35% respectively and after 1 year was 81 and 70% respectively as compared to day 0. The change in mass of PCBs for the higher chlorinated homologs is less than 20% for both the sediment and the abiotic control compared to day 0. This could be because the higher chlorinated PCBs are not the substrate of aerobic transformation, and since the mesocosm was exposed to air, anaerobic dechlorination could have been inhibited. Comparison between the sediment and the abiotic control shows that the difference between the two mesocosms for di, tri, and tetrachlorobiphenyls is 43, 29, and 8% after 60 days and 23, 49, and 21% after 1 year.

In the sediment within 60 days of incubation the mass of di and trichlorobiphenyls in the sediment slurry had decreased by 75 and 54% compared to day 0. The rate of decrease in PCB mass slowed down for dichlorobiphenyls and after 1 year of incubation the difference compared to day 0 was 86%. For trichlorobiphenyls the decrease was 85% after 1 year as compared to day 0 indicating similar removal (Figures 3.7 and 3.8). The percent difference in the mass of total PCBs (in the sediment and the foam plug) for the sediment and the sediment treated with azide as compared to day 0 for di and trichlorobiphenyl congeners is shown in Table 1. The sediment slurry shows a greater reduction in PCB mass compared to the abiotic control indicating biological removal of PCBs. The mass balance of selected congeners (Table 2) shows that for tetra and higher chlorinated PCBs the recovery is greater than 80% for both the sediment and the abiotic control. However, for di and trichlorobiophenyls the PCB recovery is only between 20-40%. This low recovery could possibly be due to microbial degradation of these congeners since the recovery in the abiotic control for di and tricholorobiphenyls is greater than 85 percent.

3.3.2.2 Mesocosms with carbon amendment

After 60 days of incubation the mass of di, tri, and tetrachloro biphenyls decreased by 32, 35, and 33% and after 1 year by 65, 69, and 59% for the AC treated system compared to day 0. This decrease is less than that of the sediment only system. This could be due to strong sorption of PCBs by the AC particles which would have led to lower recovery during sediment extraction. For both the carbon amended and the abiotic carbon amended systems the change in the PCB profile of the homologs after one year of incubation is shown in Figure 3.6. For the abiotic carbon amended system the decrease in PCB mass of di, tri, and tetrachlorobiphenyls after 60 days is 16, 20, and 22% respectively and after 1 year of incubation is 51, 56, and 43% respectively (Figure 3.9). The difference in mass between the AC treated sediment and the abiotic AC treated sediment might indicate that some biological removal of PCBs is occurring even in the presence of AC. No significant change in mass of PCBs was observed for the higher chlorinated PCBs between the abiotic AC treated system and the sediment treated with AC.

3.3.3 Change in PCBs in foam plug

3.3.3.1 Mesocosms without carbon amendment

The mass of PCBs captured in the foam plug represents the loss of PCBs from the sediment slurry due to volatilization (Figure 3.11). The PCB mass lost due to volatilization is higher in the azide treated system than in the sediment alone. As the lower chlorinated PCBs have a higher Henry's constant so they are more volatile and as expected is present in greater mass in the foam plug than the higher chlorinated homologs. The difference between the volatile loss of PCBs from sediment without azide and the abiotic control for di, tri, and tetrachlorobiphenyl is 86, 57,

and 16% respectively with loss from the abiotic control being greater. This could be because aerobic biological processes oxidatively removed the lower chlorinated PCBs thus reducing the fraction of volatile loss. The difference between the mass of penta and hexachlorobiphenyl detected in the foam plugs for the sediment and the killed control is 6 and 7 percent respectively, which is not statistically significant indicating that perhaps no biological transformation of these homologs occurred and also that the higher chlorinated homologs are less volatile. The change in the mass of di and trichlorobiphenyls both in the sediment and foam plug for two time points (60 and 365 days) is depicted in Figure 3.10. The decrease in the mass of PCBs for the sediment was rapid for the first 60 days and then slowed down, indicating that the readily available PCBs were rapidly degraded leaving behind the more recalcitrant molecules.

3.3.3.2 Mesocosms with carbon amendment

Comparison between the volatile loss in the sediment slurry and the AC amended sediment shows that the difference between the mass of PCBs captured in the two systems for di, tri, tetra, penta, and hexachloro biphenyls are 21, 82, 74, 23, and 19% with a higher loss in the volatile PCBs for the unamended sediment. The mass of dichlorobiphenyls captured in the foam plug for the sediment slurry is less than the other homologs. This could be due to greater removal of the dichlorobiphenyls by microbial processes resulting in less volatile loss. For the AC amended system and the abiotic AC amended system the mass of volatile PCBs captured in the foam plugs for the two systems is comparable across all homologs.

Vasilyeva et al. (2010) observed less volatilization of PCBs from soil amended with 7% granular AC and no loss in soil amended with 3.5% powdered AC. The decrease in the volatile loss of PCBs from AC amended soil and sediment could be attributed to strong sorption of PCBs to the AC particle which reduces PCB fugacity and subsequently reduces volatilization.

3.4. CONCLUSIONS

The present study showed that the microbial transformation and volatililization are important processes regulating fate of PCBs in aerobic sediment. Addition of AC as a sorbent for stabilization of PCB contaminated sediment can greatly reduce volatilization loss of the lower chlorinated PCB homolgs that are most prone to this loss process. AC addition also lowers bioavailability of PCBs for aerobic microbial transformation, however, our results indicate that slow aerobic biodegradation of lower chlorinated PCBs continue in the presence of AC in sediments.

3.5 References

Cornelissen, G., Gustafsson, O., Bucheli, T.D., Jonker, M.T.O., Koelmans, A.A., Van Noort, P.C.M., 2005. Extensive sorption of organic compounds to black carbon, coal, and kerogen in sediments and soils: mechanisms and consequences for distribution, bioaccumulation, and biodegradation. Environmental Science & Technology, 39, 6881-6895

Ghosh,U., Luthy, R.G., Cornelissen, G., Werner, W., Menzie, C.A., 2011. In-situ sorbent amendments: A new directionin contaminated sediment management. Environmental Science & Technology, 45, 1163-1168

Ghosh U, Weber AS, Jensen JN, Smith JR. 2000. Relationship between PCB desorption equilibrium, kinetics, and availability during land biotreatment. Environ Sci Technol 34:2542-2548.

Ghosh U, Zimmerman JR, Luthy RG. 2003. PCB and PAH speciation among particle types in contaminated sediments and effects on PAH bioavailability. Environ Sci Technol 37:2209-2217.

Kjellerup, B.V., Sun, X., Ghosh, U., May, H.D., Sowers, K.R., 2008. Site-specific microbial communities in three PCB-impacted sediments are associated with different *in situ* dechlorinating activities. Environmental Microbiology, 10, 1296-1309.

Rhodes, A.H.; Carlin, A.; Semple, K.T. 2010. Impact of black carbon in the extraction and mineralization of phenanthrene in soil. Environmental Science & Technology, 42, 740-745.

Vasilyeva, G.K.; Strijakova, E.R.; Nikolaeva, S.N.; Lebedev, A.T.; Shea, P.J. 2010. Dynamics of PCB removal and detoxification in historically contaminated soils amended with AC. Environmental Pollution, 158, 770-777.

Yang, Y., Wesley, H., Tao, S., Crowley, D., Gan, J., 2009. Effect of AC on microbial bioavailability of phenanthrene in soils. Environmental Toxicology and Chemistry, 28, 2283-2288

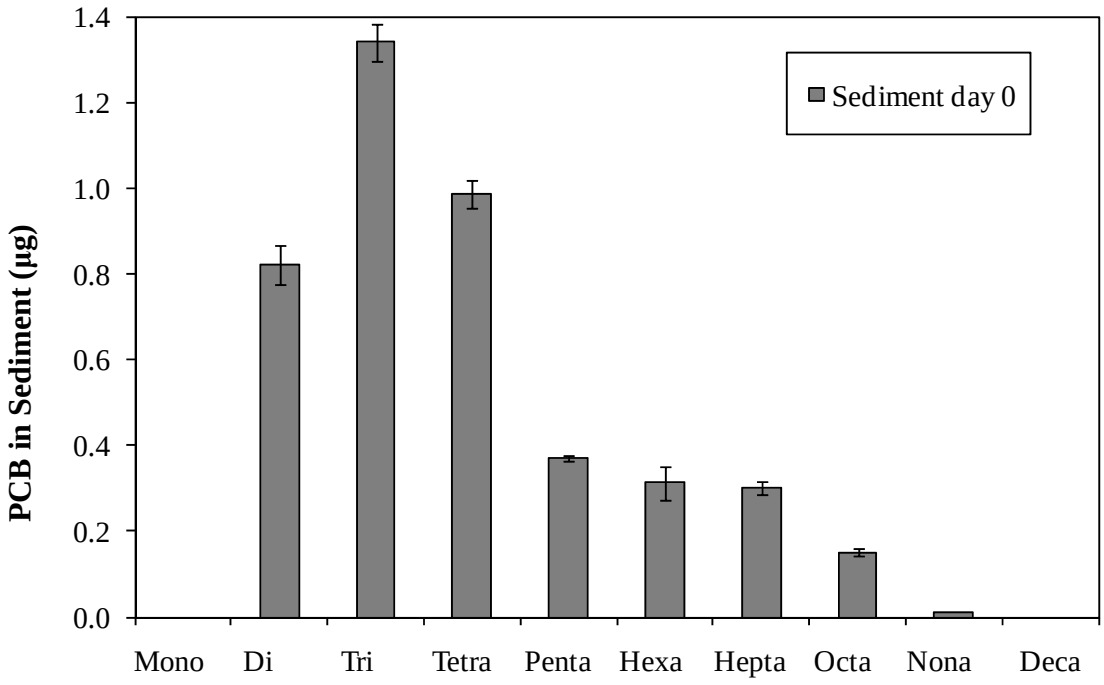

Figure 3.1. PCB distribution by homolog in study sediment.

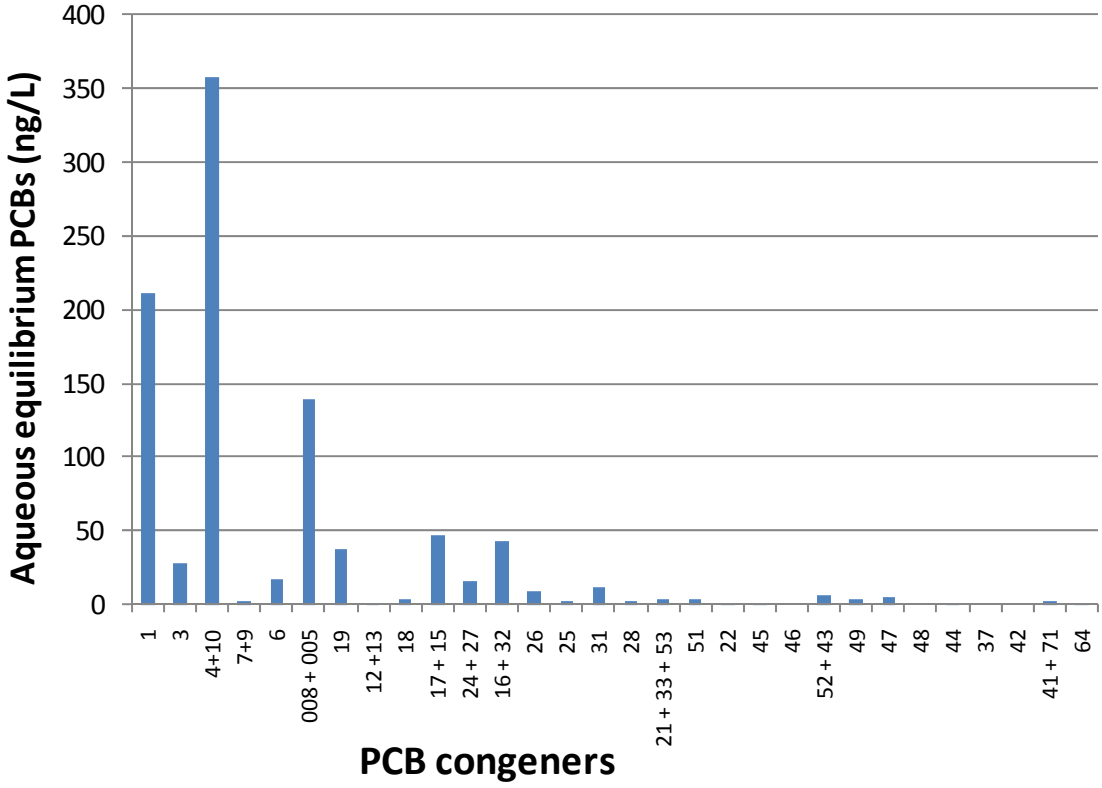

Figure 3.2. PCB concentration in the aqueous phase at equilibrium with sediment.

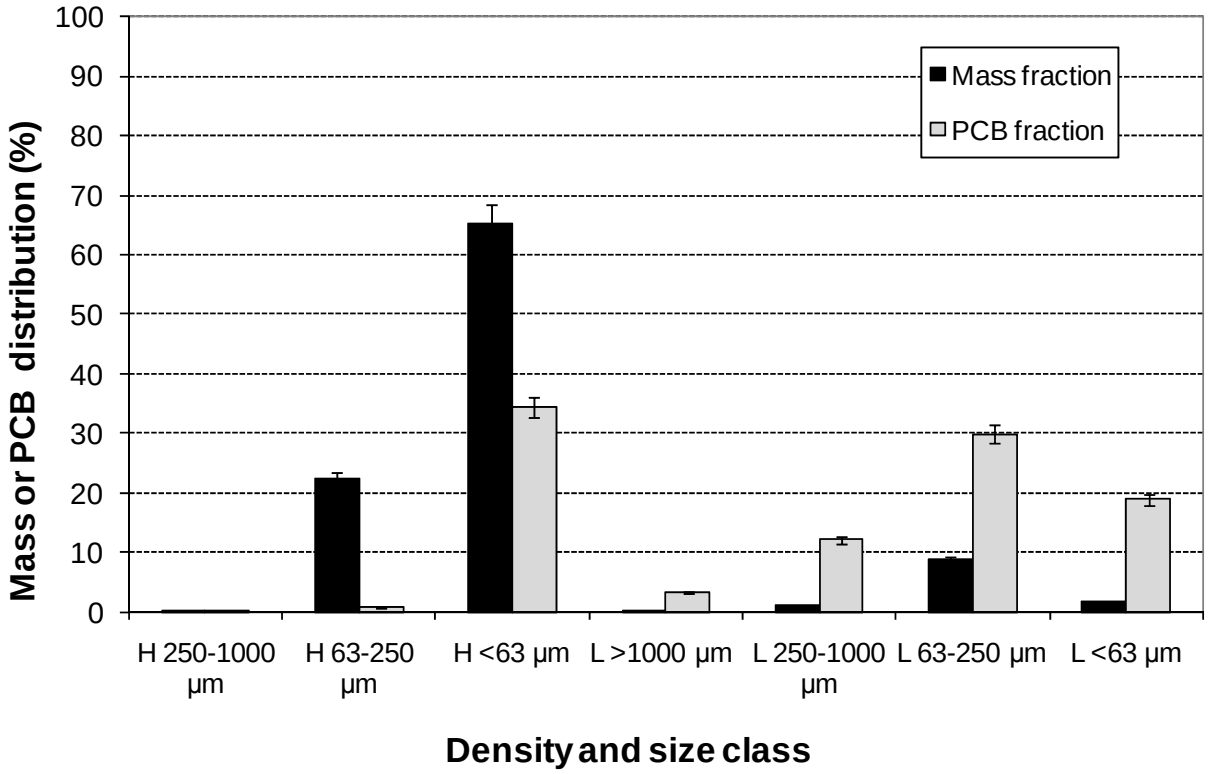

Figure 3.3. Size and density class fractions in Grasse River sediments.

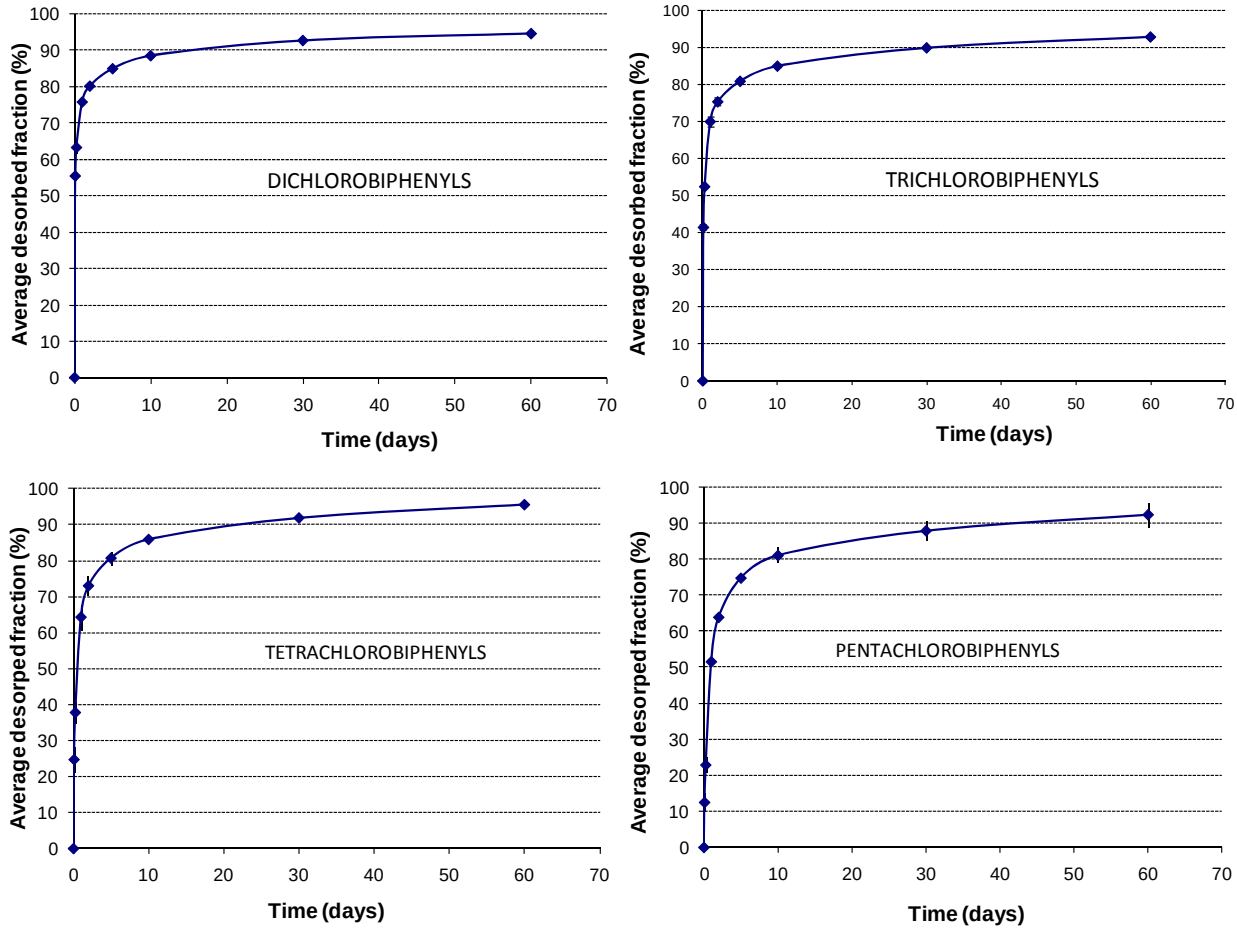

Figure 3.4. PCB desorption kinetics from Grasse River sediments.

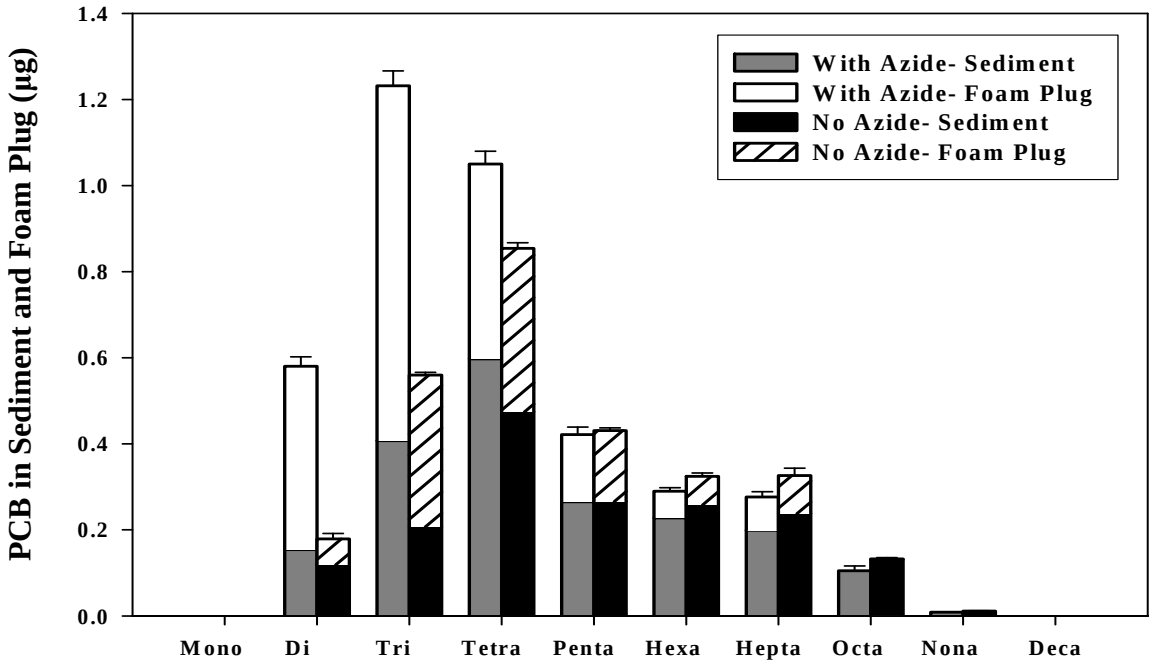

Figure 3.5. PCB Distribution by homolog for 1 year time point: sediment and control.

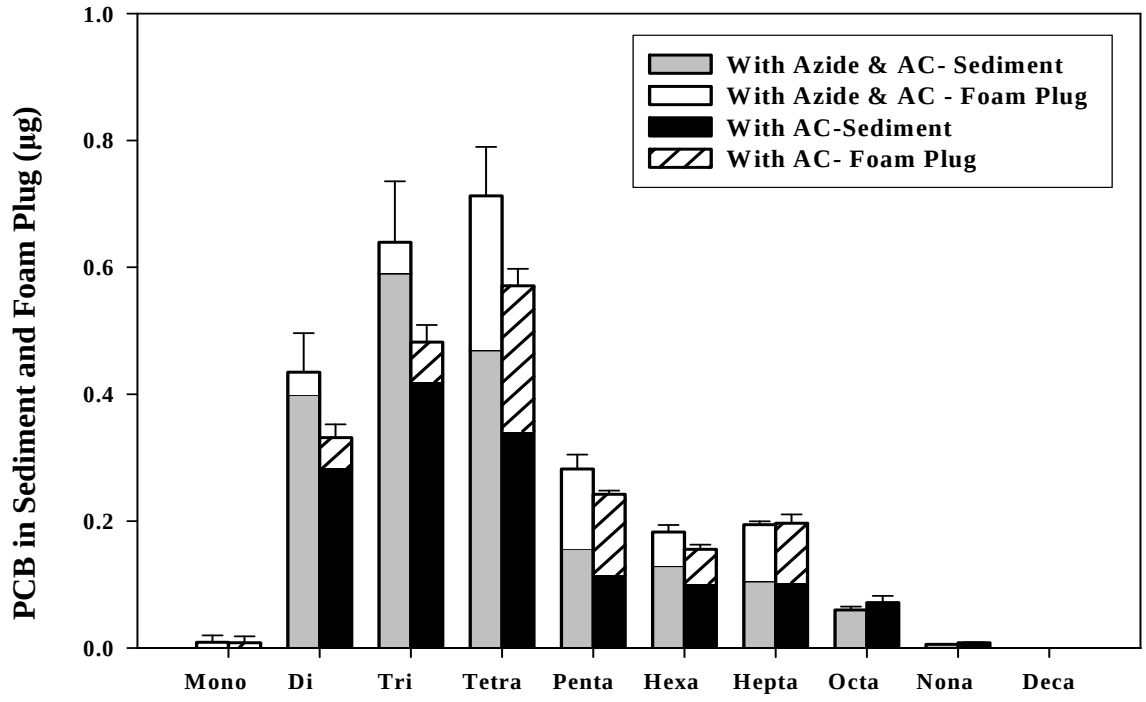

Figure 3.6. PCB distribution by homolog for 1 year time point: sediment treated with AC and control.

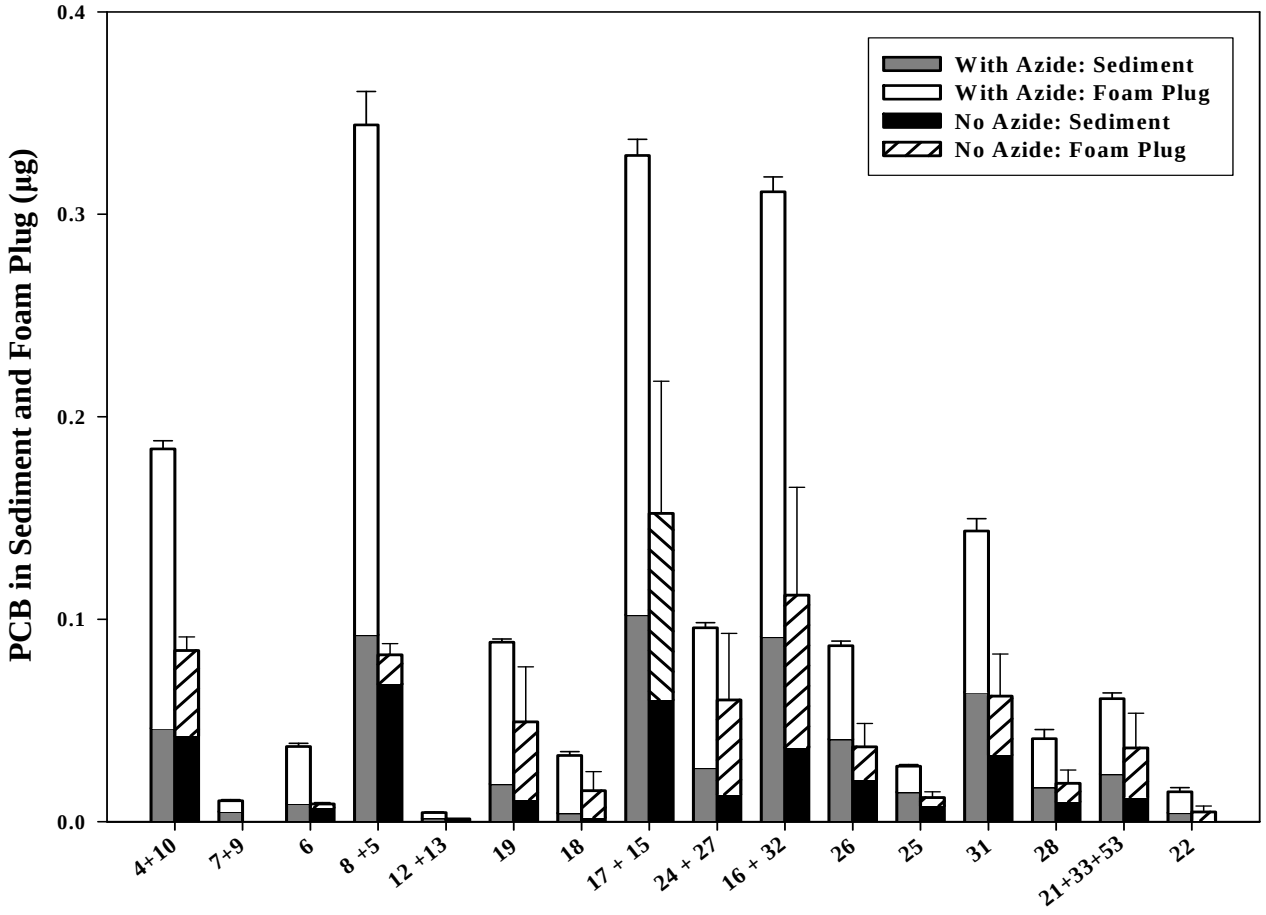

Figure 3.7. PCB distribution by congener (di and trichlorobiphenyls) for one year time point: sediment and control.

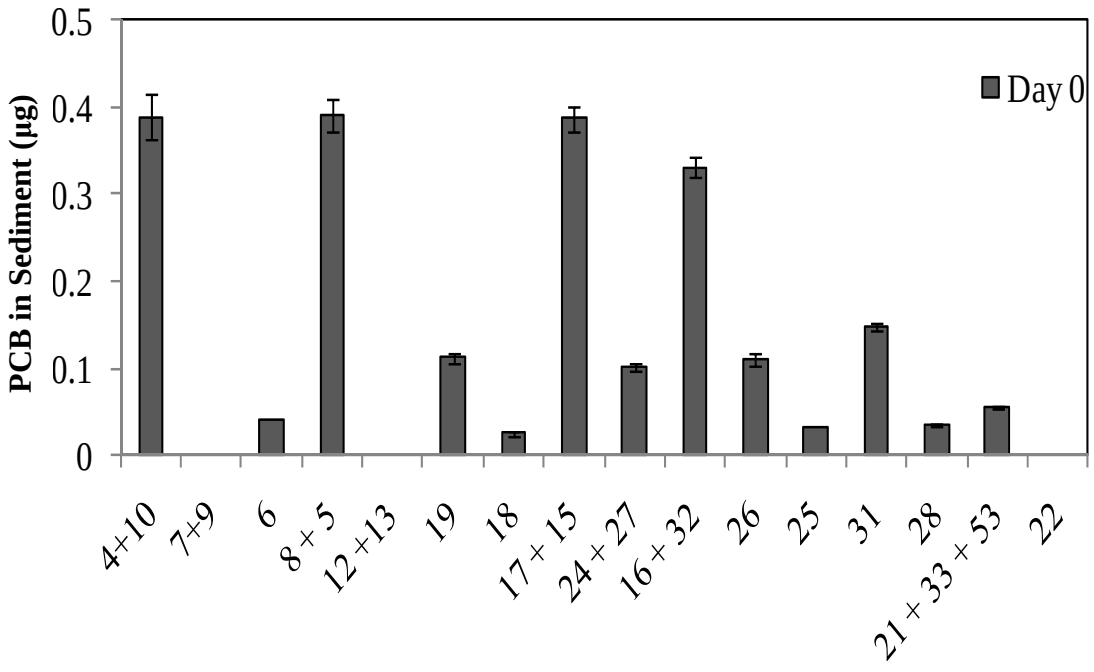

Figurure 3.8. PCB distribution by congener (di and trichlorobiphenyls) for day 0.

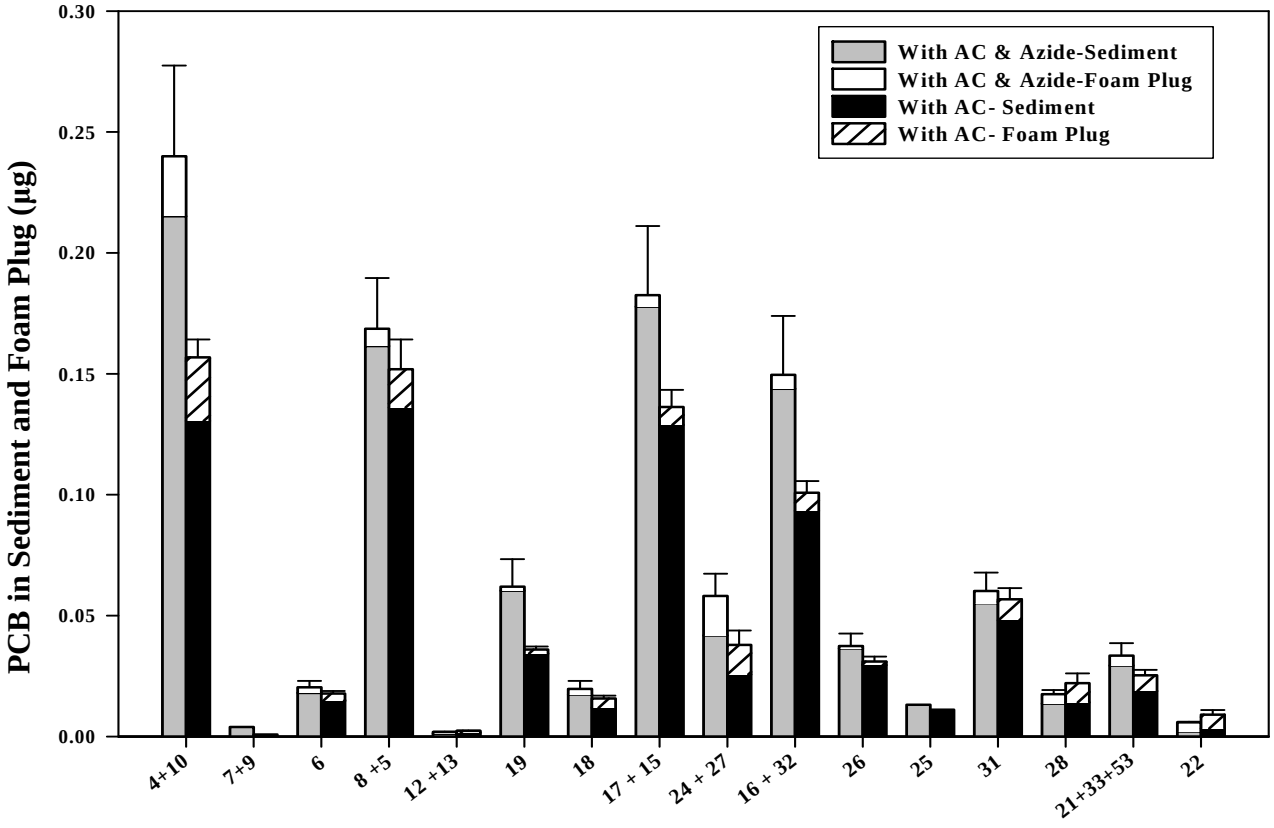

Figure 3.9. PCB distribution by congener (di and trichlorobiphenyls) for one year time point: sediment treated with AC and control.

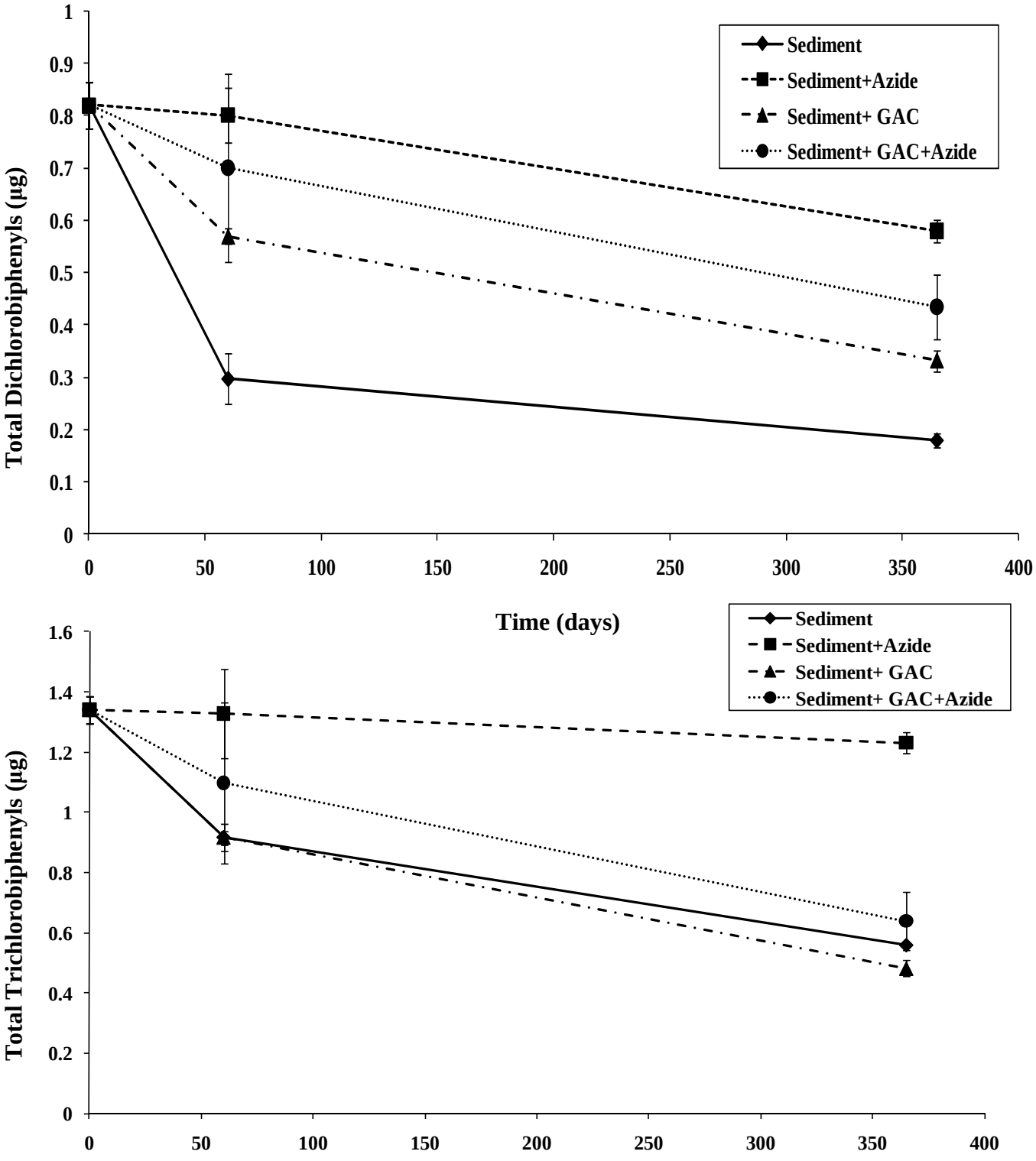

Figure 3.10. Change in the mass of total (fraction of PCB in sediment + foam plug) di and trichlorobiphenyls over one year time period.

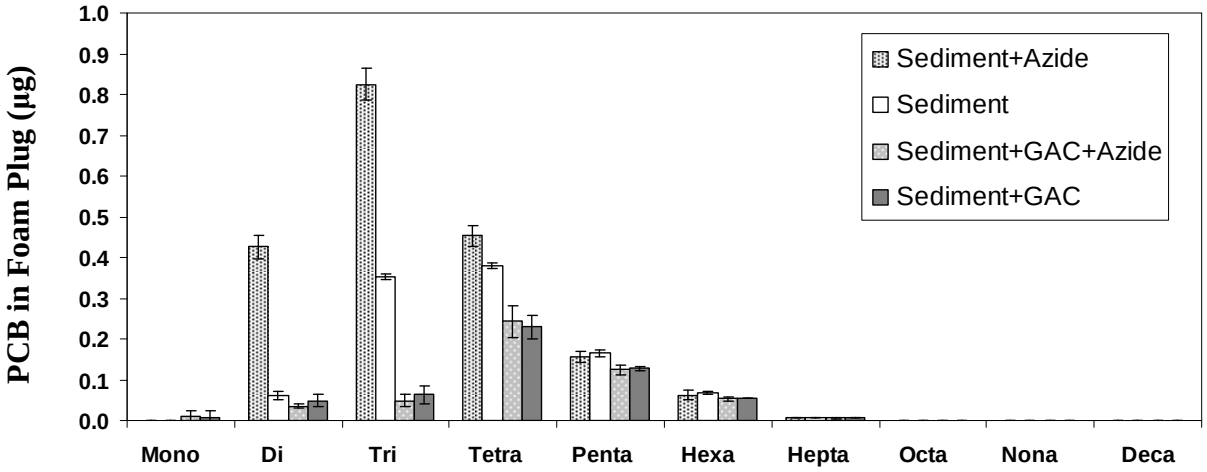

Figure 3.11. Loss of PCB mass due to volatilization after one year time period.

Table 3.1 Percent change in the mass of total (fraction in sediment and foam plug) PCBs for di and trichlorobiphenyls as compared to day 0 after one year time period.

Congeners	Sediment	Sediment+ Azide	Sediment+ AC	Sediment+ AC+Azide
4+10	78	53	60	38
7+9	-	-	-	-
6	78	7	56	49
8 + 5	79	12	61	57
12 +13	-	-	-	-
19	56	21	68	45
18	41	-26	40	24
17 + 15	61	15	65	53
24 + 27	41	6	63	43
16 + 32	66	6	70	55
26	67	21	72	66
25	62	12	64	58
31	58	2	61	59
28	45	-19	36	49
21 + 33 + 53	34	-10	54	40
22	-	-	-	-

Table 3.2 Mass balance (%) of selected congeners.

Homolog	Congeners	Chlorine Position	Sediment	Sediment+Azide
DiCB	4+10	22' 26	22	47
DiCB	8 + 5	24' 23	21	88
TriCB	17 + 15	22'4	39	85
TriCB	16 + 32	22'3 24'6	34	94
TetraCB	49	22'45'	82	90
TetraCB	47	22'44'	70	85
PentaCB	92+84+89	22'355' 22'33'6 22'346'	82	95
PentaCB	101	22'455'	129	121
HexaCB	149+123	2344'5 22'34'5'6	93	82
HexaCB	158	233'44'6	85	80

Study 4. Modeling the Impact of Flocculation on the Fate of Organic and Inorganic Particles during Resuspension Events in an Urban Estuary

4.1 Abstract

Organic particles play an important role in the fate of organic contaminants in natural waters. These organic particles move by sedimentation and erosion and their size distribution may be influenced by flocculation and disaggregation. Previous OC transport models assume organic particles have the same settling velocity either as slow as phytoplankton or as fast as total suspended solids (DELPCB, 2003 and Chang 2002). Di Toro (2001) used sediment oxygen demand (SOD) to back-calculate the field OC settling flux. He suggested the effective net organic particle settling velocity should between these two types of particles, which hints that flocculation plays an important role in OC settling in a hetrogeneous particle environment. Later studies also suggested flocculation is a major factor controlling the suspended particle residence time in the estuarine turbidity maxima (ETMs) zone, where significant amounts of inorganic solids, plankton, and organic detritus are trapped (Rengasamy *et al.*, 1996; Sanford *et al*, 2004). Two types of flocculation models that have been developed are the multi-cluster flocculation model (Lick and Lick, 1988; O'Melia and Tiller, 1993; Jackson, 1995) and the D_{50} flocculation model (Winterwerp, 1996). These models assume that flocs are composed of a single primary particle type and that floc properties are the same for all sizes of flocs, in contrast to many field observations (Lee, 2004). In this study, a new flocculation model that simulates the flocculation for both OC and inorganic solids ranging in diameter from 2 to 1000 μm has been developed. This model simultaneously calculates temporally variable, floc size-dependent properties, including the OC content, density, stickiness coefficient, and the settling velocity under different conditions. The model was calibrated using Shear Turbulence Resuspension Mesocosms (STORM) tank experiments that mimic resuspension and settling of contaminated Hudson River sediment with realistic bottom shear stress (Schneider et al., 2007). The objective of this study is to develop a flocculation model that includes the interactions between organic and inorganic particles in estuaries. In addition, including flocculation of heterogeneous particle populations will improve models of organic contaminants in estuaries.

4.2 Introduction

Flocculated particles (flocs) are cohesive particles formed in the water column or on the sediment surface by aggregation of the complex matrix of microbial communities, organic detritus, and inorganic particles (Dyer and Maning, 1999). Flocs are fragile (Krone, 1962) and have higher fractional organic carbon (f_{OC}), porosity, water content, contact area and intraparticle viscosity compared to same-sized solids. Aqueous flocs have been studied since the 1970s because of their importance in water treatment. Recent research notes the importance of flocs in the fate of HOCs including their impact on HOC partitioning and sorption rates, and on particle OC contents (Alkhatib and Weigand, 2002; Wu and Gschwend, 1986; Borglin *et al.*, 1996; Jepsen *et al.*, 1995; Lick and Rapaka, 1996; Rounds and Pankow, 1990).

The importance of flocs on the fate of natural organic matter has also been reported by Kiorboe and Hansen (1993), Hill (1998), Kiorboe *et al.* (1998), Serra and Logan (1999), and Droppo (2001). Richardson and Jackson (2007) demonstrated that floc formation scavenges picoplankton from surface waters, resulting in an additional important OC source for zooplankton in the deep ocean. Tiselius *et al.* (1998) and Peperzak *et al.* (2003) indicated that although single diatoms settle slowly their aggregates rapidly settle and are enriched in carbon content. Variable

flocculation may explain the wide range in OC settling rates reported in field studies. For example, Graf and Rosenberg (1997) report carbon settling fluxes ranging from 0.025 to 70 gCm^{-2} d^{-1}, and those of large marine snow and fecal pellets settling velocity can exceed 100 m d^{-1} (Stemmann *et al.*, 2004).

When inorganic solids aggregate with organic matter, these flocs exhibit different sedimentation rates and residence times. Rengasamy *et al.* (1996) reported the effectiveness of adding clay to control algal blooms in open water. Sanford *et al*. (2004) also suggested flocculation is the major factor controlling the suspended particle residence times in the ETM zone, where significant amounts of inorganic solids, plankton, and organic detritus are trapped.

The net result of particle aggregation is a wide, mixed hetrogeneous particle distribution in the water column, with size-variable OC settling velocity, f_{OC} and effective density. Flocculation may play an important role in transporting OC and associated pollutants through the water column. When organic substrates surround inorganic solids, the settling velocity of OC is influenced by the properties of both the organic and inorganic substrates. Many researchers have tried to find a universal strategy to simulate OC sedimentation rate. Some particle transport models use rules of thumb to estimate an invariant sedimentation rate, such as 0.1 m d^{-1} for biotic particles and 1.0 m d^{-1} for particulate organic particles in the DELPCB model (DRBC, 2003). Other models apply field-measured suspended solid dry density in the Stokes law equation to estimate the particle settling velocity (Chang *et al.*, submitted). Alternatively, Di Toro used SOD to constrain OC settling velocity delivering oxygen-depleting materials to the sediment surface. That analysis suggests that the OC settling velocity lies between those of discrete clay particles and algal cells (Di Toro, 2002). Therefore, a model that simulates the flocs composed by organic detritus and inorganic solids can be a better tool to simulate the fate of OC in natural waters.

The process of the aggregation of particles resulting from the attachment of those particles colliding with each other is called flocculation. Salinity, pH , shear stress, total suspended solids concentration (TSS), and the floc character, density and porosity affect the flocculation rate (O'Melia, 1972; Farley and Morel 1986; Lick and Lick, 1988; and Lick *et al.*, 1993). O'Melia (1972) described flocculation as a two-step process: particle transport resulting in collisions (as parameterized by the collision probability β) and particle destabilization (*e.g.*,the probability of each collision resulting in an aggregate, as parameterized by the 'stickiness coefficient' α). There are three major mechanisms that control the collision probability: Brownian motion, differential settling, and fluid shear, which depend on temperature, particle size, dynamic viscosity of the fluid, shear stress, effective particle density, and particle settling velocities (Ali *et al.*, 1985, Burd and Jackson, 2002; Jackson, 1995; Lick and Lick, 1988; Lick *et al*., 1993; Dyer and Manning, 1999). In estuaries, Brownian motion plays a minor role in particle transport relative to those processes driven by turbulent mixing.

The stickiness coefficient α is the ratio of the particle attachment rate to the particle collision rate (O'Melia, 1972). Edzwald *et al*. (1974) indicated that this step is concerned with eliminating or nullifying the repulsive energy barrier that exists between two approaching particles. Environmental factors like ionic strength, pH, salinity, temperature, and flocs composition factors (*i.e.* exopolymeric material, algae type, and algae concentration) are the major controls determining the stickiness coefficient (Edzwald *et al*., 1974, Gibba, 1983, Kiorboe and Hansen, 1993; Winterwerp, 2002). Ali *et al*. (1984) reviewed and summarized reported stickiness coefficients, which range from 0.01 to 1 depending on the transport method, coagulant, and colloid composition. The effect of organic substances on the stickiness coefficient is complex. Gibbs (1983) compared sediment flocculation rates with and without organic substances such as

humic acid and dissolved organic carbon (DOC). The sample with the organic substance removed had a stickiness coefficient α four times larger than the natural sample for salinity ranges between 0.6 to 20‰. Weilenmann *et al*. (1989) observed that humic materials act as a stabilizing agent in Swiss lakes. But, algae like diatoms and green algae often act as strong destabilizing agents in the summer. Furthermore, the way that the stickiness coefficient relates to diatom concentration is controversial. Some studies determined that the diatom stickiness coefficient increases during blooms, while others have observed that the coefficient actually decreases during this period because diatoms release mucus that prevents the diatom from sticking together.

Smoluchowski (1917) was the first to develop a mathematical model to describe the aggregation of particles. Later, Edzwald *et al.* (1974) solved Smoluchowski's equation as a function of porosity φ, velocity gradient G and the stickiness coefficient α. O'Melia (1972) described flocculation as a two-step process. Recent studies have expanded these concepts into three types of flocculation models. The multi-cluster flocculation model developed by Lick and Lick (1988) simulates the flocs being transported among differently sized floc clusters. Each floc cluster represents a certain volume-based size of flocs. When two flocs form a new floc, the volume of new floc equals the sum of the previous floc volumes, and the new floc is assigned to the corresponding volume-based size floc cluster. Variables like settling velocity and number concentration vary temporally in each cluster of flocs. Later Jackson (1995) applied this concept to simulate OC flocculation within algae populations. He extended this concept and assumed that flocculation involves the balance between gain from smaller particles and loss to form larger particles by inter-particle collisions.

The traditional multi-cluster flocculation models use either volume (O'Melia and Tiller, 1993) or solid mass (Jackson, 1995) as the floc cluster unit interval. In other words, floc cluster N's volume or mass equals N times the volume or mass of floc cluster N=1. Therefore, the particle diameter does not increase linearly with floc cluster number N. This method simplifies tracking the conservation of volume or mass, but requires very large arrays in the computer program. Therefore, the model can simulate only a very limited floc size spectrum. Furthermore, these models only simulate the flocculation by either pure organic or inorganic solids and lack the ability to describe a wide, mixed hetrogeneous particle distribution.

A second type of flocculation model uses the steady state mean floc diameter (D_{SS}) to represent the floc characteristic. Lick and Lick (1988) conducted a series of experiments to examine the relationships among velocity gradient G, steady state floc diameter and TSS concentration in Lake Erie samples. They concluded that at steady state a simple approximate relationship among concentration, median diameter and shear stress is described by the product of TSS, shear stress, and square of D_{SS}. This model provides a quick tool to predict the steady state flocs' diameter based on given TSS and shear stress.

Winterwerp (1998) developed a 1 DV Point flocculation model that uses the median particle size, D_{50}, to represent the entire floc spectrum. This is the first flocculation model to use fractal geometry to describe flocculation. This model first describes the transport of the sediment's flocculation and includes the sediment's settling velocity. The model was tested against field measurements in the ETM along the border between Netherlands and Germany. It simulated the aggregation and disaggregation processes using sediment concentration and turbulence, reaching a reasonable agreement with observations from settling column tests. This model can properly describe the impact of flocculation and disaggregation on D_{50}, and has a good agreement with

calibrated data. This model also provides a equation to simulate the relationship between fractal geometry and flocs settling velocity.

However, Winterwerp's model has a few disadvantages. First, there are more than ten empirical parameters and formulations in this model. To adjust these parameters to fit our study would require several experiments to determine parameter values. Second, this model assumes that f_{OC} and the stickiness coefficient are constant throughout the entire period. This assumption goes against field and mesocosm observations, where measured particle characteristics vary both temporally and spatially (Ko *et al*., 2003; Richardson and Jackson, 2007). Therefore, the model could misestimate the flocs density and the flocculation rate. Third, unlike the O'Melia and Lick models, this model simulates the mean particle diameter of the flocs instead of that of the individually sized class particles, and assumes that all sizes of flocs have the same porosity, composition, and density. However, the observations by Ko *et al*. (2003) demonstrate that neither D_{50} nor D_{SS} can accurately represent the behavior and characteristics of all sizes of OC in a heterogeneous mixture of particles. Flocculation between organic matter and inorganic particles results in flocs with time-variable characteristics, such as f_{OC} (Ko *et al*., 2003), stickiness coefficient (O'Melia and Tiller, 1993), and effective floc density (Khelifa and Hill, 2006), which in turn affects the erosion and settling flux of OC (Burns and Rosa, 1980). Again, these reports indicate the necessity of simulating these kinetically varied processes to better predict hetrogeneous particle behavior.

Several strategies have been suggested to model particle collision rates and flocculation rates, including fractal geometry (Winterwerp, 1996), disaggregation (Alldredge *et al*., 1990), a curvilinear collision kernel (Han and Lawler, 1991), the adjusted settling velocity equation (Allen, 1985), and the inclusion of hetrogeneous particles (Jackson, 1995; Winterwerp, 1996; Hill, 1998). Fractal geometry has recently been used to describe the structure, porosity, and settling velocity of flocs (Winterwerp, 1996). Jackson (1998) and Flesch *et al*. (1999) have combined the fractal factor concept with a multi-cluster flocculation model to derive relationships among particle length, mass, and fractal scaling. Aggregates are modeled as fractals comprised on primary particles, and the fractal factor value varies between one and three (Mandelbrot, 1983). Flocs are assumed to be composed of pure inorganic solids (Yao *et al.*, 1971) or algae cells (Jackson, 1995). Aquatic particles are composed of many different solids including clay and plankton. Many fractal factor indexes have been reported to address this fact, such as the Sierpinski Carpet fractal dimension D_{SC}, and the fractal dimension of the pore boundaries D_B (Lee, 2004). Several authors have employed unique methods to estimate fractal factors for field-collected aggregates, including a multi-stage-fractal-factor (Li and Logan, 1997), a gross field fractal factor estimated using a computer image technique (Lee, 2004), and a linear combination between oil and clay (Sterling *et al*., 2005). Many authors suggest the fractal factor value in estuarine water ranges from 1.7 and 2.3 (Winterwerp, 1998). However, Sterling *et al.* (2005) reported the fractal factor for clay-oil system was higher than previous values and between 2.6 and 3.0.

Disaggregation is another important issue in many flocculation simulation models. However, Alldredge *et al*. (1990) concluded that physical disaggregation is important only in the upper ocean layer during storm events when the energy dissipation rate ε is larger than $10^{-3}cm^2s^{-3}$. Stemmann *et al*. (2004) also suggested that disaggregation is more likely controlled by biological mechanisms such as bacteria-mediated dissolution and biologically-derived shear stress. Several disaggregation equations have been reported. Most of them use a similar form as the flocculation equation but with a disaggregate coefficient replacing the stickiness coefficient, and the floc is

broken into 2, 3, or 4 pieces of smaller floc. In the absence of erosion or other external particle sources, the particle size distribution shifts to smaller particles (the D_{50} value decreases) when disaggregation is stronger than aggregation.
Several floc settling velocity equations have been developed by including a shape factor, effective viscosity, hindered effect, Reynolds number, or fractal dimension factors to modify the Stokes law equation (Allen, 1985; Sanford and Halka, 1993; Schnoor, 1996; Winterwerp, 1998). Among these equations, the method developed by Winterwerp agrees well with observed data (Winterwerp, 2002).
A heterogeneous particle size distribution may also impact the flocculation mechanism and alter the OC settling velocity. Crump and Baross (2000) used an Owens tube to compare the relationship between settling velocity and the percentage of OC in particles from flood tide ETM samples. McCave (1984) also used multi-effective density equations for differently sized particles in his sedimentation model to match the observed data. These reports all suggest a wide, mixed hetrogeneous particle distribution in the water column and that the OC settling velocity, f_{OC} and effective density vary in each size of hetrogeneous particles.

4.3 Model Developments

4.3.1 Objectives

The first objective of this study is to develop a flocculation model that includes the interactions between organic and inorganic particles in a shallow water estuary. The second objective is to determine how flocculation affects the water column residence times and sedimentation rates of OC under varying conditions.

Model Processes

4.3.2.1 General Model Structure

In this study, the flocculation model simulates the movement and concentration of flocculated particles in the water column and in the top sediment layer. The major model equations include the concepts from Smoluchowski (1917), Lick and Lick (1988), O'Melia and Tiller (1992), Kiorboe and Hansen (1993), Winterwerp (1998), and Grant *et al*. (2001). Equation 4.1 describes how the number of particles per volume per time varies with settling velocity, flocculation, and bed-water exchange.

$$\frac{\partial N_i}{\partial t} = F_i + \left(W_{S,i} / x \times N_i \right) + E_{b,i} \qquad \text{Equation 4.1}$$

where, N is number of particle of class i per volume, $W_{S,i}$ is the floc setting velocity, F_i is the flocculation effect on particle number balance, x is the water column depth, and $E_{b,i}$ is the pure sediment resuspension flux that is calculated with a sediment erosion model.
The flocculation process is based on the same concept and equations used in Lick and Lick (1988). Flocculation involves two processes; gaining from the smaller particles and losing to form the larger particle by inter-particle collisions. The first term on the right-hand side Equation 4.2 represents the rate of formation of flocs of size k by cohesive collision between particle sizes i and j. The second term is the loss of size k flocs or solids by cohesive collision with other size particles.

$$F_k = \frac{1}{2} \sum_{i+j=k} \alpha_{i,j} \beta_{i,j} N_i N_j - N_k \sum_{i=1}^{\infty} \alpha_{i,k} \beta_{i,k} N_i \qquad \text{Equation 4.2}$$

where α is the stickiness coefficient, $\beta_{i,j}$ represents the cohesive collision frequency between particle i and j, and N is the floc number concentration.

There are three major mechanisms involved in estimating collision frequency: fluid shear, differential settling, and Brownian motion (Equations 2.4 to 2.6). Because only particles larger than 2 μm are included in this model, Brownian motion is ignored. Although OC and number concentration have different units, both variables use the same flocculation rate at each time step for a given floc cluster. Further, a proper selection of the collision kernel is necessary for a particular simulated environment. Differential settling and fluid shear may be modeled by either a rectilinear or a curvilinear form of the collision algorithm (Han and Lawler, 1991). The rectilinear kernel assumes that any flocs within a radius of 2 flocs' centerline would be intercepted by the settling particle. The curvilinear kernel assumes only smaller particle hit the centerline of larger one is swept. In general, the predicted collision rate by curvilinear kernel and rectilinear kernel ratio varies from 10^0 to 10^{-5} (Lawler, 1993). In this study, the curvilinear kernel is applied to the flocculation model because this type kernel is a better approach to the field environment in that particles would move following the streamline (Jackson, 1998). To convert the kernel from rectilinear to curvilinear, we used the formula from Han and Lawler (1991) and Li and Logan (1997).

$$\beta_{i,j} = \beta_{shear\_i,j} + \beta_{settling\_i,j} + \beta_{Brownian\_i,j} \qquad \text{Equation 4.3}$$

$$\beta_{recrilinea\,r\_shear} = \frac{G}{6}(D_i + D_j)^3 \qquad \text{Equation 4.4}$$

$$\beta_{recrilinea\,r\_settling} = \frac{\pi}{4}(D_i + D_j)^2 \left| W_{S,i} - W_{S,j} \right| \qquad \text{Equation 4.5}$$

$$\beta_{Brownian} = \pi(Diff_{floc,i} + Diff_{floc,i})(D_i + D_j) \qquad \text{Equation 4.6}$$

$$\beta_{curvilinea\,r} = \left(\frac{(D_i - 2D_j)^2}{(D_i + D_j)^2} \right) \times \beta_{recrilinea\,r} \qquad \text{Equation 4.7}$$

where β_{shear}, $\beta_{settling}$, $\beta_{Brownian}$ are the collision frequencies from shear stress, differential settling, and Brownian motion, G is shear stress gradient, $D_{i\ or\ j}$ is the floc diameter, Diff is the ideal floc diffusion coefficient, and $W_{S,i}$ is the floc setting velocity

Disaggregation is another important process. In this study, the LISST temporal volume concentration distribution profiles represent net aggregation in the STORM tank experiments, which are described in a later section (Schneider *et al.*, 2007). The shear stresses in the STORM experiments were likely not sufficient to disaggregate particles Therefore, this study does not explicitly simulate gross disaggregation but focus instead on net aggregation. We assume that the disaggregation process would only slow the flocculation process in the low shear stress environment. In practice, the stickiness coefficient value could be decreased to model disaggregation.

In this study, an essentially unlimited sediment supply has been assumed and the top layer sediment solid mass is assumed to be the same as the steady state total suspended solid mass in

the water column in the STORM experiment. The mass erosion equation was based on the concept from Sanford and Maa (2001):

$$E_{b,i} = \sigma\left(\frac{\tau_b}{\tau_c} - 1\right) \qquad \text{Equation 4.8}$$

where $E_{b,i}$ is the pure sediment resuspension flux (g m^{-2} sec^{-1})), σ is a calibration coefficient, τ_b is bottom shear stress, and τ_C is critical shear stress.

There are many equations to estimate the floc settling velocity. In this study, the settling velocity equation was adapted from Winterwerp's model (1998), because fractal geometry was used to describe the flocs mass, volume, and porosity:

$$W_S = \frac{a}{18b}\frac{(\rho_{floc,dry} - \rho_W)}{\mu} D_P^{3-nf} \frac{D_f^{nf-1}}{1 + 0.15\,\mathrm{Re}^{0.687}} \frac{1}{1 + 2.5\phi} \qquad \text{Equation 4.9}$$

where W_S is the floc settling velocity, a and b are shape parameters, $\rho_{floc,}$ dry and ρ_W are the solid floc and water densities, nf is the fractal dimension, Re is the Reynolds number, D_f is the floc diameter, D_P is the diameter of primary particle, and φ is the floc porosity.

4.3.2.2 Special Methods in This Study

Simulating the formation and movement of a wide range of mixed hetrogeneous particles is the major task in this model. The model requires that both dry mass and dry density are conserved, and is based on the multi cluster flocculation model from Yao *et al*. (1971) and Lick and Lick (1988). In this model, the term volume means the conserved spherical equivalent volume. This model calculates spherical equivalent volume and dry mass concentrations with the flocculation equations for each size floc cluster simultaneously:

$$V_{dry,i} = N_i \times V_{spherical\_equivant\_cluster,i} \qquad \text{Equation 4.10}$$

$$C_{dry,i} = V_{dry,i} \times \rho_{dry,i} \times (1 - \phi_i) \qquad \text{Equation 4.11}$$

where V_{dry} is the solid volume concentration (m^3 m^{-3}), N_i is the floc number concentration, $C_{dry,i}$ is the solid floc mass concentration (g m^{-3}), ρ is the solid floc density (g m^{-3}), and the φ is the floc porosity.

The f_{OC}, which is calculated as the ratio of OC over total "dry" mass for each particle size at each time step, ranges between 0 and 0.5 and equals half of the fraction organic matter (f_{OM}). Two equations estimate the mass in this model. The first estimates the dry mass concentration which is converted from the number concentration and dry floc density of each floc cluster. The second estimates the OC mass resulting from mass transport mechanisms and uses mass concentration as a unit. This study assumes two basic types of particles; clay (f_{OC} =0, density = 2.65 g/cm^3) and biotic-substrate (f_{OC} =0.5, density = 1.05 g/cm^3).

Floc porosity is assumed to be a constant in each floc cluster, and calculated from the fractal factor, the smallest particle size, and floc diameter with the compaction concept (Kranenburg, 1994).

$$\phi_f = [1 - (\frac{D_f}{D_P})^{nf} (\frac{D_P}{D_f})^3] \qquad \text{Equation 4.12}$$

where the φ is the floc porosity, D_f is the floc diameter, D_P is the diameter of primary particle, and nf is the fractal factor.

Khelifa and Hill (2006) suggested that the stickiness coefficient and the dry floc density should have a linear relationship with f_{OC} and this concept has been applied to this model. We ignored the possibility that the stickiness coefficient for the biotic substrate could lessen during

phytoplankton blooms. Similarly, the bulk floc density has a linear relationship with porosity and dry floc density and varies temporally. All variables are calculated by:

$$\rho_{dry,i} = 2 \times f_{OC,i} \times \rho_{biotic} + (1 - 2 \times f_{OC,i}) \times \rho_{clay} \quad \text{Equation 4.13}$$

$$\rho_{bulk,i} = \rho_{dry,i} \times (1 - \phi_i) + \rho_{water} \times \phi_i \quad \text{Equation 4.14}$$

$$\alpha_i = 2 \times f_{OC,i} \times \alpha_{biotic} + (1 - 2 \times f_{OC,i}) \times \alpha_{clay} \quad \text{Equation 4.15}$$

where $\rho_{dry,i}$ is dry floc density (g/m^3), $\rho_{bulk,i}$ is bulk floc density (g/m^3), [illegible] ss coefficient for floc at size i, f_{OC} is fraction of OC for floc at size i, ρ_{biotic}, ρ_{clay} are OC and inorganic carbon dry density (g/m^3), ρ_{water} is water density (g/m^3), φ_i is floc porosity for floc at size i, and α_{biotic}, α_{clay} are OC and inorganic carbon stickiness coefficient respectively.

It is difficult to use traditional multi-floc-cluster flocculation models to simulate a wide range of floc sizes due to limitations on the floc cluster intervals and computer array sizes. In the STORM tank experiment, the flocs sizes measured varied between 2 to 1000 μm. However, with the traditional approach using fixed volume intervals, a model would require a matrix with more than 150 thousand elements to represent the particle properties when the primary particle size range from 2μm (8μm^3 in volume) to 1000μm (10^9μm^3 in volume). In addition, variables like number and OC concentrations, stickiness coefficient, collision efficiency, floc density, settling velocity, and f_{OC} are all calculated for each floc size at each time step, which is not practicable. To solve this problem, a fixed floc cluster diameter interval is used, meaning that floc cluster N's diameter is N times longer than floc cluster one. The floc spherical equivalent volume is calculated based on floc diameter in each floc cluster. The volume and mass concentrations are varied temporally in each floc cluster, but the gross dry mass and volume are conserved. In this model, the particle sizes vary between 2 to 1000 μm with a 1 μm interval. Therefore, the model has one thousand particle floc clusters or variables to represent each individual floc property.

4.3.3 Calibration Data

Schneider *et al*. (2007) conducted STORM tank experiments that mimic resuspension and settling of contaminated upper Hudson River sediment with realistic bottom shear stress and water column turbulence. The average instantaneous bottom shear stress was about 1 dyne cm^{-2} and the volume-weighted average water column turbulence intensity and energy dissipation rate were 0.55 cm s^{-1} and 0.0032 cm^2 s^{-3}, respectively. Hudson River sediment was added to a depth of 5 cm and allowed to consolidate for 10 days. This experiment included both erosion and free settling periods. During erosion, the mixing paddle continuously generated bottom shear stress for 53 hours to ensure suspended solids reached steady state. During the one hour free settling period, the paddle was turned off to allow suspended particles to settle. Particle size distribution, dissolved and particulate PCBs, TSS, DOC, particulate carbon, nitrogen, and chlorophyll *a* were measured throughout the resuspension and settling portions of each experiment (Schneider *et al.*, 2007).

Because observations were made at the mid-depth of the tank, the free-settling scenario assumes the water column depth to be 0.5 m. The erosion scenario assumes the water column depth is 1 m because of the tank is well-mixed. In the STORM experiment, the suspended particle size analysis was conducted using LISST-100C (Sequoia Scientific, Inc.). The LISST measures the particle size distribution between 2 and 500 μm, in 32 size bins in a log scale, providing the

steady-state particle size distribution for the erosion period and the initial particle size distribution for the free settling period.
The sediment grain size analysis was conducted using the Beckman Coulter LS100 Laser Diffractometer. This instrument works on the same principles as the LISST and measures the size distribution of suspensions of nonsieved sediments 0.4 to 1000 μm in diameter using the laser diffraction technique. The size distribution of the homogenized Hudson River sediment was tri-modal with a large peak in the volume size distribution at 145 μm and two lesser peaks at 61 and 473 μm respectively. The volume median diameter of the sediment grains was 63 μm. This analysis result was applied to this model as an initial sediment particle size distribution (Figure 4.1).

4.3.4 Numerical Method

The system was solved on 1000 floc clusters for each variable. The above equations form the basis of our model, which was written in double precision Fortran 90 and used a fourth-order Runge-Kutta numerical algorithm to solve the set of nonlinear ordinary differential equations. The model was stable with a time step of one minute and a 53 simulation hours run was completed in 75 CPU minutes on a Sun Ultra-60 workstation. Both dry mass and dry volume were conserved during the two period simulations. At the end of the free settling period simulation, 7.25 g OC and 411 $\mu m^3 m^{-3}$ dry floc volumes remained distributed among two reservoirs, water and sediment, demonstrating that there is no systematic numerical drift within the model.

4.3.5 Parameterization and Initial Conditions

Several parameter values and initial conditions were estimated from a combination of observations during the STORM experiment and literature reports, including the fractal factor, the primary particle character, the porosity, and initial particle volume and the f_{OC} size distribution and corresponding values for each individual floc cluster.
In this model, the fractal factor is the dominant parameter controlling particle porosity, and therefore the settling velocity. The sampled particles were predominately flocs (Schneider, 2007), so the fractal factor is less than 3.0. We used the highest estuarine fractal factor value suggested by Winterwerp (1998) of 2.3 because the eroded sediment was consolidated for 10 days prior to analysis. The influence of the fractal factor was evaluated in the sensitivity analysis described below. The primary particle is assumed to be a solid of 2 μm diameter which does not disaggregate and is the lowest LISST reading in the STORM experiment. The porosity of each floc cluster is estimated by Equation 4.7.
The model is initialized with a particle size distribution derived from the STORM experiments. To interpolate the measured size distribution, we used the strategy of Mikkelsen *et al.* (2005), in which both the total volume concentration and the shape of the particle size distribution are conserved. The same method was used to interpolate the sediment size distribution measurements to initialize the sediment particle size distribution in the model.
The LISST integrates all flocs > 500 μm into one group, and in the STORM experiments Schneider *et al.* (2007) ignored all flocs larger than 250 μm. However, Mikkelsen *et al.* (2005) used a digital camera to measure the larger floc size distribution from Hudson River sediment, and showed that the particle size distribution for the larger floc decreased with particle size. Present model results show the similar behavior for the larger particles. Therefore, the initial particle size distribution was extrapolated to 1000 μm iteratively based on stead state model

results for the sediment layer during the erosion period simulation and suspended particles during the free settling period simulation.
The next step was to set the eroded particle size distribution. Published models estimate the erodable particle size as a function of particle density, size, critical shear stress, and bottom shear stress. However, the eroded particle size distribution was also impacted by aggregation-disaggregation along with the given bottom shear stress. To simplify the model simulation, the first measured suspended particle LISST profile was selected to represent the net eroded particle size distribution (Figure 4.1) and assumed no suspended particles in the water column at time zero. This distribution does not vary temporally in the model.
The f_{OC} distribution plays an important role in this model. Because there is no method to measure the f_{OC} in the individual sized particles, we have to make a reasonable assumption for this variable. Three types of distributions were tried (Figure 4.2): a uniform f_{OC} distribution across all sizes, f_{OC} concentrated in the small flocs, and a size-variable f_{OC} distribution based on the predicted steady state f_{OC} distribution resulting from a two type particle erosion scenario which described in detail later. Because the model is very sensitive to the f_{OC} distribution, each assumption causes a different trend in the steady state. Compared the model simulation results with STORM experiment measurement, the first two f_{OC} distributions could only match the particle size distribution during the early stage of resuspension and each missed the later trend. The third scenario gave the best overall agreement with measurements at steady state. However, the third f_{OC} distribution could not be directly applied to the model because of the conservation of TSS, TVC, and f_{OC}. To solve this problem, the individual floc cluster f_{OC} value was back calculated from Equation 4.5 to 2.9, because TSS, TOC concentration, and total volume concentration were measured values, and fractal factor value and individual volume concentration were assigned.
To ensure that the model eroded a realistic amount of mass under the given shear stress, we compare model results with Upper Chesapeake Bay data (Sanford, unpublished). In Figure 4.3, we compared the relationship between eroded mass and eroded flux from STORM experiment and field data. This figure shows that the relationship between eroded flux and eroded mass under a given shear stress in STORM tank experiment was similar to field observations.

4.3.6 Sensitivity Analysis

The flocculation model was first evaluated be exploring the sensitivity of key outputs (the gross floc settling velocity for TSS [Ws_{TSS}], residence time, steady state TSS concentration, and particle size distribution trends) to several parameters. The model was initialized with 1 to 3 discrete sizes of flocs under the same conditions as the STORM experiments, including the experiment duration, eroded shear stress, and tank size during the both the free settling and erosion periods. In this chapter, the residence time was calculated as the concentration weight average for size of flocs.

$$\mathrm{Re}\,sidence\_Time = \sum[C_{dry,i} \times \left(\frac{V_{\tan k}}{Area \times W_S} \right)] \Big/ \sum C_{dry,i} \qquad \text{Equation 4.16}$$

where V_{tank} is the experimental tank volume (m^3), area is the sediment surface area (m^2), $C_{dry,i}$ is the solid floc mass concentration (g m^{-3}), and $W_{S,i}$ is the floc setting velocity.
The first sensitivity test examines the impact of the fractal factor on the gross settling velocity for TSS (Ws_{TSS}) during a one hour free settling period. The gross settling velocity for TSS during

the free settling period was estimated as a first order equation which was only used in this section:

$$\frac{\partial TSS}{\partial t} = -\frac{w_{S,TSS}}{x} TSS \qquad \text{Equation 4.17}$$

In this test, the model first simulated 0.1 g of clay packaged into 20 μm flocs settling in a one meter tank for 1 hour without flocculation. Three fractal factor values (1.0, 2.0, and 3.0) were evaluated. When the fractal factor equals 3.0 the 20 μm particles are solids, and particle settling is predicted by Stokes' law. When the fractal factor is less than three the porosity increases and the floc bulk density decreases, resulting in a smaller settling velocity. This analysis demonstrates that the fractal factor strongly controls particle settling, as Ws_{TSS} decreased from 19 m/day to 0.1 m/day as fractal factor decreased from three to one.

The second sensitivity test examined the impact of flocculation on Ws_{TSS}. In this test, the model simulated 0.1 g/m^3 of clay particles in flocs with an initial 20 μm diameter and a fractal factor of 2.0 which settled through one meter for 1 hour. The stickiness coefficient (α) varied between zero (no flocculation) and 1 (every collision results in flocculation). Under these conditions, Ws_{TSS} is 30% higher when α=1 than without flocculation due to the formation of larger flocs.

Previous particle transport models use D_{50} to represent the entire particle spectrum and use this value to estimate the Ws_{TSS} (Winterwerp, 1996). However, as discussed before, a size distributed suspension may increase the flocculation rate due to differential settling-induced collisions. Thereafter, the gross Ws_{TSS} for cohesive particles may have different value between multi-size-particle and D_{50} runs. The third test compares the impact of flocculation on Ws_{TSS} between D_{50} and the multi-size-particles. The model again simulated 0.1 g/m^3 clays with a D_{50} of 20 μm diameter settling through one meter for 1 hour with a fractal factor of two. Three sizes of floc clusters, 10, 20 and 30 μm, having the same average volume concentration size value as D_{50} run, were selected to compare with the D_{50} simulation results. The stickiness coefficient varied between one and zero to control the extent of flocculation. Without flocculation, there is less than 2% in difference for the Ws_{TSS} between multi- and single size flocs scenarios. This result implicates that D_{50} is a workable tool to estimate Ws_{TSS} for a broad size distribution of non-cohesive particles. After including flocculation, the multi-size scenario increases Ws_{TSS} around 55% compared to the single size scenario. Flocculation occurs more rapidly in the multi-size scenario since there is a higher collision probability. This result implies that assuming a single particle of size D_{50} maybe underestimate the Ws_{TSS} for the broad size distribution of cohesive flocs.

The fourth test examines the impact of particle characteristics on Ws_{TSS}. Separate simulations with 20 μm diameter clay (density = 2.65 g/cm^3) and biotic (density = 1.05 g/cm^3) particles, each with and without flocculation, are compared. For both particle types Ws_{TSS} increases with flocculation due to the formation of larger, faster settling flocs. Without flocculation, Ws_{TSS} calculated for clays was 2.5 times faster than for biotic substrates because of differences in the floc density. With flocculation, the Ws_{TSS} for clay was only 1.2 times larger than that of the biotic substrates during the one hour simulation. Flocculation impacts the settling velocity of the biotic particles more than clay. Unlike clay, most low density biotic flocs remained in the water column in both runs, having a better opportunity to coagulate with other flocs during the one hour simulation period and one meter water depth.

Clay has been widely used to remove algae from wastewater treatment plants and from open water (Rengasamy *et al.*, 1996). To ensure that the flocculation model could work with erosion

and sedimentation processes, the fifth test simulates flocculation's impact on a simple clay and diatom mixture. The model used two sizes of particles that were constantly eroded by bottom shear stress in a 1 m deep tank: a 20 μm (f_{OC} = 0) clay floc and a 22 μm (f_{OC} = 0.5) biotic floc. The critical shear stress and bottom shear stress were the same as in the STORM experiments. Three tests were done in which the model constantly eroded clay only, diatoms only, and both together from the sediments at rates of 2.4 (f_{OC} = 0), 1.05 (f_{OC} = 0.5) and 3.45 (f_{OC} = 0.14) μg $m^{-3}s^{-1}$, respectively. The model was run with a one minute time interval for a 1000 hour to ensure that the model reached steady state. Further, three runs were done in each test, and all runs had the same parameters and settings, except the stickiness coefficients, which varied between 0, 0.5 and 1.0 to represent the strength of flocculation

Figure 4.4 shows the steady state TSS concentration, calculated residence time, D_{50}, and simulated particle size volume concentration distribution both at steady state and in transitory periods for all runs. In general, the steady state TSS and water column residence times decrease with stronger flocculation due to forming larger flocs. Before reaching steady state, we observed that the model run with more flocculation had a higher volume concentration of the larger flocs in all tests because those runs had a faster flocculation rate to form larger flocs. Comparing the three tests, the residence time value corresponded to floc densities. In this study, the residence time for the diatom-only test decreased almost 53% and 41% with half and full flocculation effects, respectively. When two types of particles started to coagulate, the residence time decreased slightly faster than in the diatom test. The difference in residence time could be more significant if we eroded a more complex floc group to alter the flocculation efficiency with increasing the differential settling and collusion number concentration.

After including the flocculation effect, the particle size volume concentration distribution showed a similar shape but different quantities for both runs at steady state in each eroded test. In addition, we observed the periodic volume concentration peak alone with increasing floc size, which has the similar trend as observed in the field (Sanford, personal communication). This is because the model started with one size of particles, and the assumption of volume conservation-floc cluster size relationship. Compared to the steady state clay-only results, the diatom-only test had larger flocs, which because of their lighter density settled more slowly than clay.

Without flocculation, the steady-state TSS concentration from the clay plus diatom mixed-erosion scenario was equal to the sum of TSS concentrations from the clay only and diatom only runs. This result suggested that the steady state TSS concentration from a group of non-cohesive particles could be estimated from the summation of the individual particle size run result. However, after including flocculation both TSS and volume concentrations from the mixed-eroded-scenario were less than the sum of TSS and volume concentrations from the clay and diatom runs at steady state. These results showed the impact of flocculation on the kinetic variation in number concentrations, floc density and settling velocity.

4.3.7 Calibration with STORM Experimental Data

To understand the effect of shear stress on TSS and D_{50} with flocculation, we applied different shear stresses in this model. Model initial conditions and environment parameters were the same as STORM tank erosion calibration scenario. Shear stress was varied from 1 to 4 dyne cm^{-2} in 1 dyne cm^{-2} increments. Each shear stress was applied constantly for 53 simulation hours to ensure that the model reached steady state. As before, disaggregation was not included in this simulation. Figure 4.5 shows how the model simulated D_{50}, and the TSS and organic carbon concentrations varied with shear stress. In general, at steady state the D_{50}, TSS, and OC

concentrations increased with higher shear stress because more mass was eroded. Further, higher shear stress and higher concentrations also increased the flocculation efficiency to form larger flocs. Thereafter, the time to reach steady state was shorter with higher shear stress. D_{50} had several peaks when shear stress was changed in the model. The sharp D_{50} increase was a combination of steady state particle size distribution under previous shear stress and additional eroded particle size distribution under new shear stress.

The flocculation model was calibrated with STORM experiment results by adjusting the stickiness coefficient and erosion coefficient. The final calibrated parameter values are listed in Table 4.1. Figure 4.6a-f showed measured and model calculated OC, TSS, and total volume concentrations during the erosion and free settling periods.

4.4 Example Applications

4.4.1 Comparison of Organic Carbon Settling Rates Predicted by the Flocculation Model with those from a Traditional Particle Transport Model

A traditional particle transport model does not include the formation and fractal nature of flocs and often fixes the OC sedimentation rate at a value between those of inorganic solids (e.g., clays) and plankton (Di Toro, 2002). To compare the TSS and OC settling velocities with and without flocculation, 4 scenarios were designed. Scenario 1 and 2 ignored flocculation, assumed flocs had constant densities as 1.05 and 1.35 g/cm^3, respectively, and used settling velocities calculated using the Stokes' law equation. The third scenario included flocculation, allowing floc density to vary temporally with floc composition (but not with floc size). The last scenario is the same as scenario three except that the setting velocity is calculated using the equation of Winterwerp (1998), which is the strategy in the model described in this report.

Figure 4.7 compares the measured and modeled TSS and OC concentrations among the four scenarios. The diatom-based scenario one results under-estimated the TSS and OC settling velocities due to low particle densities. This under-prediction is similar to those seen in other OC particle transport models like the DELPCB model (DRBC, 2003). These results suggest that the impact of inorganic solids on organic matter settling cannot be ignored in estuaries and other algal-rich waters.

The other interesting finding is the result from scenario 2, in which the particle density was estimated from field observations of settling, which is the approach commonly used in many particle transport models. The result suggested that in organic rich environments, modifying the particle density to improve the OC settling velocity does not work well and under-estimates the OC residence time because flocculation continues to alter the particle size and gross bulk density.

Scenario three and four started with the same initial condition, giving us an initial look at the impact of equations 4.4 and 4.11 on the fate of flocs. Scenario three predicted that both TSS and OC concentrations decreased much faster than observations. But scenario four had a good agreement with observations. These results agreed with the suggestion from Winterwerp to use a fractal geometry-based equation to estimate the settling velocity for flocs.

4.4.2 The Impact of Eroded f_{OC} Distributions on the Behavior of Organic Carbon

As discussed before, the model performance is sensitive to the f_{OC} distribution. Because there is no method to measure the f_{OC} of the individual sized particles, we have to make a reasonable assumption for this variable. Three types of distributions were considered in this study: a

uniform f_{OC} distribution across all sizes, which has the same effect as assuming all particles have the same composition, f_{OC} concentrated in the small flocs, which has been adapted by the other models (Gong and DePinto, 1998), and a size-variable f_{OC} which we believed to be closest to the actual distribution (Figure 4.2). Each distribution has a unique impact on the gross particle residence time, settling velocity, and steady state concentration, after including the flocculation, erosion, and settling. In this section, we use this model to explore the impact of the f_{OC} distribution and flocculation on the fate of eroded sediment carbon.

We designed a series of model runs to estimate the steady state concentrations and calculated the residence time for bulk OC and TSS with varying stickiness coefficients and three types of f_{OC} distributions. All runs had the same gross OC and inorganic solids erosion fluxes, and erosion was based on the same particle size distribution and fractal factor. To simplify the model settings, here clay and organic matter were assumed to have the same stickiness coefficients. The stickiness coefficient varied from zero, representing no flocculation, to 1, representing full flocculation, in 0.2 increments. Each set was tested with the three f_{OC} distributions. There were total 18 runs in this case, and each run was executed for 200 simulated hours to reach steady state.

The steady state D_{50} increases and both the OC concentrations and the time to reach steady state decrease when the model includes flocculation (Table 4.2). However with flocculation the variations in steady state TSS and OC concentrations were very limited among different stickiness coefficient runs for each f_{OC} distribution because at steady state all runs predicted similar OC and TSS volume size distributions. The only difference was the time to reach steady state. Increasing flocculation (higher stickiness coefficient) reduced the time to reach steady state. Compared with the other f_{OC} distributions, the varied distribution runs reached steady state more quickly and had the least difference between the residence time and steady state OC concentrations with and without the flocculation because these runs were initialized with a steady state f_{OC}. These runs did not reach steady state immediately because the initial particle size distribution was not the same as the steady state particle size distribution.

These trends agree with the other reports that when particles start to form flocs, the gross settling velocity increases as larger particles form. Schneider (2005) used a first order equation to estimate the TSS based floc settling velocity with a mean of 0.12 cm s^{-1} for the upper Hudson River. Fugate and Friedrichs (2002) reported a TSS-based settling velocity at the Cherrystone site in the Chesapeake Bay by an acoustic doppler ranging from 0.07 to 0.13 cm s^{-1}. Sanford *et al*. (2005) used a video camera technique to measure upper Chesapeake Bay floc settling velocities ranging from 0.02 to 0.50 cm s^{-1}, with a mean of 0.15 cm s^{-1}. The model calculated TSS-based settling velocities ranged between 0.09 to 0.16 cm s^{-1}, and OC based settling velocities ranged between 0.03 to 0.18 cm s^{-1}, which was within the report range of values.

When the eroded OC is initially concentrated in small flocs, flocculation more significantly impacts the OC steady state concentration. In addition, the OC residence time and steady state concentration with full flocculation ($\alpha = 1$) were one third of the results without flocculation because without flocculation all OC was in small, low density flocs with slower settling velocities. As they coagulated, the organic matter aggregated into larger, denser particles, resulting in faster settling and lower steady state OC concentrations. On the contrary, the runs under size-variable f_{OC} distribution are least impacted by flocculation. The OC residence time and steady state concentration with full flocculation are only 5% different than without flocculation.

Furthermore, because f_{OC} varies temporally among different floc sizes in this model, bulk TSS and OC may settle with different velocities depending on the initial f_{OC} distributions. When f_{OC} is evenly distributed among all sizes of flocs, all flocs have the same density and there is no difference between OC and inorganic solids steady state concentration distributions. However, when f_{OC} varied with particle size distribution, density varies with floc size, altering the size-dependent settling velocity distribution. In the small flocs dominated distribution runs, the TSS settling velocity was almost three times faster than OC settling velocity. For the varied distribution scenario, the OC settled 13% faster than TSS.

The floc dry density, which controls the settling velocity, depends on the f_{OC} of each floc size cluster. In this model, within the same floc size cluster organic and inorganic substrates have the same settling velocity. As a result, under the uniform f_{OC} distribution both gross TSS and OC are predicted to have the same settling velocity. On the contrary, TSS and OC should have the different settling velocity when the model is initialized with an uneven f_{OC} distribution. When OC is enriched in the larger flocs, faster settling velocities lower steady state OC concentrations compared to the same amount of organic substrates beginning in smaller flocs. Therefore, the OC in the small f_{OC} dominated distribution had the longest time to reach steady state compared to the other two f_{OC} distributions.

These results suggest that the OC size distribution in the sediment is an important factor controlling the residence time, gross settling velocity, and steady state concentration of solids and organic matter. Most particle transport models assume that f_{OC} is constant and evenly distributed across the entire range of particle sizes, and that OC has the same settling behavior as TSS. In this study, we found these models might either under or over estimate the fate of OC when f_{OC} is not evenly distributed, with results depending on the nature of the f_{OC} distribution in the sediment.

4.5 Summary

The behavior of organic particles, which strongly influences the fate of organic contaminants in natural waters, is controlled by settling and erosion fluxes. However, there is no universal method to estimate the behavior of organic matter when it forms flocs with itself or with inorganic solids. In this study, a flocculation model that simulates the flocculation of both OC and inorganic solids ranging in diameter from 2 to 1000 μm has been developed. This model simultaneously calculates the temporally varying OC content, density, flocculation coefficient, and settling velocity for each size of particles under different scenarios. The model was calibrated using the STORM tank experiments that mimic resuspension and settling of contaminated Hudson River sediment with realistic bottom shear stress. This model was effective in predicting the temporal variability in the behavior of wide spectrum hetrogeneous flocs in the mesocosm.

The model predicted that the water column residence time of TSS and OC decrease and the median size of particles (D_{50}) is less with increased flocculation and fractal factor. Several settling velocity strategies were tested based on the same initial condition for a hetrogeneous source particle population. A fractal geometry-based settling velocity equation agreed best with the STORM observations. The results also suggested that using a modified but temporally-invariant particle density over-estimates the OC settling velocity in OC rich environments due to the influence of flocculation on settling velocities. Including flocculation in the multi-size scenario increases Ws_{TSS} 55% compared to the single size scenario. This result suggests that

modeling settling with a single particle of size D_{50} may underestimate the Ws_{TSS} for the broad size distribution of cohesive flocs.

OC size distribution is another important factor influencing the water column residence time, gross settling velocity, and steady state concentration of solids and organic matter. In this study, we found that the relationship among individual floc cluster density, gross OC, and TSS settling velocity were impacted by the f_{OC} distribution. They have the same settling velocity and individual floc cluster density only when f_{OC} does not vary with particle size and is evenly distributed over all sizes of particles. The settling velocity of OC plays an important role in predicting the fate of particle-reactive chemicals in the water column. When a wide spectrum of hetrogeneous flocs is present, it is necessary to apply a multi-sized floc strategy to simulate gross particle behaviors. The next step of this study will apply this flocculation model to simulate the fate of organic contaminants in an urban estuary.

4.6 Figure Captions

Figure 4.1: The initial volume size distribution for sediment and eroded flux during the erosion period and of suspended particles at the beginning of free settling period.

Figure 4.2: Three f_{OC} distribution trends: small, uniform, and a size-variable. All trends are estimated by the same gross f_{OC} (0.115), gross TSS (43.5g/m3), and gross TVC (190uL/L) as in the STORM experiment

Figure 4.3. Model predicted TSS, residence time, D_{50}, and simulated particle size volume concentration distribution both at steady state for clay eroded only (f_{OC}=0), biotic-substrates eroded only (f_{OC}=0.5), and clay-biotic-substrate-co-eroded (f_{OC}=0.14) scenarios. In each scenario, the model was tested with three different stickiness coefficients (0, 0.5, and 1).

Figure 4.4: Model predicted TSS, OC concentrations, and D_{50} variation with different shear stress values. Shear stress varied from 1 to 4 dyne cm^{-2}. Each shear stress was applied for 53 simulation hours. Fractal factor is 2.3 with TSS equal to 43.5 g m^{-3}, TVC equal to 191 µl/L, and gross f_{OC} equal to 0.115.

Figure 4.5: Comparison of the experimental eroded flux-eroded mass relationship with Upper Chesapeake Bay field measurements (Sanford, unpublished)

Figure 4.6 a and b: Comparison of model-predicted and measured TSS and OC concentrations during the STORM free settling period. Fractal factor is 2.3 with TSS equals to 63 g/m^3, TVC equal to 410 µl/L, and gross f_{OC} equal to 0.115.

Figure 4.6 c, d, e, and f: Comparison of model predicted and measured TSS, TVC, OC concentrations, and D_{50} during the STORM resuspension period. Fractal factor is 2.3 with TSS equals to 43.5 g/m^3, with TVC equal to 191 µl/L, and gross f_{OC} equal to 0.115.

Figure 4.7: Comparison of measured and model-predicted TSS and OC concentrations among four scenarios. All runs started with the same initial conditions for an one hour duration at one meter water depth: Fractal factor is 2.3 with TSS equal to 63 g/m^3, TVC equal to 410 µl/L, and gross f_{OC} equal to 0.115.

Figure 4.1 The initial volume size distribution for sediment and eroded flux during the erosion period and of suspended particles at the beginning of free settling period

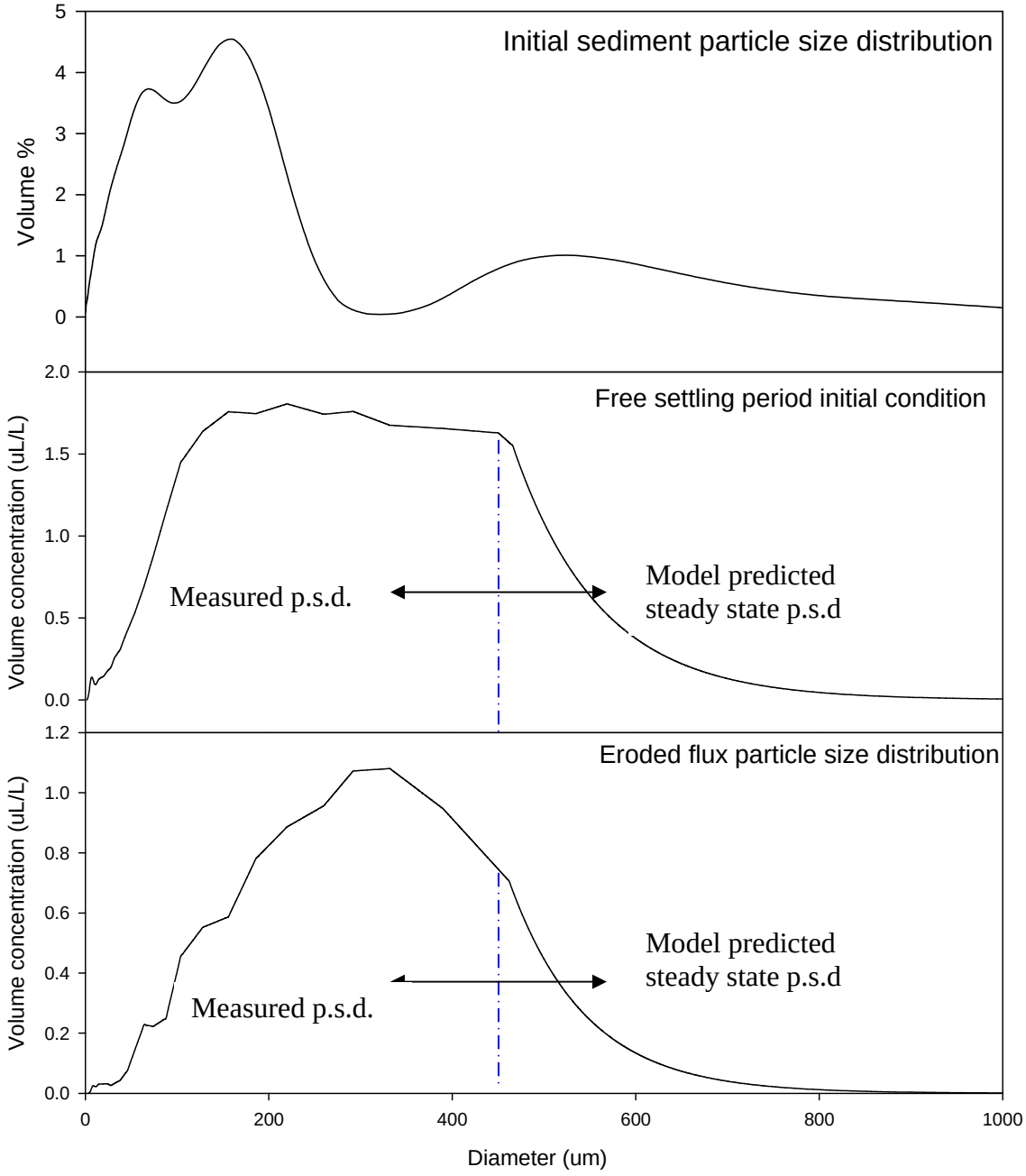

Figure 4.2 Three f_{OC} distribution trends.

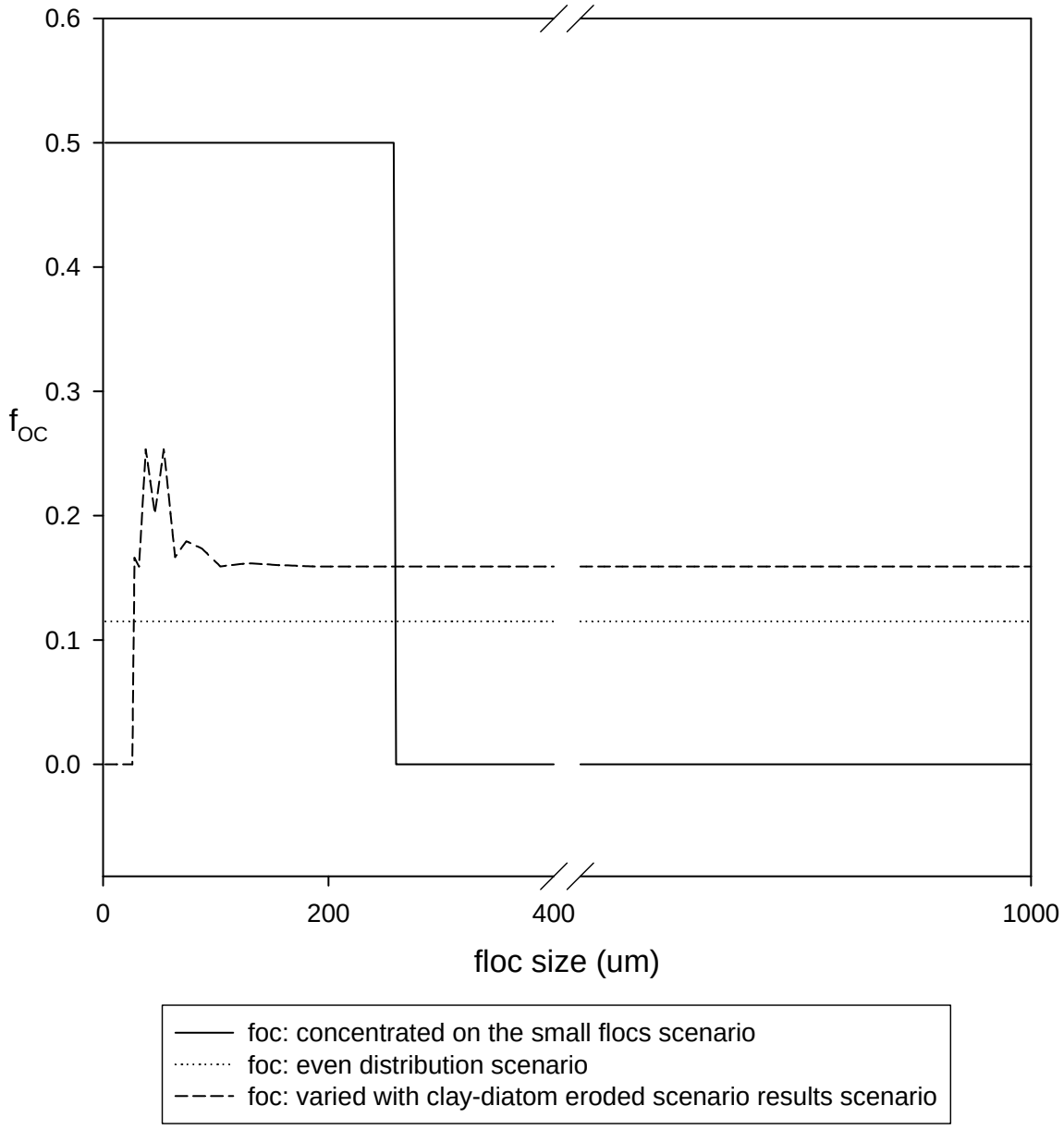

Figure 4.3a Model predicted TSS, residence time at steady state for diatom eroded only.

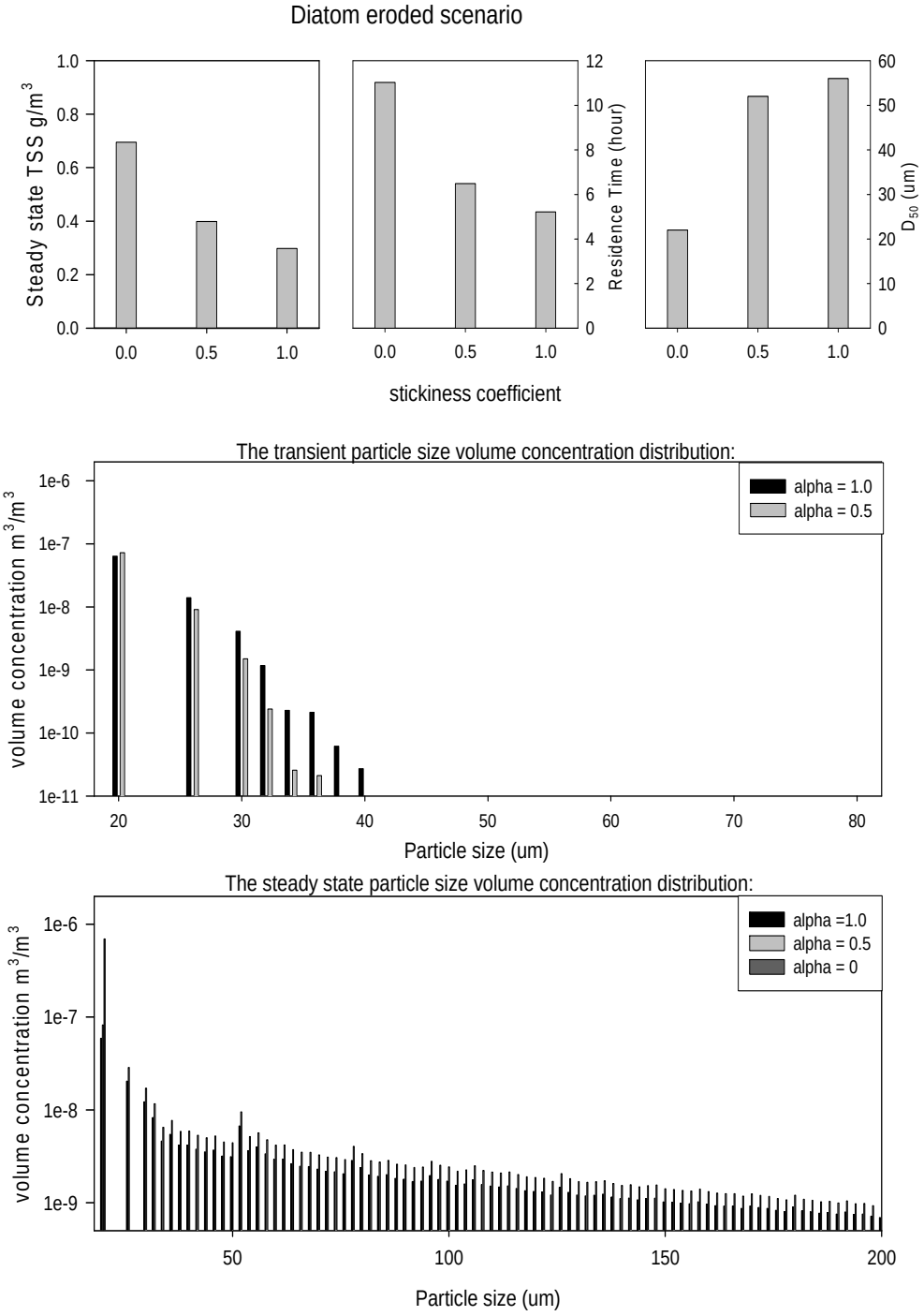

Figure 4.3 b Model time predicted TSS, residence time at steady state for clay eroded only.

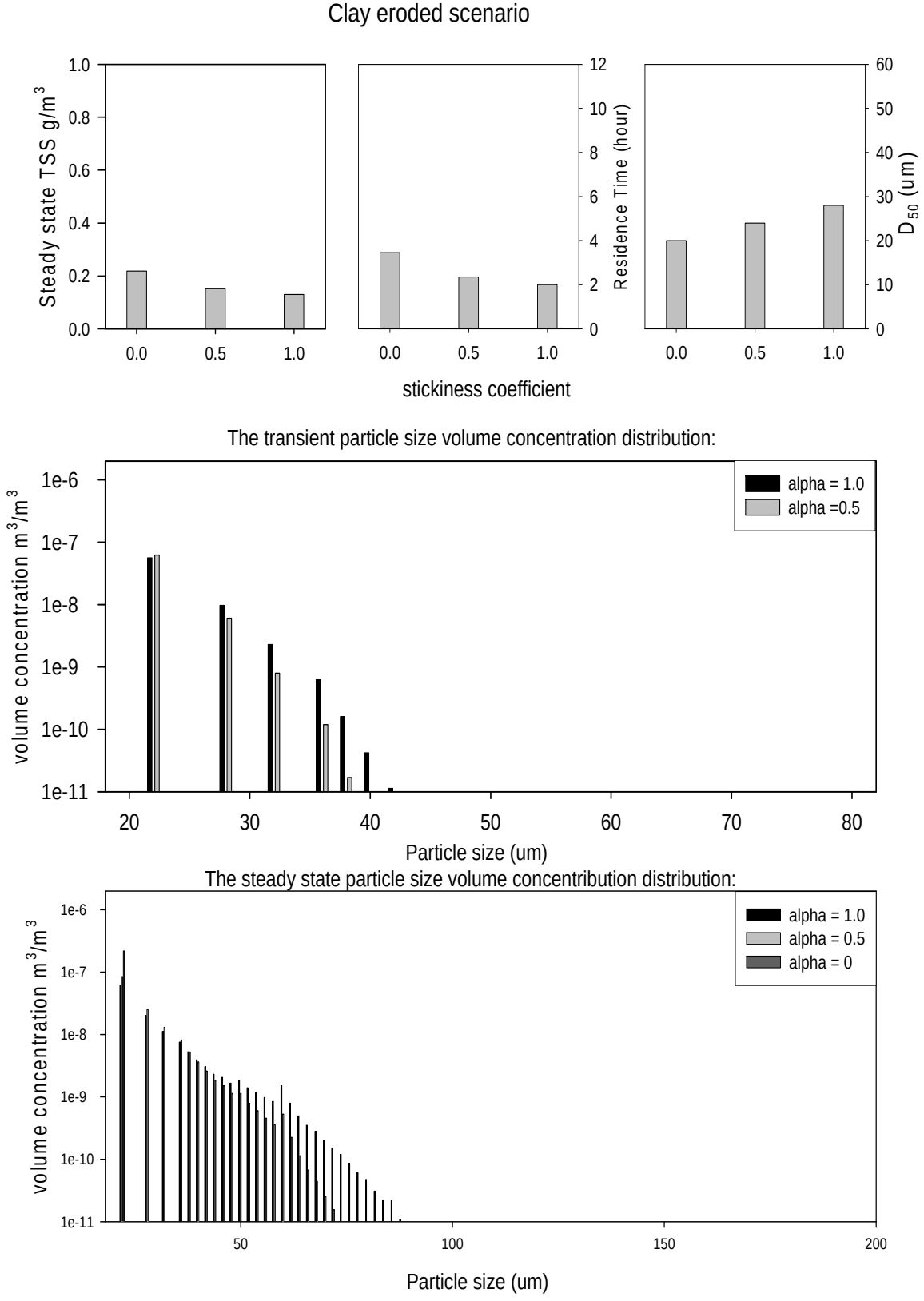

Figure 4.3c Model time predicted TSS, residence time steady state for clay and diatom mixed eroded.

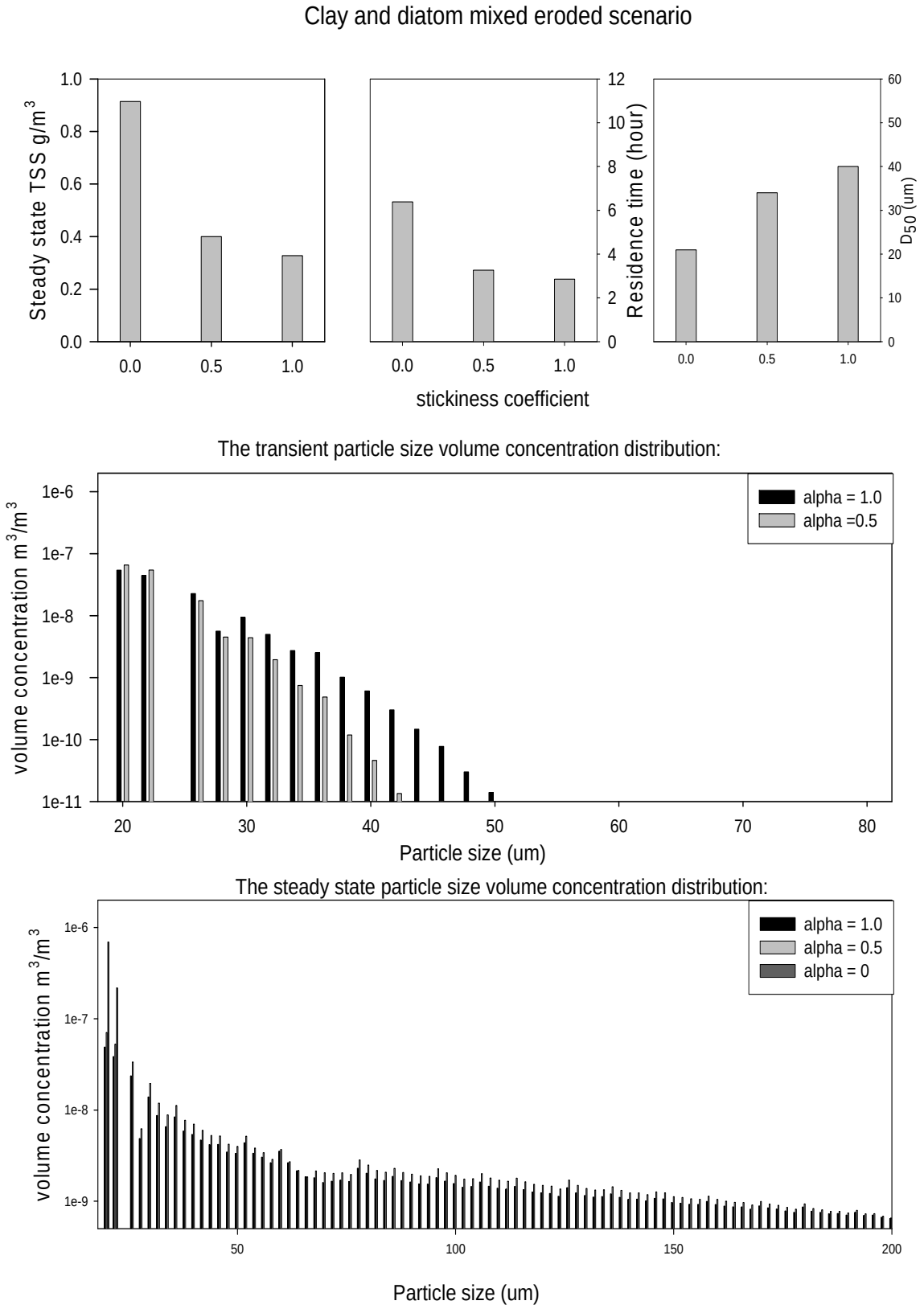

Figure 4.4 Model predicted TSS, OC concentrations and D_{50} variation with different shear stress values.

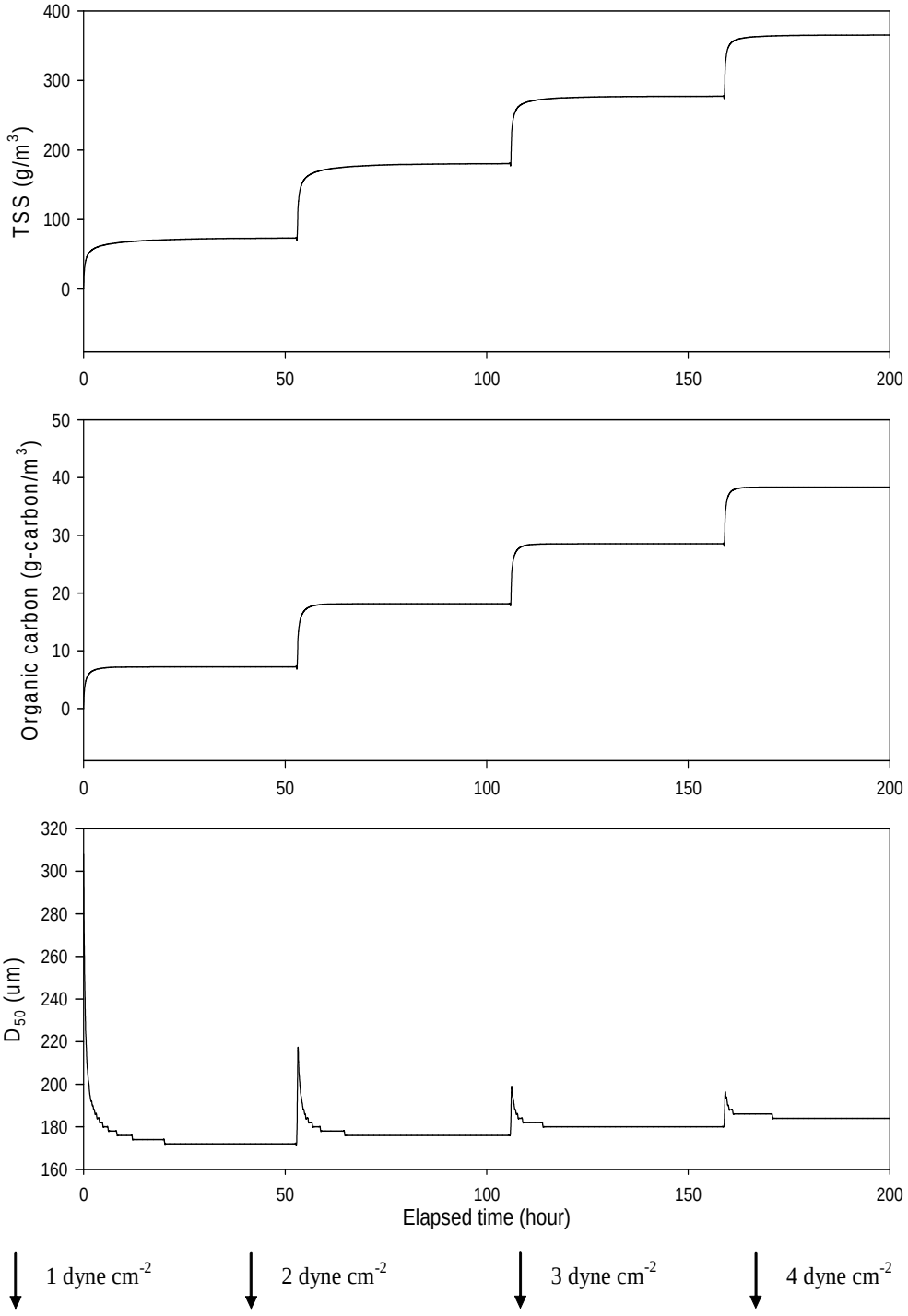

Figure 4.5 Comparison of the experimental eroded flux-eroded mass relationship with Upper Chesapeake Bay field measurements (Sanford, unpublished).

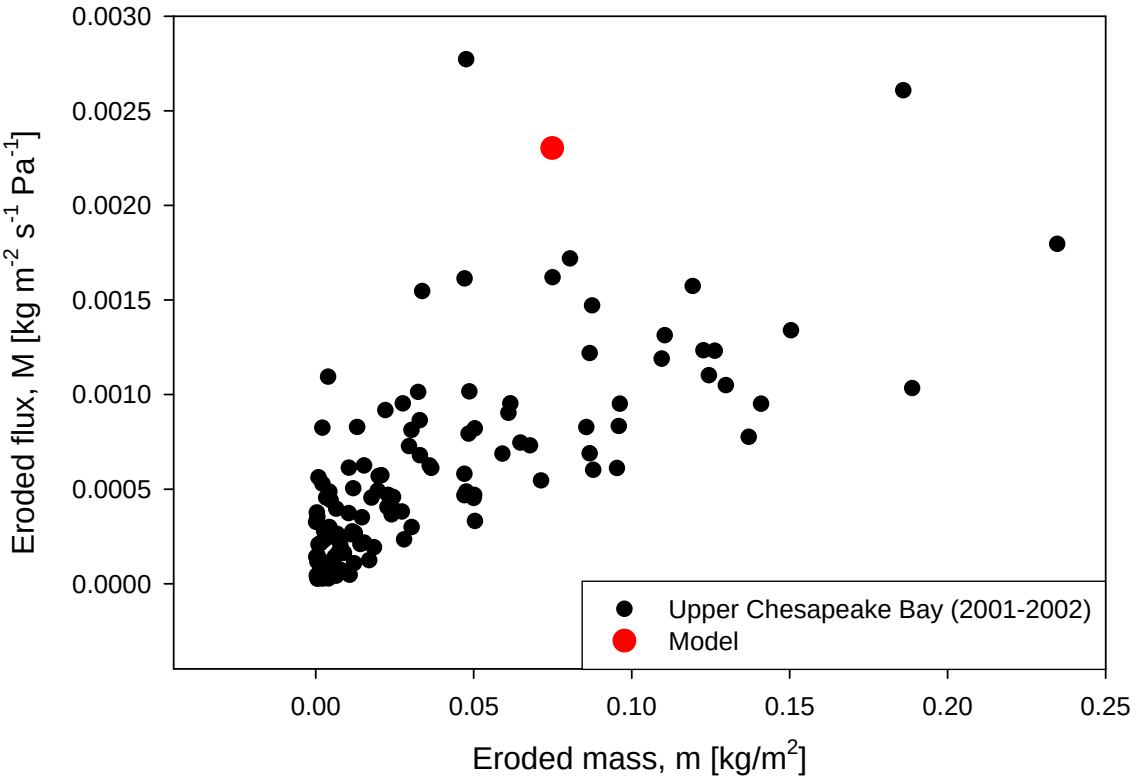

Figure 4.6 a and b Comparison of model-predicted and measured TSS and OC concentrations during the STORM free settling period.

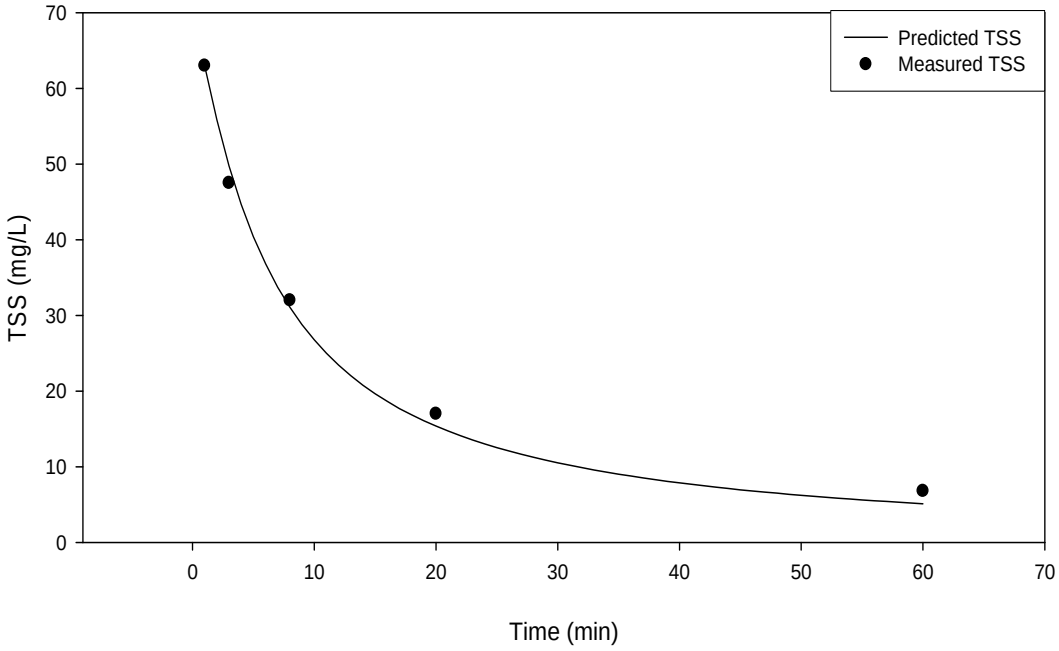

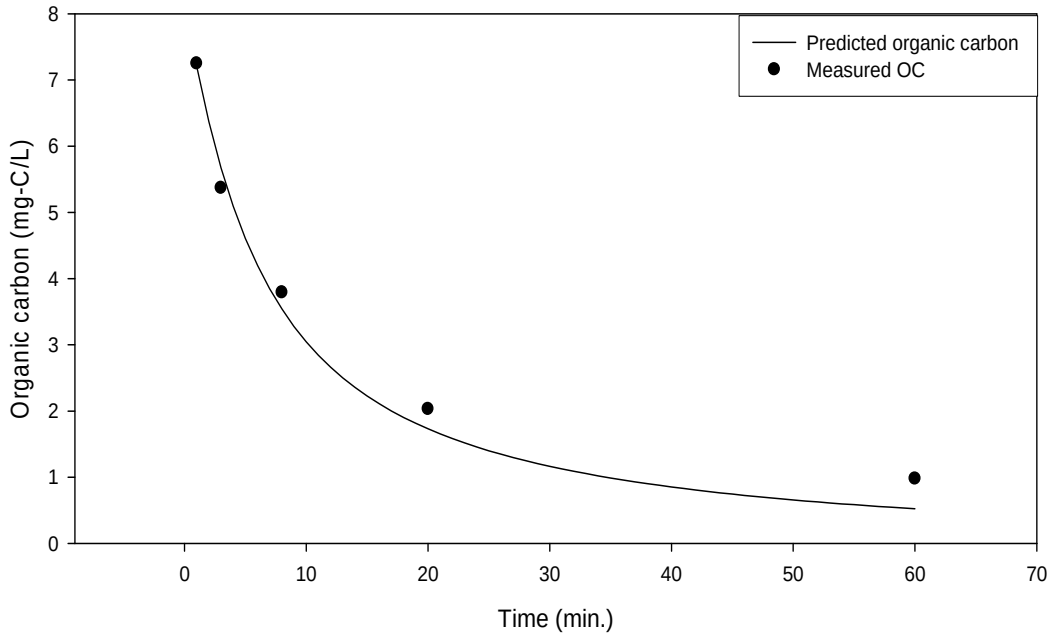

Figure 4.6 c and d Comparison of model predicted and measured TSS, TVC, OC concentrations, and D_{50} during the STORM resuspension period.

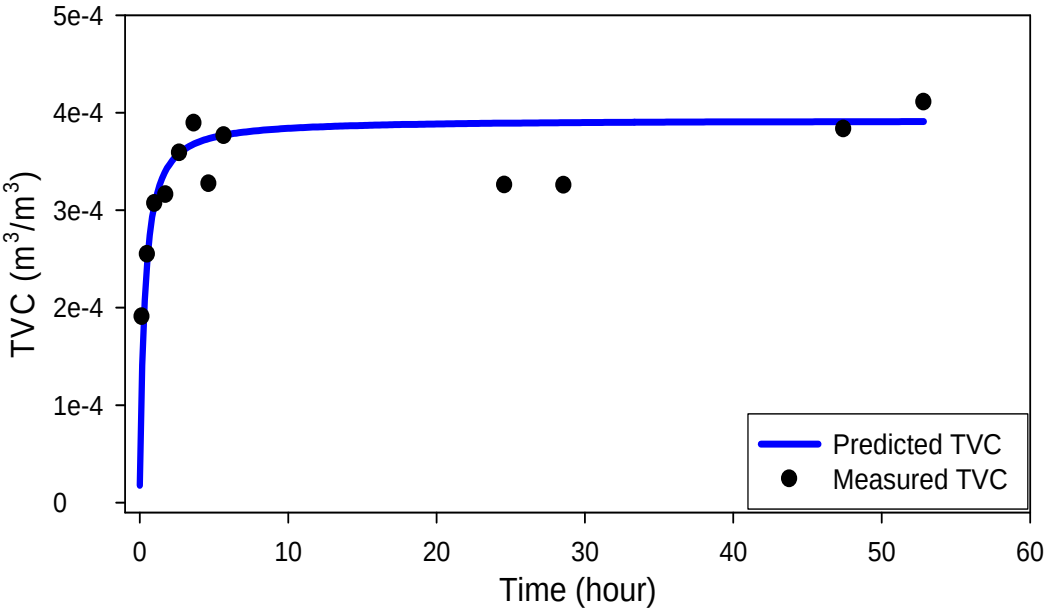

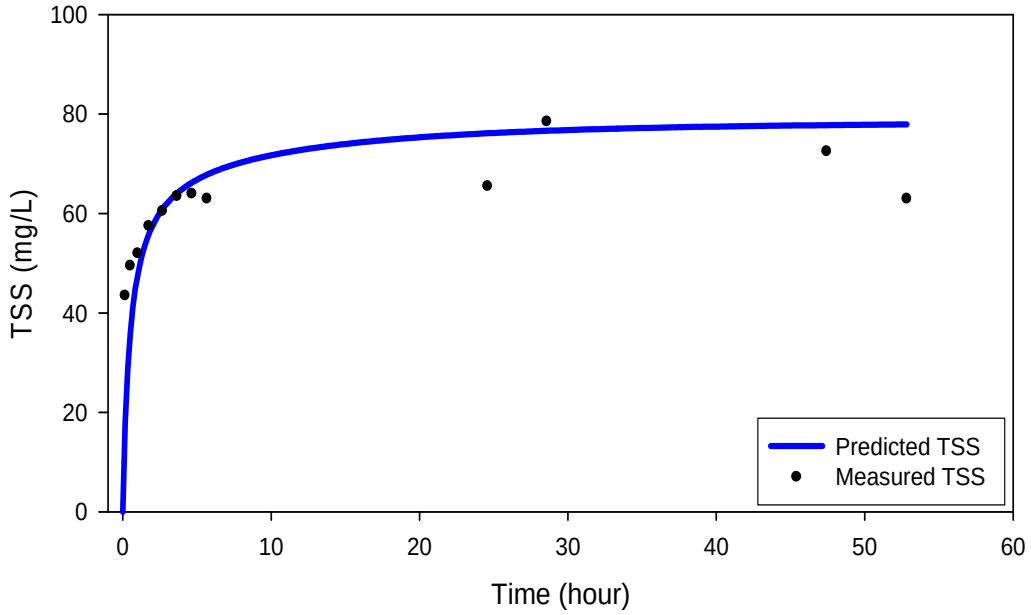

Figure 4.6 e and f Comparison of model predicted and measured TSS, TVC, OC concentrations, and D_{50} during the STORM resuspension period (continued).

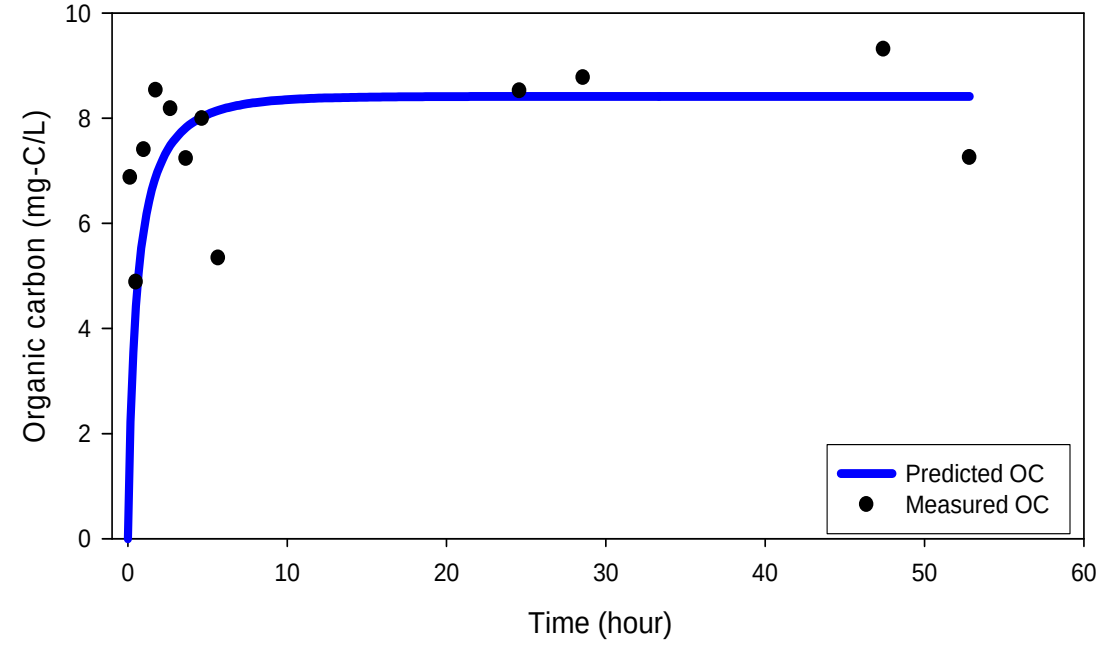

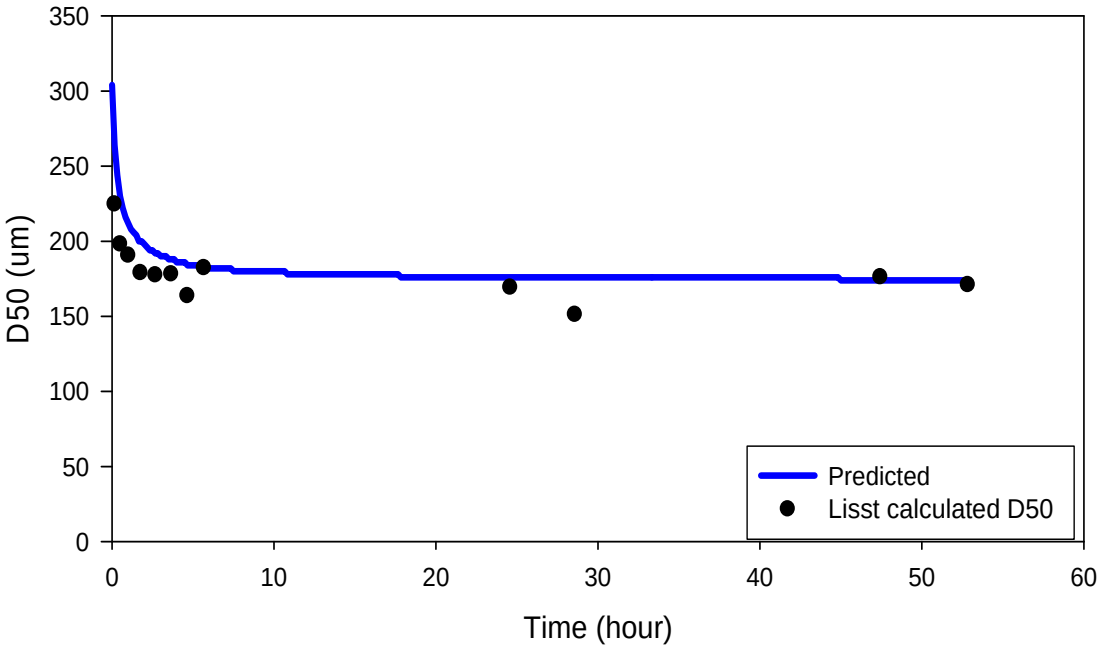

Figure 4.7 Comparison of measured and model-predicted TSS and OC concentrations among four scenarios.

	Scenario name	density (g/cm^3)	Settling velocity equation.
Three scenarios without the flocculation:	**1. diatom**	1.05	Stokes' Law
	2. field data estimated based	1.65	Stokes' Law
	3. clay	2.65	Stokes' Law
This model: One scenario with the flocculation:	**4. flocculation**	varied with floc composition	Winterwerp

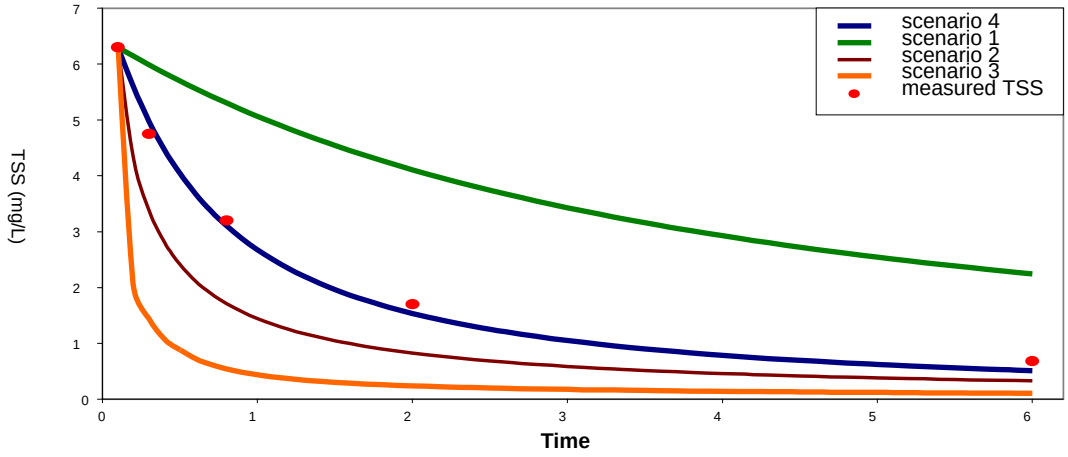

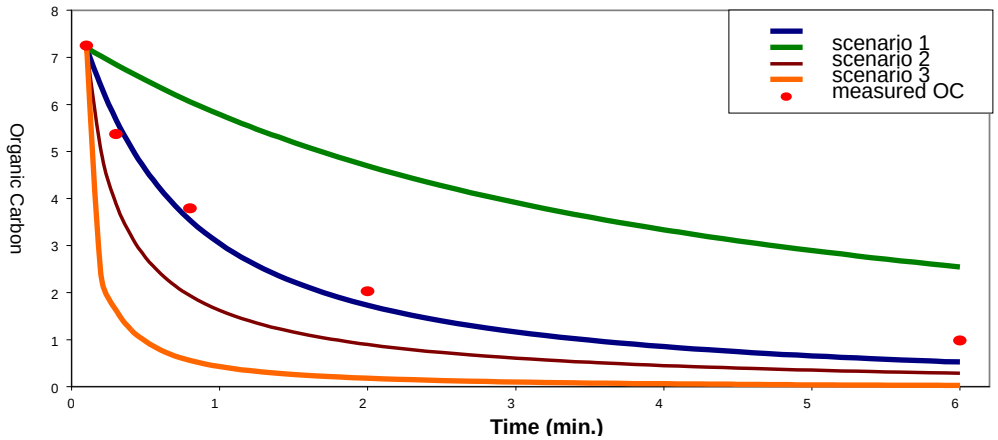

Table 4.1: The final parameter values at the end of calibration.

nf	2.3	Fractal factor (dimensionless)	Model assumption
D_P	2	Primary particle size (μ m)	Model assumption
α_{Clay}	0.1; 0.4	Stickiness coefficient (w/wo stress)	Calibrated value
$\alpha_{biotic\_substrate}$	0.5; 0.8	Stickiness coefficient (w/wo stress)	Calibrated value
M	2.3E-9	Eroded mass flux (kg/m^2 sec Pa)	Calibrated value
ρ_{water}	1E6	density of water (kg/m^3)	Model assumption
$\rho_{biotic\text{-}substrate}$	1.05E6	density of biotic substrates (kg/m^3)	Model assumption
ρ_{clay}	2.65E6	density of inorganic solids (kg/m^3)	Model assumption
μ	1	dynamic viscosity of fluid (g/m-sec)	STORM data
τ_c	0.0998	critical stress (dynes cm^{-2})	Calculated value
τ_b	1	bottom shear stress (dynes cm^{-2})	STORM data
g	9.81	Gravitational acceleration (m/sec^2)	Default value

Table 4.2: Impact of f_{OC} distribution on the behavior of OC. `2337890

f_{OC} = small flocs dominated initial distribution

stickiness coefficient	**0**	**0.2**	**0.4**	**0.6**	**0.8**	**1**
[TOC] at SS	36.3	30.7	28.6	27.3	26.0	25.8
TOC [time hr.] reaching SS	190.5	123	71.3	50	41.5	31.5
TSS Residence time [sec]	1107	1002	909	909	909	870
OC Residence time [sec]	2987	2529	2353	2249	2174	2120
Ws TSS weight avg [cm/sec]	0.09	0.10	0.11	0.11	0.11	0.11
Ws OC weight avg [cm/sec]	0.03	0.04	0.04	0.04	0.05	0.05

f_{OC} = even initial distribution

stickiness coefficient	**0**	**0.2**	**0.4**	**0.6**	**0.8**	**1**
[TOC] at SS	9.2	8.7	8.3	8.0	7.8	7.6
TOC [time hr.] reaching SS	50	47.3	43	37.5	32.2	27.7
TSS Residence time [sec]	769	667	667	625	625	625
OC Residence time [sec]	769	714	667	667	625	625
Ws TSS weight avg [cm/sec]	0.13	0.15	0.15	0.16	0.16	0.16
Ws OC weight avg [cm/sec]	0.13	0.14	0.15	0.15	0.16	0.16

f_{OC} = varied initial distribution

stickiness coefficient	**0**	**0.2**	**0.4**	**0.6**	**0.8**	**1**
[TOC] at SS	7.3	7.2	7.1	7.0	7.0	6.9
TOC [time hr.] reaching SS	10.8	10.2	9.5	9	8.5	8.2
TSS Residence time [sec]	711	667	667	625	625	616
OC Residence time [sec]	600	588	588	588	588	567
Ws TSS weight avg [cm/sec]	0.14	0.15	0.15	0.16	0.16	0.16
Ws OC weight avg [cm/sec]	0.17	0.17	0.17	0.17	0.17	0.18

Study 5. Erosion of Activated Carbon-Amended River Sediments Under Controlled Experimental Conditions.

These experiments address key project questions of whether treating contaminated Grasse River sediments with AC alters their physical properties, especially cohesion, erodibility, and tendency to form flocs. The long-term feasibility of *in situ* remediation depends on the stability of the treated sediment. These experiments explored three questions: how does the erodibility of AC compare to that of native sediment? does adding AC to sediments at treatment levels change the sediment properties? and, are the added AC particles resuspended under realistic bottom shears, either as individual particles or as sediment aggregates?

To explore these questions, we conducted a series of experiments with Grasse River sediment and AC using a bench-scale particle entrainment simulator (PES) (Tsai and Lick, 1986). Three types of particles were tested under different bottom shear stress: AC, untreated Grasse River sediment, and Grasse River sediment amended with 3.43% (by dry weight) AC. Each sediment sample was securely positioned in the PES (Figure 5.1) and re-suspension experiments were conducted according to previously papers (Tsai and Lick, 1986; Latimer *et al*., 1999). Each particle sample was subjected to artificial resuspension under shear stress ranging from 0.05 to 0.4 Pa, using the calibration relationship between grid oscillation frequency and bottom shear developed by Lavelle and Davis (1987). TSS, particle size distribution, total AC, particulate PCBs, and dissolved PCBs were measured at the end of each shear stress period. The PES was run for 30 minutes at each shear stress level to ensure SPME fiber having enough time to absorb dissolved PCBs.

Figure 5.1. Schematic view of PES (Latimer et al., 1999)

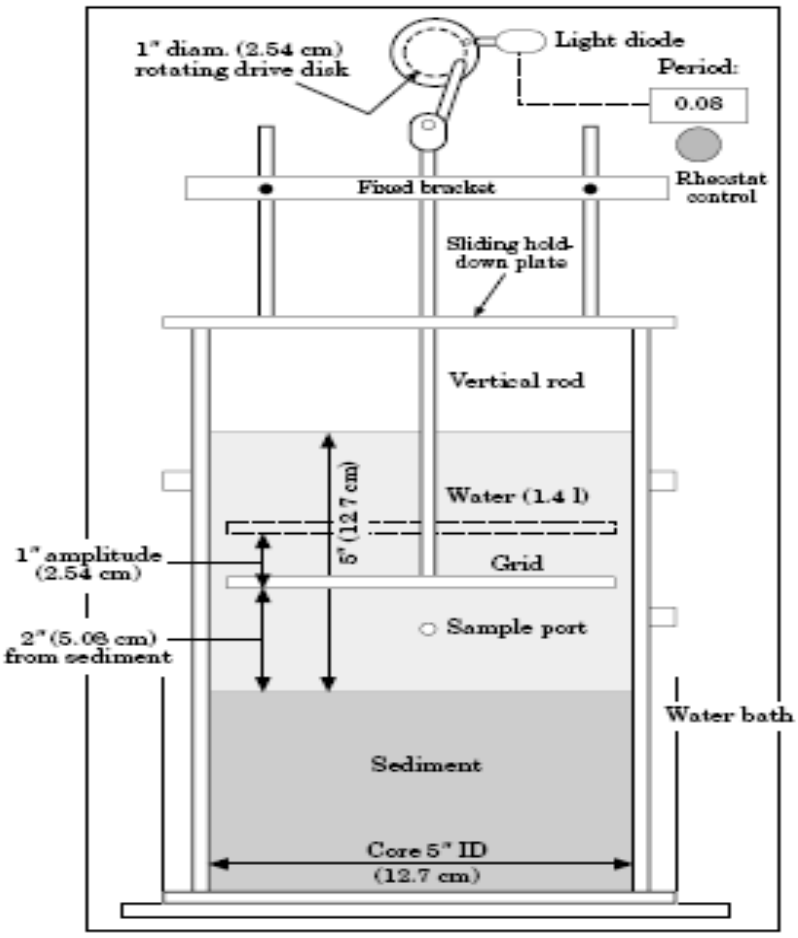

Table 5.1 shows the critical shear stress (τ_C) for 3 types of particles, as determined by the minimum shear required to visually resuspended material. AC has the smallest τ_C value due to its relatively large particle size, low density, and lack of self-aggregration. The Grass River sediment showed a two-stage τ_C. Because Grass River sediment shows a non-uniform particle size distribution (Figure 5.2), the first τ_C, corresponded to erosion of the fine particles while the second τ_C reflected erosion of larger particles and flocs. Adding AC

to the Grass River sediment decreased its critical shear stress, indicating the amended sediment is more susceptible to re-suspension.

Figure 5.2

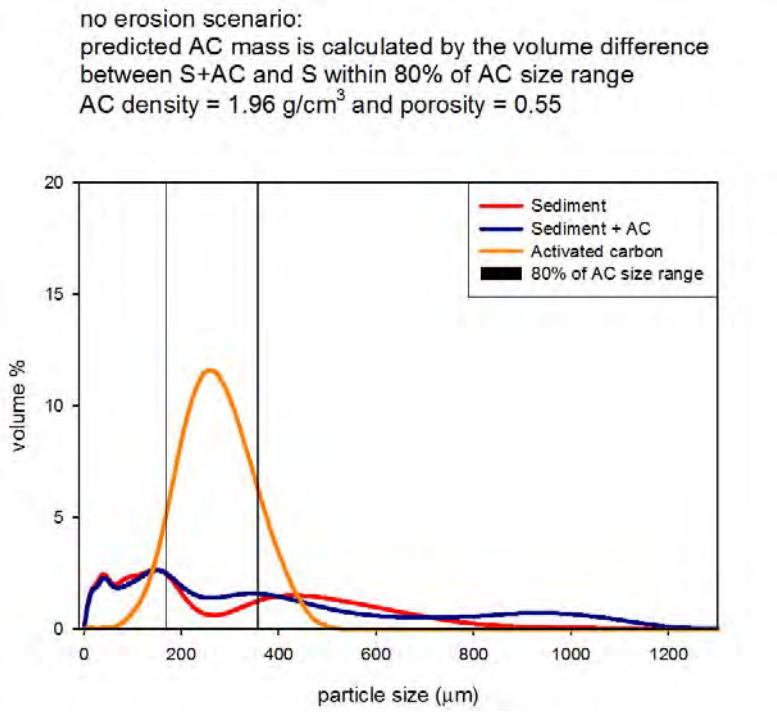

Table 5.1

T_c	Active Carbon	Sediment	Sediment + Active Carbon
Initial shaking	0.033	0.048	0.045
Erosion begins	0.033	0.080	0.070

T_b for upper Chesapeake Bay = 0.2 - 0.8 Pa

T_C for upper Chesapeake Bay = 0.2 - 0.28 Pa

Figure 5.3 shows the relationship between TSS and bottom shear stress. In general, the TSS concentration increased with higher shear stress for all sediments.

Figure 5.3

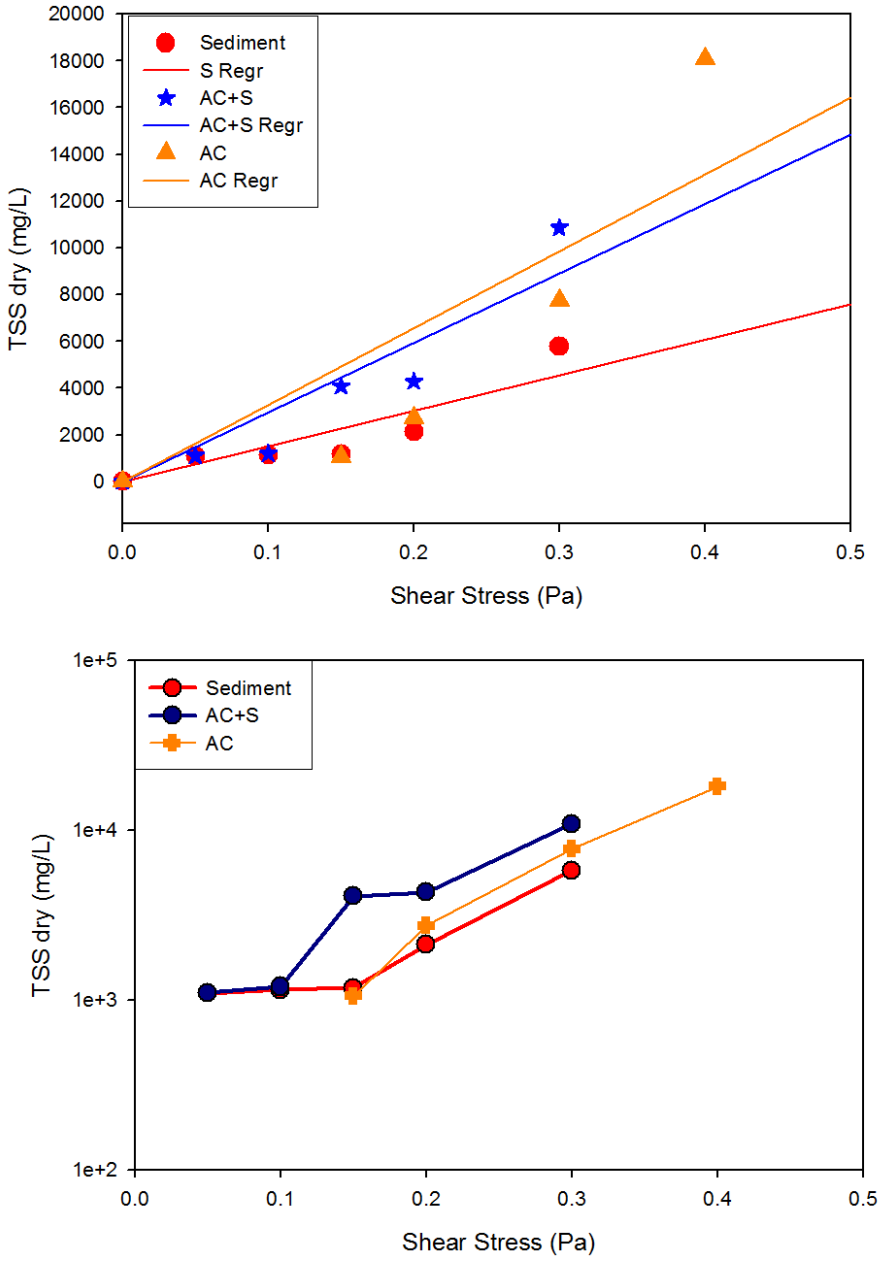

These experimental results are similar to those reported by Tsia and Lick (1986). Under low shear stresses, the suspended solids concentration increased very little, with larger increases occurring only beyond 0.1 Pa. At a given level of bottom shear, more treated Grass River

sediment is resuspended relative to untreated sediment, consistent with the measurements of D_{50} and τ_C for treated and untreated sediments (Figure 5.4).

Figure 5.4

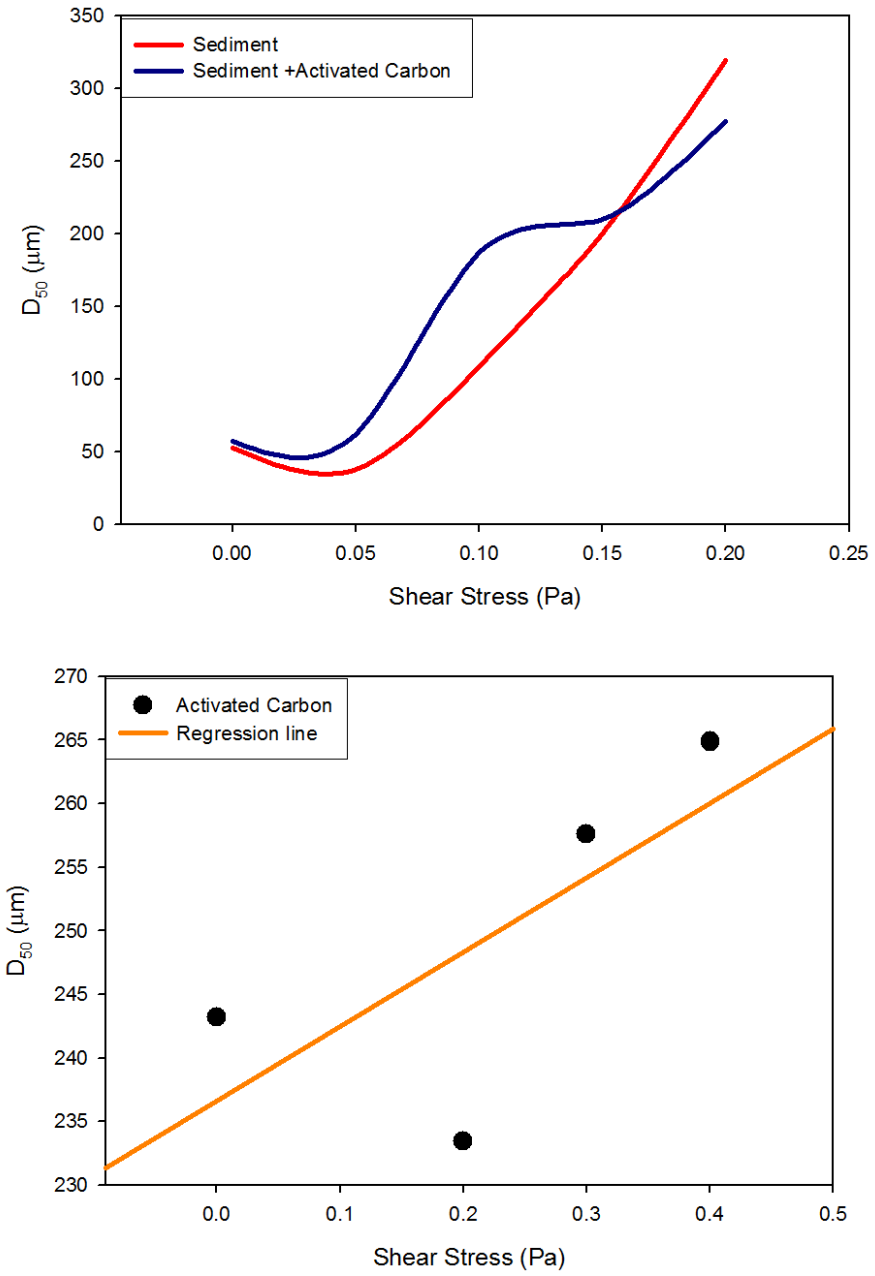

Two possible factors that may explain this observation are: added AC may alter the physical properties of the sediment and mixing of the sediment with added carbon for 30 days may have altered the grain size of the amended sediment. In addition, D_{50} increased with increasing τ_C, which suggests that resuspended Grass River sediment forms flocs.

The amount of AC resuspended under each applied bottom shear was estimated from the measured particle size distributions as follows. The AC has a narrow particle size range with D_{50} ~238 µm. The contribution of AC to the amended sediment was first calculated from the additional volume concentration of particles in the AC size range (using a range that included 80% of the AC size distribution) in the treated versus untreated Grass River sediment, assuming AC density = 1.96 g/cm^3 and porosity = 0.55. The calculation result (3.47%) is similar to the known amount of added AC % (3.43%), validating the approach. Figure 5.5 showed the particle size distribution between two types of sediments along with four bottom shear stress levels.

Figure 5.5

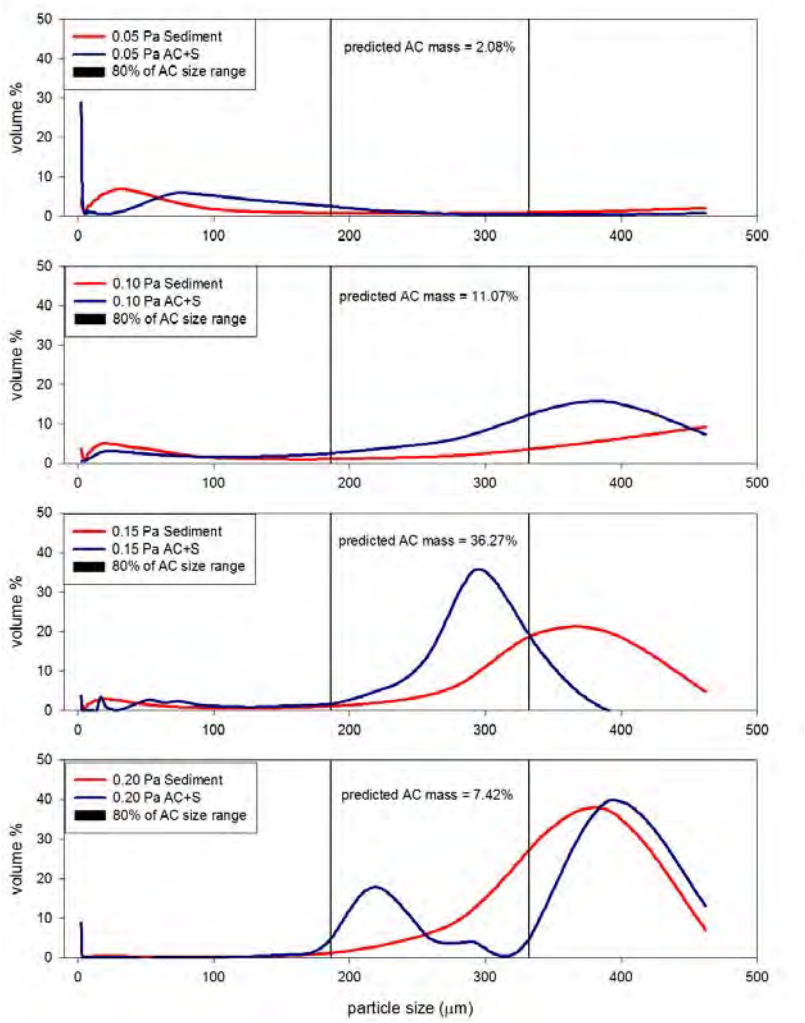

The predicted contribution of AC to the suspended solids pool increased with shear stress, and indicates that AC is selectively resuspended relative to bulk Grasse River sediment.
These laboratory experiments confirm that amending river sediments with AC to reduce PCB bioavailability may enhance the sediment resuspension and transport of PCB-enriched AC particles in the overlying water. Modeling simulations (see Study 6 below) suggest that although the PCB flux from the sediment to the water column due to erosion may be enhanced by the amendments, very little of the eroded PCB is released into the more bioavailable dissolved phase in the water column.

Study 6. Modeling the Impact of Flocculation on the Fate of PCBs during the Resuspension Event in an Urban Estuary

6.1 Abstract

A multi-class flocculation-based contaminant fate model was adapted to describe desorption kinetics for contaminants associated with flocculated particles during a resuspension event. The model was effective in predicting transport of hydrophobic organic contaminants among different size flocs, water, and two sediment layers. The model also demonstrated the impact of fractal geometry, bottom shear stress, particle composition, floc size, f_{OC}, K_{OC}, and TSS on contaminant desorption rates and residence times. Under different scenarios, results from this model supported the importance of multi-floc-size, sediment-water interaction, and of flocculation on the contaminant desorption rate in the water column. Both equilibrium and kinetically-limited models predict the same dissolved and particle contaminant concentrations at steady state. However, during the first three hours of a simulated resuspension event, equilibrium and radial diffusion models overestimate the PCB desorption rate by 50% and 20% respectively. This result suggests equilibrium behavior may not be the best choice for prediction of desorption kinetics during fast events, like dredging, tidal events, or storm water runoff. The radial diffusion model, a common tool to describe desorption kinetics for a single floc, is limited by several factors during a resuspension event, as it fails to include the contaminant exchange with surrounding flocs, it has numerical difficulties in calculating the impact of various boundary conditions, and it ignores indirect impacts on contaminant concentration from sediment-water exchange.

Further, in a floc-rich environment flocculation is an important mechanism redistributing contaminants among flocs. When flocculation is considered in a dynamic particle environment that includes sediment resuspension, settling, and kinetic-limited HOC partitioning, the steady state total PCB concentration in the water column decreases by 20 % and the water column HOC residence time decreases by 36%.

6.2 Introduction

Hydrophobic organic contaminants (HOCs) are important pollutants in urban estuaries. HOCs include polycyclic aromatic hydrocarbon (PAH), PCB, and polybrominated diphenyl ethers (PBDEs). Sorption to resuspended particles and sediments plays an important role controlling the water column residence times and spatial distributions of HOC in aquatic environments. Pollutant residence times and the time required to reach sorptive equilibrium depend on properties of the chemical, of the particles, and of the surrounding environment. If rates are sorption are fast *relative* to particle residence times, HOC behavior may be described using equilibrium partitioning models. In contrast, in highly dynamic particle environments such as algal blooms, shallow water sediment-water interfaces, and during dredging operations, HOC behavior may be better described using kinetically-limited partitioning models. In laboratory studies, sorption of HOC takes from a few hours to a hundred days to reach equilibrium (Lick and Rapaka, 1996; Jespen *et al.*, 1995). The time for HOCs to reach sorption equilibrium with algae also varies from a few minutes to a few days (Ko, 1994). Many studies suggest that PCB sorption can be described as sequential rapid

(labile) and slow (resistant) steps. Carroll *et al*. (1994) suggest that the labile stage be defined as that which is adsorbed within 24 hours and a resistant stage as that which requires over one year to fully absorb. Other studies have made similar observations, finding that the first stage could be as fast as 15 minutes for PCBs in algae (Ko, 1994) and 4.5 hours for PCBs in Hudson River sediment (Schneider, 2006). The second stage may last more than 200 days for PCBs in intact sediment (Werner *et al.*, 2006). The time for each stage varies according to the type of particles examined and the molecular weight of the PCBs.

In the water column, particles are transported by many mechanisms, including water flow, sedimentation, resuspension, and grazing by biota. In the field, the particle settling velocity has a wide range (from 0.01 m day^{-1} to in excess of 100 m $day^{-1)}$ depending on the particle size, shape, and bulk density (Graf and Rosenberg, 1997; Stemmann *et al.*, 2004). Therefore the particle residence time in a 1 meter water column varies from less than 15 minutes to longer than 24 hours. Sediment resuspension, another important particle transport mechanism, occurs when the bottom shear stress generated by wind, current, or human activity exceeds the critical shear stress required to lift a particle off of the bed. In the Upper Chesapeake Bay, the resuspension flux reached up to 82.5 g m^{-2} day^{-1} (Sanford, unpublished). Particle residence times in the deep ocean or in closed engineered systems may be months or years, but in a dynamic environment such as Baltimore Harbor the particle residence time in the water column maybe less than 4 hours due to strong water currents and upstream flushing. Human activity including boating and dredging may also increase particle residence times.

The process of aggregation resulting from the attachment of particles colliding with each other is called flocculation. It is an important internal transport processes affecting the particle residence time in the water column. Coagulated particles are formed either in the water column or on the sediment surface, often facilitated by microbial communities. Recent research has noted the importance of flocculation in the fate of HOCs, including that flocs will affect the fate of HOC by altering the measured partition coefficient, OC content, and sorption rates (Alkhatib and Weigand, 2002, Wu and Gschwed, 1986; Borglin *et al*., 1996, Jepsen *et al.*, 1995; Ko *et al*., 2003; Lick and Rapaka, 1996; Rounds and Pankow, 1990). The flocculation rate is a function of the stickiness coefficient and collision probability. The three major mechanisms that control collision probability are Brownian motion, differential settling, and fluid shear stress (O'Melia, 1972). The stickiness coefficient α is defined as the ratio of the particle attachment rate and the particle collision rate. Edzwald *et al*. (1974) indicated that this step is concerned with eliminating or nullifying the repulsive energy barrier that exists between the two particles. In general, exopolymeric material, suspended solids concentration, ionic strength, pH, temperature, algae type, and algae concentration are the major factors that determine the stickiness coefficient (Edzwald *et al*., 1974, Gibbs, 1983, Kiorboe and Hansen, 1993, Liss *et al*., 1996; Elmaleh *et al*., 1996; Rengasamy *et al*., 1996; Crump and Baross, 2000; Jun *et al*., 2001; Han and Kim, 2001; Hamm, 2002). The time to form flocs may vary from a few seconds to a few days and depends on the particle character and features of the surrounding environment, including water column depth, salinity, shear stress, and temperature (Jackson, 1989).

The question follows as to whether the population of particles changes fast enough that HOCs do not have sufficient time to reach sorptive equilibrium. If the answer is positive, how does rapid particle transport affect the HOC's sorption rate? In the water column, under conditions with rapidly changing particle populations like resuspension events

and algae blooms, dissolved HOC concentrations in the water column are affected in many ways. For example, if the time for a resuspended particle-associated contaminant to resettle to the bottom is shorter than the time for the HOC to reach sorptive equilibrium, less contaminant is desorbed into the water column. Further, rapid increases in phytoplankton biomass results in an under-saturation of HOC concentrations in the algae relative to equilibrium (Swackhamer and Skoglund, 1991; Ko, 1994). Under these conditions, the chemical contaminant diffusion gradient from water to phytoplankton is strongest during peak primary production (Dachs and Eisenreich, 2000). Resuspension events also last on the order of a few hours to a few days and are significantly shorter than the time needed to reach sorptive equilibrium. Cheng *et al*. (1995) compared the particle residence time under the impact of turbulence with the PCB residence time for the Buffalo River. They concluded that the PCB residence time was much longer than the particle residence time during the resuspension period under all scenarios.

For an internal process like flocculation, the time to reach sorptive equilibrium for HOC and the time to form flocs both vary widely, and we can not easily determine which process is faster under a given condition. Lick and Rapaka (1996) conducted a series of experiments to examine the relationship between the time required for floc size to reach steady state and the time required to reach sorptive equilibrium under a given suspended solids concentration and water column shear stress. Under certain environments, like those with higher TSS concentrations, the time to form flocs is faster than the time to sorptive equilibrium (Lick and Rapaka, 1996). However, their experiments also involved a dynamic disaggregation process. Therefore, the time difference between forming a single floc with flocculation process and a sorbing PCBs to the reach equilibrium is still not clear.

Recent research has noted the importance of flocculation on the fate of HOCs, including that flocs will affect the fate of HOCs by altering the partition coefficient, the OC content of the flocs, and the sorption rates (Alkhatib and Weigand, 2002, Wu and Gschwed, 1986; Borglin *et al*., 1996, Jepsen *et al.*, 1995; Ko *et al*., 2003; Lick and Rapaka, 1996; Rounds and Pankow, 1990). Flocculation can impact the fate of HOC in two ways. The direct impact is changing the mass transfer velocity that controls the sorption process. Mass transfer velocity is a function of floc size, porosity, K_{OC}, f_{OC}, the molecular diffusion coefficient, and floc dry density. The porosity, floc size, contact area, f_{OC}, and dry density vary as flocs are formed. The second indirect impact of flocculation on HOC cycling results from changing the particle water column residence times. When flocs are formed, the particle settling velocity changes and the adsorbed contaminant have different residence times in the water column.

The particle size distribution varies with time in the water column as flocs are formed and change properties. Contaminant partitioning also varies in the water column due to changes in f_{OC}, the particle porosity, the diffusion distance from particle distance from center to the shell, and the particle dry density. Several papers have discussed the relationship between grain size and field measured partition coefficient for methyl-mercury and HOCs in the sediment, water, and atmosphere (Krauss and Wilcke, 2002; Hayes *et al.*, 1998). These papers suggest the contaminant residence time changes along with the variation of particle contact area. Schneider *et al*. (2007) conducted mesocosm experiments that mimic resuspension and the settling of contaminated upper Hudson River sediment with realistic bottom shear stress and water column turbulence. In that study, they also observed that both

the measured PCB partition coefficient (K_P) and the particle size distribution varied temporally throughout the experiments.

Therefore, the objectives of this paper are to explore the question of how HOC sorption is affected in a rapidly changing particle environment, especially changes resulting from flocculation. Four approaches to modeling HOC sorption have been previously developed to simulate HOC-particle interactions, including equilibrium partitioning (Di Toro, 1985), a single box partitioning model (Oddson *et al.*, 1970), a two compartment diffusion model (Pignatello and Xing, 1996; Gong and DePinto, 1998), and a radial diffusion model (Wu and Gschwend, 1986). Equilibrium partitioning is the simplest approach that assumes dissolved and particulate HOC concentrations are invariant and a function of particle porosity, TOC, fraction of OC, and the octanol-water partition coefficient. A single box partitioning model assumes that sorption process can be calculated as a first order function and controlled by a single rate constant estimated from laboratory experiments. The two compartment diffusion model separates particles into two compartments: an exterior compartment that has a faster exchange rate, and an interior compartment that has a slower exchange rate in order to have better agreement with the experimental data. The radial diffusion model considers the sorption-retarded diffusion within flocculated particles (flocs). Wu and Gschwend (1988) used the radial diffusion model to simulate desorption of HOCs within and between porous particles, the sediment surface layer, and the surrounding water.

In the field, the sorption process shows a two-step sorption behavior and often takes a long time to reach equilibrium (Gong and DePinto, 1998). Therefore, the equilibrium and single box model behaviors are often too simple to predict the fate of HOCs over short periods. Further, both models assume a static particle composition. Therefore, they may poorly estimate the HOC residence time and dissolved and particle-sorbed concentrations in dynamic environments. However, these relatively simple partitioning models may still be applicable for long-term predictions if the short term dynamics average out. Dynamic environments also affect the performance of the radial diffusion model, because this model assumes a fixed boundary on a single particle (Gong and DePinto, 1998). Natural sediment particles have complex composition and therefore it may not be proper to use a single-sized particle like median particle diameter (D_{50}) to represent the entire particle spectrum. Therefore, modelers often adjust the particle size along with other physical and chemical parameters to fit experimental data from resuspended sediment HOC desorption experiments (Werner *et al.*, 2006; Schneider, 2007). Furthermore, the complex boundary condition setting required for the radial diffusion model limits its application when particle properties are varying. Application of the two compartment diffusion model in a dynamic environment has a different problem. Three independent fitting sorption rate constants, including the fraction of exterior particle volume to the total particle volume, the sorption rate between surrounding water and the exterior compartment, and the sorption rate between exterior and interior compartments, must be specified. These input parameters are often difficult to estimate and vary among different experiments or environments.

In an urban estuary, both resuspended and bottom sediment particles show non-uniform, non-normal size distributions (Schneider, 2007). The contaminant also has different residence times or times required to reach steady state, which correspond to the different floc size within the rapidly varying boundary condition. Therefore, models need the ability to simulate how the entire spectrum of particles varies in space (sediment versus water column) and time (*i.e.*, before, during, and after resuspension events). A new model that can

simultaneously simulate the varying particle population and contaminant partitioning would better describe resuspended contaminated sediment in an urban estuary. The model should also be able to simulate the dynamics of particle exchange across sediment/water interface, settling of particles and contaminants through the water column, production of flocs, and HOC sorption and desorption rates.

6.3 Model Development

6.3.1 Objectives and Strategies

1. Develop a model to investigate how flocculation influences the fate of organic contaminants when both HOCs and sorbent concentrations vary rapidly.
2. Evaluate whether a kinetic sorption model more accurately describes the fate of PCBs during a resuspension event compared to equilibrium.
3. Discuss the impact of kinetic processes such as flocculation and erosion/deposition on the fate of PCBs; for example, the time to reach a steady state, the desorption rate, the dissolved and particulate PCBs concentrations at steady state, and the temporal variation in the deviation from sorption equilibrium during the resuspension event.
4. Discuss the differences between D_{50} and multi-floc-size models. This objective responds to the conclusion from DePinto (1998) that the radial diffusion model is too simple and does not reflect the composition and properties of real sediment.

6.3.2 Model Assumptions and Structure

In this work, the structure of the model is optimized for hydrophobic organic contaminants (HOCs), a broad class of chemicals that include PCBs, dioxins and furans, PAHs, many brominated flame retardants, and organochlorine pesticides. The model tracks particles, OC, and HOCs in the water column and in the sediment. In principle, any chemical contaminant with a known affinity for OC can be modeled within this framework. In the previous chapter, the model described the exchange of particles between water and sediment surface layers and related flocculation mechanisms. However, many HOC fate models have emphasized the importance of a deeper sediment layer on the long term HOC fate. Therefore, a deeper sediment layer and related surface-deeper sediment exchange mechanisms are added to the model in this study (Figure 6.1). Porewater also plays an important role in this contaminant model by linking HOC among surficial sediment, deeper sediment, water, and resuspended particles. In this model, porewater HOC is defined as the dissolved contaminant concentration in the sediment layer; it connects the HOC source from the deeper sediment layer and allows diffusive exchange with the overlying water column.

In the STORM resuspension experiments (Schneider *et al*., 2007), properties of the resuspended particles vary with time in many ways. The median diameter (D_{50}) of particles in the water column varied, flocs in the sediment and water column had different D_{50} and particle size distributions, and flocs rapidly exchanged between the sediment and the water column. These observations indicate that flocs properties are not constant during the experiment. In addition, the dynamic resuspension-settling and flocculation processes might cause particle-related HOCs to not have enough time to reach steady state in the water column. The traditional radial diffusion model may fail to simulate the fate of field HOCs because of the complexity of particle properties and the broad particle size distribution, which complicates parameterization and setting boundary conditions. The traditional one box

or two-compartment diffusion models cannot directly model situations where particles are changing rapidly, because both HOCs and related flocs varied rapidly, which violates assumptions of constant particle concentrations and characteristics.

The HOC sub-model simulates chemicals being transported among particles, and uses particle models as a platform to transport HOCs among flocculated particles, surrounding water, sediment porewater and sediment particles. This model also tracks the fluxes of particle-related HOCs among all particle size clusters. These fluxes include both flocculation and resuspension-settling. To resolve the above concerns and achieve the study objectives, a new kinetically-limited diffusion model was developed.

First, we assume that the HOC will immediately reach equilibrium or become well-mixed between pore water and solids within each flocculated particle to simplify the boundary condition and numerical techniques. For example, it is difficult to set the intra-floc HOC distribution and related boundary condition after two different size flocs coagulate to form a new larger floc. To compensate for the overestimated HOC concentration gradient, we modified the chemical diffusive exchange rate by including the floc size effect and adjusted diffusion coefficient. Further, to simplify the model, we assumed no stagnant film layer between floc exterior shell and surrounding water in this study. The detail of these assumptions will be explained in the next section.

Second, flocs sizes are varied between 2 and 1000 μm in 1 μm intervals. Each cluster is a state variable and represents a specific size of floc. Number and OC concentrations, particulate HOC concentration, mass transfer velocity, stickiness coefficient, floc density, settling velocity, and f_{OC} are calculated for each cluster simultaneously at each time step. The floc spherical equivalent volume and area are calculated based on floc diameter in each cluster. The volume and mass concentrations vary temporally in each cluster, and the gross dry mass and volume are conserved. In addition, only flocs that contain OC transport HOCs and we assume no diffusion exchange of contaminant into pure inorganic flocs. To include bioturbation and mixing from the deeper sediment layer, the model simultaneously simulates HOCs being transported among the water column, top sediment layer (0.1 cm), and deeper sediment layer (4.9 cm).

6.3.3 Major Model Equations

The water column particle model in this chapter adapts the same equations and assumptions used in the previous chapter:

$$\frac{\partial N_i}{\partial t} = F_i + \left(W_{S,i} / x \times N_i \right) + E_{b,i} \qquad \text{Equation 6.1}$$

where N represents the number of particles of class i per volume, $W_{S,i}$ is the floc setting velocity, F_i is the flocculation effect on particle number balance, x is the water column depth, and $E_{b,i}$ is pure sediment resuspension flux that is given by the sediment erosion model.

Regarding the sediment layer, a few additional terms are added in this chapter. To simulate the particle exchange between the surface and the deeper sediment, this model adapts the strategy from Di Toro (2001) that simulates this process as a simple diffusive exchange. In order to simplify this process, the model ignores consolidation in both layers and focuses on bioturbation exchange. The sediment consolidation rate is relatively slow compared with other mechanisms in a 53 hour simulation period.

$$\frac{\partial N_{i,surface}}{\partial t} = -\frac{m_{1,2}}{(sz_1 \times sz_2)}\left(N_{i,surface} - N_{i,deeper}\right) - E_{b,i} \qquad \text{Equation 6.2}$$

$$\frac{\partial N_{i,deeper}}{\partial t} = \frac{m_{1,2}}{(sz_1 \times sz_2)}\left(N_{i,surface} - N_{i,deeper}\right) \qquad \text{Equation 6.3}$$

where N represents the number of particles of class i per volume in the surface or deeper sediment layer, $m_{1,2}$ is the particle mixed rate between two sediment layers, which is controlled by the bioturbation effect; sz_1 is the top sediment thickness, and sz_2 is the deeper sediment thickness.

The contaminant model simulates HOCs being transported among resuspended flocs, dissolved water, porewater in the sediment, and sediment particles. There are 3000 state variables, including 1000 state variables in the water column and 2000 state varies in the two sediment layers, to represent the HOCs in the flocs from size 2 to 1000 μm. In addition to the state variables for solid HOCs, the model also includes three state variables representing the dissolved HOC concentrations in the water column and in porewater in two sediment layers. In general, each floc state variable gains or looses contaminants through diffusive exchange, and by contaminants 'piggybacking' on the OC flows calculated by the flocculation submodel

$$\frac{\partial HOC_i}{\partial t} = HOC\_flux_{F_N, floc} + J_{i,j} \qquad \text{Equation 6.4}$$

where HOC_i represents the HOC concentration in the floc cluster i with the unit of $\mu g/m^3$, $HOC\_Flux_{Fn,\ floc}$ represents the HOC flux due to particle transport by flocculation, resuspension, settling, or bioturbation in the water column or sediment layer, and $J_{i,j}$ represents the HOC being transported between particles variable i and surrounding water variable j.

In this study, the diffusive contaminant uptake and release has a specific equation to emphasis the temporal varied OC concentration. The rate of diffusive exchange between the dissolved contaminant pool and each carbon phase is calculated as the product of a diffusional gradient and a mass transfer velocity. The diffusional gradient is defined as the difference between the instantaneous contaminant concentration in the carbon phase and that at equilibrium with the surrounding dissolved contaminant concentration. The equilibrium condition, as parameterized by K_{oc}, is an input to the model. The mass transfer velocity equals a velocity term multiplied by the specific interfacial area of the carbon phase. Overall, the bi-directional diffusive flux equals:

$$J_i = k \times A \times N_i \times \left(HOC_{dissolved} - \frac{HOC_i}{OC_i \times K_{OC}} \right)$$

where represents the HOC being transported between particles variable i and surrounding water variable j, k is the mass transfer velocity (m/sec), A is the specific interfacial exchange area (m^2/floc), OC_i is the OC state variable concentration (g-carbon/m^3), $HOC_{dissolved}$ is the dissolved HOC concentration (ng-HOC/m^3), HOC_i is the particulate HOC state variable i concentration (ng-HOC/m^3), and K_{OC} is the OC normalized partition coefficient (m^3/g-carbon).

The first important element in the diffusion flux equation is that the model includes the mass transfer velocity (k). In this study, we therefore calculate the effective diffusion

Equation 3.5

coefficient based on the dry density, porosity, K_{OC} and f_{OC} of the floc (Schwarzenbach *et al.*, 1993),

$$k = \frac{D^*}{z} = \frac{\phi_f \, fDm}{z \times (K_{OC} f_{OC} \times (1-\phi_f) \times \rho_{f,solid} + \phi_f)} \qquad \text{Equation 6.6}$$

where k is the mass transfer velocity (m/sec), z represents the volume-weighted effective interior diffusion distance, f is the tortuosity factor, ρ_f is floc dry density (g/m^3), φ_f is porosity (m^3/m^3), D* is the adjusted diffusion coefficient (m^2/sec), and D_m is the molecular diffusion coefficient of the chemical in water (m^2/sec).

Since effective interior diffusion thickness, porosity, f_{OC}, and floc dry density vary, either with floc size or temporally, the chemical diffusive exchange rate is not a constant and also varies temporally along with floc size in this study.

The second important element in the diffusion flux equation is that the model includes the total floc contact area. The traditional radial diffusion model describes diffusion within a single flocculated particle. However, the sorption/desorption rate has been observed to vary with particle mass or number concentrations (Schwarzenbach *et al.*, 1993). For example, the dissolved PCB concentration should be higher after resuspending many contaminated particles than for adding a single particle during a given time period. To simulate this effect, the total diffusion contact area has been added to the diffusion equation as the product of area per floc (A, m^3/floc) and total floc number concentration (N, number of flocs/m^3). This raises the question of how to estimate the area per floc. Our model is based on the floc volume being equal to that of spherical primary particles combined in flocs following fractal geometry (Winterwerp, 1998). Therefore, the method of estimating the interior floc contact area per aggregated particle becomes complex. The distance between the floc center and the shell is floc radius r. Therefore, the contact area per floc particle is simply estimated as $4\pi r^2$.

Many papers suggest effective radial diffusional distance should be equaled to half the floc radius to estimate the effective of floc thickness (Gong and DePinto, 1998; Werner *et al*, 2006). In this study, the volume-weighted average distance (z) from the interior of a sphere to the outer shell of the sphere is R/4 instead of R/2, where R is the radius of the sphere (Sanford, personal communication) (Figure 6.2). The radial diffusion model calculates that during resuspension into clean water the HOC concentration will be highest at the floc center and will approach $HOC_{dissolved}$ at the outer shell, where $HOC_{dissolved}$ represents the dissolved concentration in the surrounding water or stagnant film layer. However, in this study we assume a uniform HOC concentration distribution within the modeled floc particle sphere shell as explained in the previous section. Therefore, with this assumption, the mass flux may overestimate the flux because the concentration difference is too great. As a result, we need to compensate for the concentration gradient (Sanford, personal communication). To calculate the volume-weighted mean distance from any point in the interior of a sphere to the outer shell of the sphere, the distance from the center of the sphere is defined as r and the radius of the sphere as R: The distance to the outer shell is (R-r) and the appropriate weighting for each of these distances is the area of the internal spherical shell of radius r. Thus, the volume-weighted average radial diffusional distance is R/4 instead of R/2:

$$(R-r) = \frac{1}{\frac{4}{3}\pi R^3} \int_0^R 4\pi r^2 (R-r) dr = \frac{\frac{1}{3}\pi R^4}{\frac{4}{3}\pi R^3} = \frac{1}{4} R = z \qquad \text{Equation 6.7}$$

6.3.4 Numerical Methods, Parameterization, Boundary Conditions, and Initial Conditions

The model requires an initial concentration for each floc size, and STORM experiment measurements (Schneider *et al*., 2007) are applied as model initial conditions. Initially only sediment layers contain HOCs and we assumed HOCs reach equilibrium between flocs and porewater in the sediment layers for all size of flocs, calculated using the given K_{OC}, OC size distribution, and experimental measurements. The f_{OC} distribution derived in Chapter Two is used to initialize the sediment carbon.

Several parameter values and initial conditions were estimated from the combination of observations during the STORM experiment and literature reports, including the fractal factor, the characteristics of the primary particle, porosity, and initial particle volume and f_{OC} size distribution. In this chapter, these parameters are derived using the strategies and references in Chapter 2. K_{OC} was estimated by measurements in the STORM tank experiments at steady state and varied among the different PCB congeners. The molecular diffusion coefficient was back calculated by algae PCB uptake rate from Ko (1994), the porewater-water diffusion coefficient was selected from the Lake Michigan PCB model (2007), and the sediment bioturbation rate was chosen from Di Toro (2001).

The system of equations was solved for 1000 floc sizes for each variable. The model was written in double precision Fortran 90 and uses a fourth-order Runge-Kutta numerical algorithm to solve the set of nonlinear ordinary differential equations. The model is numerically stable with a time step of one minute, and a 53 hour simulation is completed in 75 CPU minutes on a Sun Ultra-60 workstation. Total dry mass, total particle dry volume, and total contaminant mass in the system are monitored to insure conservation of solids and contaminant mass during the simulations.

6.3.5 The Impact of Floc Property on the Mass Transfer Velocity and Desorption Rate

Mass transfer velocity (k) is a function of floc size, porosity, K_{OC}, f_{OC}, D_m, and floc dry density. It is the most important parameter in the radial diffusion model controlling the sorption/desorption rate. The first objective of this section is to test the response of mass transfer velocity by using our new diffusion equation with the given conditions. The second objective in this section is to discuss the impact of these variables on the HOC desorption rate.

To have a better understanding of the mass transfer velocity in this new diffusion model, several simple model scenarios and assumptions are tested in this section. Initially, the impact of fractal geometry, total contact area, and the concentration gradient between dissolved and particulate phases are ignored to explore two different porosity-size distributions. The first and simplest relationship is that all flocs have the same porosity. The second relationship is that the porosity and floc size follow fractal geometry.

6.3.5.1 The Influence of Constant Porosity on the Desorption Rate

In the first case, the floc porosity is constant for all sizes, resulting in the mass transfer velocity decreasing with floc size, which implies that HOC require a longer time to diffuse to the floc outer edge in larger flocs (Figure 6.3a). Further, based on the equation 6.5, a faster desorption rate should be observed in the higher mass transfer velocity run. Table 6.1 shows the settings and the corresponding assumptions of Runs 1 to 7. Based on Equation 6.6, the mass transfer velocity will increase with increasing D_m and porosity, and decrease with

increasing floc size, K_{OC}, f_{OC}, and solid density. As shown in Figure 6.4 and Table 6.1, the desorption rate has a strong positive correlation with the mass transfer velocity. Results from Run 1 to Run 7 demonstrate that our new HOC fate model follow the proper trends, namely that the desorption rate increases with increasing D_m and porosity, and decreases with a increasing floc size, K_{OC}, f_{OC}, and dry floc density.

We next discuss the impact of more than one parameter or variable on the desorption rate. From Run 1 to Run 7, we observed that the mass transfer velocity increases with some parameters and decreases with others. However, when two or more parameters influence the mass transfer velocity calculation, their combined effect on the desorption rate is not clear. For example, when f_{OC} is increased the particle solid density also decreases since OC is less dense than clay. An increase in K_{OC} should lead to a decrease in D_m and an increase in floc size should result in an increase in porosity. However based on the Run 1 to Run 7 results, these parameters have the opposite influence on the mass transfer velocity calculation and trend in the desorption rate.

Lick and Rapaka (1996) also observed that the run with larger floc, lower solid density, and higher porosity has a faster desorption rate than the run with smaller floc, higher solid density, and lower porosity. Lick's experimental data can be used to examine the impact of more than one parameter or variable on the desorption rate (Runs 8 and 9, Table 6.1 and Figure 6.5). These model runs ignore the impact of TSS, fractal geometry, total contact area, and the gradient between dissolved and particle HOCs. The model simulation results agree with the observations of Lick and his colleagues that the larger and more porous flocs showed a faster desorption rate than small and lower porosity flocs.

6.3.5.2 The Influence of Size-Dependent Porosity on the Desorption Rate

In the model runs above, we assumed porosity is constant for all floc sizes to isolate the influence of porosity independent of size-specific behavior. Here the particle sub-model is based on fractal geometry and to emphasize the importance of flocs the fractal factor was set less than 3.0 and greater than 1.0 in all runs. Here we explore the influence of fractal geometry on the HOC mass transfer velocity (Figure 6.3b). The floc character described by Lick and Rapaka (1996) has a similar trend in the mass transfer velocity as predicted using fractal geometry. When the fractal factor is less than 3.0, the larger floc has a lower solid density and a higher porosity. One interesting finding is that for a given fractal factor the mass transfer velocity only varies significantly for smaller flocs. For mid- to large-sized flocs, the dependence of the mass transfer velocity on floc size is very limited. There are two points in this section: First, discuss how fractal geometry impacts the mass transfer velocity. Then discuss the impact of fractal geometry on the total contact area, concentration gradient, desorption rate, and diffusion equation.

To simplify the model setting, in this section the influence of the total contact area and the concentration gradient between the dissolved and particulate phases are ignored. Therefore, for a given floc size the runs with the higher fractal factor contains less porous flocs and smaller mass transfer velocity (Table 6.2). For a given fractal factor, larger flocs have higher porosity and higher mass transfer velocity than smaller flocs. In general, based on these assumptions, model results showed a similar trend as the fixed porosity runs in that the desorption rate increased with increasing Dm, and porosity, and decreasing floc size, K_{OC}, f_{OC}, and dry floc density (Figure 6.6).

Next, the model runs allow the number concentration and contact area to vary with mass concentration, fractal factor, and floc size. We have discussed the relationship between fractal geometry and the mass transfer velocity in the previous section. The fractal factor not only impacts the mass transfer velocity because porosity is a function of the fractal factor, but also affects the number concentration for a specified total solid volume and mass concentrations. Also, the diffusion flux is controlled by the mass transfer velocity, total contact area, and concentration gradient between the dissolved and particulate phases. The total contact area is a product of contact area per floc and number concentration, which is determined by the mass concentration, the fractal factor, and the floc size. The detailed model settings are listed in the Table 6.3. The model was executed for 300 simulation days without flocculation, deposition, and erosion. All model runs start with a concentration of 1 ng/g PCB 52. Run 18 behaviors are a reference for runs 19 to 22. Run 19 applies the same parameters except the fractal factor equals 1.5 to increase floc porosity to 0.996; Run 20 increases the floc size from 50 to 120 μm; run 21 doubles the initial f_{OC} of the floc, and run 22 increases the TSS concentration ten fold to examine the influence of total contact area and concentration gradient on the desorption rate.

Most model run results showed similar trends to those in Tables 6.1 and 6.2 that increasing the solid density or decreasing the porosity decreases the diffusion rate (Figure 6.7). However, run 20 showed an opposite result from run 13 regarding to the floc size influence that the net diffusion flux is faster for the smaller floc. A larger floc has a higher mass transfer velocity than a smaller one with the same fractal factor. However, under the same solid mass concentration, the smaller floc has a higher total contact area. Thus, the net product of mass transfer rate (k) and total contact area (A*N) is higher for the smaller floc since the diffusion flux includes the total contact area. Run 22 results also showed the importance of the total contact area. Comparing runs 18 and 22, the mass transfer velocity are the same for both runs because they have the same floc characters. However, run 22 has a higher total contact area in the water column. Therefore, the net diffusion flux is higher in run 22, which is why we observe a higher desorption rate in the sediment than in the water column for the same type of particles. Porosity plays a dominant role in the diffusion flux, and when the fractal factor decreases the difference in desorption rates with particle size diminishes. In some extreme situations, a larger floc has a faster desorption rate than a smaller floc under the same initial conditions due to its high porosity which compensates for the disadvantages arising from the total contact area and size adjustments.

6.3.6 Model Data

Schneider *et al*. (2007) conducted STORM tank experiments that mimic resuspension and settling of contaminated upper Hudson River sediment with realistic bottom shear stress and water column turbulence. The maximum instantaneous bottom shear stress was about 1 dyne cm^{-2} and the volume-weighted average water column turbulence intensity and energy dissipation rate were 0.55 cm s^{-1} and 0.0032 cm^2 s^{-3}, respectively. Hudson River sediment was added to a depth of 5 cm and allowed to consolidate for 10 days. The two periods of this experiment are the erosion and the free settling. During erosion, the mixing paddle continuously generated bottom shear stress for 53 hours to ensure suspended solids reached steady state. During the one hour free settling period, the paddle was then turned off to allow suspended particles to settle. Particle size distribution, dissolved and particulate PCBs, TSS, DOC, particulate carbon, nitrogen, and chlorophyll *a* were measured throughout the

resuspension and settling portions of each experiment. The detailed PCBs measurement methods were reported by Schneider *et al*. (2007).

The flocculation particle sub-model was calibrated using Shear Turbulence Resuspension Mesocosm (STORM) tank experiments. Further, STORM tank experiments also provided data for the HOC sub-model, including the initial sediment PCB concentration and the K_{OC} parameter value. Later, results from the HOC sub-model are compared without further calibration with the STORM experiment measurements.

6.4 Model Applications

6.4.1 The Impact of Flocculation on the Steady State Contaminant Concentrations and on the Desorption Rate

This section discusses the impact of flocculation and floc transport on the water column residence time of contaminants.

Settings: In this section, the following settings were applied to the model: the fractal factor is equal to 2.0, f_{OC} is equal to 0.1 and the bottom shear stress is the same as the STORM experiment as 1 dyne cm^{-2}. Particles are assumed to be well mixed in the tank without disaggregation, deposition or erosion or any other interaction with sediment layers. The model was executed for 300 simulation days beginning with 1 ng/g of PCB 52 on 50 μm flocs without flocculation in the base case run (Run 23). Run 24 and Run 25 had the same settings except the stickiness coefficient was increased from 0 to 0.25 and 0.5 respectively. Run 26 had the same settings as the base case run except the1 ng/g of PCB 52 began on 400 μm flocs. To examine the impact of flocculation on contaminant residence time, the model used data from the STORM free settling period for the floc submodel settings and for initial conditions in the contaminant submodel.

Results and discussion: Table 6.4 showed the detail model simulation results in all runs. The run with flocculation had a slower PCB 52 desorption rate than runs without flocculation (Figure 6.8), consistent with previous results described above that the PCB desorption rate is slower for larger flocs than smaller flocs under the same initial conditions. These results are also consistent with the concept that the number concentration or total contact area is a dominant factor controlling the diffusive flux. Larger flocs have a faster desorption rate due to higher porosity and corresponding higher mass transfer velocity. However, as mention above, the diffusive flux is also controlled by the total contact area. Under the same solid mass and fractal factor value, larger flocs have a lower number concentration than smaller floc, which impacts the desorption flux. Therefore, desorption rate for run 23 was 50% faster than run 26. Desorption rates calculated from runs 24 and 25 were slower than from run 23, because large flocs were formed faster with the higher stickiness coefficient. Therefore, the total water column contaminant residence time decreases with enhancing flocculation process.

There in no sediment resuspension during the STORM free setting period, highlighting the influence of flocculation on contaminant residence time. With flocculation (Run27), the total water column HOC residence time is five times shorter than without flocculation (Run 28) (Figure 6.9). Because the particulate HOC residence time is shorter in the flocculation run larger flocs formed. This result implies that in calm floc-rich water the particulate HOCs are transported more quickly from the water column to the surficial sediment.

6.4.2 The Impact of Deposition-Erosion on the Steady-State Contaminant Concentrations and Desorption Rate

Previous flocculation models (Lick and Rapaka, 1996) did not simulate sediment erosion and settling under realistic bottom shear stress, and were designed with well-mixed sediment particles forming flocs during a long mixing period. However, during shorter events, such as tidal periods, or in dynamic environments, contaminated particles might not have enough time to desorb contaminants to the surrounding water. This is especially true for large particles. The objective of this section is to discuss the impact of deposition and erosion on the PCB desorption rate under realistic bottom shear stresses.

Settings: In this section, the following settings were set for the model: the fractal factor is equal to 2.0, f_{OC} is equal to 0.1, and flocculation is not included in the three runs. The sediment PCB 52 concentration is 702 ng/g-carbon, consistent with the STORM measurements. The model was executed for 300 simulation days three separate times, with the bottom shear stress equal to 0, 1, and 2 dyne/m^2 (Run 29, Run30, and Run 31) respectively.

Results and discussion: In Figure 6.9 PCB 52 desorption rates are compared between runs with no erosion and with two different bottom shear stresses. In general, because these runs ignore flocculation, the higher bottom shear stress run erodes more flocs from the sediment to the water column. The results are consistent with runs discussed in the previous section that showed that higher TSS increases the desorption rate because more flocs are eroded from the sediment to increase the total floc contact area in the water column.

The PCB desorption rate is faster in the run without erosion and settling compared with the run under identical conditions except particles are exchanging between the sediments and overlying water (Figure 6.12). This trend was observed more clearly for the larger flocs or after including flocculation. The overall PCB desorption rate is slower in the desorption-erosion run for two reasons. As showed in the Figure 6.11, the porewater contaminant reaches equilibrium in a short time because of the higher concentration of solids in the sediment. Thereafter the contaminant has a smoother diffusion gradient between sediment and porewater to decrease the desorption rate. Second, the time that flocs remain in the sediment due to deposition will delay the overall desorption rate than the run without deposition-erosion. In past studies, particles are often entirely suspended in the water column under a given bottom shear stress with no deposition, which may lead to errors in estimates of the desorption rate.

In the previous section, we developed a basic understanding of impacts from diffusion, flocculation, and resuspension-settling mechanisms on the HOC diffusion rate. Now we can begin to discuss the effects arising from both flocculation and resuspension-settling. When we include both flocculation and resuspension-settling into the model, the PCB desorption rates are fastest in the diffusion-only run (Run 32), followed by the flocculation-only run (Run 33), the deposition/erosion-only run (Run 34), and finally the full process run (Run 35) (Figure 6.12). With flocculation, the steady-state OC concentration in the water column decreased 28%, the total HOC concentration decreased 57%, and desorption rate decreased 13% relative to the run that only included resuspension-settling and kinetic-limited HOC partitioning without flocculation.

The deviation from equilibrium was also observed for each floc cluster as a function of time, assuming that the equilibrium state is defined by K_{OW},

Deviation from equilibrium = $(C_{p,t} - C^*_{p,t,})/C^*_{p,t,}$ Equation 6.8

where $C_{p,t}$ is the concentration of chemical contaminant in a particle phase (g contaminant/m^3 water) at time *t* and $C^*_{p,t,}$ is the corresponding particle phase contaminant concentration in equilibrium with the surrounding dissolved phase at time *t* ($C_{d,t}$, g contaminant/m^3-water),

$$C^*_{p,t,} = K_{OW} C_{d,t} C_{dry,i} \quad \text{Equation 6.9}$$

where K_{OW} is the octanol-water partition coefficient and $C_{dry,i}$ is the flocs concentration (g OC/m^3-water). Note that if $C_{p,t}$ exceeds $C^*_{p,t,}$, the particles are oversaturated with contaminant with respect to the dissolved phase, resulting in net desorption. In the opposite case, chemical contaminant diffuses into the particulate carbon phase. Because $C_{p,t}$, $C_{d,t}$, and F each vary somewhat independently, the deviation from equilibrium and, therefore, the diffusive flux is constantly changing for each particle type throughout the model simulation.

Under the given assumptions and initial conditions, the diffusion-only run reached sorption equilibrium faster than did the flocculation, deposition/erosion, and full process runs as discussed in the previous section. However, the deviation from equilibrium from the full process and the deposition/erosion runs are quite similar. This result hints that deposition/erosion is the dominant mechanism for slowing the approach to equilibrium. Furthermore, during the rapid transport between water and sediment, the contaminated flocs do not have enough time to fully desorb contaminants to the dissolved phase.

6.4.3 Examining the Impact of Floc Size Distribution on the Desorption Rate

Up to this point, the model has simply used a single floc size parameter to represent the entire spectrum. However, D_{50} may not well represent the behavior of the entire particle size spectrum. In the previous chapter, the field-measured particle size distribution was used as an initial condition for the floc sub-model. Therefore, here we test the impact of including a full size distribution on the desorption rate in simulations including flocculation and deposition/erosion.

Settings: To test the model performance and desorption rate with a full floc size distribution (multi-size-flocs that D_{50} was calculated as 216 μm in the previous chapter) as an initial condition, the model combined the particle size distribution described in Chapter 2 with the PCB data measured in the STORM experiments. To compare the model results from previous runs, all runs are normalized to an initial TSS of 1 mg/L. Values for other parameters for flocculation and deposition/erosion were the same as in previous sections.

Results and discussion: The PCB 52 desorption rates among three single floc runs (50, 216, and 400 μm) (Run 23, Run 36, and Run 26) and the multi-size run (Run 37) are compared in Figure 6.13. The desorption rate for a multi-size run was intermediate between the two single floc runs (Run 23 and Run 26). This result suggests that when the fate of HOC is controlled only by diffusive exchange between flocs and the surrounding water, the floc size is the dominant parameter and that D_{50} value for multi-size run (216 μm) is between two sizes used in the single size runs (50 μm and 400 μm respectively). D_{50} may be a useful tool when diffusion is the only transport mechanism and has a normal particle size distribution because there the desorption rates are equal between the multi-size and single-size runs. However, when flocculation or deposition/erosion is included and particle size distribution is not shown as normal distribution, the multi-size run performs differently than the single-size run (D_{50}), and desorption rates are controlled by the particle size distribution. For example, when the distribution is skewed to smaller flocs, the multi-size run desorption rate is faster than that of the single-size run. Therefore, using D_{50} to estimate desorption rate would miscalculate the short term results. Furthermore, the multi-size run results show a similar

trend as the single floc run, with the full effect run having the slowest desorption rate, followed by the resuspension-settling run, the flocculation run and finally the diffusion only run (Figure 6.14). The multi-size run results were intermediate between the small and larger floc size single run results, because its medium floc size is located within these ranges.

6.4.4 Comparing Modeled PCB Behavior and Observations from STORM Experiments

Here the fully-developed, flocculation-based contaminant model is used to predict the behavior of four PCB congeners under the STORM mesocosm conditions and to compare the results with measured data. Note that while the particle transport model was calibrated with STORM observations, the HOC submodel was not tuned to PCB measurements made during these experiments. These model results are used to explore the role of flocculation and resuspension on the fate of HOCs in the STORM experiments.

Settings: The floc sub-model used the settings and parameters calibrated from the resuspension stage of the STORM experiment, as described in Chapter Two. The initial f_{OC}, PCBs concentrations, K_{OC} values, and sediment PCBs concentrations were the same as STORM measurements and varied with corresponding PCB congener. In this section, the initial f_{OC} and PCBs concentrations are assumed the same between upper and deeper sediment layers.

Results and discussion: The model was tested with di, tri, tetra, and penta PCB congeners and the results were compared with STORM experiment measurements (Figure 6.15-6.18). The model results agreed well with the STORM measurements of particulate and dissolved phase concentrations of four PCB congeners without calibration. The larger PCB congeners required a longer time to reach steady state than the less chlorinated PCBs due to their smaller mass transfer velocity. The more chlorinated PCB congeners have a higher steady-state particulate-bound PCB concentration because of their higher K_{OC} values.

When flocculation is considered in a dynamic particle environment that includes sediment resuspension, settling, and kinetic-limited HOC partitioning, the steady state total PCB concentration in the water column is decreased by 20%, and time to reach steady state in the water column decreased by 36%, consistent with earlier findings at section 6.1.

6.4.5 The Impact of Surficial Sediment Contaminant Concentrations on Steady State Dissolved PCBs Concentrations

Settings: There are three runs in the section, runs 41-43. All are based on the same floc transport model and related parameters including bioturbation coefficient and chemical diffusion coefficient between each layer. The physical environment is the same as the resuspension period in the STORM experiment throughout 53 simulation hours for each run. The surficial sediment thickness is 0.1 cm and the deeper sediment layer thickness is 4.9 cm. All three runs assumed that top sediment layer PCB 52 concentration was 702 ng/g dry weight. However, deeper sediment layer PCB 52 concentrations were assigned values of 702, 0.702, and 7020 ng/g dry weight respectively in the three runs to test the influence of deeper sediment PCB levels on subsequent water column concentrations.

Results and discussion: Run 41, where there was no PCB concentration gradient in the sediment, is the base case. The deeper sediments in run 42 are depleted in PCBs relative to the surface sediment layer. The PCB 52 concentration in the water column increased during the first few hours following by a smooth decline in both dissolved and particulate phases (Figure 6.19) because the surficial sediment was eroded and PCB quickly desorbed during

the first few hours. When sediment was eroded to the water column, the deeper cleaner sediment was recruited to replace the lost surficial layer. At the same time, before contaminated sediment reaches equilibrium, it might cycle between the water column and sediment. As a result, the dissolved and particulate PCB concentrations did not decrease dramatically. In addition, the sediment-water diffusion flux buffers the dissolved PCB concentration, making the dissolved PCB decrease slower than the particulate PCB between five and ten simulation hours. When the model reached steady state, the PCB concentrations in the run 42 with cleaner deeper sediment was almost 10 times less than in the base case, which was similar to the ratio of deeper sediment concentrations between the two scenarios. Run 43 simulated a deeper sediment layer containing10 times higher PCB levels compared to the surficial later. Both the dissolved and particulate PCB 52 concentrations were 10 times higher than the base case. These results indicated that deeper sediment concentration not only impacts the long term water column contaminant concentrations, but also temporally impacts the variation in desorption rate.

6.4.6 Comparing kinetically limited partitioning and equilibrium behaviors on the steady state contaminant concentrations

Objectives: Several papers suggest that the traditional radial diffusion model and equilibrium partition model overestimate the rate of desorption during resuspension events (Cornelissen *et al.,* 1997; Gong and Depinto, 1998; Wener *et al.,* 2006). In this study we apply our new multi-class flocculation-based contaminant fate model to several scenarios and compare the results predicted by the model with equilibrium and radial diffusion models under the same physical conditions. Finally, we compare the model predictions from three models with results from the STORM experiments.

Settings: The first scenario estimated the desorption rate between kinetically limited partitioning and equilibrium behaviors (run 44) with flocculation, deposition, and resuspension. In this scenario, the model was used to test two kinetically-limited partitioning behaviors including radial diffusion (run 45) and our new kinetically-limited behavior (run 47). In these runs, the model used the settings derived from the STORM experiment during the erosion period for the floc-sub model and included flocculation, deposition, and erosion. Values for all chemical parameters for PCB 52 were based on the experimental measurements or from calculations: K_{OC} equals to1.1 m^3/g, D* equals 2.75 x 10^{-6} cm^2/s, and sediment C_P is 702 ng/g for both sediment layers. Further, the median particle radius D_{50} for the radial diffusion model, and TSS, dry density, and f_{OC} for the equilibrium model were all calculated outputs from the floc-submodel. The equilibrium partitioning calculation included contaminant transport with floc movement by settling and resuspension. Further, for the radial diffusion behavior, the resuspension-settling process had been simulated using the measured temporal varied D_{50} values (Schneider, 2007). Furthermore, for the radial diffusion behavior, the temporal varied D_{50} values had also been adjusted to fit the STORM measurements (run 46). The second scenario starts with clean water and dirty suspended particles and uses the same settings for the floc sub-model derived from the STORM experiment during the beginning of the free settling period. The first two runs (run 47 and 48) in this scenario compared the water column residence time of PCBs predicted by the equilibrium and kinetically-limited partitioning behaviors that included flocculation and settling.

Results and discussions: As described in the previous chapter, OC and TSS reach steady state concentrations and size distributions during the first few hours of constant erosion in the STORM experiment. The equilibrium partitioning model predicts an instantaneous increase in the dissolved PCB concentration at the onset of resuspension. However, as showed in Figure 6.20, only about 50% of the contaminant is desorbed relative to the equilibrium value during the first 3 hours of the resuspension experiment. After 12 hours of constant resuspension, desorption reached 83% of equilibrium during the first 12.5 hours. Even during the STORM free settling period experiment, the equilibrium partitioning model predicts PCB water column residence times that are two times longer than the kinetically-limited partitioning model (Figure 6.21). One important difference between this study and previous models (DRBC, 2003) that assume partitioning equilibrium is that a contaminant does not reach sorptive steady state within a tidal period. In other words, even from a long term point of view, an equilibrium model may not be a proper choice to describe HOC behavior in an estuary or other dynamic tidal area.

The radial diffusion model also overestimates measured dissolved PCB concentrations. Most previous experiments were designed so that all particles were resuspended and well mixed in a container that lacked the interaction between sediment and water column (Lick and Rapaka, 1996). Therefore, some parameters have to be manually adjusted in order to apply the radial diffusion model to a field project. Several possible factors might explain the overestimation.

First, as shown in the previous section, the radial diffusion model only implicitly includes the feedback from the sediment layer from D_{50} values, which decreased the desorption rate for the resuspended particles in the water column. Second, the radial diffusion model does not simulate contaminant gain and loss from a floc size from flocculation. Flocculation not only changes the concentration gradient between floc and surrounding water, but also changes the boundary conditions for the floc particles. A single floc particle will not only lose contaminant by diffusion but will also gain or lose contaminant as it is coagulates with flocs with different contaminant concentrations. Third, although we applied measured D_{50} as boundary for the radial diffusion model, this strategy might not appropriate to model this variation within the given time interval, which caused numerical problems by temporally altering the boundary and initial conditions. In addition, to fit the STORM measurement, the model had to manually increased 70% of the given D_{50} values to decrease the desorption rate.

6.5 Conclusions

A new multi-class flocculation-based contaminant fate model was adapted to describe desorption kinetics for contaminants associated with flocculated particles during a resuspension event. The model was effective in predicting transport of hydrophobic organic contaminants among different size flocs, water, and two sediment layers. The model also demonstrated the impact of fractal geometry, bottom shear stress, particle composition, floc size, f_{OC}, K_{OC}, and TSS on contaminant desorption rate and residence time.

Under different scenarios, this model results supports the importance of size distributed flocs, sediment-water interaction, and flocculation for the contaminant desorption rate in a water column. Both equilibrium and kinetically-limited partitioning approaches predict the same dissolved and particle contaminant concentrations at steady state. However, during the first three hours of a simulated sediment resuspension event, the equilibrium and radial diffusion behavior overestimated dissolved PCB concentrations 50% and 20% respectively.

This result suggested equilibrium behavior overestimates the initial PCB release from contaminated sediments during relatively rapid events like dredging, tides, or storm water influx. The radial diffusion model, a common tool to describe desorption kinetics for a single floc, is limited by several factors, as it fails to include the contaminant exchange with surrounding flocs, it has numerical difficulties in calculating the impact of various boundary conditions, and it ignores indirect impacts from sediment-water exchange.

Flocculation could alter the contaminant residence time in many ways such as by changing the particle settling velocity and diffusion flux. Further, in a floc-rich environment, flocculation is an important mechanism redistributing contaminants among flocs. When a full flocculation is considered in a dynamic particle environment that includes sediment resuspension, settling, and kinetic-limited HOC partitioning, the steady state total PCB concentration in the water column is decreased by 20 % and water column HOC residence time decreased by 36%.

6.6 Figure Captions

Figure 6.1: The conceptual diagram of the HOC fate model.

Figure 6.2: The conceptual diagram of the contaminant distribution within a single flocculation particle

Figure 6.3: Mass transfer velocity (m sec^{-1}) varied with floc size with two porosity-floc size trends. The first trend (2a) assumed porosity was a constant along all size of flocs; the second trend (2b) assumed porosity was a function of fractal factor and floc size.

Figure 6.4: Variation in desorption rates under different scenarios. Assumed all sizes of flocs have the same porosity and a constant product between number concentration and floc contact area. The detail settings are shown in Table 1.

Figure 6.5: Using Lick *et al*. (1996) experiment data to compare the impact of multi-floc-property on desorption rates as model Run 8 and Run 9 in Table 1.

Figure 6.6: Comparing desorption rates under different scenarios including base case run, smaller fractal factor run, larger fractal factor run, larger floc size run, higher f_{OC} run, lower solid density run, higher K_{OC} run, and higher Dm run. Assumed porosity is controlled by the fractal geometry and a constant total floc contact area.

Figure 6.7: Comparing desorption rates under different scenarios including base case run, smaller fractal factor run, larger floc size run, higher f_{OC} run, and higher TSS run. Assumed porosity and total floc contact area are controlled by the fractal geometry.

Figure 6.8: Comparing the impact of flocculation on desorption rates including based run, stickiness coefficient = 0.25 run, stickiness coefficient = 0.5 run, and stickiness coefficient =0 alone with floc size = 400 μm run.

Figure 6.9: Comparing the particulate PCB 52 residence time with and without flocculation using non-equilibrium partitioning behavior based PCBs fate model during the free settling period.

Figure 6.10: Comparing the impact of bottom shear stress on the PCB 52 desorption rate. The bottom shear stress varied from 0, 1, and 2 dynes/m^2

Figure 6.11: Comparing the impact of resuspension-settling on the desorption rate in the dissolved water and sediment porewater.

Figure 6.12: Comparing the impact of diffusion, flocculation, resuspension-settling and all above processes on the desorption rate that was initiated with 50 um and 1mg/L flocs.

Figure 6.13: Comparing the PCB 52 desorption rate among three initial conditions: 50 μm, 400 μm, and STORM particle size distribution respectively. All runs were involved diffusion only.

Figure 6.14: Comparing the impaction of diffusion, flocculation, resuspension-settling and all above mechanisms on the desorption rate when initiated with normalized STORM experiment particle size distribution with 1mg/L flocs for 300 days.

Figure 6.15-6.18: The model was tested with di (PCB 4 and10), tri (PCB 19), tetra (PCB 52), and penta (PCB 77 and 110) PCB congeners and the results were compared with STORM experiment measurements.

Figure 6.19: Comparison of the temporal concentration variations for particulate and dissolved PCB 52 under three deeper PCB 52 concentrations: Run27: L1=14.01 ug/g-OC (702 ng/g -dry) ; L2= 14.01 ug/g-OC; Run 28: L1=14.01 ug/g-OC (702 ng/g -dry) ; L2= 1.401 ug/g-OC; Run 29: L1=14.01 ug/g-OC (702 ng/g -dry) ; L2= 140.1 ug/g-OC.

Figure 6.20: Comparison model simulated PCB 52 desorption trends among measured, equilibrium behavior, radial diffusion model, and this study under STORM experimental conditions.

Figure 6.21: Comparing the particulate PCB 52 residence time between equilibrium and non-equilibrium partitioning behaviors using calibrated flocculation model during the STORM experiment free settling period.

Figure 6.1:

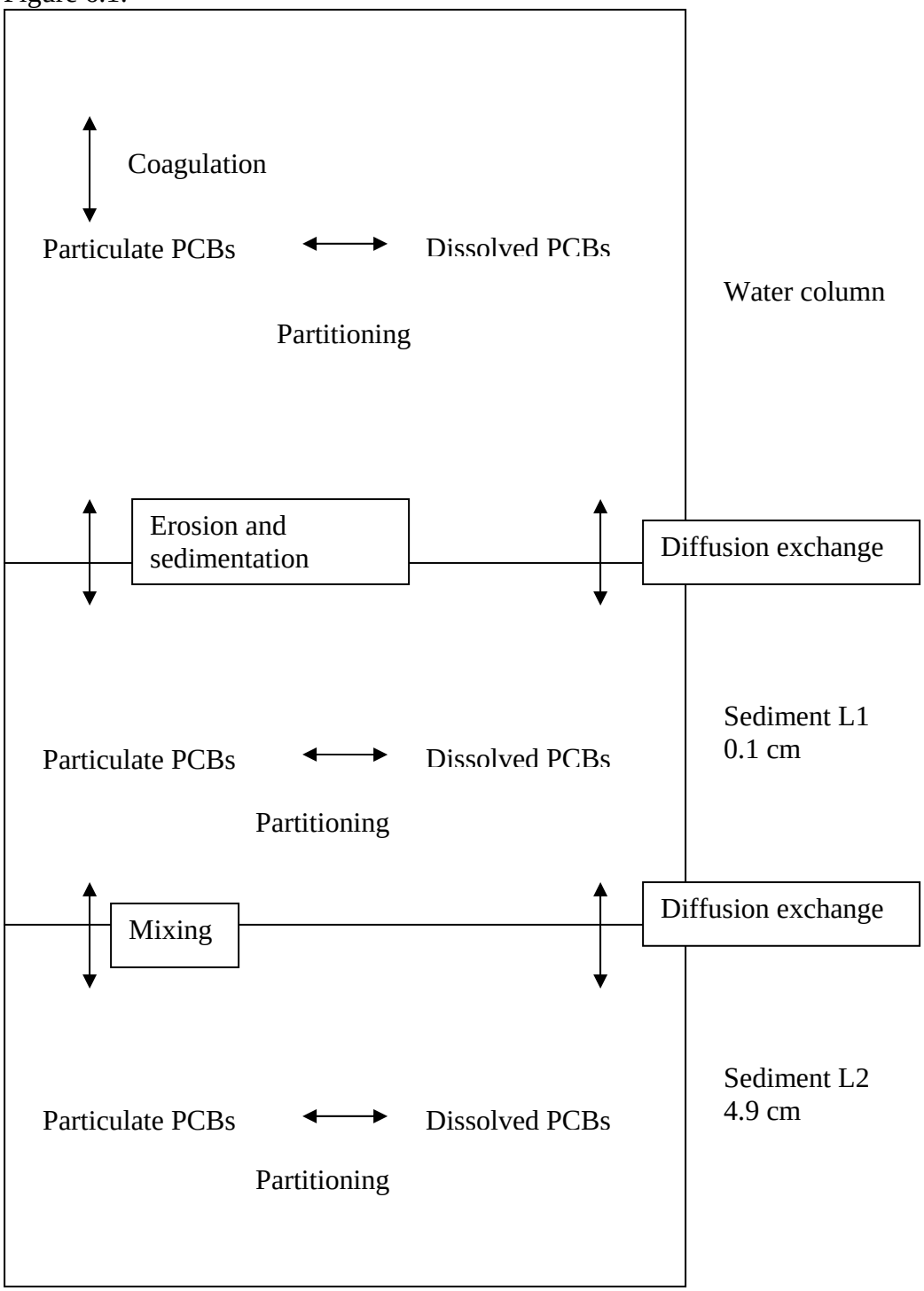
Coagulation
Particulate PCBs
Dissolved PCBs
Water column
Partitioning
Erosion and sedimentation
Diffusion exchange
Sediment L1
0.1 cm
Particulate PCBs
Dissolved PCBs
Partitioning
Mixing
Diffusion exchange
Sediment L2
4.9 cm
Particulate PCBs
Dissolved PCBs
Partitioning

Figure 6.2

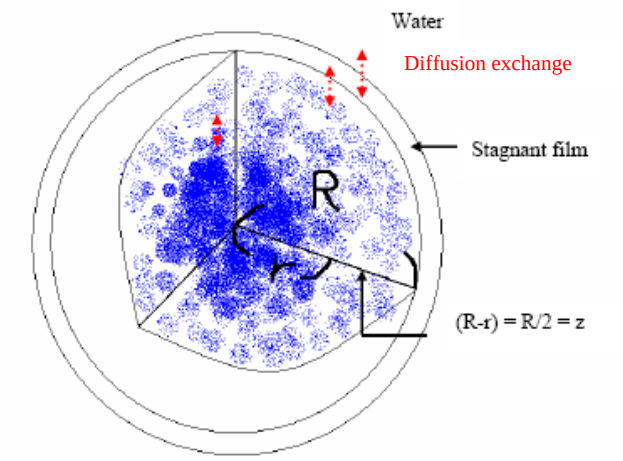

Figure 3.2a: The ideally conceptual diagram of the contaminant distribution within a single flocculation particle, where the blue dots represent the contaminants

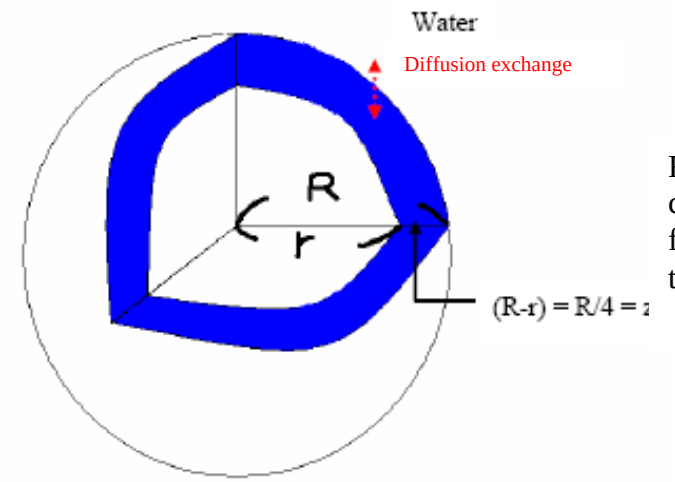

Figure 3.2b: The conceptual diagram of the contaminant distribution within a single flocculation particle in this study, where the blue dots represent the contaminants

In reality, the concentration will be high at the center and will approach $HOC_{dissolved}$ at the outer shell, where $HOC_{dissolved}$ is the dissolved concentration in the surrounding water (Figure 6.2 a). This study assumes a uniform HOC concentration distribution within the modeled floc particle sphere shell to simply the boundary condition when two flocs collided to form a new one (figure 6.2 b). Thus, writing the mass flux as may overestimate the flux because the concentration difference is too large.

$$J_i = \frac{D^*}{z} \times A \times N_i \times \left(HOC_{dissolved} - \frac{HOC_i}{OC_i \times K_{OC}} \right) \qquad \text{Equation 3.5}$$

Therefore, we have to compensate by changing the length scale slightly

Old: $(R - r) = \frac{1}{2} R = z$

New: $(R - r) = \frac{1}{4/3 \pi R^3} \int_0^R 4\pi r^2 (R - r) dr = \frac{\frac{1}{3}\pi R^4}{\frac{4}{3}\pi R^3} = \frac{1}{4} R = z$ Equation 3.7

Figure 6.3:

Figure 6.3a

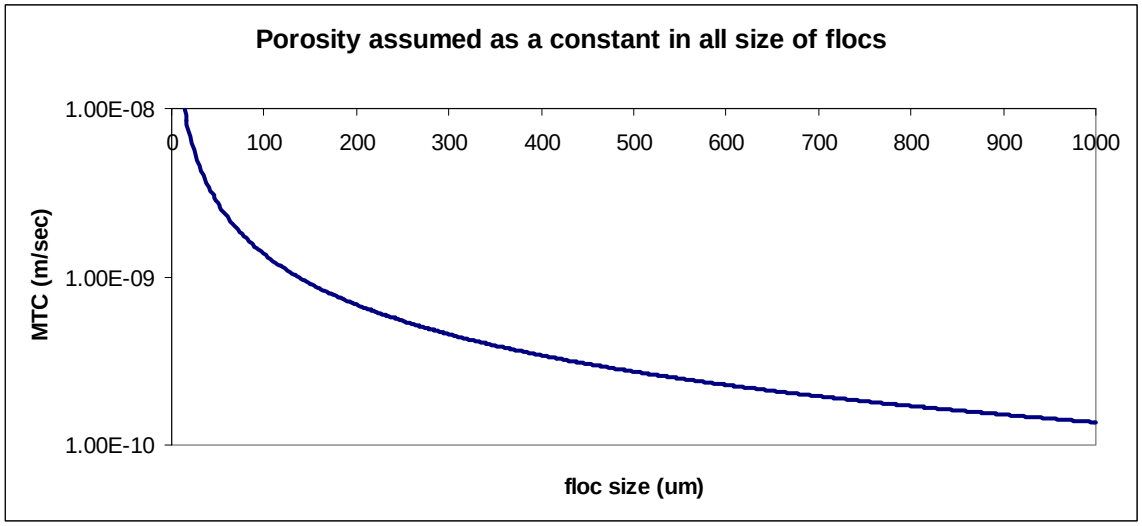

Figure 6.3b

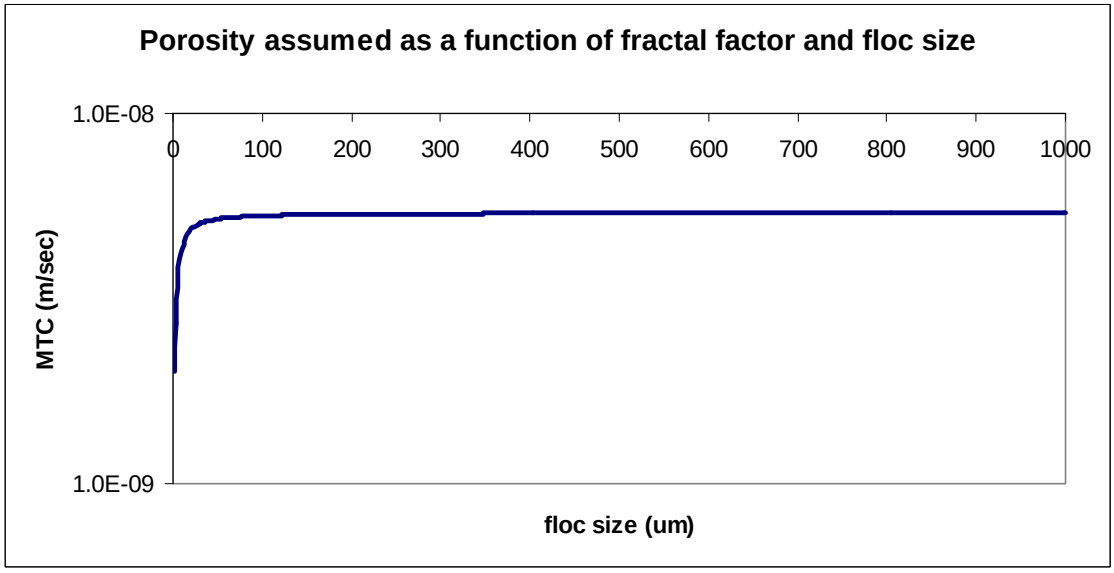

Figure 6.4:

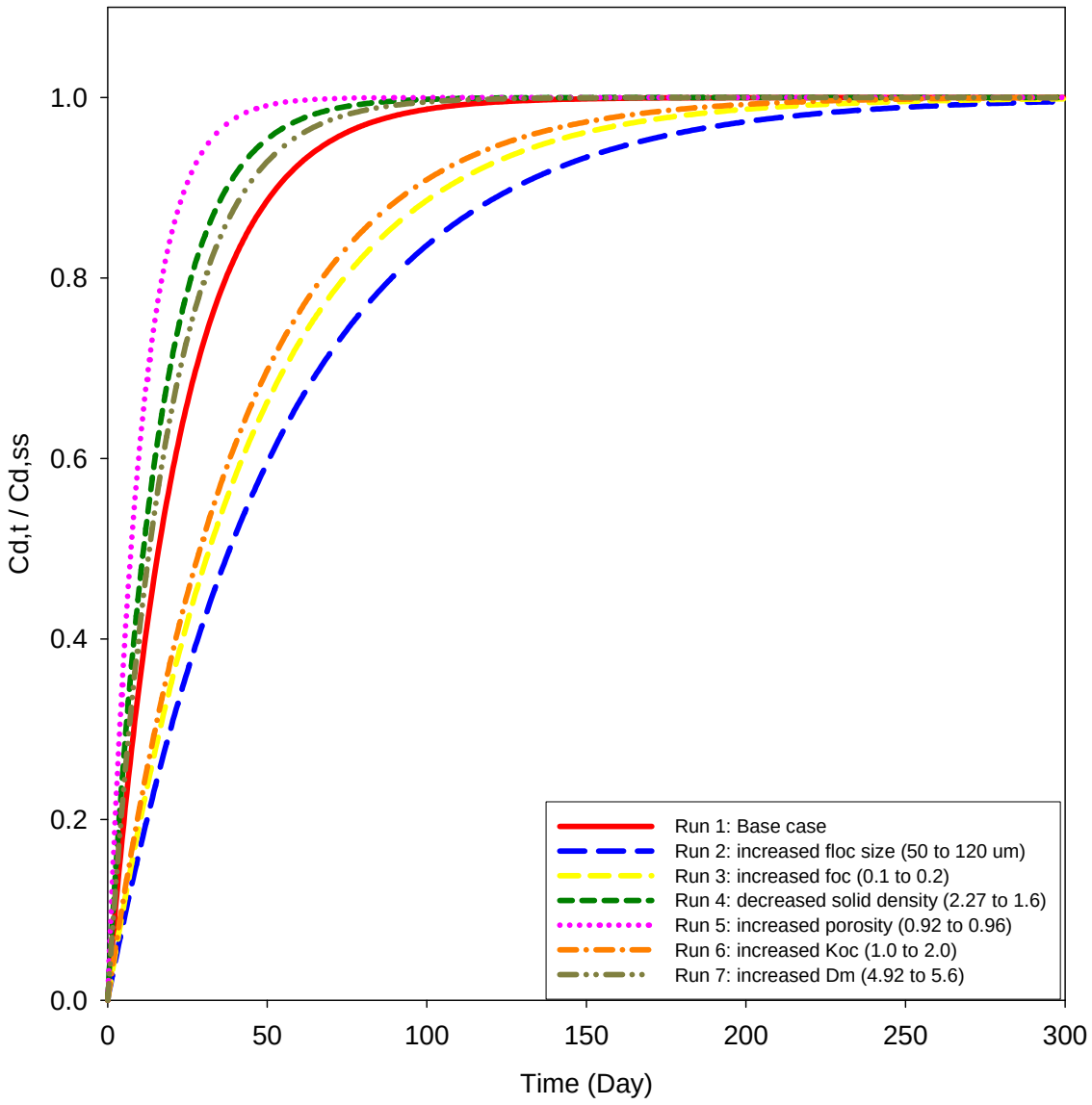
1.0
0.8
0.6
0.4
0.2
0.0
Cd,t / Cd,ss
0
50
100
150
200
250
300
Time (Day)
Run 1: Base case
Run 2: increased floc size (50 to 120 um)
Run 3: increased foc (0.1 to 0.2)
Run 4: decreased solid density (2.27 to 1.6)
Run 5: increased porosity (0.92 to 0.96)
Run 6: increased Koc (1.0 to 2.0)
Run 7: increased Dm (4.92 to 5.6)

Figure 6.5

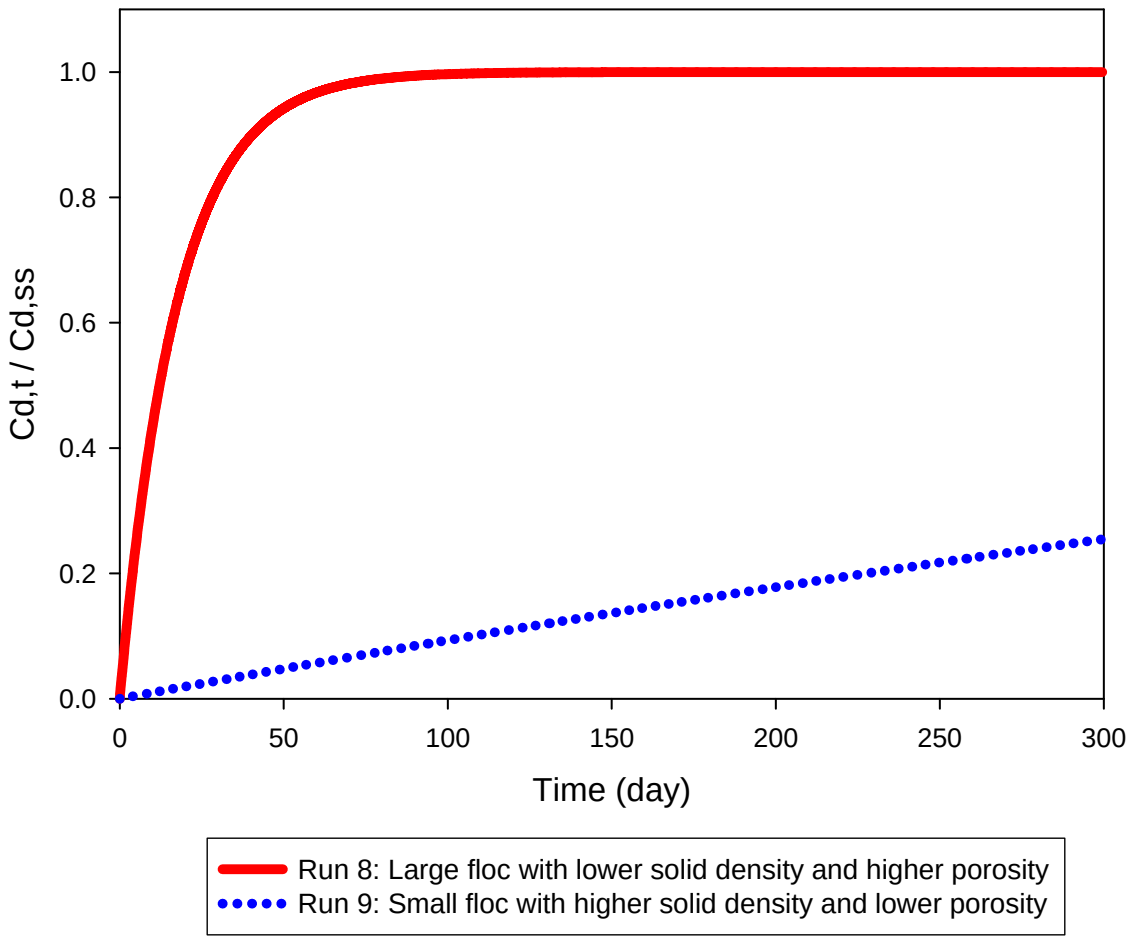
1.0
0.8
0.6
0.4
0.2
0.0
Cd,t / Cd,ss
0
50
100
150
200
250
300
Time (day)
Run 8: Large floc with lower solid density and higher porosity
Run 9: Small floc with higher solid density and lower porosity

Figure 6.6:

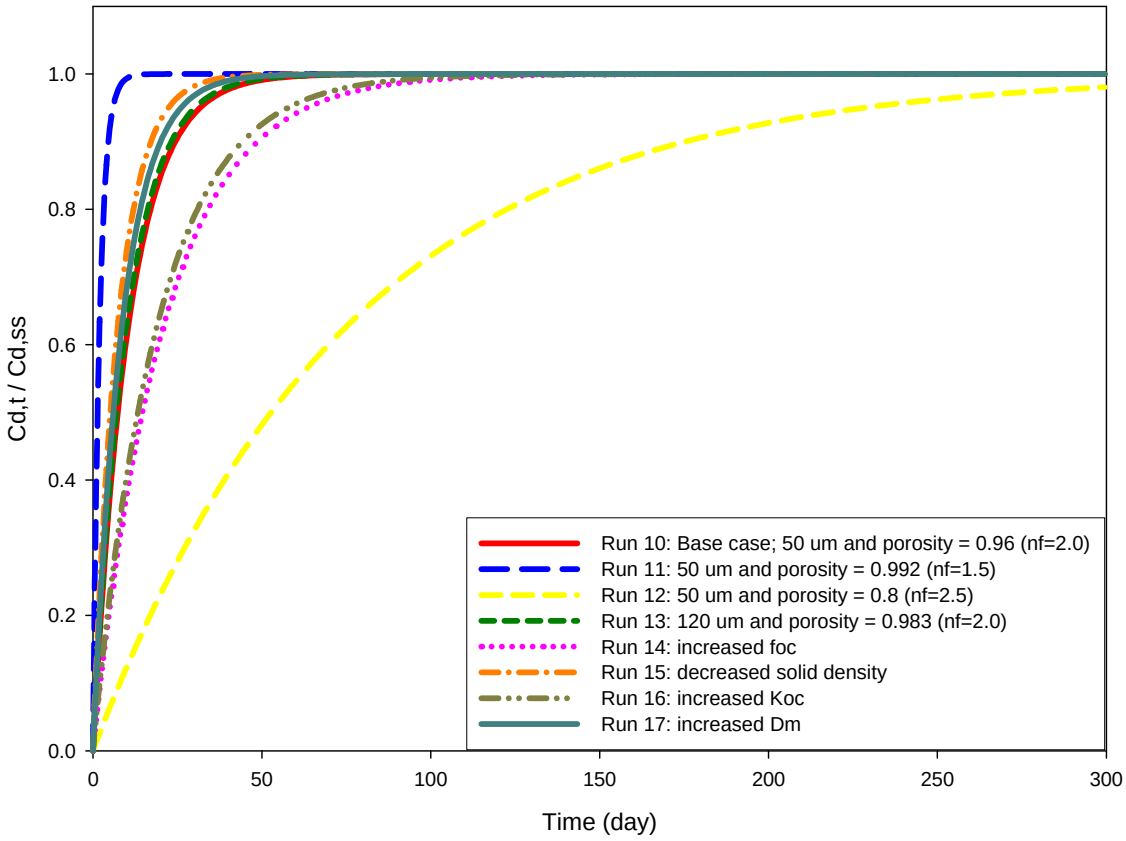
Cd,t / Cd,ss
Time (day)
0.0
0.2
0.4
0.6
0.8
1.0
0
50
100
150
200
250
300
Run 10: Base case; 50 um and porosity = 0.96 (nf=2.0)
Run 11: 50 um and porosity = 0.992 (nf=1.5)
Run 12: 50 um and porosity = 0.8 (nf=2.5)
Run 13: 120 um and porosity = 0.983 (nf=2.0)
Run 14: increased foc
Run 15: decreased solid density
Run 16: increased Koc
Run 17: increased Dm

Figure 6.7:

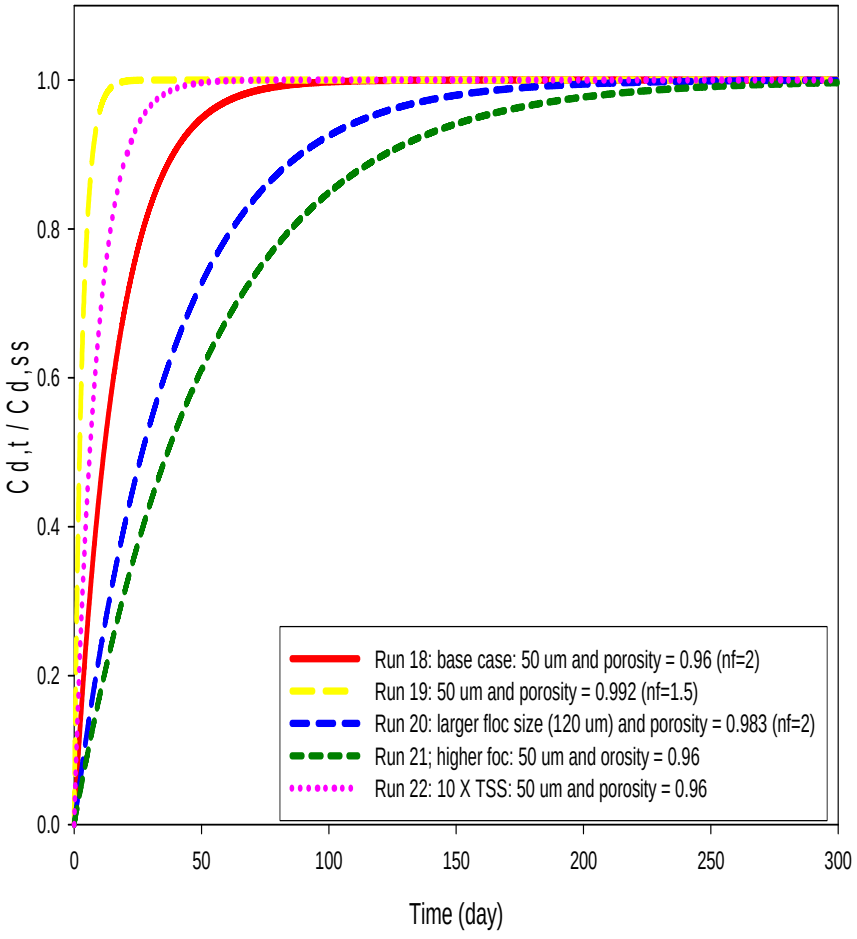
1.0
0.8
0.6
0.4
0.2
0.0
C d,t / C d,ss
0
50
100
150
200
250
300
Time (day)
Run 18: base case: 50 um and porosity = 0.96 (nf=2)
Run 19: 50 um and porosity = 0.992 (nf=1.5)
Run 20: larger floc size (120 um) and porosity = 0.983 (nf=2)
Run 21; higher foc: 50 um and orosity = 0.96
Run 22: 10 X TSS: 50 um and porosity = 0.96

Figure 6.8:

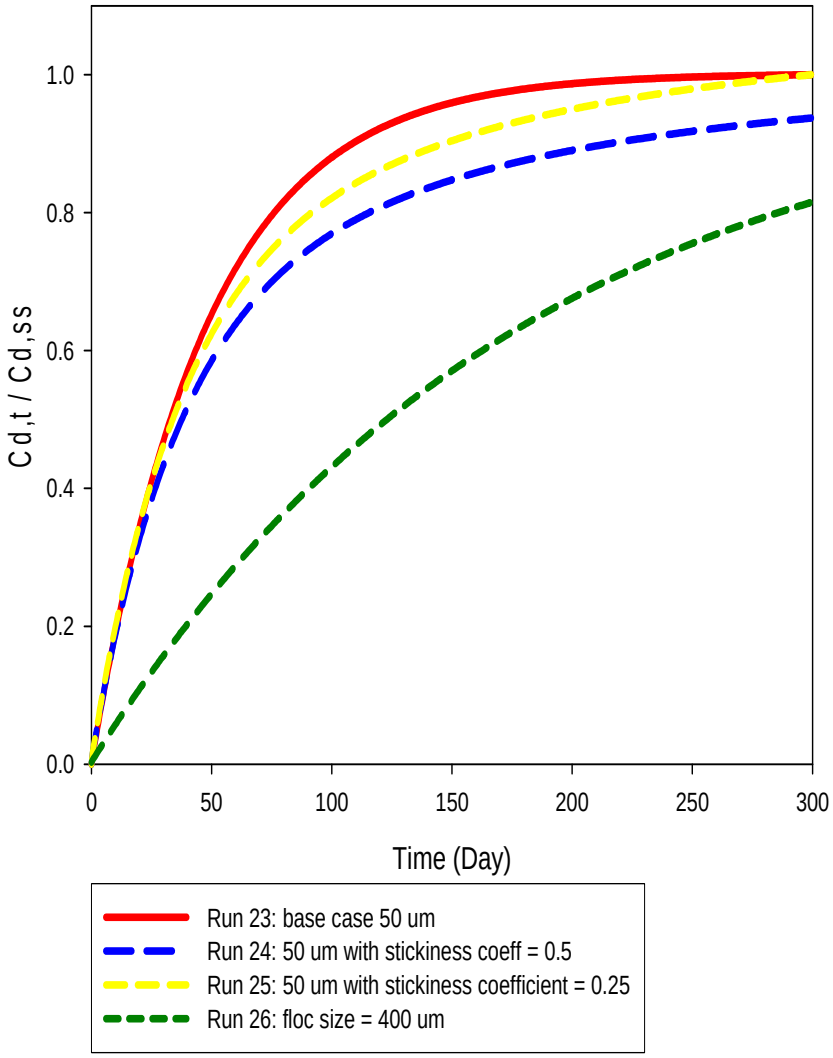
1.0
0.8
0.6
0.4
0.2
0.0
Cd,t / Cd,ss
0
50
100
150
200
250
300
Time (Day)
Run 23: base case 50 um
Run 24: 50 um with stickiness coeff = 0.5
Run 25: 50 um with stickiness coefficient = 0.25
Run 26: floc size = 400 um

Figure 6.9:

Run 27: $R_{T,\ with\ coagulation}$ = 42 min.
Run 28: $R_{T,\ without\ coagulation}$ = 216 min.

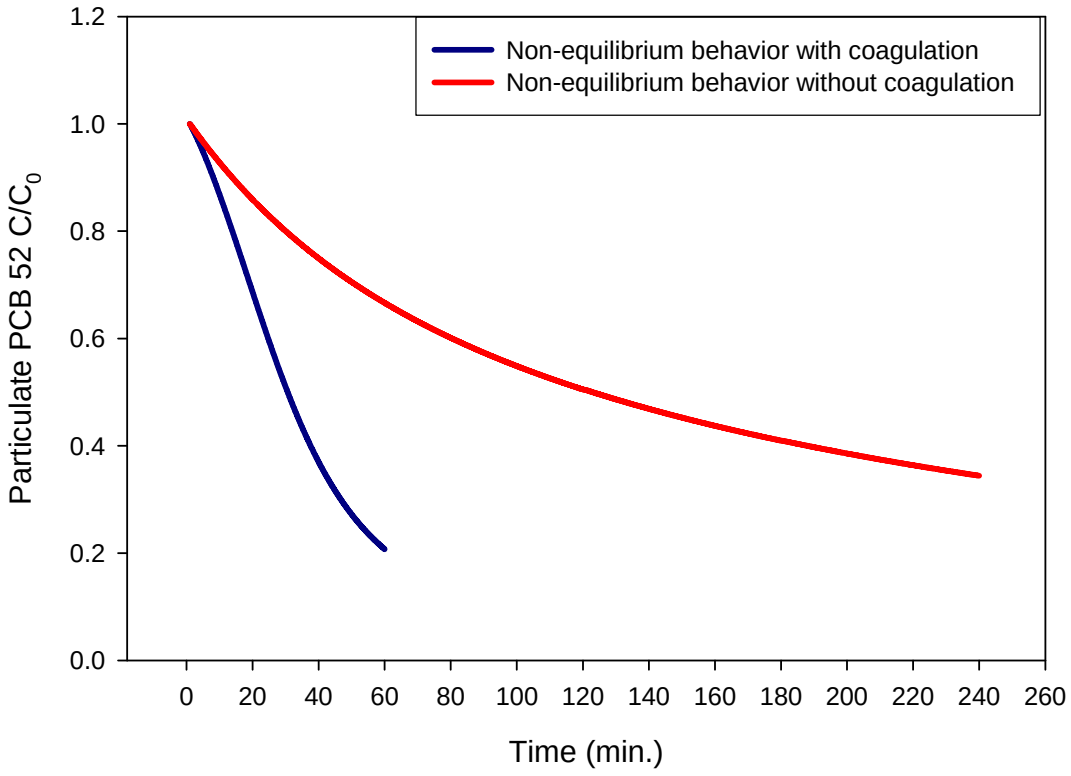

Figure 6.10:

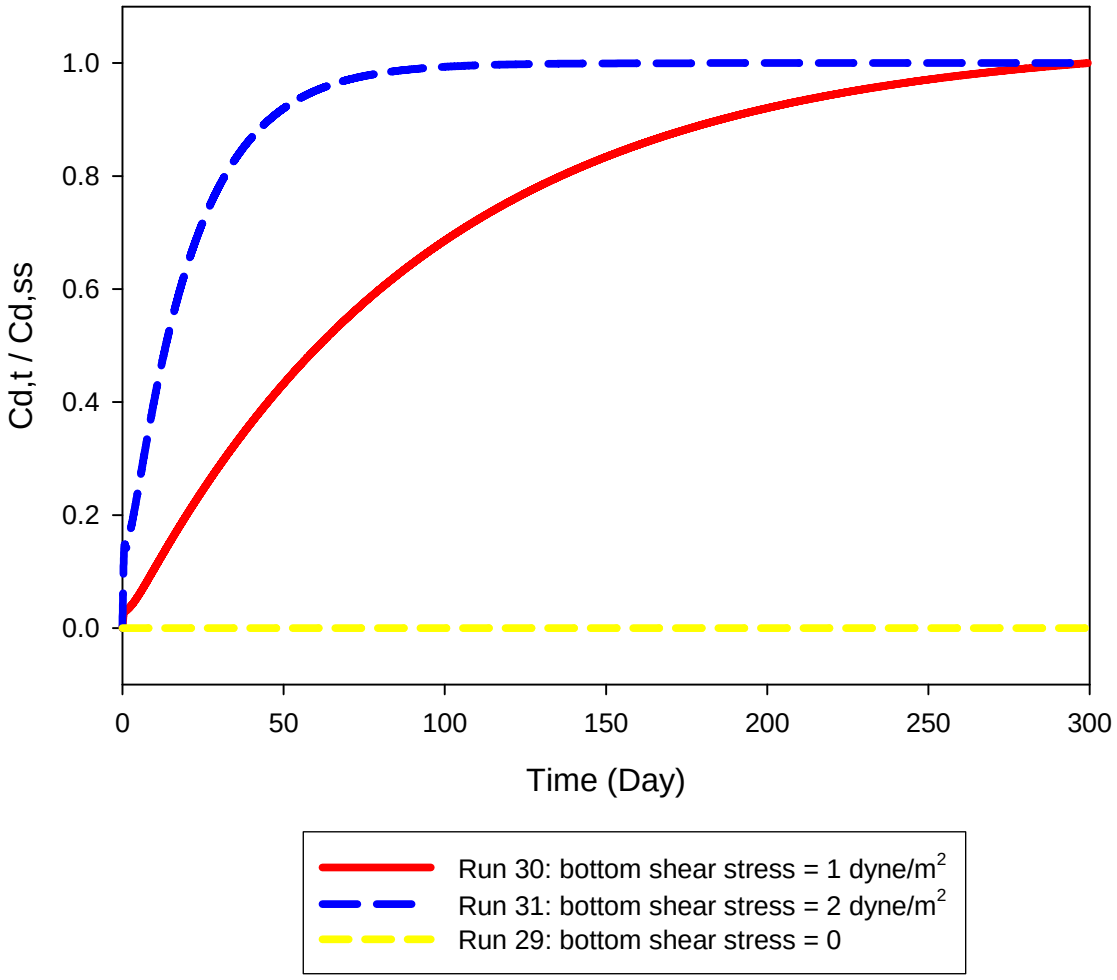
1.0
0.8
0.6
0.4
0.2
0.0
Cd,t / Cd,ss
0
50
100
150
200
250
300
Time (Day)
Run 30: bottom shear stress = 1 dyne/m2
Run 31: bottom shear stress = 2 dyne/m2
Run 29: bottom shear stress = 0

Figure 6.11

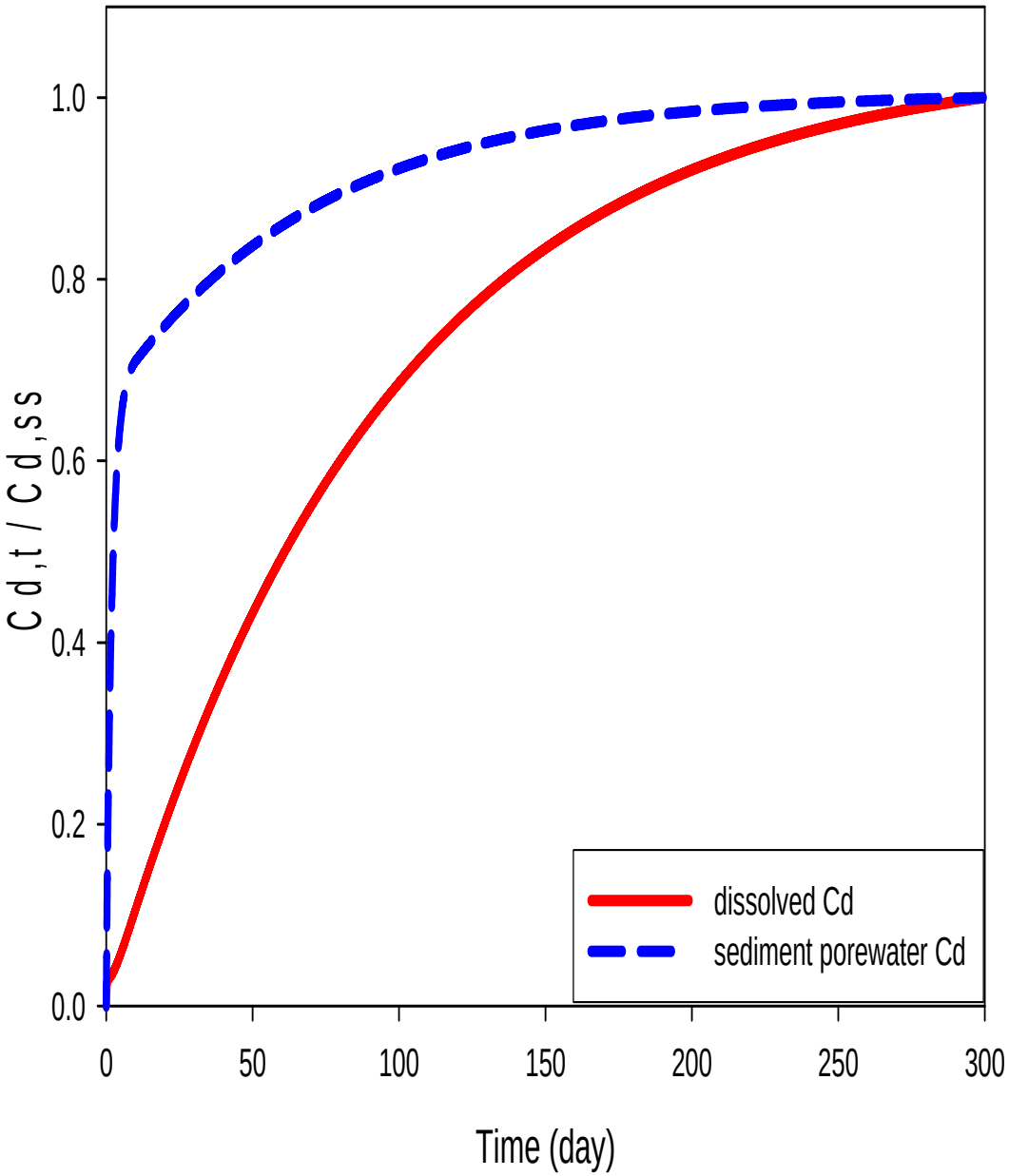
1.0
0.8
0.6
0.4
0.2
0.0
C d,t / C d,ss
0
50
100
150
200
250
300
Time (day)
dissolved Cd
sediment porewater Cd

Figure 6.12:

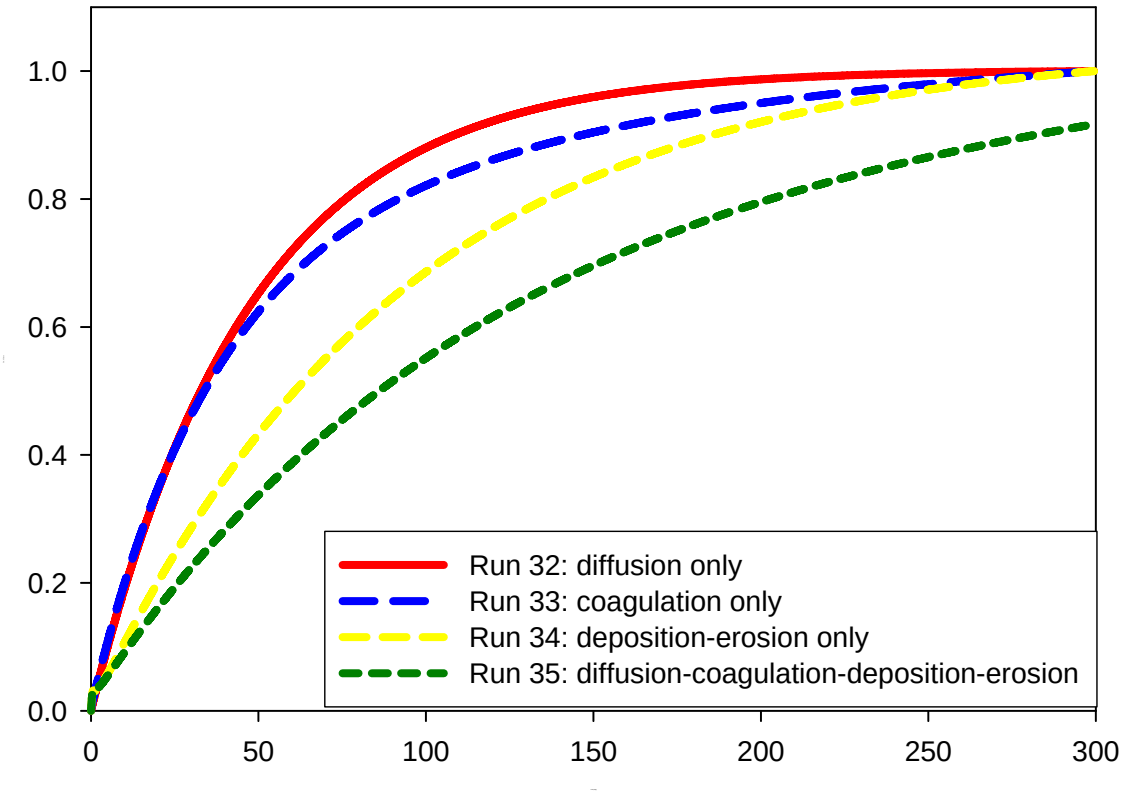
1.0
0.8
0.6
0.4
0.2
0.0
0
50
100
150
200
250
300
Run 32: diffusion only
Run 33: coagulation only
Run 34: deposition-erosion only
Run 35: diffusion-coagulation-deposition-erosion

Figure 6.13:

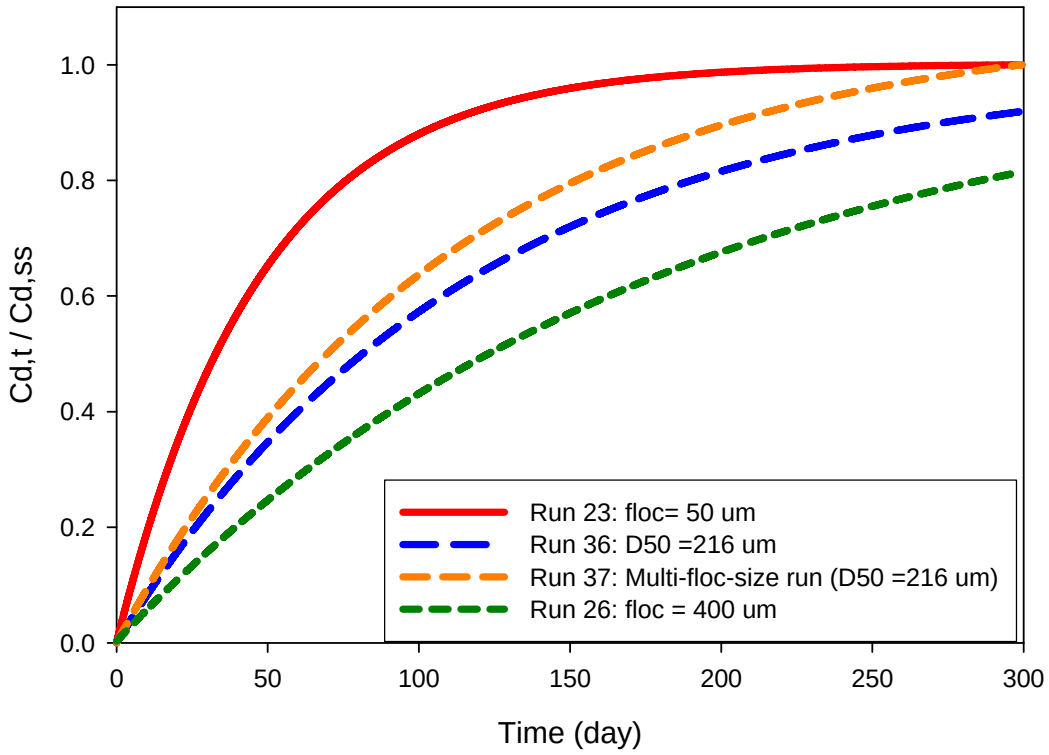
1.0
0.8
0.6
0.4
0.2
0.0
Cd,t / Cd,ss
0
50
100
150
200
250
300
Time (day)
Run 23: floc= 50 um
Run 36: D50 =216 um
Run 37: Multi-floc-size run (D50 =216 um)
Run 26: floc = 400 um

Figure 6.14:

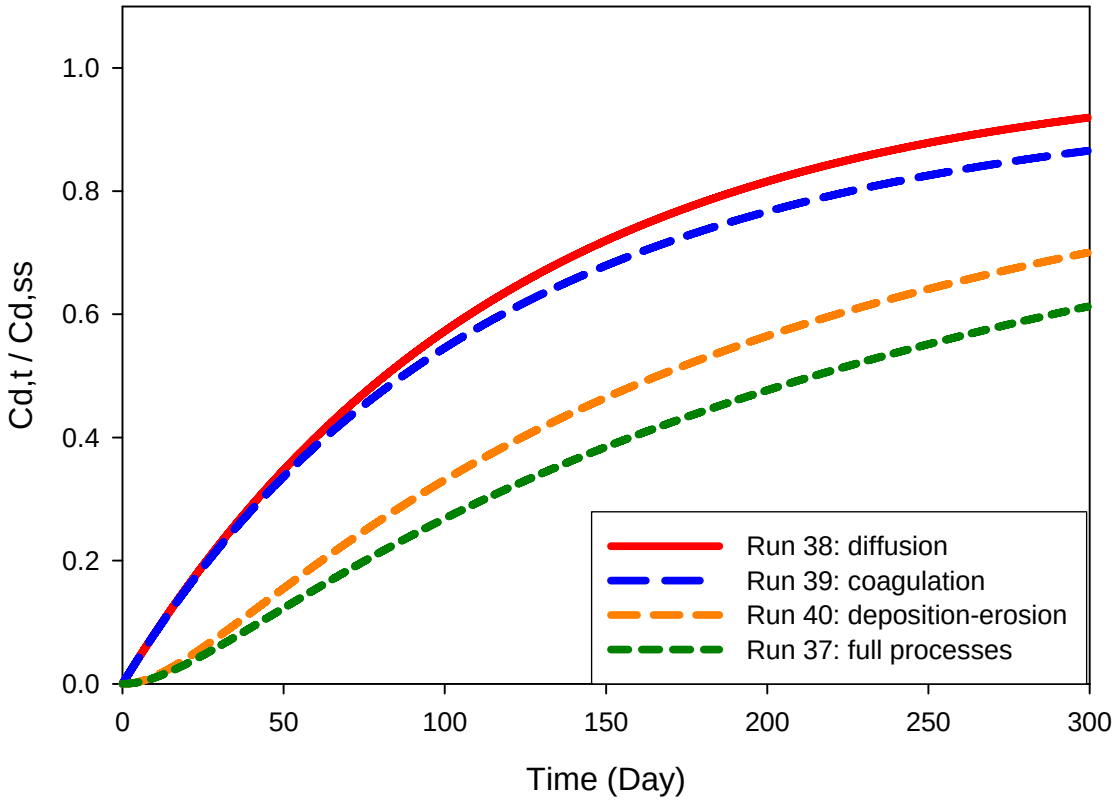
1.0
0.8
0.6
0.4
0.2
0.0
Cd,t / Cd,ss
0
50
100
150
200
250
300
Time (Day)
Run 38: diffusion
Run 39: coagulation
Run 40: deposition-erosion
Run 37: full processes

Figure 6.15:

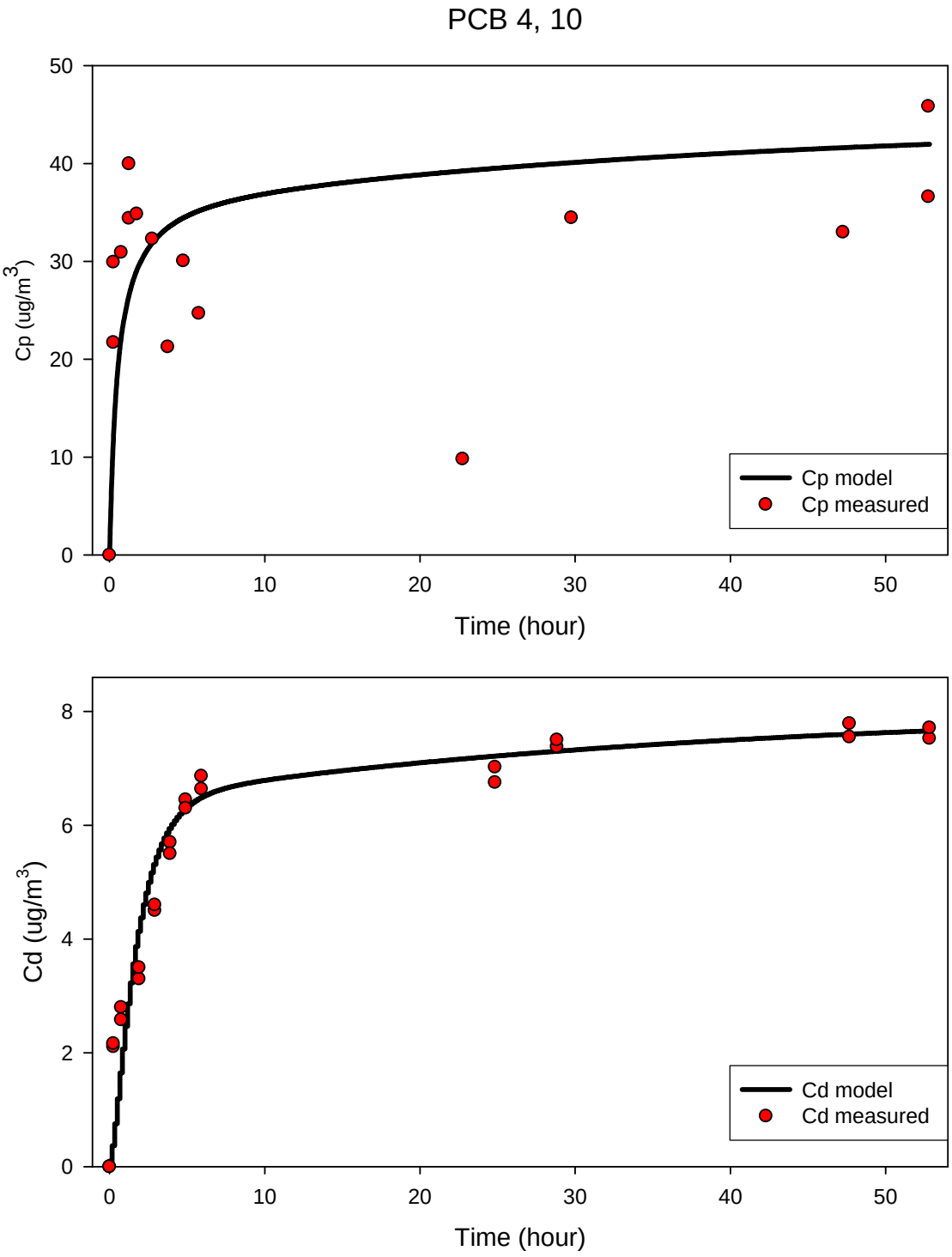
PCB 4, 10
Cp (ug/m3)
Time (hour)
Cp model
Cp measured
Cd (ug/m3)
Time (hour)
Cd model
Cd measured

Figure 6.16:

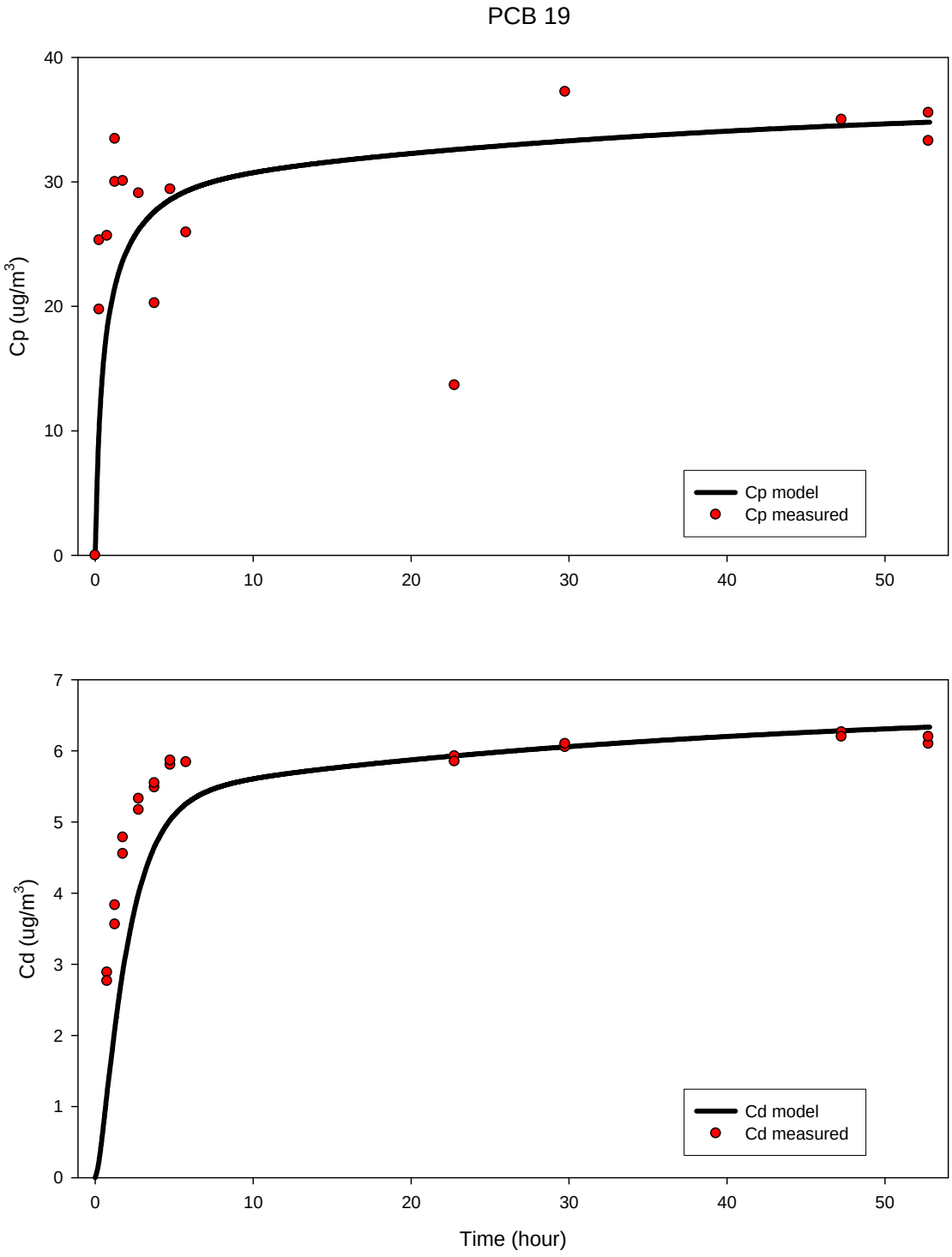
PCB 19
Cp (ug/m3)
Cp model
Cp measured
Cd (ug/m3)
Cd model
Cd measured
Time (hour)

Figure 6.17:

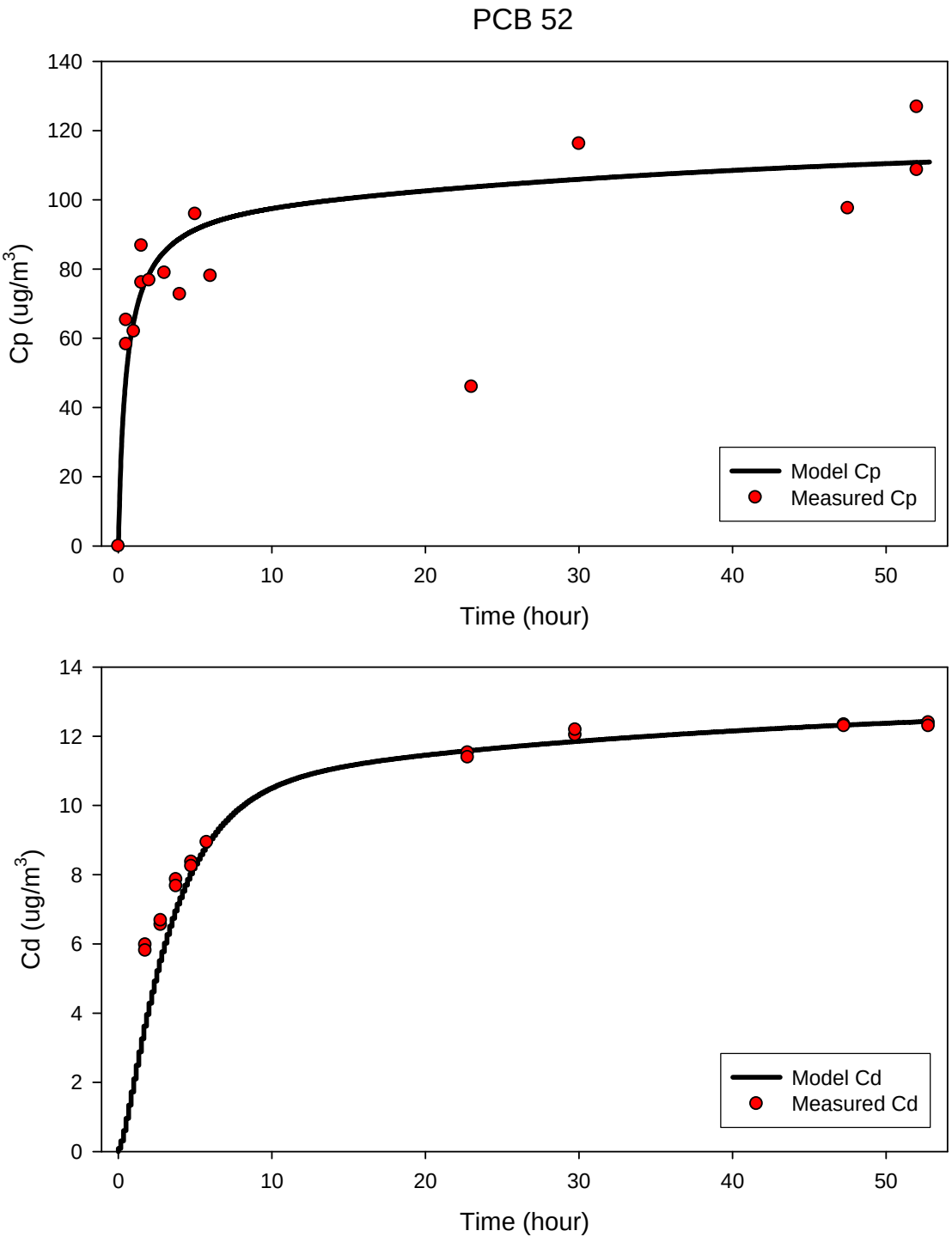
PCB 52
Cp (ug/m3)
Time (hour)
Model Cp
Measured Cp
Cd (ug/m3)
Time (hour)
Model Cd
Measured Cd

Figure 6.18:

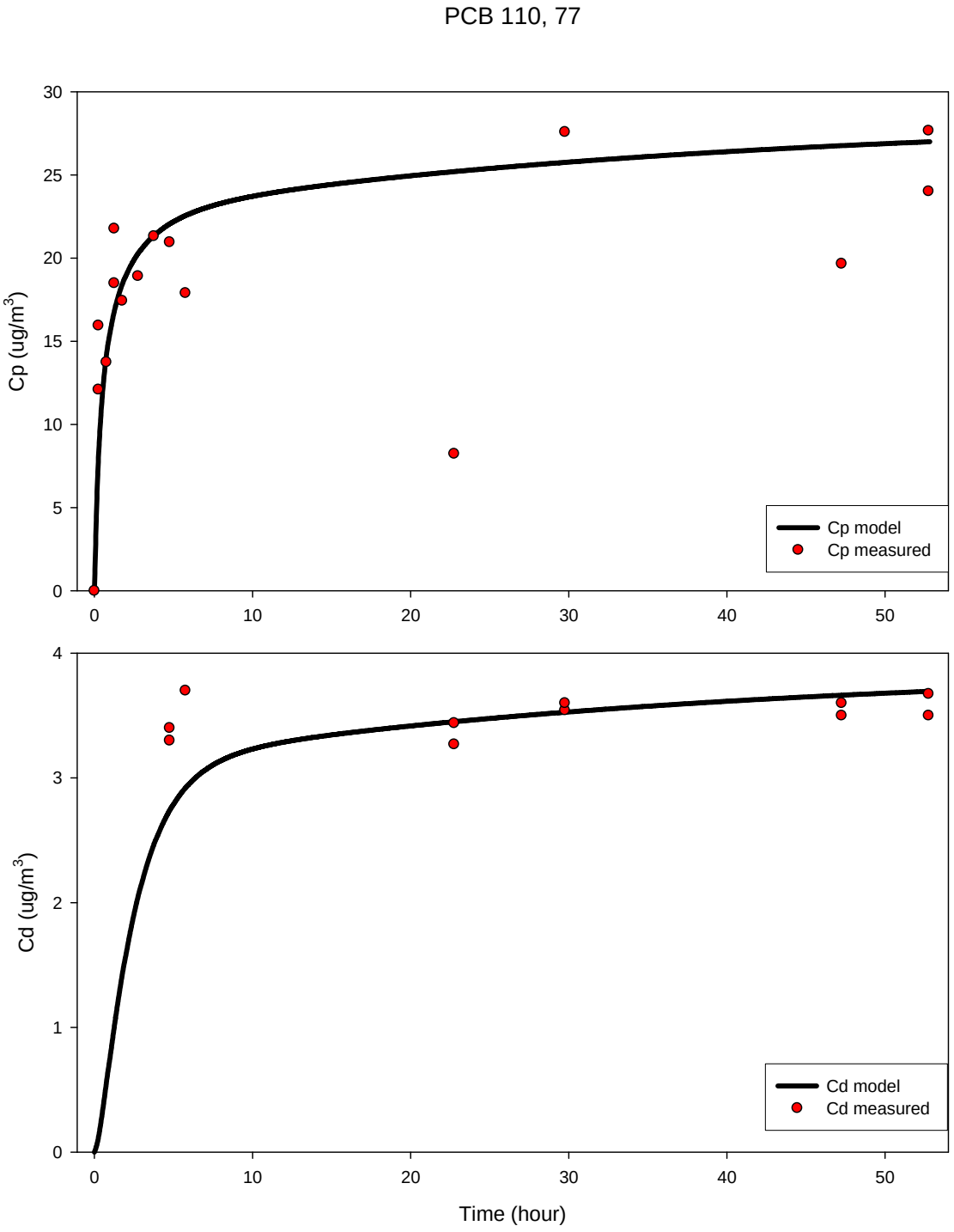
PCB 110, 77
Cp (ug/m3)
Cp model
Cp measured
Cd (ug/m3)
Cd model
Cd measured
Time (hour)

Figure 6.19:

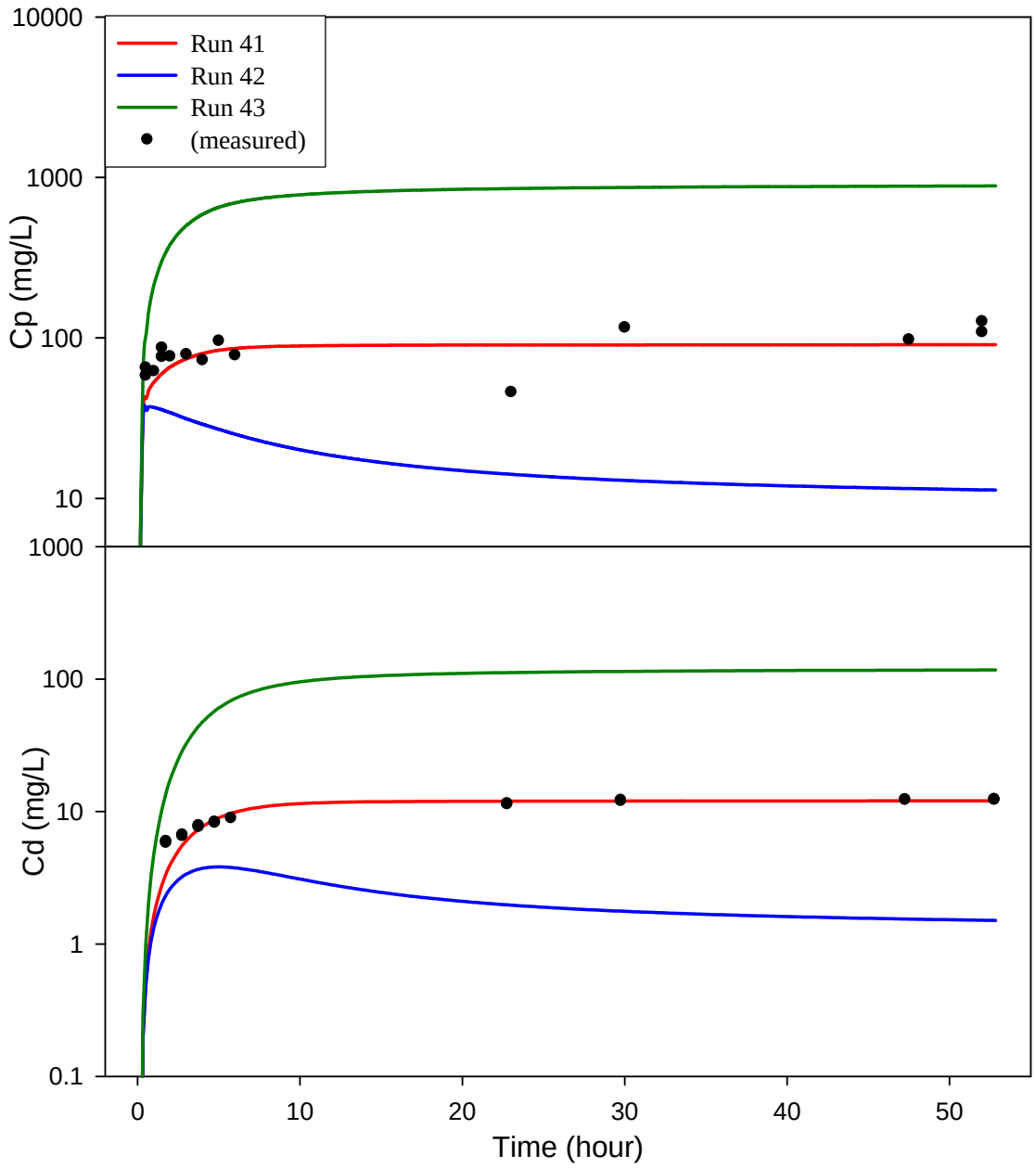
Run 41
Run 42
Run 43
(measured)
Cp (mg/L)
10000
1000
100
10
1000
Cd (mg/L)
100
10
1
0.1
0
10
20
30
40
50
Time (hour)

Figure 6.20:

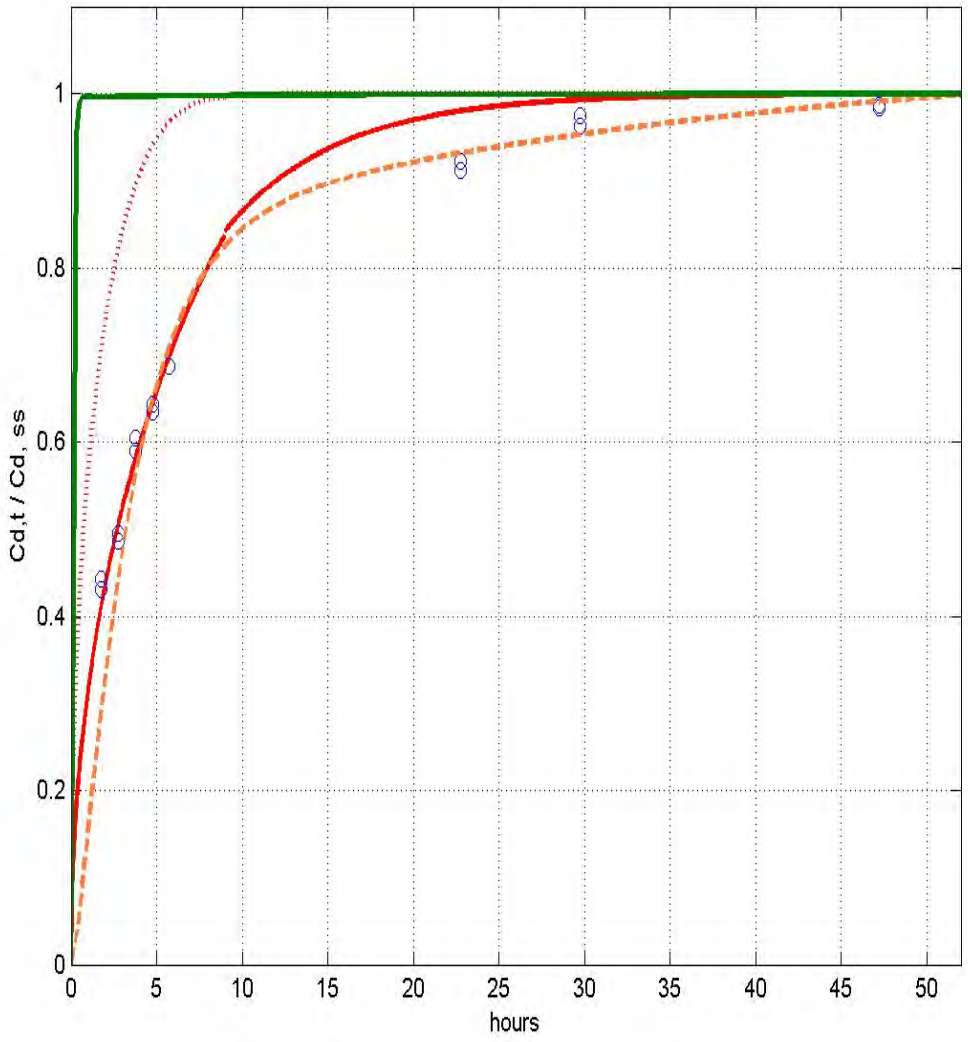

Run 44: Equilibrium Partition

Run 45: Radial diffusion behavior (before floc size adjustment)

Run 46: Radial diffusion behavior (after floc size increased 70%)

Run 47: New kinetic-limited behavior in this study

STORM measurements

OOOOOO

Figure 6.21:

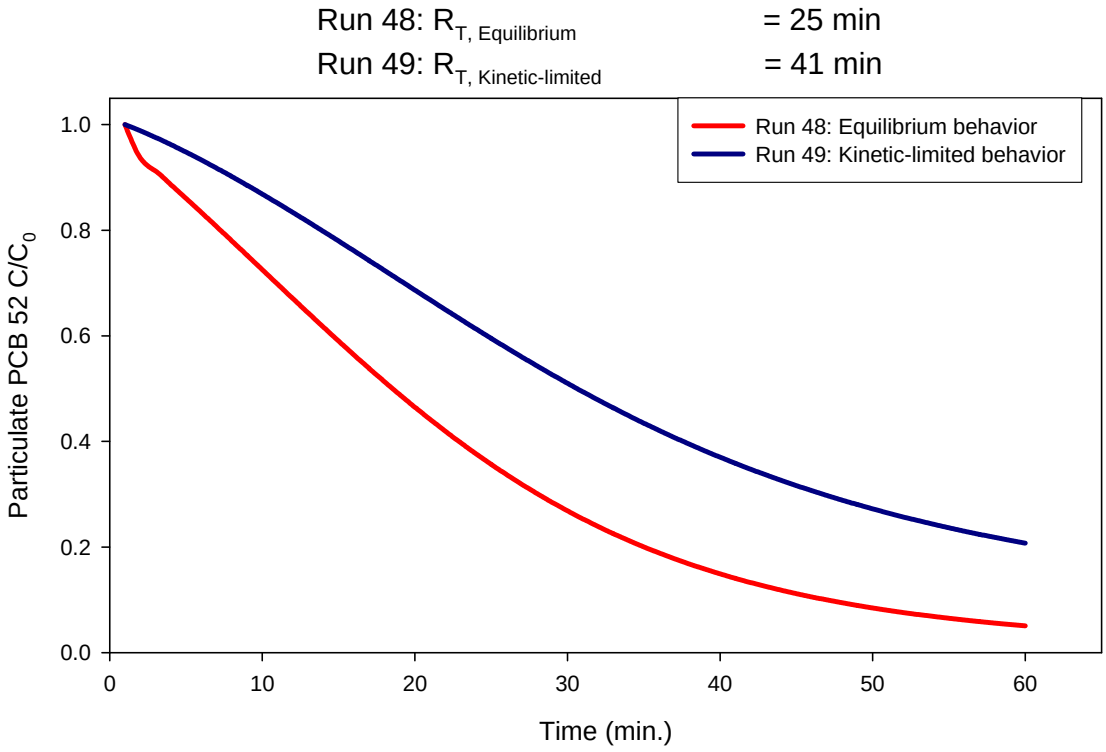
Run 48: $R_{T,\ Equilibrium}$ = 25 min
Run 49: $R_{T,\ Kinetic\text{-}limited}$ = 41 min
Run 48: Equilibrium behavior
Run 49: Kinetic-limited behavior
Particulate PCB 52 C/C_0
1.0
0.8
0.6
0.4
0.2
0.0
0
10
20
30
40
50
60
Time (min.)

Table 3.1: The settings and the corresponding assumptions of Runs 1 to 9

Run	diameter (um)	TSS (g)	f_{OC}	solid density	porosity	K_{OC}(m^3/g-OC)	Dm	HOCPOC (ug/m^3)	N*A	MTV (m/sec)
1	50	1	10.0%	2.27	0.92	1.1	4.92E-06	1.404	base case	3.90E-10
2	120	1	10.0%	2.27	0.92	1.1	4.92E-06	1.404	same as run1	1.62E-10
3	50	1	20.0%	2.27	0.92	1.1	4.92E-06	1.404	same as run1	1.95E-10
4	50	1	10.0%	1.6	0.92	1.1	4.92E-06	1.404	same as run1	5.53E-10
5	50	1	10.0%	2.27	0.96	1.1	4.92E-06	1.404	same as run1	8.49E-10
6	50	1	10.0%	2.27	0.92	2.0	4.92E-06	1.404	same as run1	2.14E-10
7	50	1	10.0%	2.27	0.92	1.1	5.60E-06	1.404	same as run1	4.75E-10
8	244	1	10.00%	1.05	0.97	1.1	4.92E-06	1.404	same as run1	5.12E-10
9	18	1	10.00%	2.2	0.25	1.1	4.92E-06	1.404	same as run1	8.80E-12

Table 3.2: The settings and the corresponding assumptions of Runs 10 to 17

Run	diameter (um)	TSS (g)	f_{oc}	solid density	porosity	nf	K_{OC}(m^3/g-OC)	Dm	HOCPOC (ug/m^3)	N^A	MTV (m/sec)
10	50	1	10.0%	2.27	0.960	2	1.1	4.92E-06	1.404	base case	8.49E-10
11	50	1	10.0%	2.27	0.992	1.5	1.1	4.92E-06	1.404	same as run10	4.53E-09
12	50	1	10.0%	2.27	0.800	2.5	1.1	4.92E-06	1.404	same as run10	1.18E-10
13	120	1	10.0%	2.27	0.983	2	1.1	4.92E-06	1.404	same as run10	8.90E-10
14	50	1	20.0%	2.27	0.960	2	1.1	4.92E-06	1.404	same as run10	4.24E-10
15	50	1	10.0%	1.6	0.960	2	1.1	4.92E-06	1.404	same as run10	1.20E-09
16	50	1	10.0%	2.27	0.960	2	2.0	4.92E-06	1.404	same as run10	4.67E-10
17	50	1	10.0%	2.27	0.960	2	1.1	5.60E-06	1.404	same as run10	1.03E-09

Figure 3.3: The settings and the corresponding assumptions of Runs 18 to 22

Run	diameter (um)	TSS (g)	f_{oc}	solid density	porosity	nf	K_{OC} (m^3/g-OC)	Dm	HOC/POC (ug/m^3)	Ni	At	MTV (m/sec)	MTV*NAF
18	50	1	10.0%	2.27	0.960	2	1.1	4.92E-06	1.404	4.10E+12	3.14E-10	8.27E-10	1.06E-06
19	50	1	10.0%	2.27	0.992	1.5	1.1	4.92E-06	1.404	2.05E+13	6.28E-11	4.41E-09	5.68E-06
20	120	1	10.0%	2.27	0.983	2	1.1	4.92E-06	1.404	7.12E+11	7.54E-10	8.68E-10	4.65E-07
21	50	1	20.0%	2.01	0.960	2	1.1	4.92E-06	1.404	4.10E+12	3.14E-10	4.79E-10	6.17E-07
22	50	10	10.0%	2.27	0.960	2	1.1	4.92E-06	1.404	4.10E+13	3.14E-10	8.27E-10	1.06E-05

Table 3.4: Model simulation results in Runs 23 to 26

run	OC_{ss} (mg/L)	TSS_{ss} (mg/L)	Cp OC (ng/L)	Cd (ng/L)	tHOCwater (ng/L)	OCSS (hr.)	Cp OC (hr.)
23	9.07	89.48	118.00	11.78	129.8	12.0	13.3
24	8.41	77.90	110.94	11.86	122.8	10.0	8.5
25	5.58	38.58	90.17	14.26	104.4	9.5	2.2
26	23.32	230.01	306.34	11.90	318.2	15.0	13.2

Study 7: Predicting the Behavior of PCBs in Activated Carbon-Amended Sediments

7.1 Abstract

Traditional contaminated sediment clean-up methods are often complex and demonstrate a poor understanding of the relationship between sediment geochemistry and bio-availability (Ghosh *et al*., 2003). As an alternative, several investigators have proposed adding granular AC *in situ* (e.g., Kosian *et al*., 1999; Lebo *et al*., 2003; Zimmerman *et al*., 2005). AC has a stronger sorption capacity for hydrophobic organic contaminants (HOCs) than do flocs of the same size and OC content. However, organic contaminants sorb more slowly to AC (i.e., have smaller mass transfer velocity) due to the relatively low porosity and higher partitioning coefficient (K_{AC}). Over long time scales, a majority of HOCs will be sequestered in the AC. However, in the absence of flocculation in a dynamic erosional and depositional environment, the initial HOC distribution in the sediment and the relatively slower sorption rate for AC are the dominant factors controlling the distribution of HOCs in the water column. The interaction time becomes a very important issue under conditions when AC does not have enough time to adsorb or compete with other organic particles. The above analysis considers the case where amended AC does not interact with natural sediments or other aquatic particles to form flocs. We found that the lower porosity and higher settling velocities of AC relative to natural OC result in lower steady-state AC concentrations in the water column and longer times to equilibrium.

In AC-amended sediment, the total water column HOC concentration is significantly lower compared to the AC free run. Further, when AC aggregates with sediment particles, this flocculated AC has the same physical properties as the floc, resulting in a slower settling velocity, longer residence time, and higher AC-associated HOC concentration in the water column. When AC is added to contaminated sediments, the total PCB concentration in the water column decreases by 90% (123.4 to 11.4 ng/L). If the AC coagulates with the resuspended sediment, this decrease is partially offset by some AC being entrained in slowly-settling flocs, and the steady-state PCB concentration is 61 ng/L

7.2 Introduction

Hydrophobic organic contaminants (HOCs) are important pollutants in urban estuarine sediments. HOCs include polycyclic aromatic hydrocarbon (PAH) and PCB. Concerns arise due to their toxicity and potential carcinogenicity to humans. Therefore, PCBs production was banned in the mid 1970s (NYS DH, 1998). The distribution and fate of HOCs are highly correlated to their sorptive behavior (Karickhoff *et al*., 1979; Wu and Gschwend, 1986). Sorption to resuspended particles and sediments plays an important role controlling the water column residence times and spatial distributions of HOC in aquatic environments. HOCs residence times and the time required to reach sorptive equilibrium are highly dependent on the chemical character, the surrounding environment, and particle types and compositions (Schnoor, 1996).

Therefore, in 1993 EPA evaluated *in situ* remediation techniques for contaminated sediment (EPA, 1993). Two types of *in situ* contaminated sediment treatments have been conducted in the field, namely biological/chemical treatment methods and solidification/stabilization treatment methods. *In situ* biological/chemical treatment involves the addition of microorganisms and/or chemicals to the sediments to initiate or enhance bioremediation. *In situ* solidification/stabilization treatment involves the addition of chemicals or cements, such as

Portland cement, to encapsulate the contaminated sediments and convert them into less soluble or mobile forms (e.g., Murphy *et al*., 1995; Chowdhury *et al*., 1996).

However, traditional *in situ* contaminated sediment clean-up methods are often complex and demonstrate a poor understanding of the relationship between sediment geochemistry and bio-availability (Ghosh *et al*., 2003). As an alternative to traditional methods of cleaning up sites with contaminated sediments, several investigators have proposed adding granular AC *in situ* (e.g., Kosian *et al*., 1999; Lebo *et al*., 2003; Zimmerman *et al*., 2005). This added carbon effectively sequesters PCBs, reducing bioavailability and therefore the level of risk associated with the contaminated sediments (Zimmerman *et al*., 2004). Zimmerman and colleagues (2005) mixed 3.4% AC with contaminated sediment at Hunters Point, San Francisco Bay, reducing the bio-availability of PCBs by 82% for worms and 70% for amphipods.

However, these methods have been demonstrated mainly in laboratory experiments. They assume AC either was well mixed with sediment suspending in the experimental chamber, or simply remained on the chamber bottom (Zimmerman *et al*., 2005; Sun and Ghosh, 2007). These experiment designs left significant operational questions remain prior to their application in the field on a large-scale. Of primary importance is the fate of the AC particles in the sediments. Are they stable? How do we tell the contribution between AC and OC on HOC remediation, which is difficult to measure in a dynamic environment (Simpson and Hatcher, 2004)? Do they aggregate with sediment particles? Are they susceptible to resuspension? If they will resuspension, do HOCs concentrations higher in the resuspended AC than other resuspended OC? Do they have a different residence time and steady state concentration than OC in the water column? Further, during the limited interaction time, do AC have the same remediation effect?

To address these questions, the model developed in the previous chapters is modified to include AC as a state variable. Scenarios are examined in which the AC particles are resuspended and aggregate with eroded sediments to explore the long-term performance of the *in situ* remediation.

7.3 Objectives

The overall objective of this chapter is to use the model to explore the behavior of AC when added to sediments as an *in situ* remediation technology.

7.4 Strategies

In this application, the previously developed dynamic sediment-water exchange/ flocculation/ HOC partitioning model was modified to include AC as a state variable (Figure 7.1 and 7.2). To simplify model parameters and environmental settings, the same STORM experiment conditions were used as in prior model development (Chapters 2 and 3). AC was added to the model in two stages, first insuring that the additional state variable behaves as expected in isolation and does not interfere with the previously calibrated parameters, then allowing for interactions (flocculation and sorption competition) among AC and sediments. This enhanced model is then used to explore the influence of AC on the fate of HOC in the water column, when AC interacts with natural sediments to form flocculated particles.

First, AC particles with specific properties were added as a state variable to the model. Model performance was verified by first focusing on the behavior of AC and OC independently, including deposition to and resuspension from the sediment bed and PCB diffusion into and from the particles. In this stage, the model was used to examine the competitive interactions between AC and OC for PCB partitioning, without allowing for flocculation.

Second, after demonstrating model performance with the additional AC state variable, we then allowed AC to coagulate with resuspended sediment particles, forming mixed AC-OC aggregates. The model explicitly calculates the size-specific physical properties (bulk density, porosity, settling velocity, and stickiness coefficient) of these mixed aggregates. The impact of these aggregates on PCB concentrations and speciation in the water column was examined.

7.5 Properties of suspended solids, OC, and AC used in these simulations

The OC and bulk suspended solids (TSS) have the same properties as in the previous chapter, which are controlled by the fractal factor, the nature of the primary particle, f_{OC}, and floc diameter. Properties of the AC are D_{50} is 150 μm, porosity is 0.55, f_{OC} is 0.44, and K_{AC} is 1000 times larger than K_{OC} (Zimmerman *et al*., 2005).

7.6 Stage one: Model evaluation with AC in the absence of flocculation

7.6.1 Model Scenarios and Settings

Eight model runs were conducted to systematically add and evaluate AC to the model (Table 7.1). Runs 1.1 to 1.3 compared rates and times to equilibrium of PCB diffusion into AC and OC for a suspension (*i.e.*, no erosion or settling). Runs 1.4 and 1.5 tested the impact of deposition-resuspension on the steady state solid concentration and dissolved and particle HOC concentrations when either OC or AC is present in the sediments and water column. Here, AC and OC of equal particle size are assumed to be resuspended at the same rate when under the same bottom shear stress.
Runs 1.6 to 1.8 examined the HOC sorption competition between AC and OC and the impact of the initial distribution of HOC between OC and AC in the sediment.

7.6.2 Results and Discussions

Before adding AC to the model, we verified that the existing model gave identical results as previous runs (Chapter 2) when using the same initial conditions. AC was added as a state variable to the model, and a run was made where all of the solids in the slurry were AC, at the same concentration as OC in the base case run. This run reached the same steady state HOC concentration in the dissolved and particle phases when the AC and OC partition coefficients were set to be equal. The only difference between these two runs was the time to reach steady state. As expected, the run with AC took longer to reach steady state than the OC-only run because AC is less porous than the same size OC flocs. The diffusion rate is controlled by the total contact area and mass transfer velocity. In run 1.3, the AC partition coefficient was increased to 1000 times that of OC. As a result, the steady state HOC concentration increased and the time to reach steady state was much longer because increasing K_{AC} significantly decreases the mass transfer velocity. In short, AC has a stronger HOC capacity than the same size OC because of the difference of partition coefficient. However, AC requires a longer time to reach steady state or equilibrium than the same size of flocs. These results could affect the HOC fate in a dynamic environment.

Run 1.4 to 1.8 expanded the simulations above to include settling and resuspension, but still did not include flocculation. AC and OC were resuspended at equal rates in these runs. Runs 1.4 and 1.5 differ in how the carbon and HOC are initially distributed in the sediment (100% in OC in run 1.4 *versus* 100% in AC in run 1.5). Under these conditions with settling and resuspension, AC reached a lower steady state mass concentration in the water more quickly than OC because

it has a faster settling velocity (higher bulk density than OC flocs for a given particle size). Further, AC has a stronger sorption capacity and a slower sorption rate than the same size of OC. As a result, the resuspended carbon concentration decreases 99.3%, and total water column HOC concentration decreases 99.5% in run 1.5 compared to run 1.4.

Run 1.6 assumed AC and OC were each 50% of the initial sediment total carbon content and sediment HOC reached equilibrium status between AC and OC as the initial condition. The steady state mass concentration of AC and OC are the same whether beginning with only one or the other in the sediments (runs 1.4 and 1.5) or both (run 1.6), verifying the particles are acting independently in this version of the model. Furthermore, although AC was responsible for 0.7% of total steady state water column carbon in run 1.6, the total water column HOC in run 1.6 decreased 98.7% compared with run 1.4.

Runs 1.6 to 1.8 compared total water column HOC concentration under three different initial sediment HOC distributions. All runs were simulated based on the same solids transport. As shown in Table 1, with limited contact time between the HOC and the AC, the initial sediment HOC in AC was lower than the equilibrium status. Under these initial conditions, the total water column HOC concentrations are 76 times higher than resuspension events where the HOCs had enough time to adsorb. These results suggest that the interaction time is a very important issue under conditions when AC does not have enough time to adsorb or compete with other organic particles.

The steady state concentrations of particulate (Cp) and dissolved (Cd) PCB 52 are much higher when OC sediments are resuspended (run 1.4) than when the PCBs begin sorbed to AC in the sediment (run 1.5). Total (dissolved plus particulate) PCB congener 52 concentrations are higher when OC is resuspended compared to AC resuspension (225 to 1.2 ng/m^3) for two reasons. First, the steady-state OC concentration in the water column is higher due to slower settling velocities. Both runs start with the same initial sediment HOC concentration and resuspension rate, and therefore the PCB gross erosion fluxes are the same. However, the lower settling velocity of OC relative to AC results in more HOC in the water column. The dissolved HOC concentration, which is proportional to the particulate HOC concentration, is also higher in the OC run. Finally, since the AC mass transfer velocity is substantially smaller than that of OC, less HOC is released to the dissolved phase as a result of AC resuspension (more time is required to desorb into the water column).

The objective of runs 1.6 to 1.8 is to examine the impact of the initial sediment HOC concentration distribution on the fate of dissolved HOC. All three runs were based on the same solid transport. Run 6 assumed sediment HOC (ng-PCB 52/m^3) was evenly distributed between AC and OC in the sediment layer. In contrast, the sediment HOC was allowed to reach equilibrium between sediment porewater, sediment Cp_{OC}, and sediment Cp_{AC} (run 1.8). An intermediate initial condition, in which the 75% of the HOC was initially associated with the AC, was also explored (run 1.7). The total HOC mass and the particle transport rates are the same among these runs, as verified by identical trends in AC and OC concentrations. However, because AC has a higher partition coefficient than OC, most HOC is associated with sediment AC rather than sediment OC. Combining the effects of the initial sediment HOC distribution and concentrations of resuspended solids, the dissolved and OC-associated PCB concentrations are much lower in run 1.8 than run 1.6, as the bulk of the PCB remains bound to AC. In run 7, in which the HOC initial distribution was intermediate, the C_d, Cp_{OC}, Cp_{AC} values are between those of run 1.6 and run 1.8.

AC has a stronger sorption capacity than flocs of the same size and OC content. However, AC has a slower sorption rate (smaller mass transfer velocity) due to its relatively lower porosity and higher K_{AC} value. Over long time scales, a majority of HOCs will be sequestered in the AC. However, in the absence of flocculation in a dynamic erosional and depositional environment, the initial HOC distribution and the relatively slower sorption rate for AC are the dominant factors controlling the distribution of HOCs in the water column. The interaction time becomes a very important issue under conditions when AC doesn't have enough time to adsorb or compete with other organic particles.

The above analysis considers the case where amended AC does not interact with natural sediments or other aquatic particles to form flocs. We found that the lower porosity and higher settling velocities of AC relative to natural OC result in lower steady-state AC concentrations in the water column and longer times to sorptive equilibrium. In the next section, we well examine what happens when these AC particles become part of larger, more porous, less dense flocs.

7.7 Stage Two: Model Evaluation with Added AC and Flocculation

7.7.1 Stage Two Descriptions and Settings

Beginning with the model described above, we now allow flocculation to occur between AC particles and the natural OC. We assume that AC, OC, and inorganic solids (INS) are components of flocs with settling velocities and porosity determined by the relative contribution of the three particle types. Floc porosity is a function of the fractal factor, the nature of the primary particle, and the floc diameter, which means that the AC content has no impact on the floc porosity for any given size of flocs. The TSS is the sum of INS, OC and AC, and the weighted fractional OC ($f_{OC,\,total}$) equals (OC+AC)/TSS. Both the floc solid density and the stickiness coefficient are calculated as linear functions of f_{OC} and f_{AC} (Equations 7.1-7.3).

$$\rho_{dry,i} = 2 \times f_{OC,i} \times \rho_{biotic} + (1 - 2 \times f_{OC,i} - f_{AC,i}) \times \rho_{clay} + f_{AC,i} \times \rho_{AC} \qquad \text{Equation 7.1}$$

$$\rho_{bulk,i} = \rho_{dry,i} \times (1 - \phi_i) + \rho_{water} \times \phi_i \qquad \text{Equation 7.2}$$

$$\alpha_i = 2 \times f_{OC,i} \times \alpha_{biotic} + (1 - 2 \times f_{OC,i} - f_{AC,i}) \times \alpha_{clay} + f_{AC,i} \times \alpha_{AC} \qquad \text{Equation 7.3}$$

where $\rho_{dry,i}$ is dry floc density (g/m^3), $\rho_{bulk,i}$ is bulk floc density (g/m^3), α_i is floc stickiness coefficient for floc at size i, f_{OC} and f_{AC} are fraction of OC and AC for floc at size i, ρ_{biotic}, ρ_{clay}, ρ_{AC} are OC, inOC, and AC dry density (g/m^3), ρ_{water} is water density (g/m^3), φ_i is floc porosity for floc at size i, and α_{biotic}, α_{clay}, α_{AC} are OC, inorganic carbon, and AC stickiness coefficient respectively.

7.7.2 Model Scenarios

Seven model scenarios were created to successively explore the interaction of AC and OC and its impact of HOC partitioning (Table 7.2). The model began with the same settings and initial conditions as described above, and PCB 52 was used as the target contaminant. In run 2.2 to 2.7, the model assumed natural OC and AC were each responsible for 50% of TOC.

1. Run 2.1: In this 'base case' run, the model started with the same settings as described above and did not contain AC. The model included flocculation and resuspension-deposition processes.
2. Run 2.2 and 2.3: AC is added as a model variable, and the model had the same resuspension flux rate as run 1 for total organic carbon (TOC = sum of OC and AC) and TSS. As an initial condition, the AC has a diameter of 150 μm and a mass concentration

equal to the sum of organic substrates for all size of flocs. The floc properties then vary temporally with the composition of AC, OC, and INS. The model is initialized with HOCs in the sediment reaching equilibrium among AC, OC, and porewater, which was the result after a 100 year simulation (Appendix 1). Runs 2.2 and 2.3 compare two different settling velocity calculations (Stokes law equation *versus* fractal geometry adjusted settling velocity equation) for AC in the absence of flocculation.

3. Run 2.4: Model starts with the same physical and chemical conditions as run 2.3. However, in this run OC is allowed to coagulate while flocculation of AC is prevented.
4. Run 2.5: The model begins with the same physical and chemical conditions as run 2.3 but AC is allowed to coagulate, which affects the floc density, mass transfer velocity, stickiness coefficient, and settling velocity.
5. Run 2.6: This run explores the possible impact of selective resuspension of AC relative to OC. The model started with the same physical and chemical settings as run 2.3 except the AC erosion rate was doubled. To simplify interpretation of the simulation results, AC did not flocculation in this run.
6. Run 2.7: Earlier we found the initial sediment HOC distribution played an important role in the fate of HOCs in the water column. In this run, the model uses the same physical setting as run 2.5, AC is allowed to coagulate, and sediment HOCs are evenly distributed between OC and AC

7.7.3 Results and Discussions

The temporally varying results for the AC, OC, TSS, and related HOC variables for all scenarios are shown in Figures 7.3 to 7.7. Similar to run 1.6, although AC only responded with 1% of TSS, the water column HOC decreased by 50% in run 2.2 compared to run 2.1 to emphasize the importance of AC on the fate of HOCs in the water column.

The settling velocity is an important factor determining the fate of AC and related HOC in the water column. Run 2.2 assumed that AC did not aggregate with flocs and that its shape did not follow principles of fractal geometry. Therefore, Stokes' law was used to calculate the AC settling velocity in run 2.2 instead of the fractal geometry adjusted settling equation used in run 2.3. Under the same resuspension flux, fractal settling was slower and the steady state AC concentration in the water column was 5.5 times higher in the run that assumed AC became a part of the floc (run 2.3) rather acting as an independent solid (run 2.2). Although the dissolved and organic carbon-associated HOC concentration did not significantly change between runs 2.2 and 2.3, the AC-related HOC concentration was 5.3 times higher when the AC particles followed fractal rather than Stokes settling.

After including the flocculation effect (run 2.5), the resuspended AC concentration and total water column HOC concentration were approximately 5 times higher compared to the run without flocculation (run 2.2). Further, runs 2.4 and 2.5 compared the effect of flocculation on OC and AC and their related HOC concentrations (Figures 7.11 and 7.12). The impact of AC as a part of the flocs was discussed in the previous paragraph. After including flocculation of AC, the suspended AC concentration decreased because of the formation of larger AC contained flocs (Figure 7.13). Thereafter, the total HOC (ng/L) in the water column decreased by 10%, especially AC-related HOC, in run 2.5 compared to run 2.4. However, the total water column HOC in run 2.5 was still 4.8 times higher than in run 2.2. When full flocculation is considered in a dynamic particle environment that includes all three types of solids, sediment resuspension, settling, and kinetic-limited HOC partitioning, the steady state total suspension solid

concentration decreased by 34%, the total PCB-52 concentration in the water column increased nearly four-fold, and the water column HOC residence time increased by 37%.

The importance of suspended AC on the water column HOC concentration was demonstrated again in run 2.6 (Figure 7.14). With the slow mass transfer velocity from AC, the sediment AC resuspension rate was doubled, and yet the dissolved HOC concentration only increased by less than 1% after a 53 hour simulation, even though the total water column HOC and AC-related HOC concentrations were almost double those used in run 2.4. Therefore, during a strong resuspension event (such as run 2.6), the dissolved HOC concentrations remained as low as those prior to the resuspension event due to the very strong sorptive capacity of the AC.

In stage one of the model developments discussed earlier in this chapter, we observed that the interaction time is a very important issue under conditions when AC has insufficient time to adsorb or compete for HOCs with other organic particles. When flocculation is added, the interaction time also demonstrated a strong influence on the fate of water column HOC (Figure 7.15). Without sufficient interaction time, the total HOC concentration in run 2.7 increased nearly eight times compared to run 2.2.

7.8 Summary

AC has a stronger sorption capacity than flocs of the same size and with the same OC content. However, AC has a slower sorption rate (smaller mass transfer velocity) due to its relatively lower porosity and higher K_{AC} value. Over long time scales, the majority of HOCs will be sequestered in the AC. However, in the absence of flocculation in a dynamic erosional and depositional environment, the initial HOC distribution and the relatively slower sorption rate for AC are the dominant factors controlling the distribution of HOCs in the water column. The interaction time becomes a very important issue under conditions when AC does not have sufficient time to adsorb or compete with other organic particles. The above analysis considers the scenario where the amended AC does not interact with the natural sediments or other aquatic particles to form flocs. We found that the lower porosity and higher settling velocities of AC relative to natural OC result in lower steady-state AC concentrations in the water column, and longer times to reaching sorptive equilibrium.

With the enrichment of AC, the total water column HOC concentration significantly decreases. Further, when AC aggregates with sediment particles, AC is going to have the same physical properties as particles of similar floc size, which results in a slower settling velocity compared to single AC particles, and will coherently have a longer residence time and higher AC related HOC concentration in the water column. When AC is added to contaminated sediments, the total PCB concentration in the water column decreases by 90% (123.4 to 11.4 ng/L). If the AC coagulates with the resuspended sediment, this decrease is partially offset by some AC being entrained in slowly-settling flocs, and the steady-state PCB concentration is 61 ng/L.

7.9 Figure Captions

Figure 7.1 and 7.2: Flow diagrams for refining the PCB fate and the flocs transport model to include (1) flocculation kinetics, (2) PCB partitioning kinetics, and (3) AC as a state variable.

Figure 7.3: Comparison of the predicted temporally varying resuspended OC, AC, and inorganic solids among different scenarios at stage two

Figure 7.4: Comparison of the predicted temporally varying water column PCB 52 (ng/L) in the OC, AC, and dissolved water among different scenarios at stage two

Figure 7.5: Comparison of the predicted temporally varying total water column PCB 52 (ng/L) among different scenarios at stage two

Figure 7.6: Comparison of the predicted steady state resuspended OC, AC, and inorganic solids among different scenarios at stage two

Figure 7.7: Comparison of the predicted steady state water column PCB 52 (ng/L) in the OC, AC, and dissolved phases among different scenarios at stage two

Figure 7.8: Predicted behavior of PCB 52 and solids in carbon-amended sediments. This is a reference run without AC (Run 2.1). The model starts with the equilibrium sediment PCB 52 between OC and porewater and includes flocculation, resuspended, and deposition processes.

Figure 7.9: Predicted behavior of PCB 52 and solids in AC-amended sediments. This is a run without flocculation that includes AC (Run 2.2). The model starts with the equilibrium sediment PCB 52 among AC, OC and porewater and includes resuspension and deposition processes. The AC settling is calculated using the Stokes' law settling velocity equation.

Figure 7.10: Predicted behavior of PCB 52 and solids in AC-amended sediments. This is a run without flocculation that includes AC (Run 2.3). The model starts with the equilibrium sediment PCB 52 among AC, OC and porewater and includes resuspension and deposition. The AC settling is calculated using the fractal geometry adjusted settling velocity equation.

Figure 7.11: Predicted behavior of PCB 52 and solids in AC-amended sediments. This is a run with flocculation of OC but not AC (Run 2.4). The model starts with the equilibrium sediment PCB 52 among AC, OC and porewater and with resuspended, and deposition processes. The AC is adapted fractal geometry adjusted settling velocity equation.

Figure 7.12: Predicted behavior of PCB 52 and solids in AC-amended sediments: this is a run with flocculation on both carbon solids and AC is involved (Run 2.5). The model starts with the equilibrium sediment PCB 52 among AC, OC and porewater and with resuspended, and deposition processes. The AC is adapted fractal geometry adjusted settling velocity equation.

Figure 7.13: Predicted steady state fraction of AC size distribution at run 2.5

Figure 7.14: Predicted behavior of PCB 52 and solids in AC-amended sediments: this is a run with double AC erosion flux, flocculation on OC and AC is involved (Run 2.6). The model

starts with the equilibrium sediment PCB 52 among AC, OC and porewater and with resuspended, and deposition processes. The AC is adapted fractal geometry adjusted settling velocity equation.

Figure 7.15: Predicted behavior of PCB 52 and solids in AC-amended sediments: this is a run with flocculation on both carbon solids and AC is involved (Run 2.7). The model was initialized with 50 % of sediment PCB 52 in AC and OC respectively. The AC is adapted fractal geometry adjusted settling velocity equation

Figure 7.1:

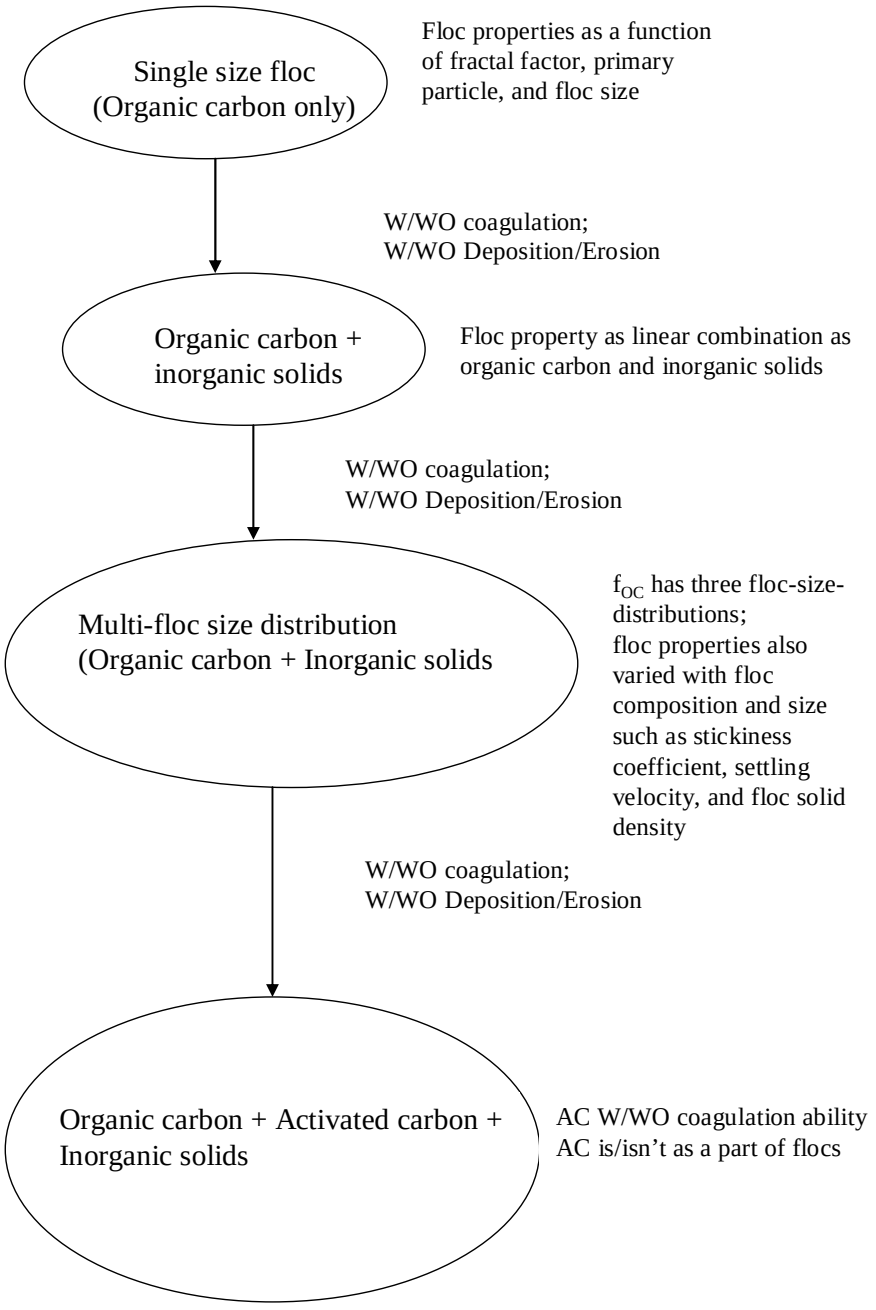
Single size floc
(Organic carbon only)
Floc properties as a function of fractal factor, primary particle, and floc size
W/WO coagulation;
W/WO Deposition/Erosion
Organic carbon + inorganic solids
Floc property as linear combination as organic carbon and inorganic solids
W/WO coagulation;
W/WO Deposition/Erosion
Multi-floc size distribution
(Organic carbon + Inorganic solids
f_{OC} has three floc-size-distributions;
floc properties also varied with floc composition and size such as stickiness coefficient, settling velocity, and floc solid density
W/WO coagulation;
W/WO Deposition/Erosion
Organic carbon + Activated carbon + Inorganic solids
AC W/WO coagulation ability
AC is/isn't as a part of flocs

Figure 7.2:

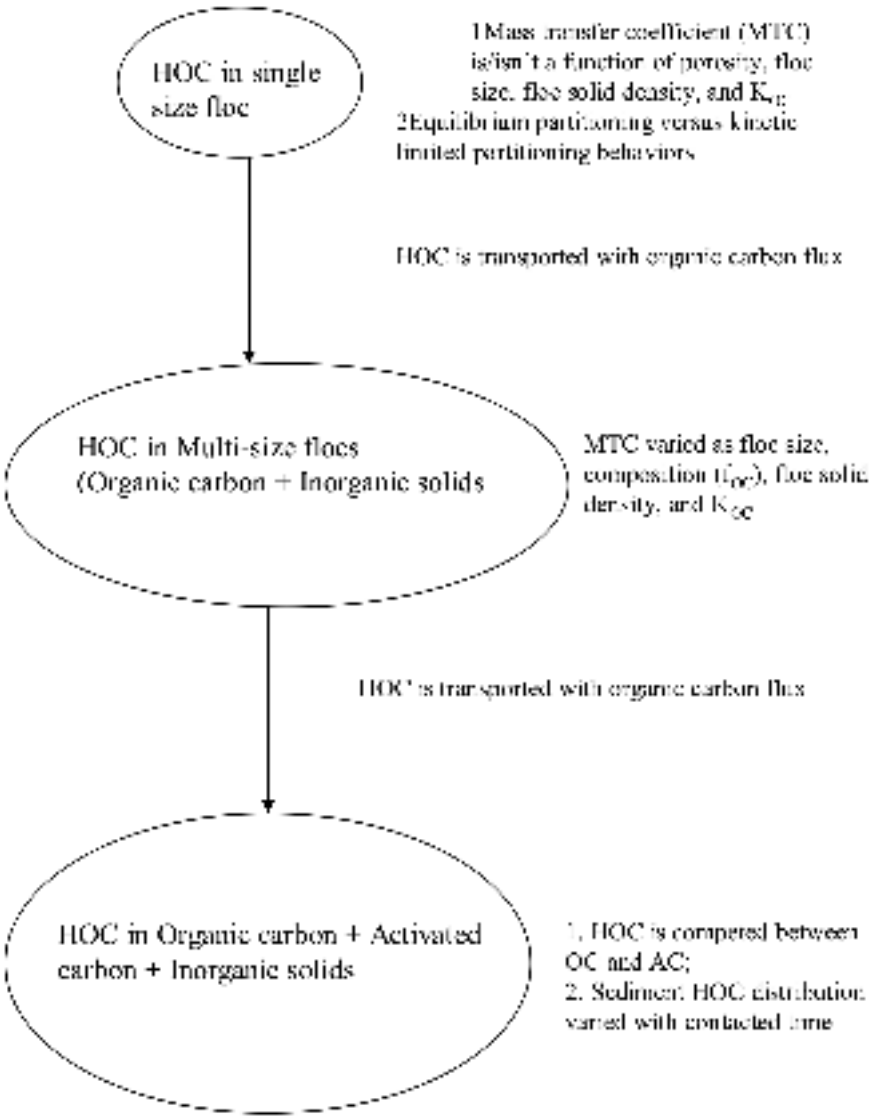
HOC in single size floc
1Mass transfer coefficient (MTC) is/isn't a function of porosity, floc size, floc solid density, and K_{ij}
2Equilibrium partitioning versus kinetic limited partitioning behaviors
HOC is transported with organic carbon flux
HOC in Multi-size flocs (Organic carbon + Inorganic solids
MTC varied as floc size, composition (f_{oc}), floc solic density, and K_{oc}
HOC is transported with organic carbon flux
HOC in Organic carbon + Activated carbon + Inorganic solids
1. HOC is compered between OC and AC;
2. Sediment HOC distribution varied with contacted time

Figure 7.3:

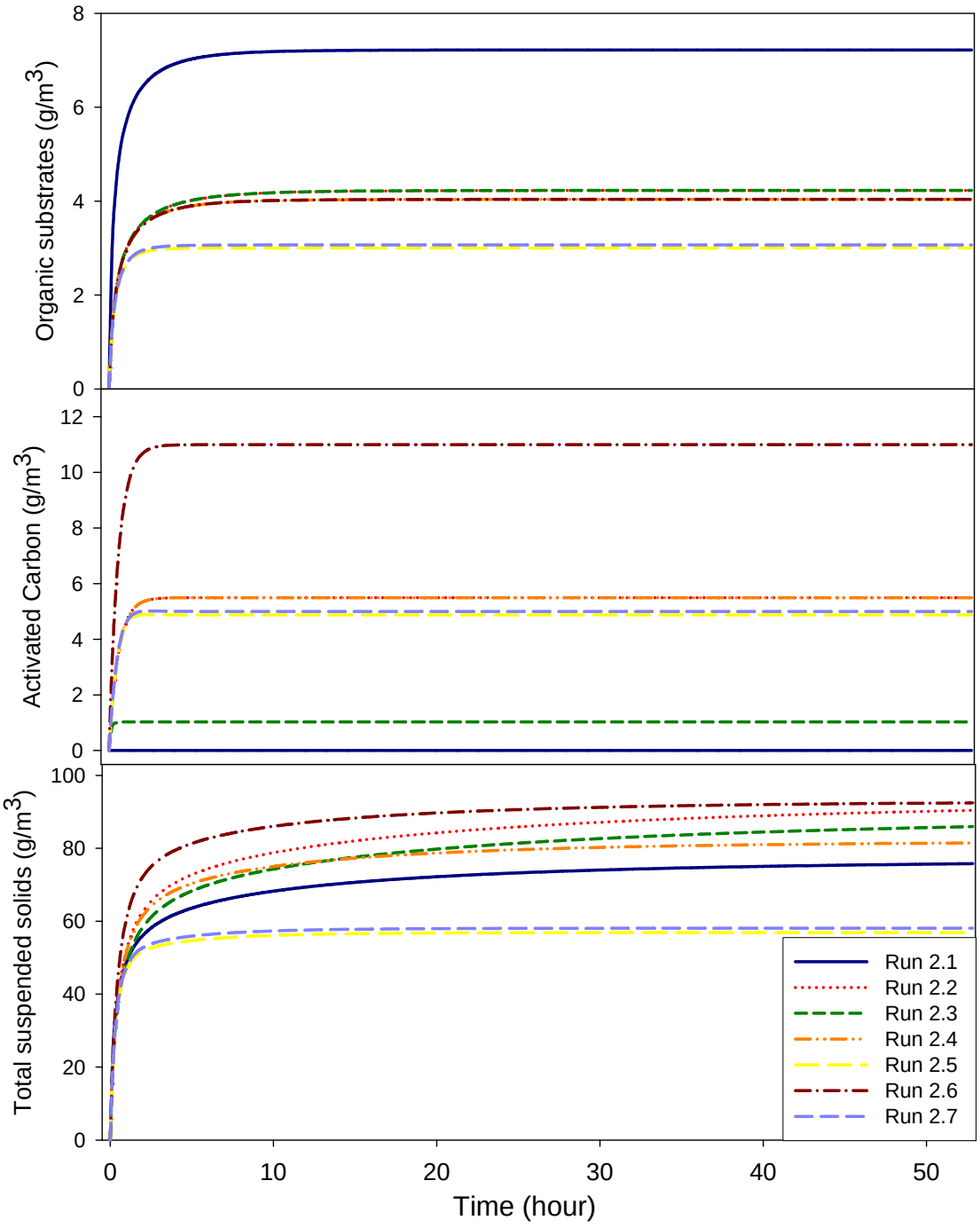
Organic substrates (g/m3)
Activated Carbon (g/m3)
Total suspended solids (g/m3)
Time (hour)
Run 2.1
Run 2.2
Run 2.3
Run 2.4
Run 2.5
Run 2.6
Run 2.7

Figure 7.4:

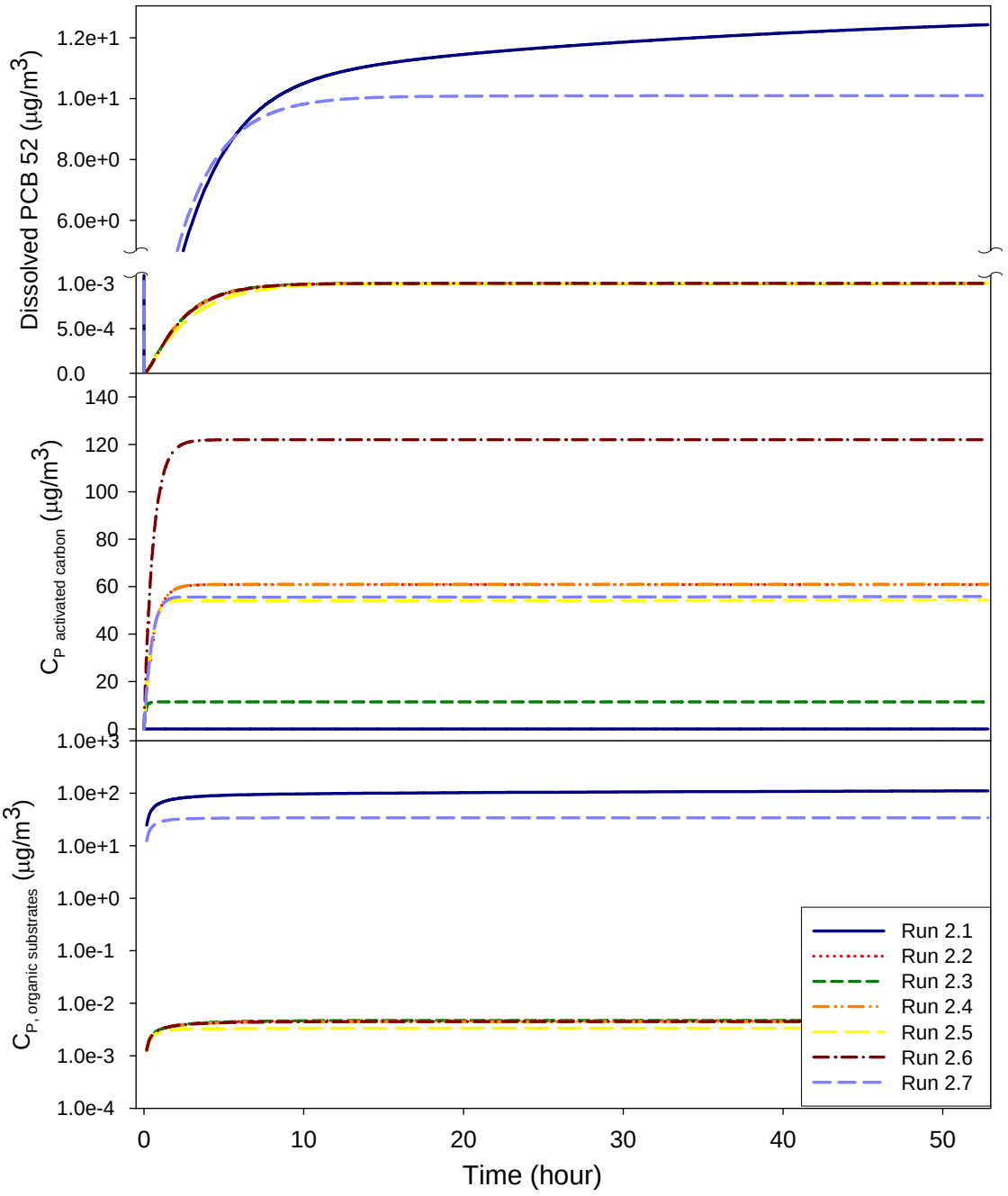
Dissolved PCB 52 (µg/m3)
1.2e+1
1.0e+1
8.0e+0
6.0e+0
1.0e-3
5.0e-4
0.0
CP activated carbon (µg/m3)
140
120
100
80
60
40
20
0
CP, organic substrates (µg/m3)
1.0e+3
1.0e+2
1.0e+1
1.0e+0
1.0e-1
1.0e-2
1.0e-3
1.0e-4
Run 2.1
Run 2.2
Run 2.3
Run 2.4
Run 2.5
Run 2.6
Run 2.7
0
10
20
30
40
50
Time (hour)

Figure 7.5:

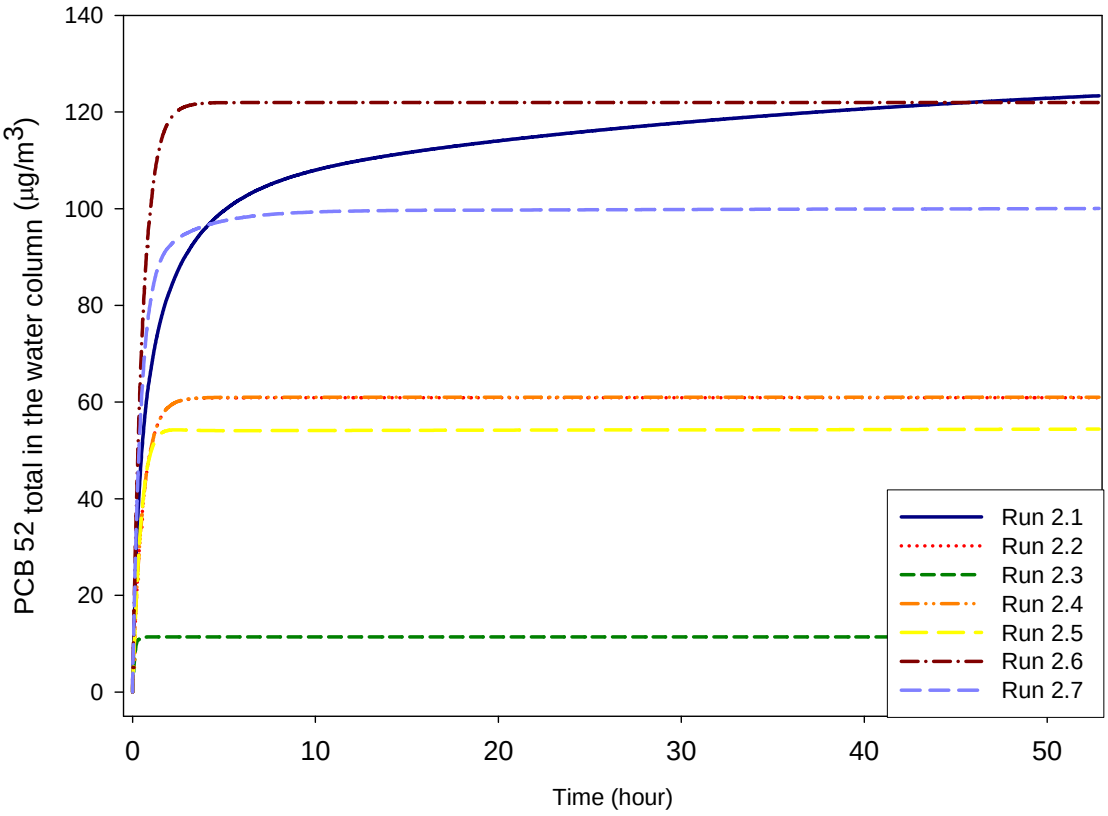
PCB 52 total in the water column (µg/m3)
Time (hour)
0
20
40
60
80
100
120
140
0
10
20
30
40
50
Run 2.1
Run 2.2
Run 2.3
Run 2.4
Run 2.5
Run 2.6
Run 2.7

Figure 4.6

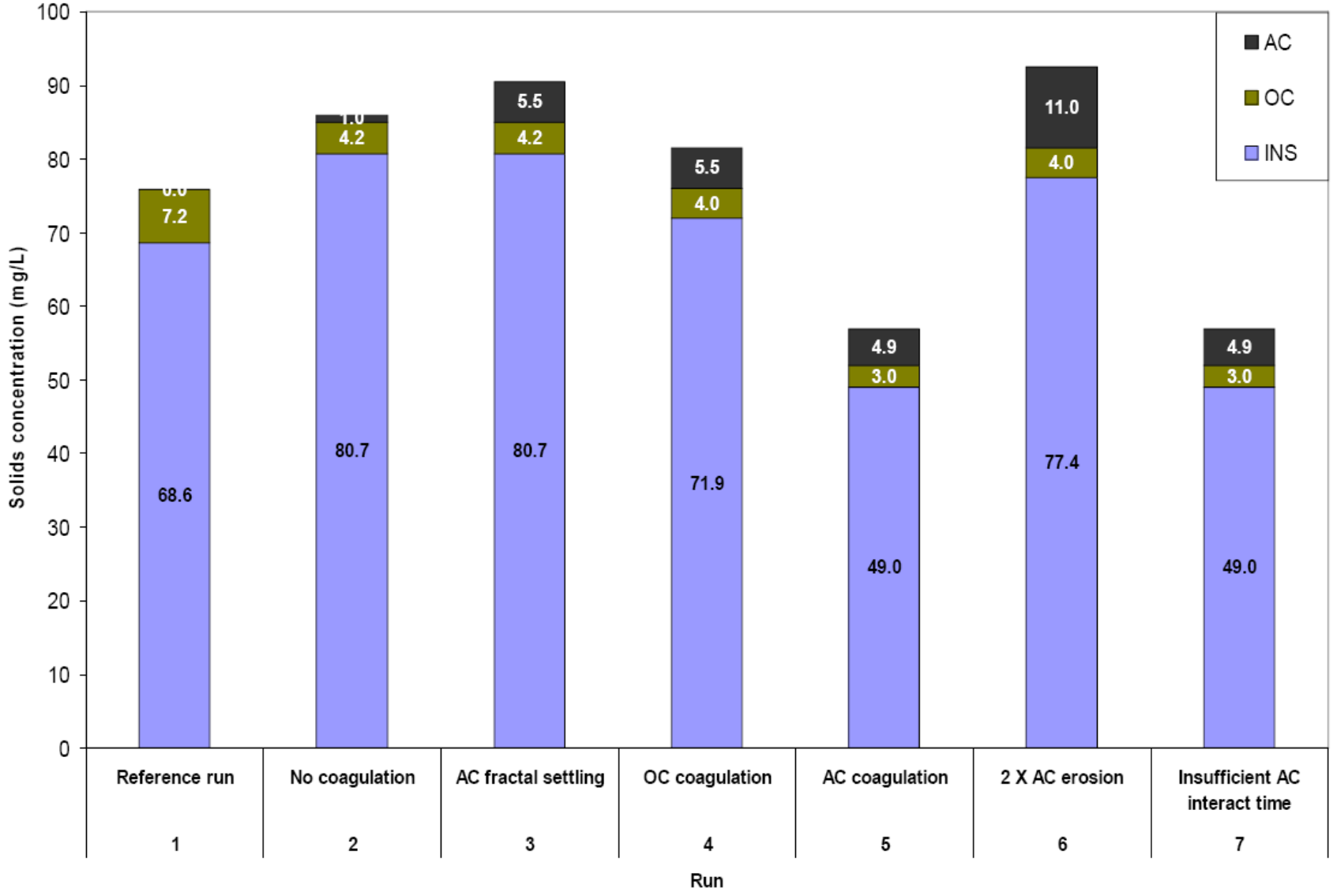
AC
OC
INS
Solids concentration (mg/L)
100
90
80
70
60
50
40
30
20
10
0
7.2
68.6
4.2
80.7
5.5
4.2
80.7
5.5
4.0
71.9
4.9
3.0
49.0
11.0
4.0
77.4
4.9
3.0
49.0
Reference run
1
No coagulation
2
AC fractal settling
3
OC coagulation
4
AC coagulation
5
2 X AC erosion
6
Insufficient AC interact time
7
Run

Figure 4.7

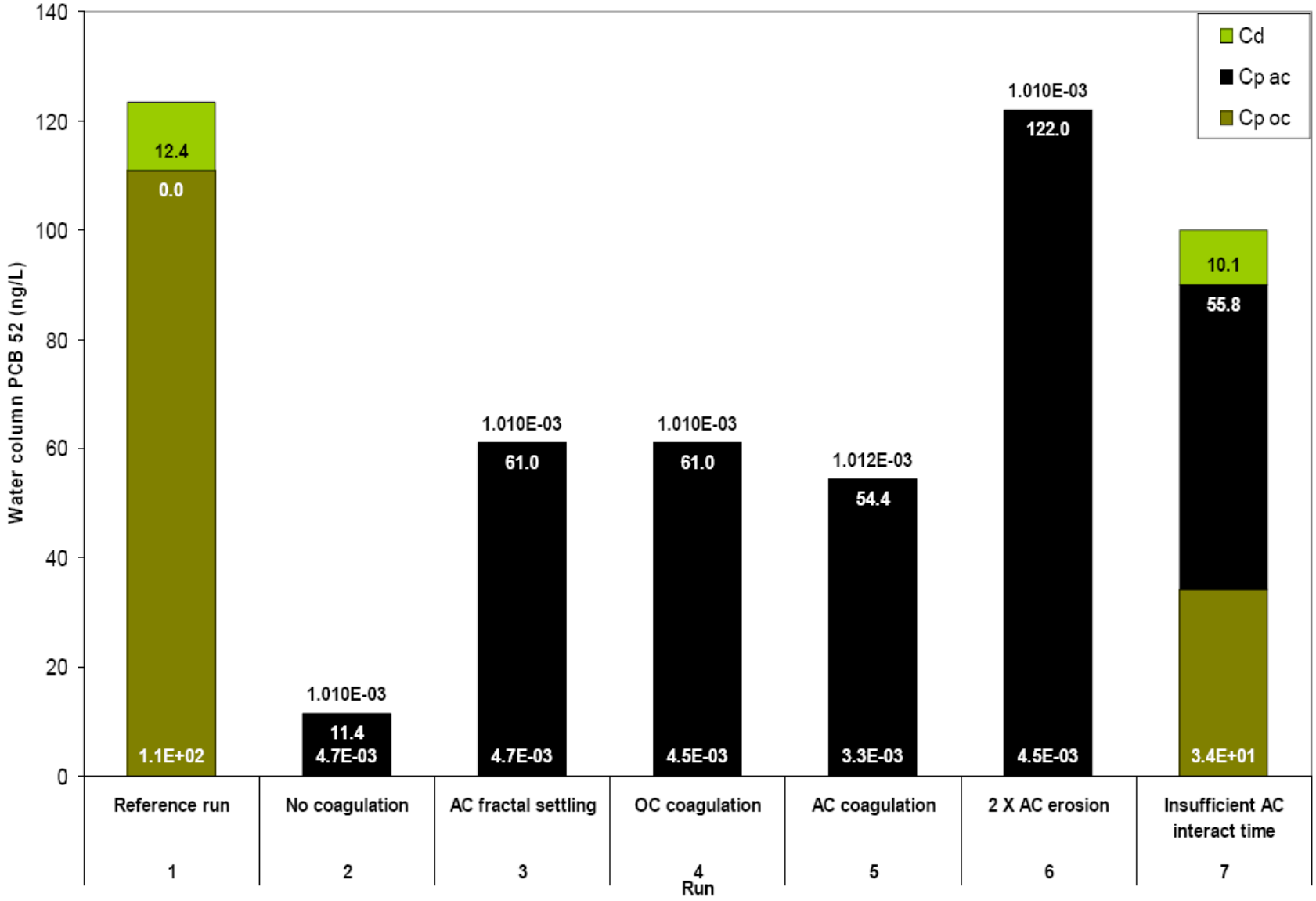
Water column PCB 52 (ng/L)
140
120
100
80
60
40
20
0
Cd
Cp ac
Cp oc
12.4
0.0
1.1E+02
1.010E-03
11.4
4.7E-03
1.010E-03
61.0
4.7E-03
1.010E-03
61.0
4.5E-03
1.012E-03
54.4
3.3E-03
1.010E-03
122.0
4.5E-03
10.1
55.8
3.4E+01
Reference run
No coagulation
AC fractal settling
OC coagulation
AC coagulation
2 X AC erosion
Insufficient AC interact time
1
2
3
4
5
6
7
Run

Figure 7.8:

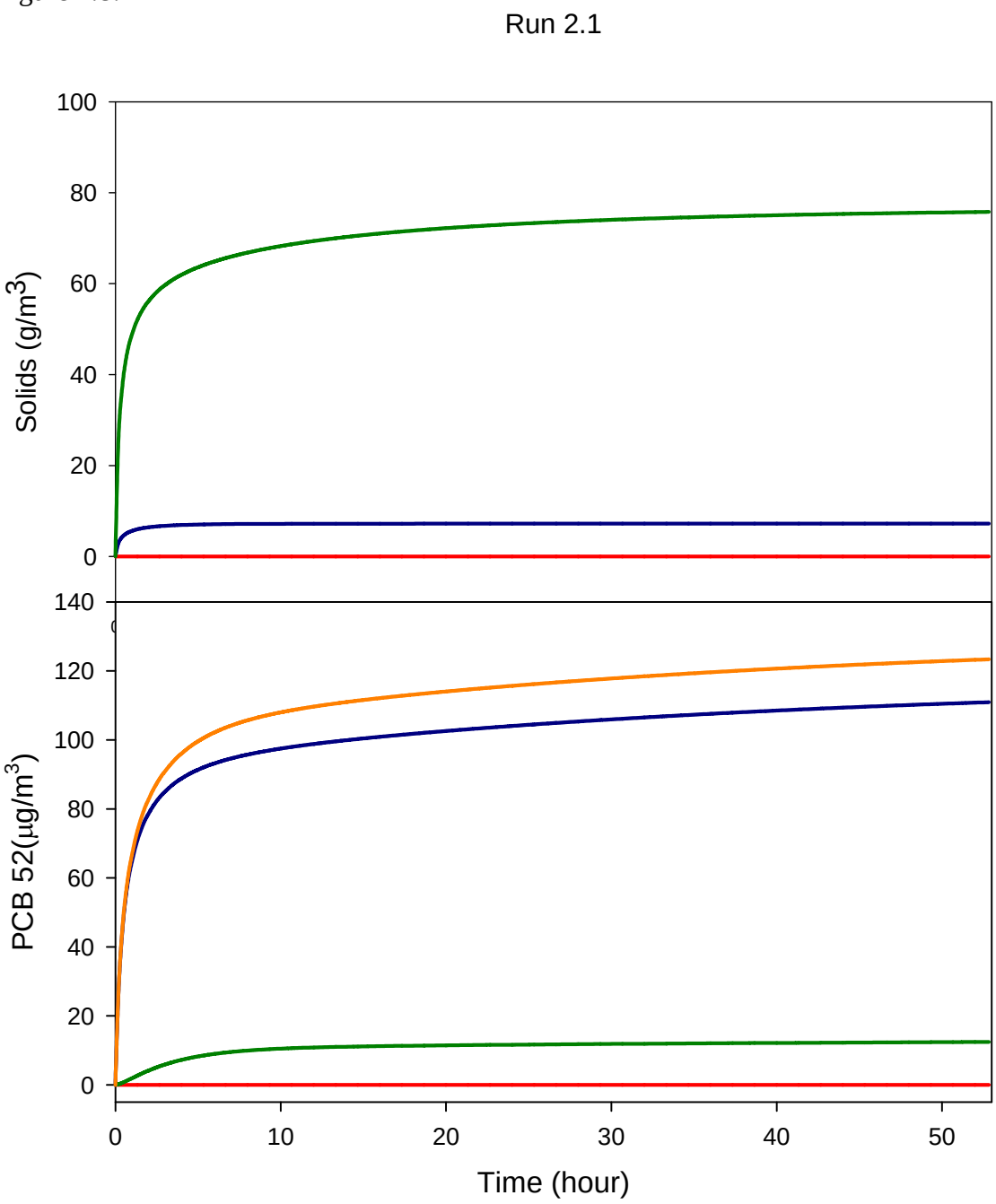
Run 2.1
Solids (g/m3)
100
80
60
40
20
0
PCB 52(µg/m3)
140
120
100
80
60
40
20
0
0
10
20
30
40
50
Time (hour)

Figure 7.9:

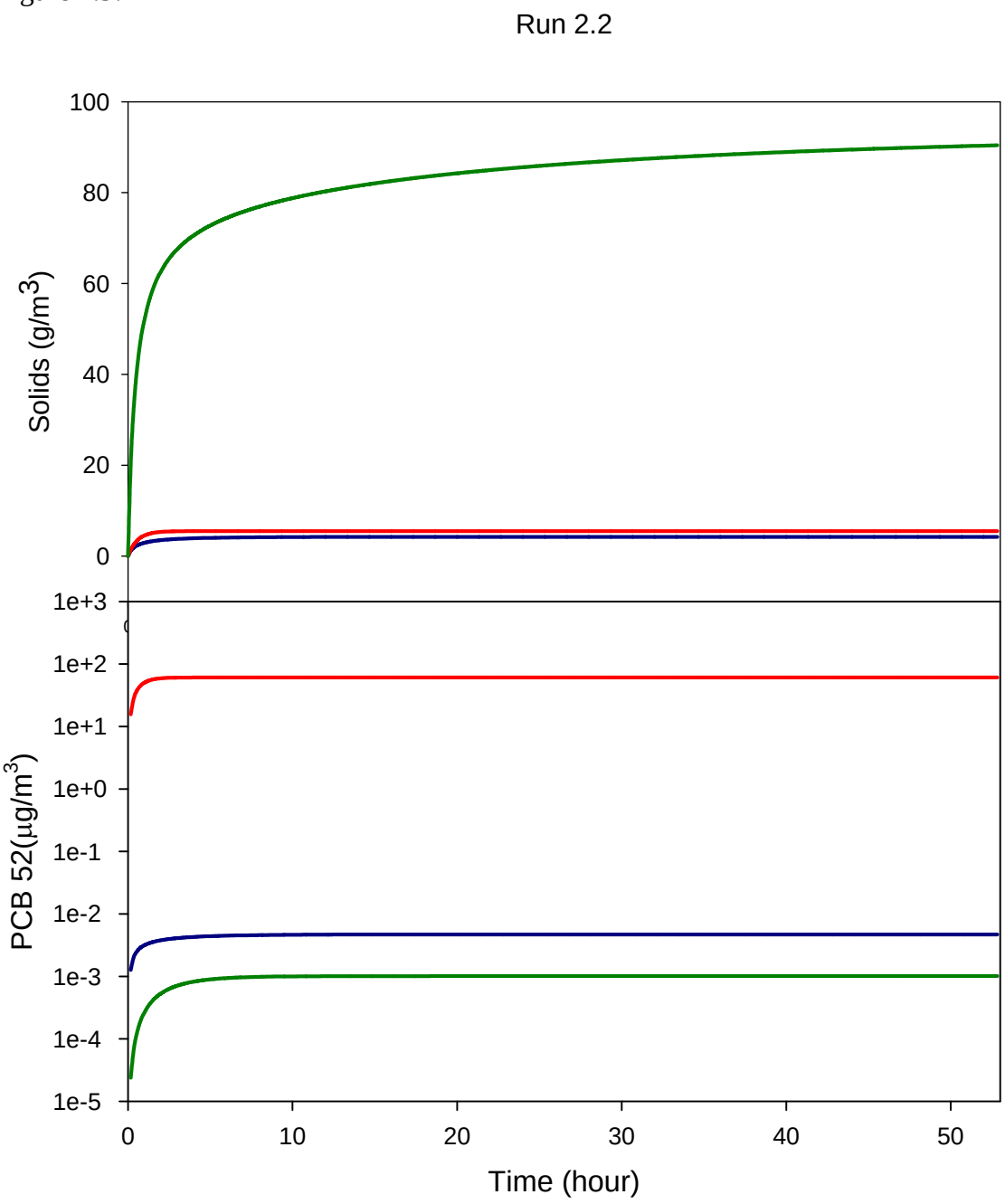
Run 2.2
Solids (g/m3)
100
80
60
40
20
0
PCB 52(µg/m3)
1e+3
1e+2
1e+1
1e+0
1e-1
1e-2
1e-3
1e-4
1e-5
0
10
20
30
40
50
Time (hour)

Figure 7.10:

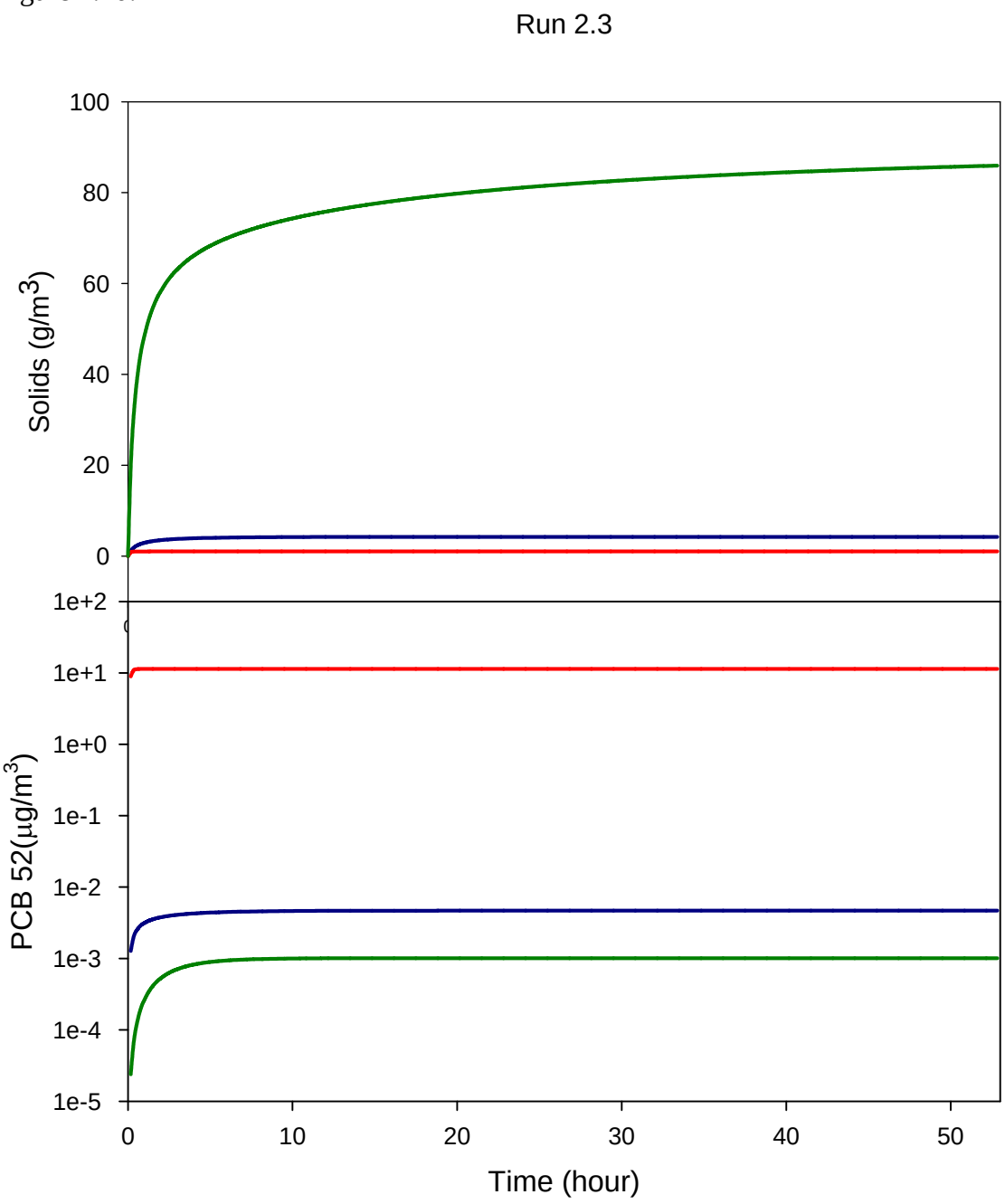
Run 2.3
Solids (g/m3)
100
80
60
40
20
0
1e+2
1e+1
1e+0
1e-1
1e-2
1e-3
1e-4
1e-5
PCB 52(µg/m3)
0
10
20
30
40
50
Time (hour)

Figure 7.11:

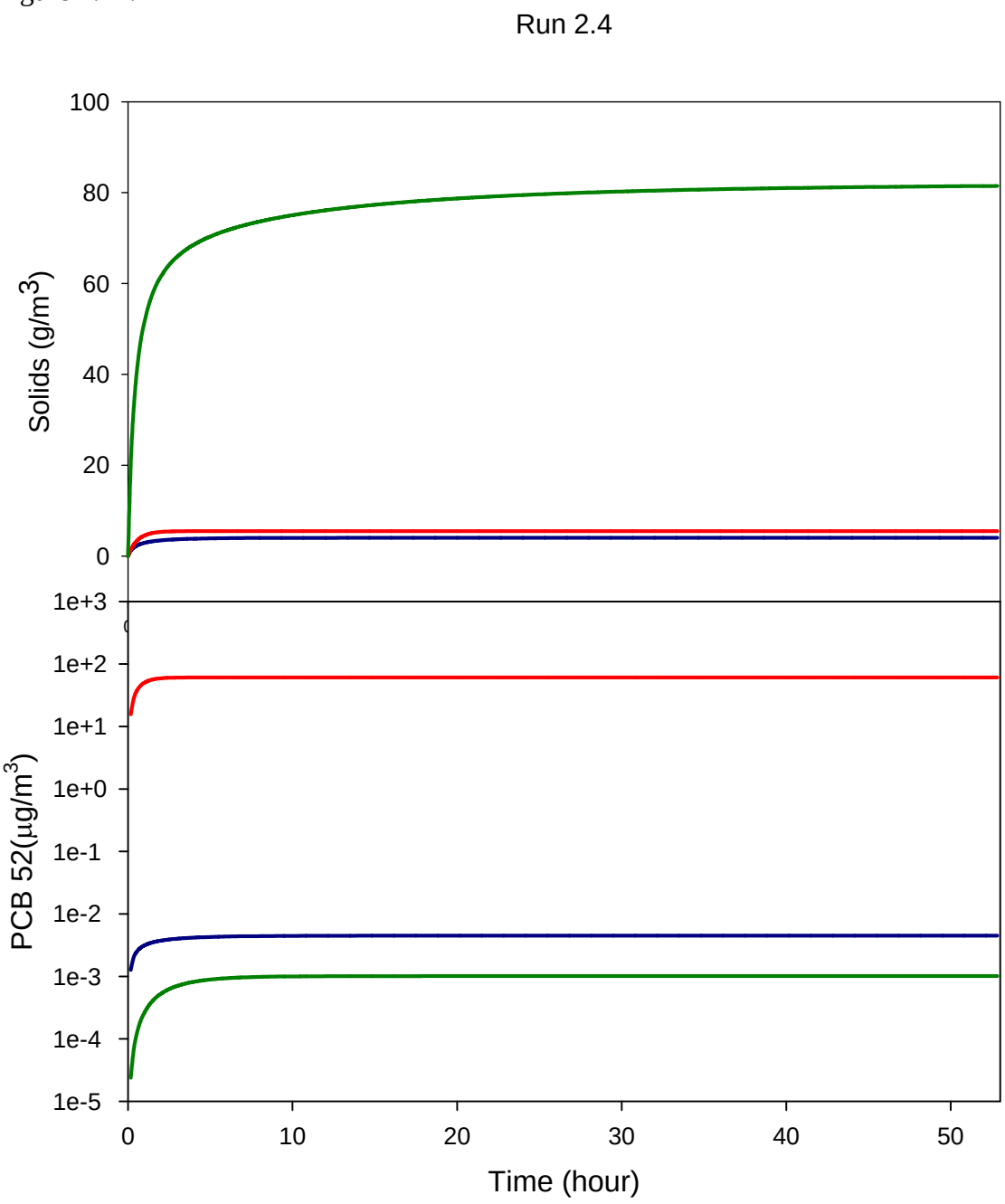
Run 2.4
Solids (g/m3)
100
80
60
40
20
0
PCB 52(µg/m3)
1e+3
1e+2
1e+1
1e+0
1e-1
1e-2
1e-3
1e-4
1e-5
0
10
20
30
40
50
Time (hour)

Figure 7.12:

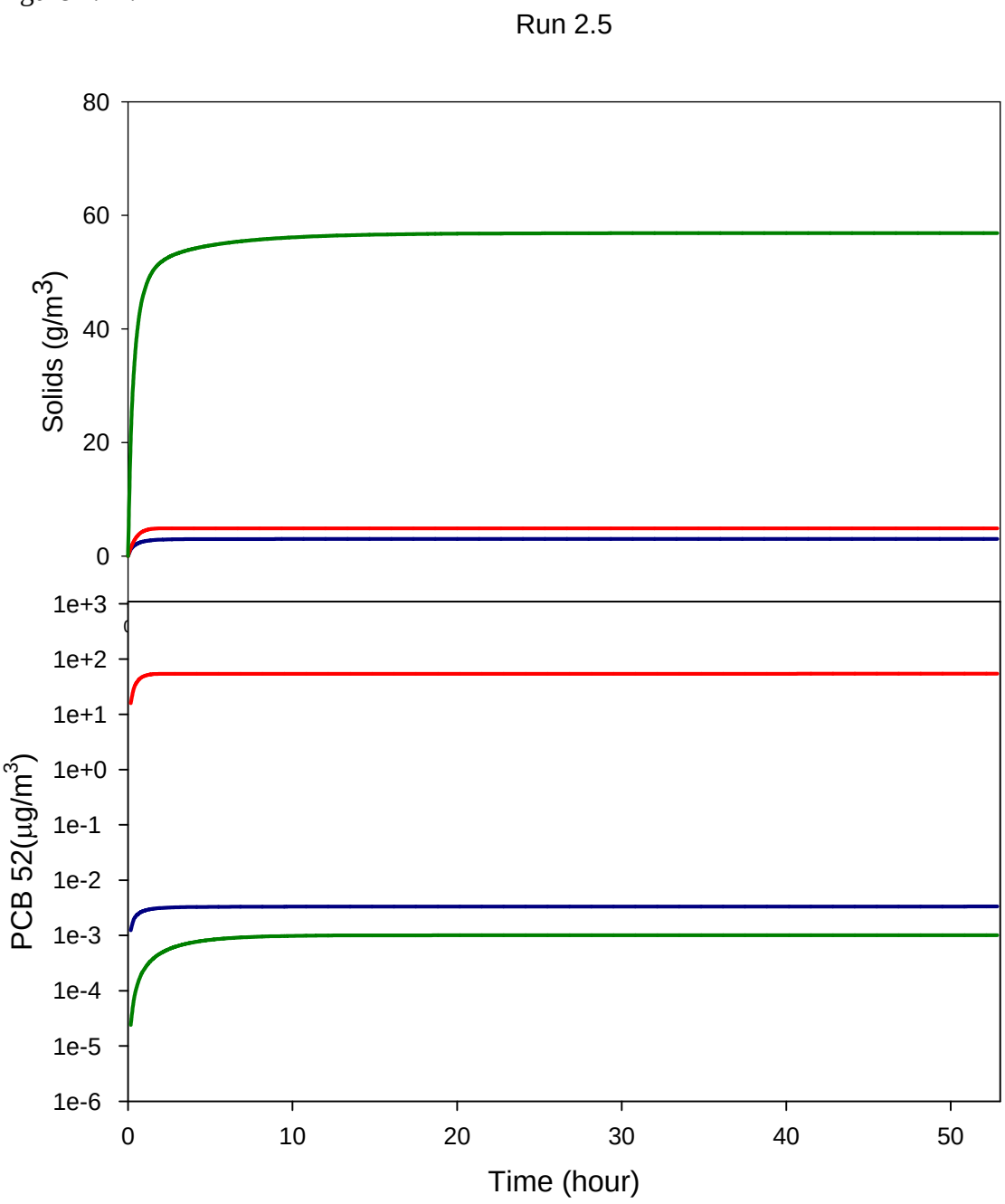
Run 2.5
Solids (g/m3)
80
60
40
20
0
PCB 52(µg/m3)
1e+3
1e+2
1e+1
1e+0
1e-1
1e-2
1e-3
1e-4
1e-5
1e-6
0
10
20
30
40
50
Time (hour)

Figure 7.13:

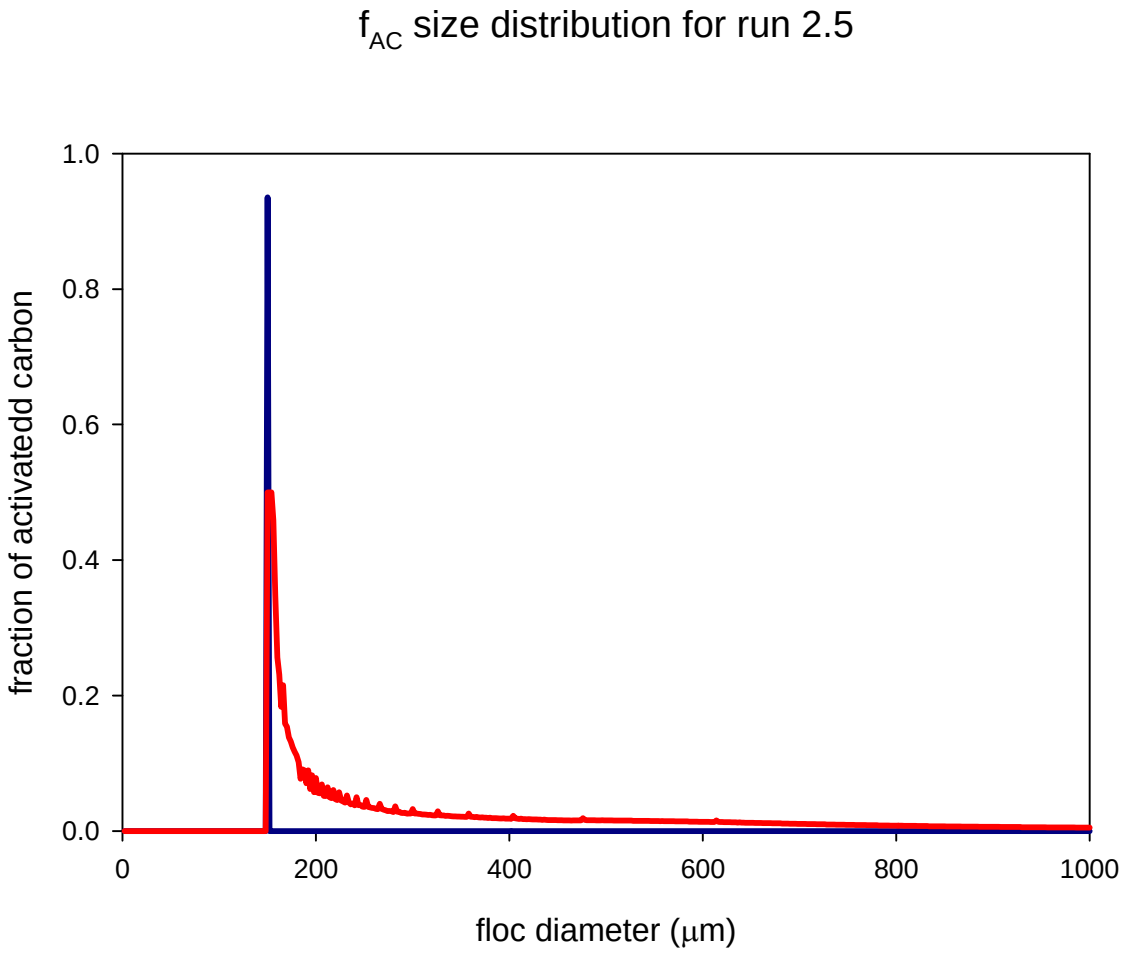
f_{AC} size distribution for run 2.5
fraction of activatedd carbon
1.0
0.8
0.6
0.4
0.2
0.0
0
200
400
600
800
1000
floc diameter (μm)

Figure 7.14:

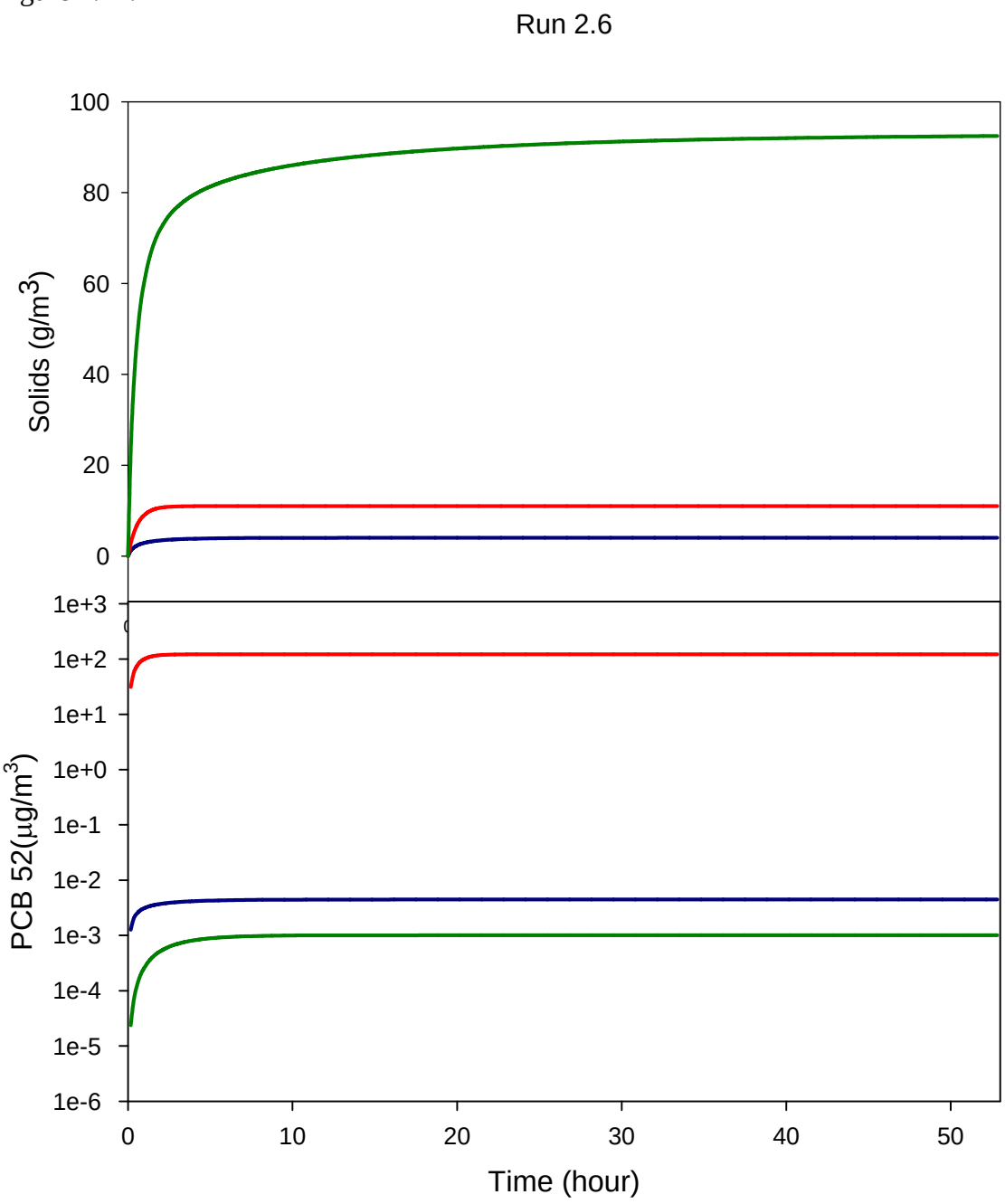
Run 2.6
Solids (g/m3)
100
80
60
40
20
0
PCB 52(µg/m3)
1e+3
1e+2
1e+1
1e+0
1e-1
1e-2
1e-3
1e-4
1e-5
1e-6
0
10
20
30
40
50
Time (hour)

Figure 7.15:

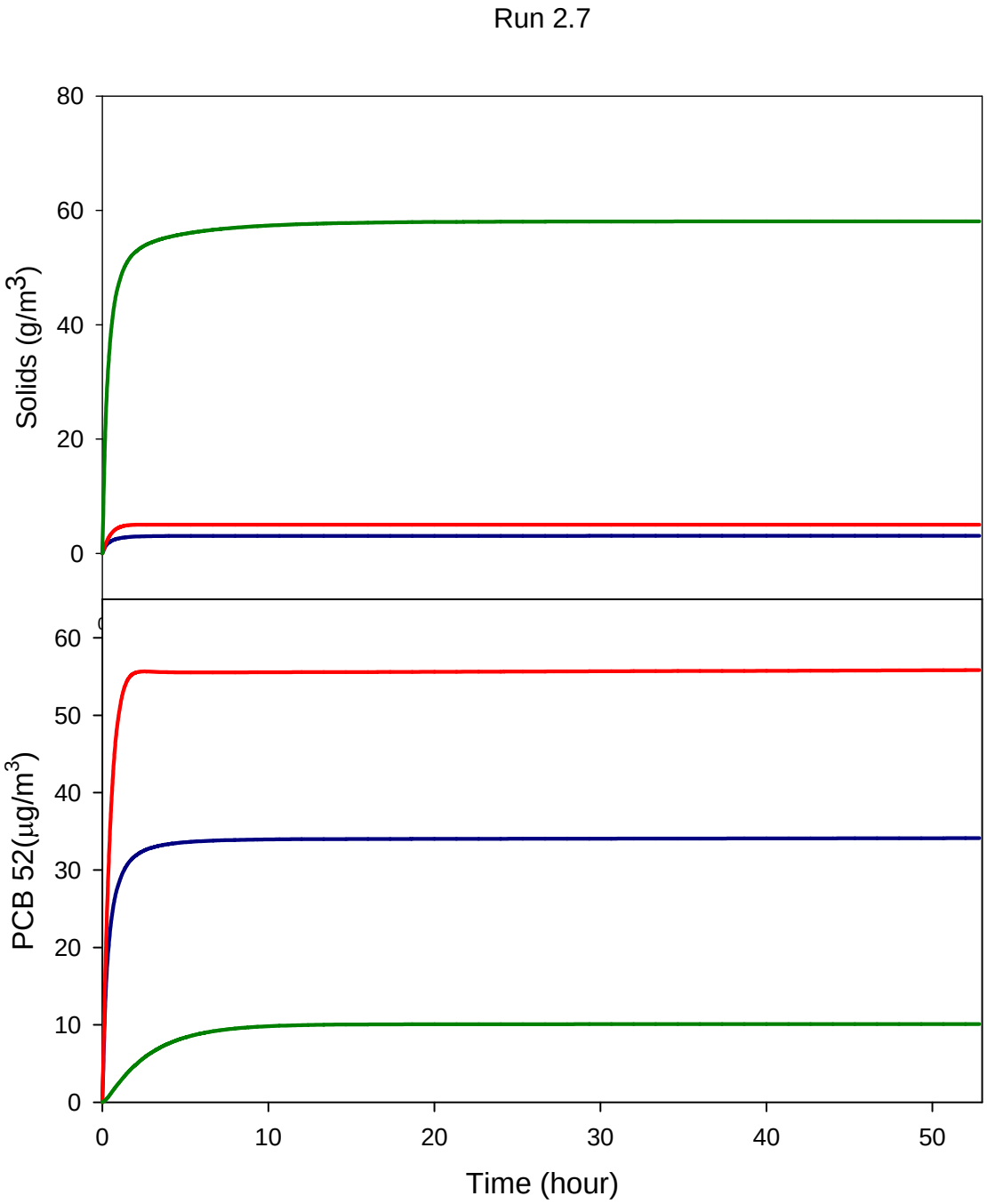
Run 2.7
Solids (g/m3)
80
60
40
20
0
PCB 52(µg/m3)
60
50
40
30
20
10
0
0
10
20
30
40
50
Time (hour)

Table 4.1: Eight model runs were conducted to systematically add and evaluate activated carbon to the model at stage one

									water column %						
run	Cp	TSS	OC	AC	K_{OC}, K_{AC}	$C_{p\,OC}$ (ug/m^3)	$C_{p\,AC}$ (ug/m^3)	Cd (ug/m$_3$)	$C_{p\,OC}$	$C_{p\,AC}$	TSS_{ss} (mg/L)	OC_{ss} (mg/L)	AC_{ss} (mg/L)	e-d	coag
0	1	1	0.10	0	1, 0	9.91E-02	0.00E+00	9.01E-01						off	off
1.1	1	1	0.44	0	1, 0	3.26E-01	0	6.74E-01						off	off
1.2	1	1	0	0.44	1, 0	0	3.26E-01	6.74E-01						off	off
1.3	1	1	0	0.44	1000, 0	0	9.97E-01	3.10E-03						off	off
1.4	1	v	v		1, 0	225.42	0	0.87			444.72	231.46	0	on	off
1.5	1	v		v	1000, 0	0	1.22	1.11E-04			444.72	0	1.54	on	off
1.6	1	v	v	v	1, 1000	225.29	1.22	0.88	99.10%	0.50%	444.72	231.46	1.54	on	off
1.7	1	v	v	v	1, 1000	112.65	1.83	0.44	98.00%	1.60%	444.72	231.46	1.54	on	off
1.8	1	v	v	v	1, 1000	0.541	2.434	0.002	18.20%	81.80%	444.72	231.46	1.54	on	off

Table 4.2: Seven model scenarios were created to successively explore the interaction of AC and OC and its impact of HOC partitioning at stage two

run	K_{OC}, K_{AC}	coagulation effect: AC	coagulation effect: OC	e-d AC flux	e-d OC flux	initial condition and special settings
2.1	1	**na**	**on**	**na**	**on**	same as chapter 3
2.2	1, 1000	**off**	**off**	on	on	**Ws=Stokes law equation for AC;** sediment HOC reaching equilibrium
2.3	1, 1000	**off**	**off**	on	on	**Ws=Winterwerp equation for AC and OC** sediment HOC reaching equilibrium
2.4	1, 1000	off	on	on	on	sediment HOC reaching equilibrium
2.5	1, 1000	**on**	on	on	on	sediment HOC reaching equilibrium
2.6	1, 1000	off	on	**X2**	on	sediment HOC reaching equilibrium
2.7	1, 1000	on	on	on	on	**AC and OC took 50% of sediment HOC** $OC+AC=OC_{run1}$; and $sum(OC)=AC_{D150um}$

PUBLICATIONS, PRESENATIONS AND PATENTS

Publications citing SERDP funding:

Kjellerup, B.V., X. Sun, U. Ghosh, H.D. May, K.R. Sowers. 2008. Site specific microbial communities in three PCB-impacted sediments are associated with different in situ dechlorinating activities. *Environ. Microbiol. 10:* 1296-1309.

Kjellerup B.V, Naff C, Paul P, Ghosh U, Baker J, Sowers, K. Effect of AC sequestration on the distribution and activity of PCB dechlorinating bacteria in weathered and non-weathered sediment from Grasse River, NY. In preparation.

Kjellerup B.V, Ghosh U, Baker J and Sowers K. Bioavailability and anaerobic dechlorination of PCB in sediment supplemented with AC. In preparation.

Invited presentations citing SERDP funding:

Dehalogenation of polychlorinated biphenyls (PCBs) by dehalorespiring ultramicrobacteria: a big task for small microbes. Dept of Biological Sciences, University of Southern California. Nov 11, 2008

Anaerobic reductive dechlorination of polychlorinated biphenyls (PCBs) by dehalorespiring bacteria. ASM-CSM Joint Symposium on Environmental Microbiology & Bioenergy. Haikou City, Hainan, China. Nov 8, 2008

Finding a Needle in the Microbial Haystack: Identification of the Microbial Catalysts that Dechlorinate Polychlorinated Biphenyls (PCBs). NSF REU in Urban Environmental Biogeochemistry, Department of Environmental Chemistry, Towson University, Towson, MD June 10, 2008.

Developments in the Anaerobic *In Situ* Treatment of Polychlorinated Biphenyls (PCBs). Kevin R. Sowers, Birthe Kjellerup, Meredith Wright, Harold D. May . Battelle Fifth International Conference on Remediation of Chlorinated and Recalcitrant Compounds Monterey, California, May 19–22, 2008. Monterey, California

Finding a Needle in the Microbial Haystack: Identification of the Microbial Catalysts that Dechlorinate Polychlorinated Biphenyls (PCBs)". Working with Extremophiles Workshop. K.R. Sowers. Annual Meeting of the Society for Industrial Microbiology, Denver, CO. July 29, 2007.

A third alternative for protein expression: the methanogenic Archaea. K.R. Sowers. Annual Meeting of the Society for Industrial Microbiology, Denver, CO. July 29-Aug 2, 2007.

Developments in the Anaerobic In Situ Treatment of Polychlorinated Biphenyls (PCBs). K.R. Sowers*, S.K. Fagervold, B. Kjellerup, G.S. Miller and H.D. May. Fifth International Conference on Remediation of Chlorinated and Recalcitrant Compounds, Monterey, California;, May 22-25, 2006.

Developments in the Anaerobic In Situ Treatment of Polychlorinated Biphenyls (PCBs). K.R. Sowers*, S.K. Fagervold, B. Kjellerup, G.S. Miller and H.D. May. UMBI, Center of Marine Biotechnology 2006 Seminar Series, May 10, 2006. Baltimore, MD.

Presentations at meetings citing SERDP funding:

Application of Tools to Measure PCB Microbial Dechlorination and Flux into Water During In-situ Treatment of Sediments (ER-1502): Microbial Degradation Results. Piuly Paul, Birthe Kjellerup, Upal Ghosh, Kevin Sowers , Joel Baker, Andrew Chang. The Partners in Environmental Technology Technical Symposium & Workshop. December 1-3, 2009. Washington, DC.

Application of Tools to Measure PCB Microbial Dechlorination and Flux into Water During *In-situ* Treatment of Sediments (ER-1502): Resupension and Desorption Results. Joel Baker*, Andrew Chang, Kevin Sowers, Birthe Kjellerup, Upal Ghosh and Piuly Paul. The Partners in Environmental Technology Technical Symposium & Workshop. December 1-3, 2009. Washington, DC.

The effect of AC on the activity of PCB dechlorinating biofilms. B. Kjellerup*, K.R. Sowers, P. Paul & U. Ghosh, J.E. Baker. Eurobiofilms 2009. September 2-3, 2009. Rome, Italy.

Effect of AC sequestration on Aroclor 1260 Contaminated Sediment from Baltimore Harbor, MD. B. Kjellerup*, K.R. Sowers, P. Paul, U. Ghosh, J. Baker. Tenth International In Situ and On-Site Bioremediation Symposium. May 5-8, 2009. Baltimore, Maryland.

Progress on Microbial In situ Treatment of Polychlorinated Biphenyls (PCBs". K.R. Sowers*, B. Kjellerup, R. Makkar, C. Chun, J. Baker, U. Ghosh and H.D. May. Tenth International In Situ and On-Site Bioremediation Symposium. May 5-8, 2009. Baltimore, Maryland.

Natural PCB dechlorination activity and spatial distribution of PCB dechlorinating bacteria in sediment samples from Baltimore Harbor, MD. B. Kjellerup*, B. Stiell, K.R. Sowers, P. Paul, U. Ghosh, J. Baker. Tenth International In Situ and On-Site Bioremediation Symposium. May 5-8, 2009. Baltimore, Maryland.

Application of Tools to Measure PCB Microbial Dechlorination and Flux into Water During *In-situ* Treatment of Sediments (ER-1502) . Joel Baker*, Andrew Chang, Upal Ghosh, Piuly Paul, Kevin Sowers, Birthe Kjellerup. The Partners in Environmental Technology Technical Symposium & Workshop. December 2-4, 2008. Washington, DC.

Effect of on-site AC sequestration on microbial reductive dechlorination of PCBs in marine sediments at Hunters Point, CA. C. Naff*, B.V. Kjellerup, U. Ghosh, J.E. Baker, K.R. Sowers. 108th Ann. Mtg. Amer. Soc. Microbiol. June 1-5, 2008. Boston, MA.

Spatial distribution and activity of PCB dechlorinating bacteria in Baltimore Harbor, MD. B. Stiell*, B.V. Kjellerup, J.E. Baker, K.R. Sowers. 108th Ann. Mtg. Amer. Soc. Microbiol. June 1-5, 2008. Boston, MA.

Aroclor 1260 contaminated soils show spatial variability of dechlorinating bacteria, PCB reducing activities and potential for bioaugmentation. Kjellerup B.V*, Paul P, Ghosh U, M, May H, Sowers, K. . 108th Ann. Mtg. Amer. Soc. Microbiol. June 1-5, 2008. Boston, MA.

Developing PCR-based molecular methods for quantifying and monitoring dechlorination of polychlorinated compounds. J-W. Park*, M. Haggblom, D. Fennell, L. Kerkhof, V. Krumins, K. Sowers, B. Kjellerup. 108th Ann. Mtg. Amer. Soc. Microbiol. June 1-5, 2008. Boston, MA.

Application of Tools to Measure PCB Microbial Dechlorination and Flux into Water During *In-situ* Treatment of Sediments (ER-1502). Joel Baker, Andrew Chang, Upal Ghosh, Piuly Paul, Kevin Sowers, Birthe Kjellerup. The Partners in Environmental Technology Technical Symposium & Workshop. December 4 - 6, 2007. Washington, DC.

Site Specific Microbial Communities in Three PCB-Impacted Sediments are Associated with Different In situ Dechlorinating Activities. Kjellerup,l B.V., Sun, X., Ghosh, U., May, H.D., Sowers, K.R. 107th Ann. Mtg. Amer. Soc. Microbiol. May 21-25, 2007. Toronto, Canada.

Developments in the Anaerobic In Situ Treatment of Polychlorinated Biphenyls (PCBs). K.R. Sowers*, S.K. Fagervold, B. Kjellerup, G.S. Miller and H.D. May. Ninth International In Situ and On-Site Bioremediation Symposium. May 7-10, 2007. Baltimore, Maryland.

Abundance and Diversity of Aerobic and Anaerobic PCB degrading Bacteria In Contaminated Soil biofilms. Kjellerup, B.V., Ghosh, U., Paul, P., May, H., Sowers, K.S. 4th ASM Conference on Biofilms, Quebec City, Quebec, Canada. March 25 – 29, 2007.

Developments in the anaerobic in situ monitoring and treatment of polychlorinated biphenyls (PCBs) in marine sediments. K.R. Sowers, B. Kjellerup, S.K. Fagervold and H.D. May. 8th International Marine Biotechnology Conference, Eilat, Israel. March 11-16, 2007.

Abundance and Diversity of Aerobic and Anaerobic PCB degrading Bacteria in PCB Contaminated Soil. Kjellerup, B.V.*, Ghosh, U., Shirtliff, M.E., May, H, Sowers, K.S. Ninth International Symposium on Microbial Ecology. August 20-25, 2006. Vienna, Austria.

Distribution, Activity and Diversity of PCB dechlorinating *Chloroflexi* in Sediment by Competitive PCR, Activity Assays and Denaturing High-Performance Liquid Chromatography. Kjellerup, B.V.*, Ghosh, U., Shirtliff, M.E., May, H, Sowers, K.S. 106th Ann. Mtg. Amer. Soc. Microbiol. May 21-25, 2006. Orlando, Fl.

Chang, C.A., Schneider, A.R. and J.E. Baker (2005) Modeling the impact of flocculation on the fate of PCBs in mesocosms. Presented at the Society of Environmental Toxicology and Chemistry North America 26th Annual Meeting, Baltimore, MD.

Chang, C. and J.E. Baker (2006) Modeling the impact of flocculation on the fate of PCBs in an urban estuary. Presented at the Society of Environmental Toxicology and Chemistry North America 27th Annual Meeting, Montreal.

Chang, C. and J.E. Baker (2006) Modeling the impact of flocculation on the fate of organic particles in an urban estuary. Presented at the Society of Environmental Toxicology and Chemistry Asia Annual Meeting, Beijing.

Patents

Organic Biofilm Substrata as a Microbial Inoculum Delivery Vehicle for Bioaugmentation of Persistent Organic Pollutants in Contaminated Sediments and Soils. Kevin R. Sowers and Birthe Kjellerup. UMBI disclosure Sowers-09-012-IDF filed 04/30/09; IPTL File: 4115-262-PRV; U.S. Provisional Patent Application No. 61/222,991 on July 3, 2009. Status: under review.